Characterization of Alaskan HMA Mixtures with the Simple Performance Tester


Authors:
Peng Li and Juanyu Liu

Date: 05/16/2014

Prepared by:

REPORT DOCUMENTATION PAGE

Form approved OMB No.

1. AGENCY USE ONLY (LEAVE BLANK)	2. REPORT DATE	3. REPORT TYPE AND DATES COVERED
4000092	05/2014	Final Report

4. TITLE AND SUBTITLE
Characterization of Alaskan HMA Mixtures with the Simple Performance Tester

6. AUTHOR(S)
Peng Li and Juanyu Liu

5. FUNDING NUMBERS

AKSAS 63693/FHWA 4000092
T2-10-10
AUTC Project No. 410020

7. PERFORMING ORGANIZATION NAME(S) AND ADDRESS(ES)
Alaska University Transportation Center
P.O. Box 755900
Fairbanks, AK 99775-5900

8. PERFORMING ORGANIZATION REPORT NUMBER

INE/AUTC 12.21

9. SPONSORING/MONITORING AGENCY NAME(S) AND ADDRESS(ES)
Alaska Department of Transportation & Public Facilities
Research, Development, and Technology Transfer
2301 Peger Road
Fairbanks, AK 99709-5399

10. SPONSORING/MONITORING AGENCY REPORT NUMBER

4000092

11. SUPPLENMENTARY NOTES

Performed in cooperation with the Alaska Department of Transportation and Public Facilities

12a. DISTRIBUTION / AVAILABILITY STATEMENT

No restrictions

12b. DISTRIBUTION CODE

13. ABSTRACT (Maximum 200 words)

Material characterization provides basic and essential information for pavement design and the evaluation of hot mix asphalt (HMA). This study focused on the accurate characterization of an Alaskan HMA mixture using an asphalt mixture performance tester (AMPT) and an asphalt pavement analyzer (APA). The tests performed on the AMPT included dynamic modulus ($|E^*|$), flow number (FN), and flow time (FT). The APA was used to measure the rutting resistance of HMA. A catalog of $|E^*|$ for typical Alaskan HMA mixtures is provided, and the prediction models of $|E^*|$ have been verified. The modified Witczak model (G^* based) is recommended for estimating $|E^*|$ HMA when measured G^* of binder is available, and the Witczak model (η based) is recommended when default inputs of binder are used. The correlations between the results from the AMPT (i.e., $|E^*|$, FN, FT) and the rutting depth obtained from the APA have been statistically analyzed.

14- KEYWORDS:
Alaska, HMA, AMPT, Dynamic Modulus, Flow Time, Flow Number, APA, Rutting, Predictive Model

15. NUMBER OF PAGES
175

16. PRICE CODE

N/A

17. SECURITY CLASSIFICATION OF REPORT	18. SECURITY CLASSIFICATION OF THIS PAGE	19. SECURITY CLASSIFICATION OF ABSTRACT	20. LIMITATION OF ABSTRACT
Unclassified	Unclassified	Unclassified	N/A

SI* (MODERN METRIC) CONVERSION FACTORS

APPROXIMATE CONVERSIONS TO SI UNITS

Symbol	When You Know	Multiply By	To Find	Symbol
LENGTH				
in	inches	25.4	millimeters	mm
ft	feet	0.305	meters	m
yd	yards	0.914	meters	m
mi	miles	1.61	kilometers	km
AREA				
in^2	square inches	645.2	square millimeters	mm^2
ft^2	square feet	0.093	square meters	m^2
yd^2	square yard	0.836	square meters	m^2
ac	acres	0.405	hectares	ha
mi^2	square miles	2.59	square kilometers	km^2
VOLUME				
fl oz	fluid ounces	29.57	milliliters	mL
gal	gallons	3.785	liters	L
ft^3	cubic feet	0.028	cubic meters	m^3
yd^3	cubic yards	0.765	cubic meters	m^3
NOTE: volumes greater than 1000 L shall be shown in m^3				
MASS				
oz	ounces	28.35	grams	g
lb	pounds	0.454	kilograms	kg
T	short tons (2000 lb)	0.907	megagrams (or "metric ton")	Mg (or "t")
TEMPERATURE (exact degrees)				
^{o}F	Fahrenheit	5 (F-32)/9 or (F-32)/1.8	Celsius	^{o}C
ILLUMINATION				
fc	foot-candles	10.76	lux	lx
fl	foot-Lamberts	3.426	candela/m^2	cd/m^2
FORCE and PRESSURE or STRESS				
lbf	poundforce	4.45	newtons	N
lbf/in^2	poundforce per square inch	6.89	kilopascals	kPa

APPROXIMATE CONVERSIONS FROM SI UNITS

Symbol	When You Know	Multiply By	To Find	Symbol
LENGTH				
mm	millimeters	0.039	inches	in
m	meters	3.28	feet	ft
m	meters	1.09	yards	yd
km	kilometers	0.621	miles	mi
AREA				
mm^2	square millimeters	0.0016	square inches	in^2
m^2	square meters	10.764	square feet	ft^2
m^2	square meters	1.195	square yards	yd^2
ha	hectares	2.47	acres	ac
km^2	square kilometers	0.386	square miles	mi^2
VOLUME				
mL	milliliters	0.034	fluid ounces	fl oz
L	liters	0.264	gallons	gal
m^3	cubic meters	35.314	cubic feet	ft^3
m^3	cubic meters	1.307	cubic yards	yd^3
MASS				
g	grams	0.035	ounces	oz
kg	kilograms	2.202	pounds	lb
Mg (or "t")	megagrams (or "metric ton")	1.103	short tons (2000 lb)	T
TEMPERATURE (exact degrees)				
^{o}C	Celsius	1.8C+32	Fahrenheit	^{o}F
ILLUMINATION				
lx	lux	0.0929	foot-candles	fc
cd/m^2	candela/m^2	0.2919	foot-Lamberts	fl
FORCE and PRESSURE or STRESS				
N	newtons	0.225	poundforce	lbf
kPa	kilopascals	0.145	poundforce per square inch	lbf/in^2

*SI is the symbol for the International System of Units. Appropriate rounding should be made to comply with Section 4 of ASTM E380.
(Revised March 2003)

EXECUTIVE SUMMARY

Material characterization provides basic and essential information for pavement design and the evaluation of hot mix asphalt (HMA). With the current trend of developing mechanistic flexible pavement design and more reliable design procedures, accurate characterization of HMA properties is needed. NCHRP Project 1-37A considers the dynamic modulus ($|E^*|$) master curve a design parameter in the AASHTO 2002 Mechanistic-Empirical Pavement Design Guide (MEPDG). NCHRP Project 9-19 (Witczak et al., 2002a), *Superpave Support and Performance Models Management* recommends simple performance tests (SPTs), including $|E^*|$, flow number (F_N), and flow time (F_T), to complement the Superpave volumetric mixture design method and ensure reliable mixture performance over a wide range of traffic and climatic conditions. In current mechanistic design methods used by the Alaska Department of Transportation and Public Facilities (ADOT&PF), resilient modulus (M_R) is used to characterize HMA instead of $|E^*|$, though research indicates that $|E^*|$ provides better characterization of HMA than M_R because it provides full characterization of the mix over temperature and loading frequencies. However, no systematic study has been conducted to create a catalog of SPT data and correlations between SPTs and HMA performance for typical Alaskan HMA mixtures.

This study focused on the accurate characterization of an Alaskan HMA mixture using an asphalt mixture performance tester (AMPT) and asphalt pavement analyzer (APA). The AMPT was used to conduct SPTs (dynamic modulus $|E^*|$, flow number F_N, and flow time F_T tests). The APA was used to measure the rutting resistance of the same HMA. Loose asphalt mixtures were collected from 21 projects in 3 regions of ADOT&PF: the Northern region (10), the Central region (9), and the Southeast region (2). Details of each job mix formula (JMF) being used in the projects were obtained. Binder rheology testing results, which are essential inputs for $|E^*|$ predictive models, were also collected. The collected information included viscosity at 135°C measured by a rotational viscometer, dynamic shear modulus (G^*) and phase angle measured by a dynamic shear rheometer (DSR), flexural creep stiffness and *m*-value measured by a bending beam rheometer (BBR), and softening point. The collected mixtures were re-heated, mixed, and compacted using a gyratory compactor (SGC) in the laboratory. The SPTs were performed on specimens that were 100 mm in diameter and 150 mm in height. The target air voids of testing specimens were the design air voids of each project, about 4%. The $|E^*|$ test was performed over 8 loading frequencies (i.e., 25, 20, 10, 5, 2, 1, 0.5, and 0.1 Hz) and 4 temperatures (i.e., 4.4, 21.1, 37.8, and 54°C) according to AASHTO T342-11. The F_N and F_T tests were performed at a temperature of 54°C. The APA testing samples were manufactured using SGC at the University of Alaska Fairbanks laboratory, and the tests were performed by the University of Tennessee. Cylindrical specimens 6 in. (150 mm) in diameter and 3 in. (75 mm) in height were compacted by the SGC, and the air void content was controlled at 7%. The APA tests were conducted in accordance with procedures specified in AASHTO T340-10. The fabricated specimens were placed in the testing chamber and conditioned to 58°C, which was the testing temperature. The

tubes were pressurized to 100 psi, and the wheel load was 100 lb. The rutting depth measurements were obtained at a seating load of 10 cycles and intermediate loadings of 25, 4000, and 8000 cycles.

Dynamic modulus was measured at 4 temperatures and 8 frequencies for 19 asphalt mixtures collected from 3 ADOT&PF regions. The testing results and master curve coefficients for each mixture are listed in Appendix A. The predictive models of |E*| (i.e., Witczak model – η based, modified Witczak model – G* based, and Hirsch model) were verified at two levels corresponding to input Levels 2 and 3, as specified in the MEPDG. Level 2 verification was only performed at the temperature upper bound of asphalt binder performance grade (PG) due to available data.

Generally, the original Witczak model over-predicted |E*|, and the modified Witczak model and Hirsch model predicted similar moduli for all JMF. At Level 3 input, the most accurate estimations of |E*| were obtained from the Witczak model (η based), and the correlation between predicted values and measured |E*| had an R^2 of 0.8435. The modified Witczak model (G* based) and Hirsch model had an R^2 of 0.8166 and 0.7894, respectively. However, none of the three models accurately predicted |E*| at high temperature. Measured |E*| varied in a wider range than predicted values, indicating that the predictive models are relatively insensitive to changes in HMA volumetric properties, especially the Hirsch model, which approximately predicts the same |E*| for all mixtures at temperature of higher end in the PG. The modified Witczak model (G* based) is recommended for estimating |E*| of hot mix asphalt when measured G* of binder is available, and the Witczak model (η based) is recommended when the default inputs of a binder are used.

The results obtained from flow tests indicate that confining pressure greatly increases F_N and F_T. To accomplish a confined flow test within 10,000 loading cycle/second, the confining pressure must be far less than 137 kPa or the compressive stress must be increased. The results also indicated that F_N correlates well with the mix design method and PG. Hot mix asphalt designed by the Superpave method had a higher F_N due to the higher compaction effort applied during specimen fabrication. The mixture with coarse aggregate gradation had a higher F_N.

Measured rutting depths from APA tests showed that 11 out of 21 mixtures had a final rutting depth of less than 6 mm. The M mixture had the lowest rutting depth, followed by FIA, GPP, PSG, AIA, GGB, FIA64, CH, DH, PW, and HNS. Findings show that mixtures with a higher high-temperature grade and dust/asphalt ratio tend to have lower rutting depth or higher rutting resistance. Correlations between F_N/F_T and rutting depth obtained from APA tests were statistically analyzed. Flow number correlated to rutting depth better than F_T, as indicated by a higher R^2 value. Higher rutting depth tends to correlate with lower F_N and F_T. When F_N was greater than 400 or F_T was greater than 40, the asphalt mixture had good rutting resistance, as indicated by a rutting depth less than 5 mm. However, when F_N was less than 400 or F_T was less than 40, the results were mixed. Rutting depth of such mixes ranged between 3 and 13 mm.

TABLE OF CONTENTS

LIST OF FIGURES

LIST OF TABLES

CHAPTER 1 INTRODUCTION

Material characterization provides basic and essential information for pavement design and the evaluation of hot mix asphalt (HMA). This study focused on the accurate characterization of Alaskan HMA mixes using an asphalt mixture performance tester (AMPT) and an asphalt pavement analyzer (APA). The tests performed using the AMPT included dynamic modulus ($|E^*|$), flow number (F_N), and flow time (F_T) tests. The APA was used to measure the rutting resistance of HMA. A catalog of $|E^*|$ for typical Alaskan HMA mixtures is provided, and the prediction models of $|E^*|$ are verified. Correlations between the AMPT results ($|E^*|$, F_N, and F_T) and the rutting depths obtained from the APA have been statistically analyzed as well.

1.1 Problem Statement

With the current trend of developing mechanistic flexible pavement design and more reliable design procedures, accurate characterization of HMA properties is needed. NCHRP Project 1-37A (ARA, Inc. 2004) considers the dynamic modulus ($|E^*|$) master curve a design parameter in the Mechanistic-Empirical Pavement Design Guide (MEPDG). NCHRP Project 9-19 (Witczak et al. 2002a), *Superpave Support and Performance Models Management*, recommends simple performance tests (SPTs) including $|E^*|$, F_N, and F_T tests, to complement the Superpave volumetric mixture design method and ensure reliable mixture performance over a wide range of traffic and climatic conditions.

Many states have been using SPTs in the evaluation of their HMA mixtures to determine if the performance tests and the MEPDG are ready for implementation by owners/agencies (Pellinen, 2001; Witczak et al., 2002a; Kim et al., 2004; Bhasin et al., 2005; Mohammad et al., 2005; Obulareddy, 2006; Williams et al., 2007). The objectives of these studies were to develop a catalog for $|E^*|$ inputs in the MEPDG, provide state departments of transportation (DOTs) familiarity with the proposed $|E^*|$ parameter, and generate information on performance of selected HMA mixtures using the new tests. Increased effort is anticipated when those SPTs are implemented at a state level.

In the current Alaska Department of Transportation and Public Facilities (ADOT&PF) mechanistic design methods, resilient modulus (M_R) instead of $|E^*|$ is used to characterize HMA, though research has indicated that $|E^*|$ provides better characterization of HMA than M_R because it provides full characterization of the mix over temperature and loading frequencies (Loulizi et al., 2006).

Simple performance tests were conducted in two completed research projects sponsored by ADOT&PF to evaluate the rutting performance of Alaskan HMA mixtures (Ahmed, 2007; Liu and Connor, 2008) and the performance of warm mix asphalt. (Liu et al., 2011; Liu and Li, 2012). However, no systematic study has been conducted to obtain a catalog of SPT data and

correlations between SPTs and HMA rutting performance for typical Alaskan HMA mixtures. Hence, the development of a catalog of |E*| values for mixture types typically used in Alaska is essential for the State of Alaska's own pavement design guide or for future implementation of the MEPDG.

An evaluation of the applicability of current test procedures and the equipment used for measuring HMA mix properties, with particular emphasis on |E*| is needed, as well as a comparison of results from SPTs with other established performance tests. The ADOT&PF should be provided with the proposed |E*| parameters and information on the performance of selected HMA mixtures in new projects, as well as feedback on the practical issues associated with future implementation of new test procedures.

1.2 Objectives

To provide the accurate characterization of HMA for both pavement design and performance evaluation, the main objectives of this project are to

1) establish a catalog of |E*| test results for typical Alaskan HMA mixtures,
2) evaluate the correlations between SPT results (|E*|, F_N, F_T by AMPT) and HMA performance (rutting tests by APA), and
3) assess the ability of the original Witczak, modified Witczak, and Hirsch models in |E*| prediction for Alaskan asphalt mixtures.

1.3 Research Methodology

The following major tasks were accomplished to achieve the objectives of this study:
- Task 1:   Literature Review
- Task 2:   Development of AMPT Testing Plan
- Task 3:   Materials Collection, Specimens Fabrication, and Performance Tests
- Task 4:   Data Processing and Analyses
- Task 5:   Project Summary and Recommendations

Task 1: Literature Review

The purpose of this task is to review the existing and current efforts in characterization of HMA mixtures using the AMPT and APA. This task was accomplished through a critical review of technical literature and research in progress. The detailed literature review is described in Chapter 2.

Task 2: Development of AMPT Testing Plan

Under this task, a HMA characterization testing plan was developed based on discussions between the research team, the technical advisory committee for this project, and professionals from the Statewide and Regional Materials Sections of ADOT&PF. The testing plan identified asphalt paving projects from different regions of Alaska considering factors such as mix design

method (such as Marshall design or Superpave design), aggregate source, aggregate gradation/nominal maximum aggregate size (NMAS), asphalt source, asphalt grade, and asphalt content. The details are presented in Chapter 3.

Task 3: Materials Collection, Specimens Fabrication, and Performance Tests

Loose HMA mixtures were collected from 21 paving projects and delivered to the University of Alaska Fairbanks (UAF) laboratory. Details of the materials and job mix formula (JMF) being used in the project construction and associated test data were obtained as well.

These mixtures were then re-heated, mixed, and compacted using the gyratory compactor (SGC) in the laboratory. Laboratory mixture characterization tests include $|E^*|$ tests at various temperatures and frequencies (according to AASHTO TP62-07 [2008]) and F_N, F_T, and APA tests (according to AASHTO TP63-09). The APA tests were performed by the University of Tennessee. Volumetric properties of mixtures (e.g., air voids and voids in the mineral aggregate [VMA]) were verified before the tests. The experimental details are summarized in Chapter 3.

Task 4: Data Processing and Analyses

A catalog of dynamic moduli for typical Alaskan HMA mixtures from the three regions was synthesized. Measured moduli of various HMA collected in this study were used to evaluate the suitability of the Witczak and Hirsch predictive models. Statistical analyses were conducted to investigate the effects of the different mixture variables on the SPTs. The correlations between SPT results and HMA rutting performance measured by APA tests were evaluated as well. The testing results and data analysis are presented in Chapter 4.

Task 5: Project Summary and Recommendations

Based on Tasks 1 through 4, research results and findings were summarized. A catalog of dynamic moduli for typical Alaskan HMA mixtures from the three regions and reliable $|E^*|$ predictive models were developed. Comments as well as recommendations for future work are presented in Chapter 5.

CHAPTER 2 LITERATURE REVIEW

This chapter summarizes the findings and conclusions from previous studies in the area of HMA characterization, SPTs (i.e. |E*|, flow number and flow time) and their testing methods, influencing factors, and predictive models for |E*|.

Since pavement design methods have migrated from the empirical design method (e.g., the AASHTO guide, version 1972–1993) to the mechanistic-empirical design method (e.g., MEPDG), modern HMA characterization should be based on a fundamental mechanistic property that can be used to evaluate HMA performance and provide material input for the mechanistic-empirical pavement design (ARA, 2004).

2.1 Characterization of HMA

Hot mix asphalt characterization is the measurement and analysis of the response of HMA to load, deformation, and/or environmental conditions (Brown et al., 2009). The results provide valuable information for evaluating material performance, understanding HMA behavior, providing essential input values for pavement design, and use in construction quality assurance.

The early HMA characterization tests were mostly empirical testing methods, based on empirical correlation between testing results and material performance. These tests include the Marshall stability test, the Hveem stabilometer test, and various loaded wheel tests. The Marshall stability test was an empirical strength measure of HMA developed in the 1940s. The Marshall test is a part of the Marshall mix design method, currently used by ADOT&PF. During the test, a compressive load is applied to a cylindrical specimen 4 in. in diameter and 2.5 in. in height along the diametrical direction through a semicircular testing head. The test is performed at 60°C to simulate the most critical field condition. Marshall stability is defined as the maximum load carried by the specimen. The total vertical deformation of the specimen at maximum deformation, which is defined as flow index or flow value, is also recorded. Marshall stability is primarily affected by the asphalt binder viscosity at 60°C and internal friction of the aggregate.

Hveem stability was developed as an empirical measure of the internal friction within a mixture. The specimen is compacted by a kneading compactor, and its final dimension is 4 in. in diameter and 2.5 in. in height. During testing, a vertical axial load is applied to a specimen with confining pressure at 60°C. The stability is calculated according to Eq. 2.1, and the value varies in the range of 0 to 100. Hveem stability is a part of the Hveem mix design method, with a required value of stability of 40 to 55 to be a qualified HMA (Vallerga and Lovering, 1985).

$$S = \frac{22.2}{\left[\frac{P_h \cdot D}{P_v - P_h}\right] + 0.222} \tag{2.1}$$

where
S = stability value,
P_h = horizontal pressure for corresponding Pv in psi (or kPa),

D   = displacement of specimen, and

P_v = vertical pressure (typically the 400 psi (2800 kPa) being applied when the vertical load is 5000 lbf (22.3 kN).

       Generally, the stabilities obtained from Marshall and Hveem tests are used to determine the optimum asphalt contents during mix design procedures. These stabilities are neither based on fundamental engineering properties nor correlation with field performance, such as permanent deformation (Brown et al., 2004) and the potential of fatigue cracking (Kandhal and Parker, 1998).

       Rutting is the permanent deformation of pavement under the wheel path and is considered a primary pavement distress. Currently, the most widely used standardized laboratory test to characterize rutting resistance is the loaded wheel test (LWT), which measures the rutting potential of HMA by applying a moving wheel load to the surface of an asphalt mixture sample. Many types of LWT equipment are available: the Georgia Loaded Wheel Tester (GLWT), the Asphalt Pavement Analyzer (APA), the Superfos Construction Rut Tester, the Hamburg Wheel Tracking Device (HWTD), the Purdue University Laboratory Wheel Tracking Device (PURWheel), and the French Pavement Rutting Tester (FPRT) (Cooley et al., 2004). Among these LWTs, the APA is a modification of the GLWT (Kandhal and Cooley, 2003). The APA features controllable wheel load and contact pressure that are representative of actual field conditions and, thus, has been widely used by many DOTs and transportation agencies in the U.S. An AASHTO test specification (T340-10) has been developed for testing rutting potential of asphalt mixtures by using the APA. Stuart and Izzo (1995) reported that the loaded wheel testers provided a very good relationship between the binder property of G*/sin δ and rutting susceptibility. The FPRT and HWTD provided reasonably good relationships with binder properties. Williams and Prowel (1999) compared three accelerated laboratory loaded wheel devices—the APA, FPRT, and HWTD—with full-scale pavement performance under controlled conditions. Results of the three laboratory rutting testers show high correlations with the field test measurements.

       The primary limitation of empirical tests (e.g., the Marshall stability test, the Hveem stabilometer, and LWTs) is that the parameters obtained from the tests are not based on fundamental mechanical principles and cannot be directly incorporated into pavement design. As conditions beyond the scope of existing material and pavement structure, the confidence of their correlations to the pavement performance would be weakened. Modern HMA characterization methods are moving toward mechanistic-based testing methods, such as the Superpave shear test, |E*| test, creep test, and indirect tensile test. Among these mechanistic-based testing methods, |E*|, flow time, and flow number tests have been recently adopted as SPTs in the NCHRP 9-19 project.

2.2 Simple Performance Test

The Superpave mix design method has been adopted nationwide. However, the design method is only based on volumetric properties, and no characterization test can be used to evaluate the field performance of designed HMA. Based on observations obtained from the WesTrack (NCHRP 9-7), the Superpave volumetric mixture design method alone is not sufficient to ensure reliable mixture performance over a wide range of materials, traffic, and climatic conditions (Cominsky et al., 1998). By contrast, strength tests have been available for the empirical Marshall and Hveem mix design methods for a long time. The paving industry was expecting a simple "push-pull" type testing method to complement the Superpave volumetric mix design method. NCHRP Project 9-19, *Superpave Support and Performance Models Management*, recommended three candidate SPTs, defined as a test method (or methods) that accurately and reliably measures a mixture response characteristic or parameter that is highly correlated to the occurrence of pavement distress over a diverse range of traffic and climatic conditions (Witczak et al., 2002a). The study indicated that rutting and fatigue cracking were the primary concerns among all pavement distresses and proposed three SPTs, including F_T, F_N, and $|E^*|$. Later, an asphalt mixture performance tester (AMPT, previously simple performance tester) was developed under the NCHRP Project 9-29, *Refining the Simple Performance Tester for Use in Routine Practice* (Bonaquist, 2008), which packed all technologies into a user-friendly testing system and greatly facilitated and popularized the SPT.

Dynamic Modulus

The MEPDG uses $|E^*|$ of HMA in structural analysis to calculate the stresses, strains, and displacements of flexible pavement under various loading and climate conditions. Dynamic modulus can also be used as an indicator of the resistance of asphalt mixture to pavement distress, such as rutting and fatigue cracking. Therefore, $|E^*|$ has been included in the SPTs and recommended as a performance test to complement the Superpave volumetric mix design procedure. Using $|E^*|$ is also considered a promising approach for integrating mix design with pavement design, which has been a long-term goal pursued by pavement engineers for decades (Witczak et al., 2002b).

Dynamic modulus ($|E^*|$) is the absolute value of complex modulus (E^*), which is a complex number and defines the relationship between stress and strain under sinusoidal loading for linear viscoelastic materials (Brown et al., 2009). Dynamic modulus is determined by applying sinusoidal loads to a specimen while measuring the deformation. Then $|E^*|$ is calculated by dividing the stress amplitude by the strain amplitude (Eq. 2.2).

$$\left|E^*\right| = \frac{\sigma_0}{\varepsilon_0}$$

(2.2)

where
$|E^*|$ = dynamic modulus, MPa,

σ_0 = peak-to-peak stress amplitude, MPa, and

ε_0 = peak-to-peak strain amplitude.

To take into account the time-temperature dependence of $|E^*|$, usually the test is performed at four temperatures (i.e., 4°C, 21°C, 37°C, and 54°C) and at least 6 frequencies (i.e., 0.1, 0.5, 1.0, 5, 10, and 25 Hz) (AASHTO TP62). Using the principle of time-temperature superposition, a master curve is constructed by shifting the data at various temperatures to the reference temperature (usually 21°C) with respect to time until the curves merge into a single smooth function (Brown, 2009).

Flow Time (F_T) and Flow Number (F_N)

Within the asphalt concrete layer, the development of pavement rut can be divided into two phases (Kaloush and Witczak, 2002). The first phase is due to the accumulation of vertical deformation, and a part of the rut in this phase is caused by post-construction densification. The second phase is due to lateral movement within the asphalt mixture caused by shear force. This phase is more critical to the stability of mixture and leads to excessive rutting depth. Flow number (F_N) and flow time (F_T) tests were developed to capture the threshold of this shear plastic movement.

It was found through uniaxial compression tests that the relationship between loading time (or the number of load repetitions) and creep compliance includes three distinct stages: the primary, secondary, and tertiary stages, as shown in Figure 2.1 (Kaloush and Witczak, 2002; Zhou et al., 2004). The primary stage is a period of rapid strain accumulation at the beginning of the test, followed by the secondary stage, which is identifiable by a constant accumulated strain rate. As the secondary stage continues and the pavement structure breaks down, a jump to the tertiary stage eventually occurs, marked by an increase in strain rate. The point at which the permanent strain rate is at its minimum and tertiary flow begins is noted as the F_T for the static uniaxial compression test or F_N for the repeated load uniaxial compression test.
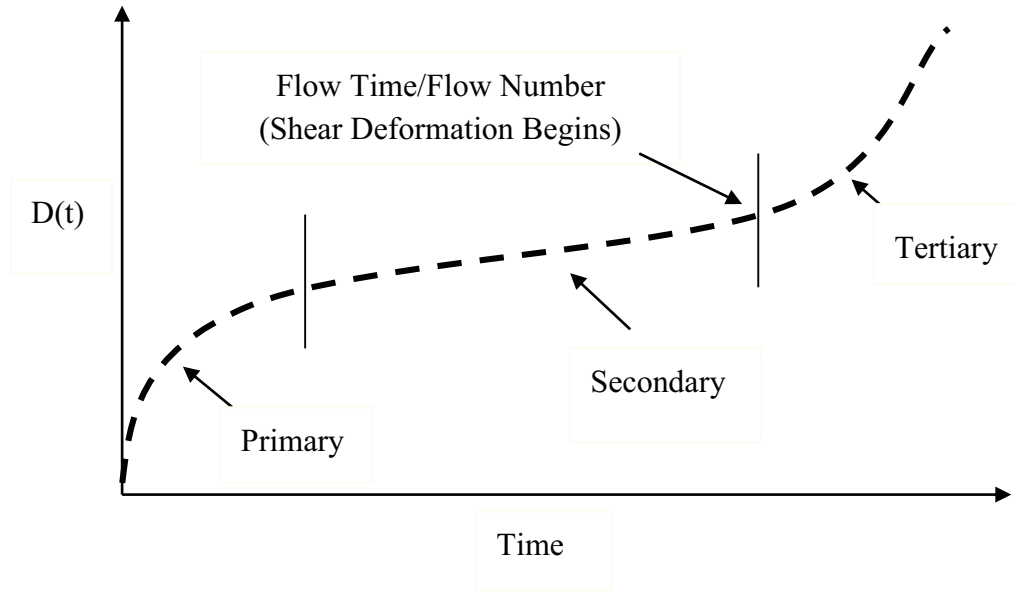
Figure 2.1 Creep compliance vs. time

Various models were developed to fit the data measured during F_N and F_T tests and improve the reliability of calculation. Through laboratory test results and field observation, Zhou et al. (2004) concluded that existing models are limited to characterizing only the primary stage. A new three-stage model was proposed to describe all three stages, and an algorithm was established to determine the model parameters from typical laboratory data. Biligiri et al. (2007) analyzed 300 F_N test data files from more than 40 mixtures in a wide range of test temperatures and several stress levels and found that previous modeling techniques for determining the F_N, which used a polynomial model-fitting approach, worked well for most conventional asphalt mixtures but not for rubber-modified asphalt mixtures. A new comprehensive mathematical model was recommended to determine F_N accurately. Dongre et al. (2009) found that algorithms currently used in the AMPT to determine F_N were extremely sensitive to noise in the data and identified erroneous F_N results, especially for modified mixes. A Francken model-based algorithm was proposed to fit F_N data, and the robustness of the new model was verified using data obtained from field projects. It was also found that steady-state slope and slope at 2% strain correlated well with F_N, and this correlation indicated that these slopes might be robust indicators of rut resistance. The instability of the calculation algorithm due to data noise was also reported by Goh et al. (2011). Based on results from 122 F_N tests, a stepwise method was used to overcome variations in testing data, and deformation rate was used to estimate F_N based on strong correlation between them. Bhasin et al. (2005) suggested that the sensitivity of F_T and F_N tests could be improved by (a) selecting the appropriate temperature and stress levels for the mixes being compared and (b) comparing mixes that have similar properties other than a broad range that can be used in APA tests.

2.3 Testing Method

Dynamic Modulus (|E*|)

The most widely used testing method for measuring |E*| is the uniaxial compression test, which theoretically produces a uniform compressive stress in the testing specimen (AASHTO T342-11, previously TP62). During the test, a uniaxial sinusoidal compression load is applied to a 100 mm diameter and 150 mm tall cored, cylindrical specimen with a continuous haversine wave form under a strain controlled mode. The test is performed over a range of loading frequencies (25, 20, 10, 5, 2, 1, 0.5, and 0.1 Hz) and four temperatures (4.4, 21.1, 37.8, and 54°C). Dynamic modulus is calculated according to Eq. 2.2.

Dynamic modulus can also be measured using the indirect tensile (IDT) test. The analytical solution to calculating |E*| under IDT mode was proposed by Kim et al. (2004). The IDT testing method was also used by Oscarsson (2011). A great advantage to using an IDT test is that |E*| can be directly measured on field cores. Tran and Hall (2006) recommend using four affixed measurement instruments (such as LVDT) and two replicate specimens for E* testing. During the uniaxial compression tests, confining pressure can be applied to specimens. Sotil et al. (2004) found that unconfined and confined |E*| tests showed a linear relationship with the applied bulk stress and were almost parallel regardless of the confinement level. Based on this observation, a reduced confined |E*| test protocol that only required one (or two) confined test(s) was proposed.

Flow Time (F_T) and Flow Number (F_N)

Typically, flow tests are performed by applying a uniaxial compressive load to a 100 mm (4 in.) diameter, 150 mm (6 in.) tall cored, cylindrical specimen at a temperature of 54°C. For F_T testing, static compressive load is applied for a maximum of 10,000 seconds or until a deformation of 50,000 microstrain is reached. For F_N testing, the compressive load is applied in haversine form with a loading time of 0.1 seconds and a rest duration of 0.9 seconds for a maximum of 10,000 cycles or until a deformation of 50,000 microstrain is reached. The F_N and F_T tests can also be performed in confined conditions, and findings have shown that the rate of permanent deformation obtained from confined repeated load tests best simulates the rate of deformation that occurs in the field (Kaloush and Witczak, 2002). A study was performed to develop guidelines for the selection of the equivalent deviator pulse characteristics used for F_N testing that best simulates the conditions encountered in pavement under traffic loads (Hajj et al., 2010). Prediction equations for estimating anticipated deviator pulse duration as a function of pavement temperature and vehicle speed were developed. In addition, ranges for the amplitude of the triaxial deviator and confinement stresses as a function of pavement stiffness properties and traffic speeds were provided.

2.4 Evaluation and Influencing Factors

Dynamic Modulus ($|E^*|$**)**

Many states have been using SPTs to evaluate their HMA mixtures in determining if this technology is ready for implementation by owners/agencies. Pellinen (2001) evaluated a total of thirty mixtures from MnRoad (Minnesota), ALF (Virginia), and WesTrack (Nevada) test sites to demonstrate that $|E^*|$ (stiffness) could be used as a performance indicator to complement the Superpave volumetric mix design system. Studies showed that $|E^*|$ testing results correlate well with rutting in field pavements, and $|E^*|$ appears to have potential as a simple performance test for fatigue cracking (Witczak et al., 2002c; Zhou and Scullion, 2003; Bhasin et al., 2005; Mohammad et al., 2005; Apeagyei, 2011). Also mentioned was that caution must be taken in interpreting the rut susceptibility of mixes based on the E* parameters, especially when evaluating mixtures containing polymer-modified asphalts (Bhasin et al., 2005). Loulizi et al. (2006) conducted a comparison of resilient modulus (M_R) and $|E^*|$ of HMA as material properties for flexible pavement design. Their results showed that the $|E^*|$ test provides a better characterization of HMA than the M_R test because it provides full characterization of the mix over temperature and loading frequencies.

Dynamic modulus was also used to evaluate the moisture susceptibility of HMA by comparing the $|E^*|$ of specimens before and after moisture conditioning (Solaimanian et al., 2006; Nadkarni et al., 2009; Bausano and Williams, 2009). The results indicated that $|E^*|$ can be used to discriminate between good and poor performance in terms of resistance to stripping and moisture susceptibility. The advantages of using $|E^*|$ rather than the traditional indirect tensile strength ratio are that the test can be performed on the same specimen, and the effects of hydraulic loading developed by pore pressure in the mixture are simulated during the test.

It has been reported that traffic level, nominal maximum aggregate size, and air void are significant factors influencing the E* of HMA (Mohammad et al., 2005; Mohammad et al., 2006; Obulareddy, 2006; Williams et al., 2007; Tashman and Elangovan, 2008). Dynamic modulus increases as traffic levels increase and air voids decrease. Binder content has a greater impact on E* than aggregate angularity. Increasing asphalt binder content by 0.3% would lead to increasing the $|E^*|$ at intermediate and high temperature. Similar observations were also reported by Kim and King (2005), who reported that the binder variables (i.e., the source, performance grade and content) have a much more significant effect on $|E^*|$ than the aggregate variables. Dynamic modulus is also affected by the overall density of testing specimens. It was found that an increase in 1.5% density can increase $|E^*|$ by 15% (Blankenship and Anderson, 2010).

Within Alaska, Ahmed (2007) used the GLWT and SPTs to examine the effect of optimized mix design on the improvement of rutting resistance of Anchorage HMA mixtures. Liu and Connor (2008) compared results of $|E^*|$ and F_N using the simple performance tester for five HMA mixtures, aimed at providing economic and effective solutions to address rutting

problems occurring at the Barrow airport. Simple performance tests were also used to evaluate the performance of warm mix asphalt for Alaskan conditions (Liu et al., 2011; Liu and Li, 2012); however, no systematic study has been done to obtain a catalog of SPTs data and correlations between SPTs and HMA rutting performance for typical Alaskan HMA mixtures.

Flow Time and Flow Number

Flow number (F_N) is effective in detecting the difference between mixtures, and accumulated microstrain at F_N was more effective in comparing the quality of specimens within a specific mixture (Zhou and Scullion, 2003; Mohammad et al., 2005; Mohammad et al., 2006; Williams et al., 2007; Bonaquist, 2009). The F_N test identified the effects of both asphalt cement and aggregate in the rutting resistance of mixtures (Huang et al., 2008). Flow number and Hamburg test results correlated fairly well (Bhasin et al., 2005; Mohammad et al., 2005; Mohammad et al., 2006). Archilla and Diaz (2008) suggested that besides |E*|, either permanent deformation model parameters or permanent deformation tests, such as the F_N test, should be included in modeling the permanent deformation of asphalt pavement in the MEPDG. The F_N test can be used to investigate moisture susceptibility of HMA by comparing results obtained on specimens in saturated conditions and unconditioned specimens in a dry test environment (Bausano et al., 2006).

The F_N test was found to be sensitive to binder stiffness, mixture stiffness, mixture volumetric properties, aggregate gradation, traffic level, NMAS, gradation type (dense vs. open), and amount of recycled asphalt pavement (RAP) (Williams et al., 2007; Apeagyei and Diefenderfer, 2011). Higher traffic level and lower air void content lead to greater F_N of HMA. It was found that specimens with higher density yielded improved F_N (Mogawer et al., 2011), and an increase in 1.5% density can increase F_N by 34% (Blankenship and Anderson, 2010).

2.5 Modeling

At both federal and states levels, efforts have been made to develop the |E*| database and predictive models. Of all published predictive models, five that have been used and discussed most were selected and reviewed: (1) the original Witczak model, (2) the modified Witczak model, (3) the Hirsch model, (4) the Al-Khateeb model, and (5) the artificial neural networks model (Fonseca and Witczak, 1996; ARA, 2004; Bari and Witczak, 2006; Christensen et al., 2003; Al-Khateeb et al., 2006; Ceylan et al., 2008; Kim et al., 2011). Hot mix asphalt volumetric properties and binder properties were included in these models to predict |E*|. The newly develop artificial neural networks model also allows users to calculate |E*| based on M_R results obtained from an IDT test.

1. Witczak |E| predictive model (Fonseca and Witczak 1996)*

The original Witczak |E*| predictive model was developed based on 1430 test data points from 149 un-aged laboratory-blended HMA mixtures that contained only conventional binders (Fonseca and Witczak, 1996). During the NCHRP 1-37A project, the model was revised based

on nonlinear regression analysis and a database that contained 2750 data points (ARA, 2004). The model is expressed by Eq. 2.3. The input parameters of this model contain the percentage passing #200, retained on #4, retained on ⅜″, and retained on ¾″ sieves, HMA volumetric properties, loading frequency, and binder viscosity.

$$\log_{10}|E*| = -1.249937 + 0.02923 p_{200} - 0.001767(p_{200})^2 - 0.002841 p_4 - 0.05809 V_a$$

$$-0.0082208 \frac{V_{veff}}{V_{veff} + V_a} + \frac{3.871977 - 0.0021 p_4 + 0.003958 p_{3/8} - 0.000017(p_{3/8})^2 + 0.00547 p_{3/4}}{1 + \exp(-0.603313 - 0.31335 \log_{10} f - 0.393532 \log_{10} \eta)}$$

(2.3)

where

p_{200}	= percentage of aggregate passing #200 sieve,
p_4	= percentage of aggregate retained on #4 sieve,
$p_{⅜}$	= percentage of aggregate retained on ⅜″ (9.56 mm) sieve,
$p_{¾}$	= percentage of aggregate retained on ¾″ (19.01 mm) sieve,
V_a	= percentage of air voids (by volume of mix),
V_{beff}	= percentage of effective asphalt content (by volume of mix),
f	= loading frequency (hertz), and
η	= binder viscosity at temperature of interest (10^6 P = 10^5 Pas).

By comparing the predicted value and laboratory measured E*, Mohammad et al. (2005) and Dongre et al. (2005) found that the Witczak equation predicted E* of mixture properties with reasonable reliability. The predicted values were higher than measured values at high temperatures and low loading frequencies (Azari et al., 2007; Gedafa et al., 2009). The original Witczak predictive equation is based on regression analysis. Therefore, extrapolation beyond the calibration database should be restricted. It has also been pointed out that the model relies on other models to translate the currently used |G*| measurement into binder viscosity (Bari, 2005). Other researchers also noted the need for improved sensitivity to volumetrics, such as the percentage of voids in the mineral aggregate (VMA), the percentage of voids filled with asphalt (VFA), asphalt concrete (AC) percentage, and air void (Va) (Dongre et al., 2005).

2. Modified Witczak |E| predictive model (|G*| based) (Bari and Witczak, 2006)*

Instead of binder viscosity parameter η, the modified Witczak model uses binder dynamic shear modulus |G*| (Eq. 2.4), which is used in the current PG binder grade system. A larger database (346 mixtures with 7400 data points) was used for regression data analysis, and the correlation between measured and predicted |E*| improved to 0.87 (R^2). However, the modified model does not significantly improve over-prediction at higher temperature and lower loading frequency. The binder phase angle is predicted using an empirical equation ($R^2 = 0.83$). This equation is one of two options for Level 3 analysis in the most current MEPDG program.

$$\log_{10}|E*| = -0.349 + 0.754|G*|_b^{-0.0052} \left(\begin{array}{l} 6.65 - 0.032p_{200} + 0.0027(p_{200})^2 + 0.011p_4 - 0.0001(p_4)^2 \\ + 0.0006p_{3/8} - 0.00014(p_{3/8})^2 - 0.08V_a - 1.06\dfrac{V_{beff}}{V_{veff} + V_a} \end{array} \right)$$

$$+ \frac{2.558 + 0.032V_a + 0.713\dfrac{V_{beff}}{V_{veff} + V_a} + 0.0124p_{3/8} - 0.0001(p_{3/8})^2 + 0.0098p_{3/4}}{1 + \exp(-0.7814 - 0.5785\log_{10}|G*|_b - 0.8834\log_{10}\delta_b)}$$

$$(2.4)$$

where

$|G*|_b$ = dynamic shear modulus of rolling thin film oven (RTFO)-aged asphalt binder (pounds per square inch), and

δ_b = binder phase angle associated with $|G*|_b$ (degrees).

3. Hirsch model (Christensen et al. 2003)

Based on the parallel model of mixtures law, Christensen et al. (2003) examined four different models and chose the model that incorporated binder modulus, VMA, and VFA as the final model listed in Eq. 2.5 to Eq. 2.7

$$|E*|_m = P_c\left[4{,}200{,}000\left(1 - \frac{VMA}{100}\right) + 3|G*|_b\left(\frac{VFA \times VMA}{10{,}000}\right)\right] + \frac{1 - P_c}{\dfrac{1 - VMA/100}{4{,}200{,}000} + \dfrac{VMA}{3|G*|_b(VFA)}} \qquad (2.5)$$

$$\phi = -21(\log P_c)^2 - 55\log P_c \qquad (2.6)$$

$$P_c = \frac{(20 + 3|G*|_b(VFA)/(VMA))^{0.58}}{650 + (3|G*|_b(VFA)/VMA))^{0.58}} \qquad (2.7)$$

where

$|E*|_m$ = dynamic modulus of HMA (pounds per square inch),

φ = phase angle of HMA, and

Pc = aggregate contact volume.

This model provides accurate results in the simplest form; it provides a reasonable prediction (Dongre et al., 2005) and shows slightly better statistical predictions than either of the Witczak models (Mohammad et al., 2005). One advantage of this model is the empirical phase angle equation, which can be used to convert |E*| to the relaxation modulus or creep compliance.

13

However, the predicted values were also greater than measured values at low loading frequencies and high temperature (Mohammad et al., 2005).

4. Al-Khateeb model (Al-Khateeb et al., 2006)

The Al-Khateeb model was also developed based on the law of mixtures for composite materials, as shown in Eq. 2.8 In this model, the different material phases (aggregate, asphalt binder, and air) are considered to exist in parallel. The model could be viewed as a simpler interpretation of the Hirsch model. Compared with the Hirsch model, its advantage is accuracy at high temperature and low loading frequency. However, this model does not include factors such as air void and binder content, which are considered very important in determining the |E*| of HMA.

$$|E*|_m = 3\left(\frac{100 - VMA}{100}\right)\left(\frac{\left(90 + 10,000(|G*|_b / VMA)\right)^{0.66}}{1,100 + \left(900(|G*|_b / VMA)\right)^{0.66}}\right)|G*|_g \tag{2.8}$$

where
$|G*|_g$ = dynamic shear modulus of asphalt binder at the glassy state (assumed to be 145,000 psi (999,050 kPa).

5. Artificial Neural Networks (ANN) based model (Ceylan et al., 2008; Kim et al., 2011)

Other than the traditional regression approach, recent studies developed new |E*| predictive models based on artificial neural networks (ANNs). The primary advantage of this approach over statistical regression is that the functional form of the relationship is not needed before the analysis. Considering that many variables affect |E*| values and their interactions, the ANN technique captures complicated nonlinear relationships between |E*| and other mixture variables better than regression analysis.

The ANN model contains a mapping ANN architecture (Figure 2.2) and is based on supervised learning. In the developed network, the learning method used is a feed forward backpropagation, which is one of the best known types of ANN models. By multiplying input parameters and weight factors such as W_{ij} or Q_{ij}, the notes at hidden layers are obtained. Then, based on the output function, the predicted value and the error between predicted and actual output value are calculated. Based on the error, weight factors would be updated until the system achieves required accuracy. The sigmoidal function was chosen as the transfer function. The actual forms of sigmoidal function and ANN architecture used by different research teams are different.
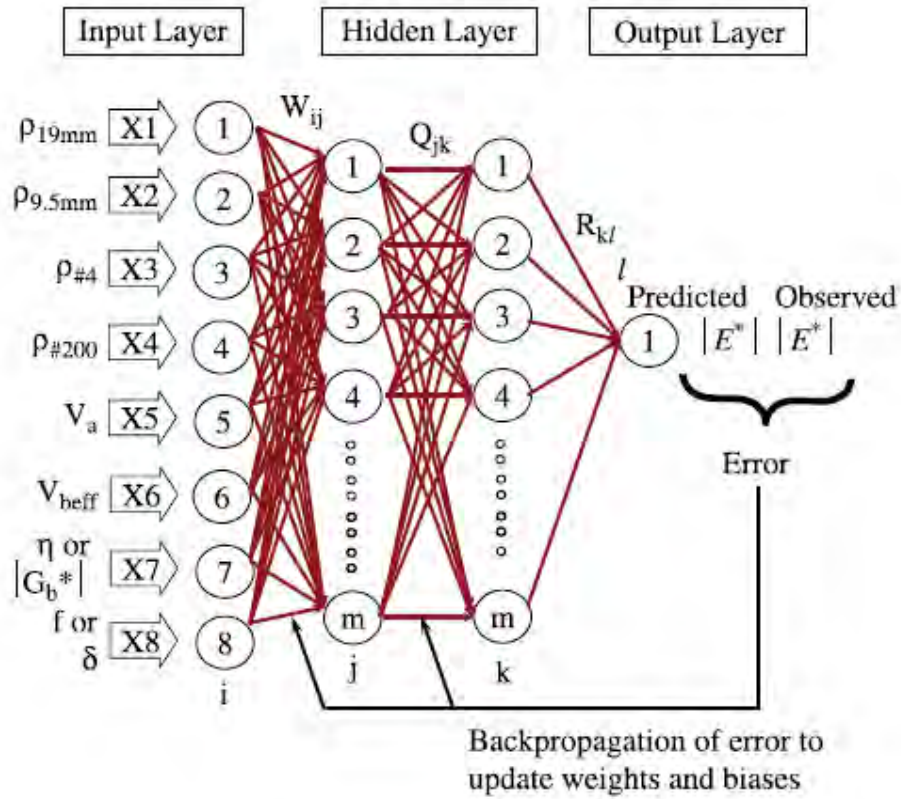
Figure 2.2 ANN architecture (Ceylan et al., 2008)

$$f(I) = \frac{2}{1 + \exp(-2I)} - 1 \tag{2.9}$$

where

$f(I)$ = sigmoidal function.

     The overall ANN models developed by Kim et al. (2011) contained five sub-models (Figure 2.3). Based on the available information, the user could choose the appropriate predictive model. Comparisons between the ANN models and the closed-form models showed that, overall, the ANN models provide better predictability than do any of the closed-form solutions and are more sensitive to input parameters. However, an ANN model could contain more than hundreds of factors (coefficients), and the structure of function would be hard to explain.
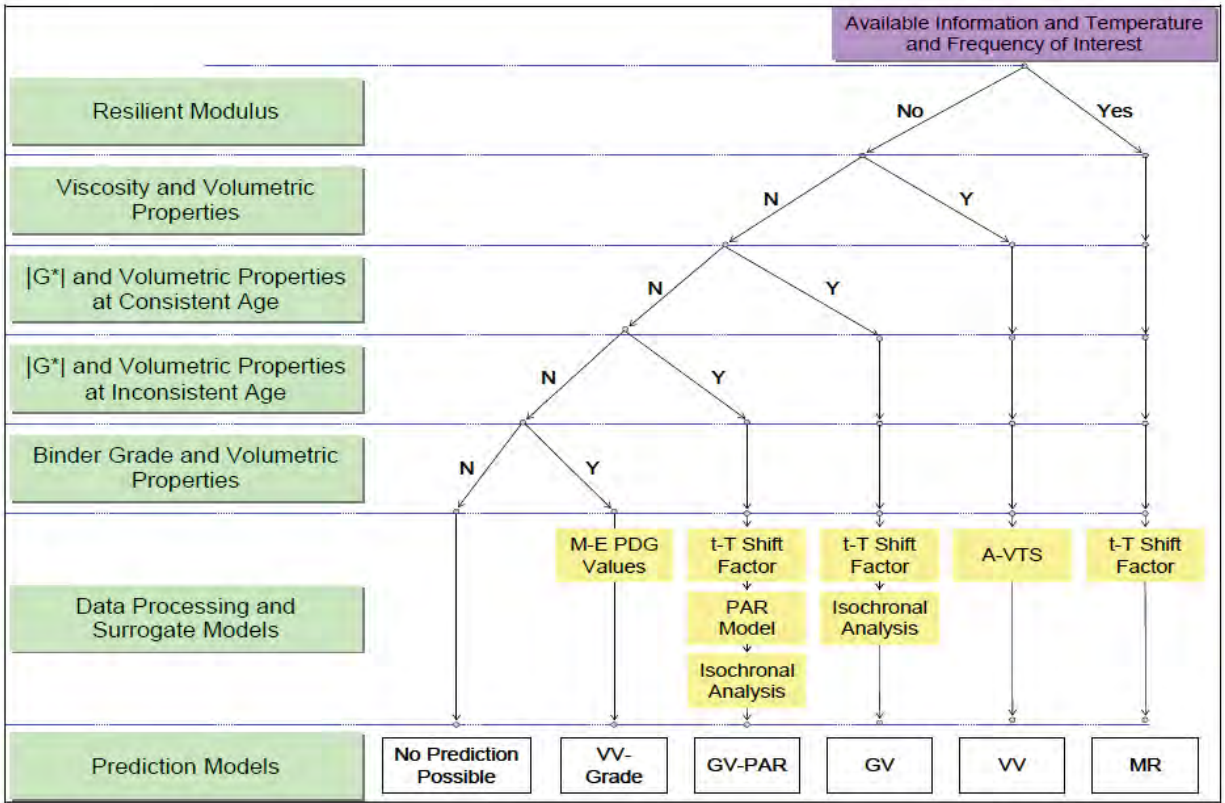
Figure 2.3 Modulus prediction model decision tree (Kim et al., 2011)

CHAPTER 3 EXPERIMENTAL DESIGN

This chapter describes the experimental details of this research, including mix collection, specimen fabrication, and laboratory tests. The main objectives of these tests were to establish a property database of typical HMA (i.e., $|E^*|$, F_N, F_T, and rutting depth) used in Alaska and to assess the applicability of currently used predictive models of $|E^*|$.

3.1 Material Collection

Loose asphalt mixtures were collected from 21 projects in 3 regions of ADOT&PF, including 10 from the Northern region, 9 from the Central region, and 2 from the Southeast region. Figure 3.1 shows the 21 project locations. All the samples were collected by ADOT&PF staff during summer time from year 2009 to 2010 and stored in testing facilities at UAF.
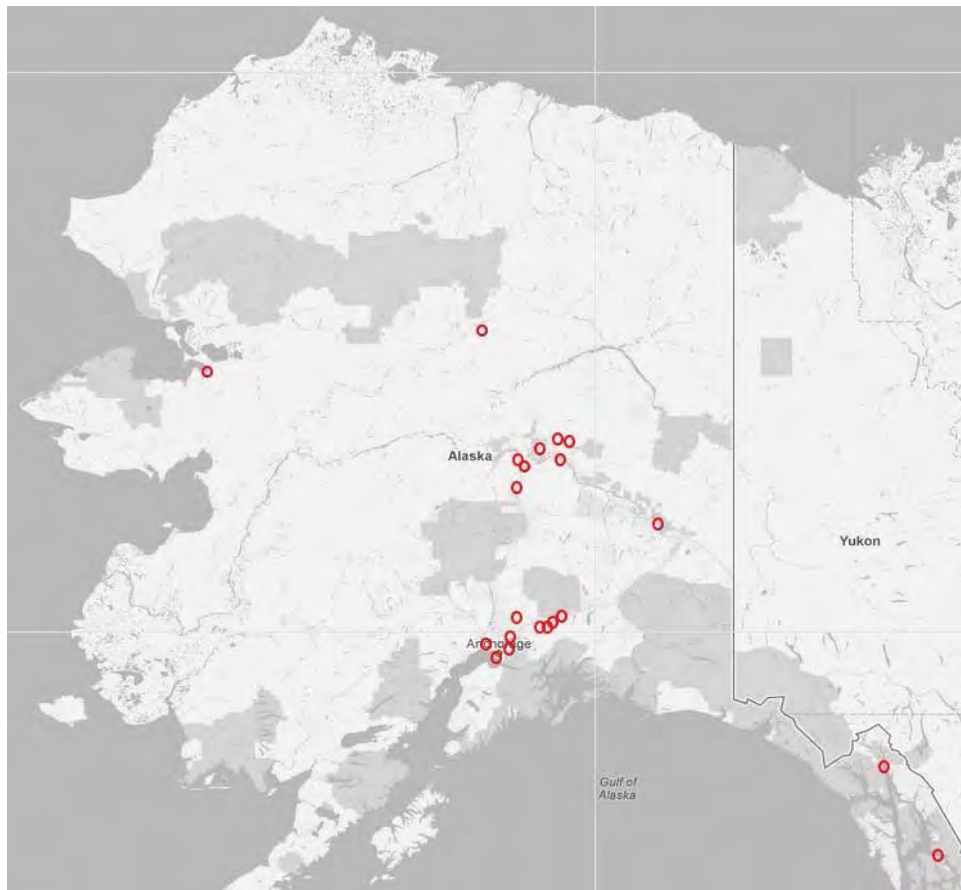
Figure 3.1 Project locations

These collected mixes covered a wide range of HMA mixtures used in Alaska. Table 3.1 is a summary of project information, and Table 3.2 shows the job mix formula (JMF) details including binder grade and content, volumetrics, and gradation. Among the 21 mixes, 4 were designed by the Superpave method and 17 were designed by the Marshall method. Crumb rubber

modified mixtures were used in 2 projects (East Dowling Road and Glenn Highway-Hiland to Eklutna Resurfacing projects). Abbreviations of each project, used consistently throughout this report, are listed in Table 3.1.

Table 3.1 Summary of project information

No.	Project	Abbreviation	Region	Mix Design Method	Other
1	AIA runway 7R_25L Rehabilitation	AIA	Central	SuperPave	
2	Chena Hot Springs Rd MP 24-56	CH	Northern	Marshall	
3	Chena Hot Springs	CH2	Northern	Marshall	
4	Fairbanks Cowles Street Upgrade	CO	Northern	Marshall	
5	East Dowling Road Extension and Recon.	D	Central	Marshall	Crumb Rubber HMA
6	Dalton Hwy. MP 175–197 Rehabilitation	DH	Northern	Marshall	
7	FIA Runway 1L_19R stage 3 (52-34)	FIA	Northern	Marshall	
8	FIA Runway 1L_19R stage 3 (64-34)	FIA64	Northern	Marshall	
9	Glenn Hwy MP 92-97 Cascade to Hicks Creek	GCH	Central	Marshall	
10	Glenn Hwy: Gambell to airport MP 0–1.5	GGB	Central	SuperPave	
11	Glenn Hwy: Hiland to Eklutna Resurfacing	GH	Central	Marshall	Crumb Rubber HMA
12	Glenn Hwy MP 34–42, Parks to Palmer Resurfacing	GPP	Central	SuperPave	
13	HNS Ferry Terminal to Union Street	HNS	Southeast	Marshall	
14	Minnesota Dr. Resurfacing: International Airport Rd to 13th	M	Central	SuperPave	
15	Parks Hwy MP 287–305 Rehabilitation	N	Northern	Marshall	
16	Richardson Hwy North Pole Interchange	NPI	Northern	Marshall	
17	Old Glenn Hwy: MP 11.5–18	OGP	Central	Marshall	
18	PSG Mitkof Hwy-Scow Bay to Crystal Lake Hatchery	PSG	Southeast	Marshall	
19	Palmer/Wasilla	PW	Central	Marshall	
20	Alaska Hwy MP 1267–1314	TOK	Northern	Marshall	
21	Unalakleet Airport Paving	UNK	Northern	Marshall	

As shown in Table 3.2, the most commonly used binders among the projects evaluated were PG 52-28 (seven projects) and PG 64-34 (nine projects). Among these binders, the highest temperature end of PG was 64°C; the lowest end of PG was -40°C for the Dalton Highway project (DH). The binder contents were between 5.0% and 6.0% except for two crumb rubber

modified mixes, which had binder contents of 7.0% for the East Dowling Road (D) project and 6.7% for the Glenn Highway Hiland to Eklutna project (GH). The design air voids were between 3.0% and 4.1%. The exact design air voids for the FIA and FIA64 paving projects were not specified in the JMF. Instead, a range of 2.8% to 4.2% was listed in the JMF. For specimen fabrication and evaluation purposes, an averaged VTM value of 3.5% was used, as shown in Table 3.2. The VMAs ranged from 13.6% to 17.0% except for the crumb rubber modified HMA, which had VMAs of about 22%. Collected mixtures had the same nominal maximum aggregate size (NMAS) of ½″. The gradations are illustrated in Figure 3.2, where it can be seen that the gradation of most material was near the maximum density line. The crumb rubber modified HMA had a coarser gradation; for example, the East Dowling Road project (D) had a percentage passing of 54% at ⅜″ sieve size, which was the lowest among all collected HMAs.

Binder rheological testing results were also obtained from ADOT&PF. The binder rheological properties are essential inputs for the |E*| predictive models. The collected information included viscosity at 135°C measured by rotational viscometer, dynamic shear modulus and phase angle measured by a dynamic shear rheometer (DSR), flexural creep stiffness and *m*-value measured by the bending beam rheometer (BBR), and softening point. The testing temperatures of DSR and BBR tests were determined based on the PG of each binder according to the AASHTO M 320. However, not all rheological properties were available. The softening points were only obtained from FIA64 and NPI projects. The collected rheological properties are summarized in Table 3.3.

Table 3.2 Summary of mix properties from JMFs

Mix	Binder		Volumetrics			Gradation, % passing									Dust/Asphalt Ratio
	PG	Binder Content (%)	VTM (%)	VFA (%)	VMA (%)	½"	⅜"	#4	#8	#16	#30	#50	#100	#200	
AIA	64-34	5.2	3.6	76	14.6	87	76	52	36	26	19	12	9	6	1.3
CH	52-28	5.4	3.9	74	15.2	89	78	53	37	28	21	15	11	6.8	1.4
CH2	52-28	5.5	4.1	74	15.5	90	75	50	32	23	19	14	8	5.9	1.2
CO	52-28	5.2	4.0	73	15	90	79	52	38	27	20	16	9	6.3	1.4
D	64-34	7.0	3.0	86	22.2	76	54	40	27	19	14	10	7	5.5	0.9
DH	52-40	4.9	3.2	77	13.9	87	77	51	34	24	17	11	8	6	1.4
FIA	52-34	5.0	3.5		14.0	90	79	51	35	24	18	12	9	5.8	
FIA64	64-34	5.1	3.5		13.0	90	79	51	35	24	18	12	9	5.8	
GCH	52-28	5.2	4.0	72	14.2	89	76	52	36	24	15	9	7	5.1	1.2
GGB	64-34	6.0	3.8	76	15.9	84	72	52	33	22	15	11	7	5	1.0
GH	64-34	6.7	3.8	82	21.7	86	70	42	28	19	14	10	7	5.4	0.9
GPP	64-34	5.5	4.0	76	15.4	87	72	54	37	25	17	10	7	4.8	1.0
HNS	58-28	5.0	3.0	78	14.5	77	62	42	29	21	15	11	8	5.5	1.3
M	64-34	5.0	3.8	73	14.0	84	69	44	31	22	15	10	7	5	1.2
N	52-34	5.0	3.5	75	14.4	86	73	52	37	27	20	13	9	5.8	1.3
NPI	64-34	5.4	4.0	74	16.0	87	74	52	39	30	25	19	8	3.5	0.7
OGP	52-28	5.3	3.8	74	14.2	88	74	55	39	25	17	12	8	5.2	1.2
PSG	58-28	6.0	3.8	78	17.0	85	69	41	26	17	12	9	7	5.5	1.0
PW	64-34	5.8	4.0	73	15.6	90	82	60	43	31	20	12	8	5.2	1.1
TOK	52-28	5.0	3.9	74.5	15.4	84	72	48	34	26	21	15	6	3.6	0.8
UNK	52-28	5.2	3.5		13.6	89	76	50	34	23	17	12	9	6.7	
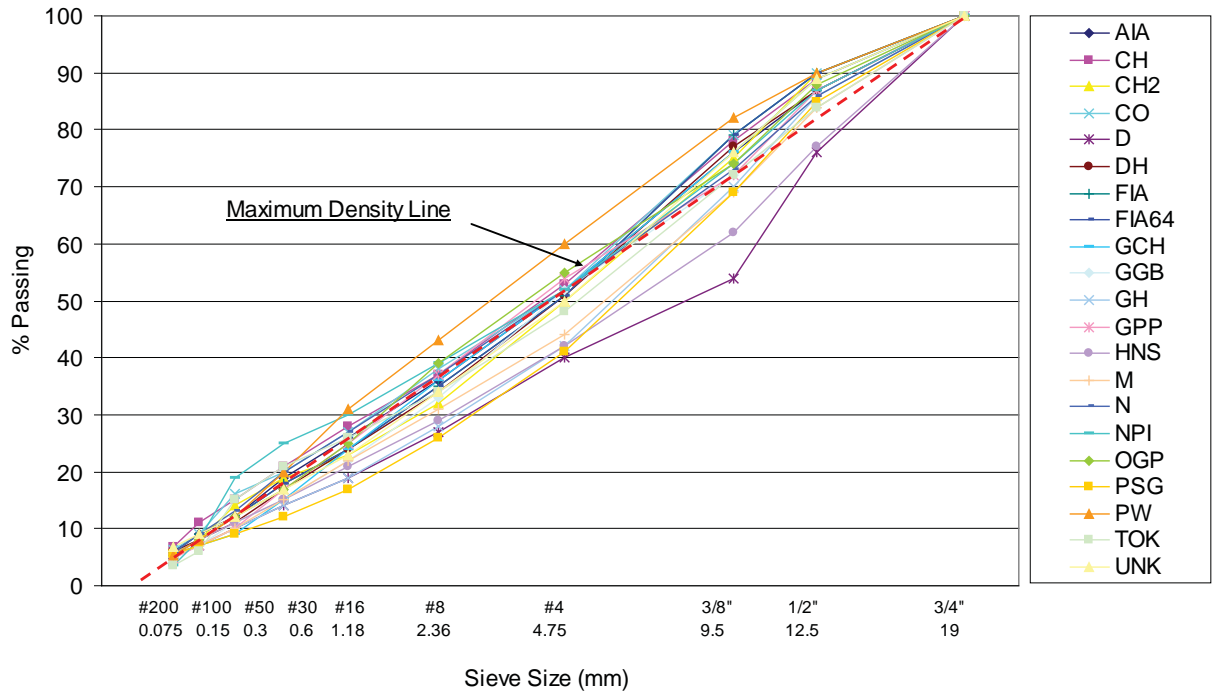
Figure 3.2 Summary of gradations

Table 3.3 Summary of binder rheology testing results

No.	Mix	PG	Viscosity @135°C (Pa·s)	DSR (Original)		DSR (RTFO)		DSR (PAV)		BBR		Softening point (°F)
				G*	Phase Angle	G*	Phase Angle	G*	Phase Angle	S(t)	m	
1	AIA	64-34	2.002	1.47	45.7	3.73	51.5	n/a	n/a	n/a	n/a	n/a
2	CH	52-28	0.196	1.68	87.9	3.14	86.5	4612.50	55.6	196.8	0.35625	n/a
3	CH2	52-28	0.196	1.68	87.9	3.14	86.5	4612.50	55.6	196.8	0.35625	n/a
4	CO	52-28	0.225	1.60	84.9	3.10	83.1	3550.00	57.1	173.0	0.37600	n/a
5	D	64-34	1.840	1.55	43.4	1.68	50.2	n/a	n/a	n/a	n/a	n/a
6	DH	52-40	0.670	1.84	55.2	2.82	53.3	916.92	59.6	170.5	0.62692	n/a
7	FIA	52-34	0.469	2.33	69.8	4.24	68.7	3964.00	53.6	259.8	0.33150	n/a
8	FIA64	64-34	0.734	1.68	55.5	2.75	58.6	2162.65	57.6	225.5	0.34587	176.7
9	GCH	52-28	0.173	1.36	88.1	2.56	86.9	n/a	n/a	n/a	n/a	n/a
10	GGB	64-34	1.162	1.45	60.2	2.08	63.1	n/a	n/a	n/a	n/a	n/a
11	GH	64-34	1.591	1.38	46.6	1.80	52.6	n/a	n/a	n/a	n/a	n/a
12	GPP	64-34	1.543	1.35	56.9	1.89	62.3	n/a	n/a	n/a	n/a	n/a
13	HNS	58-28	0.440	1.72 (G* sinδ)		3.54 (G* sinδ)		3374.00 (G* sinδ)		210.2	0.31689	n/a
14	M	64-34	1.272	1.49	59.6	2.15	63.4	n/a	n/a	n/a	n/a	n/a
15	N	52-34	0.528	2.29	67.8	3.79	67.5	2425.00	59.3	244.7	0.35250	n/a
16	NPI	64-34	1.204	1.51	46.8	2.13	50.1	1176.67	59.6	207.8	0.34750	180.2
17	OGP	52-28	0.174	1.38	88.1	2.59	86.9	n/a	n/a	n/a	n/a	n/a
18	PSG	58-29	0.433	2.00	76.0	4.13	73.2	3355.60	(G* sinδ)	226.0	0.30100	n/a
19	PW	64-34	1.584	1.33	47.6	1.92	52.9	n/a	n/a	n/a	n/a	n/a
20	TOK	52-28	0.196	1.61	88.4	3.14	86.7	4692.50	63.5	197.3	0.36525	n/a
21	UNK	52-28	0.198	1.63	87.6	3.43	85.6	4400.00	52.6	186.0	0.35025	n/a

3.2 Dynamic Modulus Test

The |E*| and phase angle of compacted HMA specimens were determined over a range of temperatures and loading frequencies. The testing results were used to develop a database of |E*| for typical HMAs used in Alaska and to evaluate the appropriateness of currently used predictive models for local application.

3.2.1 Testing Apparatus

Dynamic modulus tests were performed using the AMPT, which is a fully integrated package specifically designed for |E*|, F_N, and F_T tests. The AMPT is a computer-controlled hydraulic testing system capable of applying cyclic/static loading over a range of temperatures and frequencies/time on the compacted HMA specimen. The machine consists of a triaxial cell, an environmental chamber, a hydraulic actuator and pump, a temperature-control unit, and a data-acquisition system (Figure 3.3). The triaxial test cell is mounted on the top left of the unit.

For |E*| tests, the deformation is measured by three LVDTs attached on the side of the specimens. An external compressed air supply is required to apply confining pressure (in this study, the confining pressure was not used for |E*| tests) and to raise and lower the triaxial cell. The integrated data-acquisition and analysis software automatically process measurements and calculate |E*| at each loading frequency.

Figure 3.3 Setup of the AMPT.

3.2.2 Specimen Fabrication

The |E*| tests were performed on specimens 100 mm in diameter and 150 mm in height. Collected loose mixtures were re-heated to 135°C. The mix was then put into the mold and compacted in the SGC. The specimens were compacted to a height of about 180 mm, and trimmed and cored to the required size. Figure 3.4 shows the cutting and coring machine that was used. Figure 3.5 shows the final specimen, cut and cored from a SGC compacted raw specimen.

Figure 3.4 Cutting and coring machine

Figure 3.5 Final specimen after cutting and coring

The target air voids of testing specimens were the design air voids of each project, generally about 4%. Trial compactions were conducted for each mixture to determine the number of gyrations at which the target air voids could be achieved. A loose mixture of 7200 g was used for trial compaction. This amount was estimated based on design air voids, maximum specific gravity of loose mixture, and raw specimen size (150 mm in diameter and 180 mm in height). The weight of loose mixture for the final compaction was corrected after the number of gyrations was determined. The trial compaction was performed in height control mode to reach a 179 mm height. During compaction, the number of gyrations and the height of specimen were recorded.

The height of specimen was used to estimate the bulk specific gravity of compacted specimens after each increment in number of gyrations (Eq. 3.1). After trial compaction, the specimen was cut and cored into the required size (100 mm in diameter and 150 mm in height). The bulk specific gravity of the specimen was measured and used to calculate the correction factor (Eq. 3.2). The estimated bulk specific gravity was corrected based on the obtained correction factor (Eq. 3.3). Figure 3.6 illustrates the estimated and corrected bulk specific gravity during compaction, using a mixture from the Chena Hot Springs Rd. MP 24–56 (CH) project as an example.

Finally, the air void was estimated using Eq. 3.4 and plotted versus number of gyrations, as shown in Figure 3.7. The number of gyrations was determined based on the design air void. In this example, the target air void was 3.9% and the corresponding number of gyrations was determined to be 27.

$$G_{mb,Estimated} = \frac{\frac{4W}{D^2 \pi H}}{\gamma_w} \tag{3.1}$$

$$F = \frac{G_{mb,Measured}}{G_{mb,Estimated,F}} \tag{3.2}$$

$$G_{mb,Corrected} = F \cdot G_{mb,Estimated} \tag{3.3}$$

$$VTM_{estimated} = (1 - \frac{G_{mb,Corrected}}{G_{mm}}) \cdot 100 \tag{3.4}$$

where,

$G_{mb.estimated}$	estimated bulk specific gravity,
$G_{mb.measured}$	measured bulk specific gravity,
$G_{mb.corrected}$	corrected bulk specific gravity,
W	weight of specimen, g,
D	diameter of specimen, 15 cm,
H	height of specimen, cm,
γ_W	density of water, g/cm^3,
F	correction factor
$VTM_{estimated}$	estimated air void, %, and
G_{mm}	maximum specific gravity of loose HMA, g/cm^3.
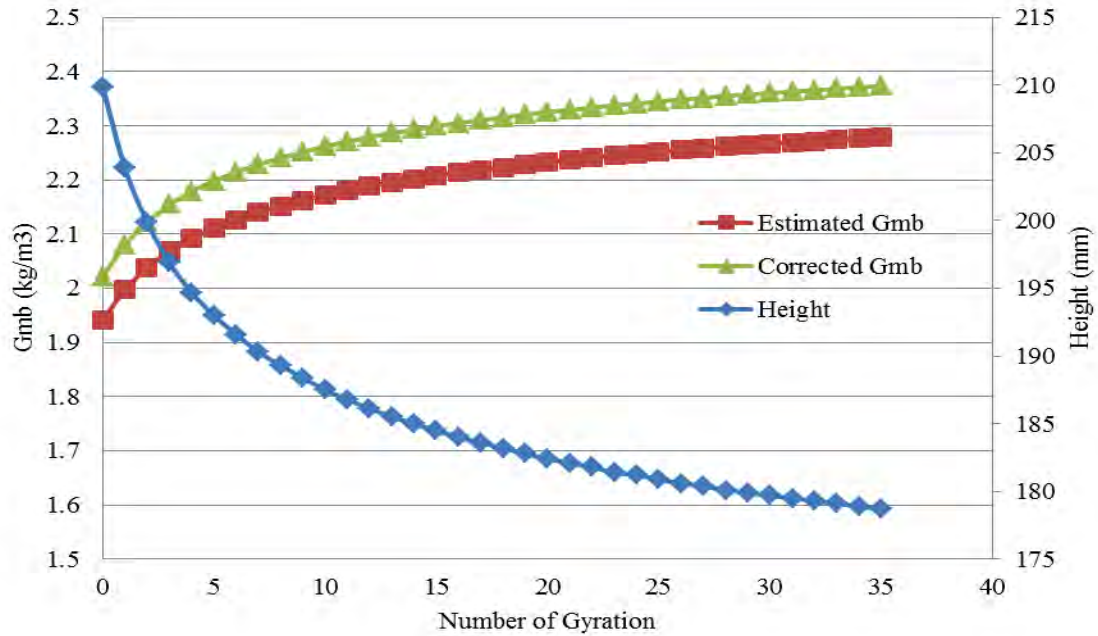
Figure 3.6 Estimated and corrected G_{mb} during the compaction process
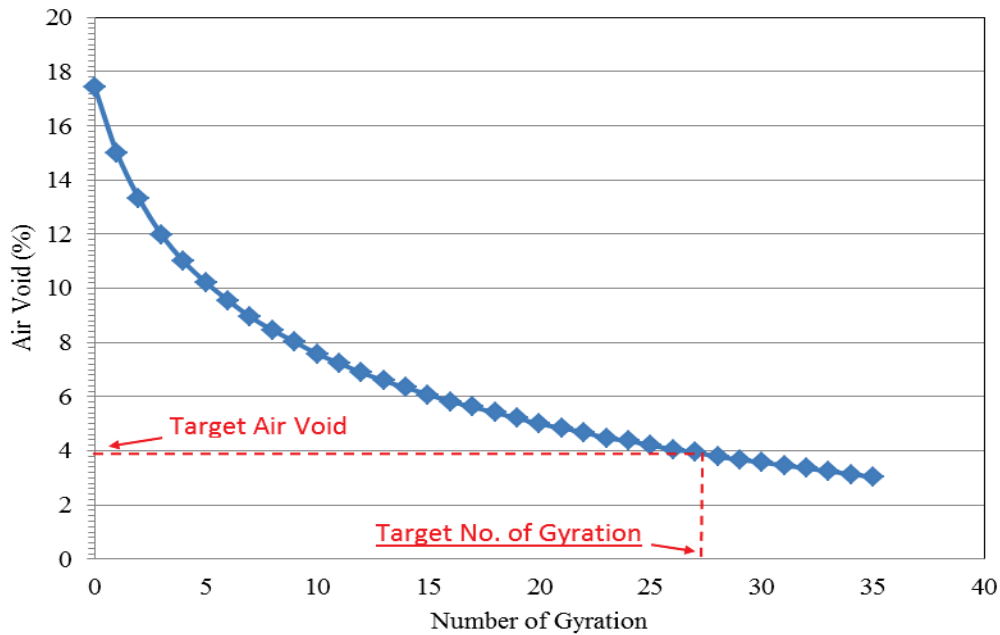
Figure 3.7 Determined target number of gyrations

The average air voids of HMA specimens are listed in Table 3.4, which shows that almost all air voids were within the range of ±0.4% of the target design air voids.

The fabrication of crumb rubber modified HMA was not successful. Due to the strong expansion caused by crumb rubber, the specimens collapsed immediately after extruding from the mold.

Table 3.4 Air voids of testing specimens

Mix	Design VTM (%)	Measured VTM (%)
AIA	3.6	2.7
CH	3.9	3.9
CH2	4.1	4.2
CO	4.0	3.9
D	3.0	n/a
DH	3.2	3.1
FIA	3.5	3.2
FIA64	3.5	3.6
GCH	4.0	3.8
GGB	3.8	3.9
GH	3.8	n/a
GPP	4.0	4.1
HNS	3.0	3.3
M	3.8	3.6
N	3.5	3.8
NPI	4.0	3.9
OGP	3.8	3.4
PSG	3.8	3.8
PW	4.0	3.9
TOK	3.9	3.9
UNK	3.5	3.6

3.2.3 |E*| Testing Procedure

The |E*| test was performed over eight loading frequencies (i.e., 25, 20, 10, 5, 2, 1, 0.5, and 0.1 Hz) and four temperatures (4.4, 21.1, 37.8, and 54°C) according to AASHTO T342-11 (2011).

Prior to testing, specimen diameter and height were measured and recorded. Three LVDT holding brackets were installed on the specimen before testing. Figure 3.8 shows the apparatus used to glue the mounting studs on the specimen, where the mounting racks were installed. The distance between two vertical mounting studs was 101.6 mm. The apparatus ensures the precision of LVDT installation.

Figure 3.8 LVDT attachment apparatus

The test was started at the lowest temperature (4°C / 40°F), followed by increasingly higher temperatures (21°C / 70°F, 37°C / 100°F and 54°C / 130°F), because less damage was induced at lower testing temperatures. The specimen was conditioned in a temperature chamber overnight (minimum 4 hours) for the test performed at 4°C. The conditioning time was reduced to 3, 2, and 1 hours for testing performed at 21°C, 37°C, and 54°C, respectively. Two hundred sinusoidal loading cycles were applied for each frequency. The integrated |E*| test software automatically collected measurements and calculated |E*|.

3.3 Flow Number (F_N) and Flow Time (F_T) Tests

Flow number and flow time tests were performed to evaluate the rutting resistance of HMA. The developed database of F_N and F_T was used to evaluate the correlation between flow tests and the APA-measured rutting depth.

3.3.1 Testing Apparatus

Flow number and flow time tests were performed using the AMPT, but without attached LVDTs. The integrated flow test software was used for testing process control, data acquisition, and calculation (Figure 3.9).
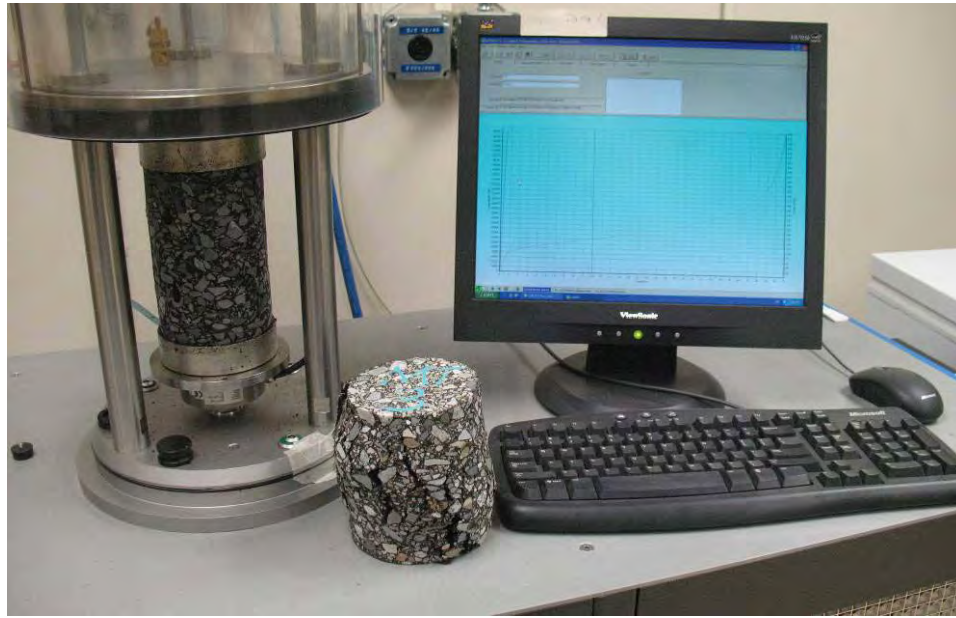
Figure 3.9 AMPT for flow test

3.3.2 Specimen Fabrication

The shape and size of the specimen used for F_N and F_T tests are same as the shape and size used for $|E^*|$. Thus, the specimen fabrication process was also the same. In addition, the F_N test was performed on the same specimen used for the $|E^*|$ test after the last loading sequence of the $|E^*|$ test at 54°C, because $|E^*|$ is considered a non-destructive test. The F_T test was performed using a new specimen.

3.3.3 F_N Procedure

During the F_N test, a repeated uniaxial compressive load is applied to a cored cylindrical specimen. The compressive load is applied in haversine form with a loading time of 0.1 seconds and a rest duration of 0.9 seconds, for a maximum of 10,000 cycles or until a deformation of 50,000 microstrain is reached. The specimens were tested at a temperature of 54°C. Permanent deformations are measured internally by the displacement of the load frame. Previous studies indicated that confined flow tests more closely match field conditions (Brown et al., 2009). In this study, confining pressure was applied for the Parks Highway (N) and the Anchorage International Airport paving projects (AIA). According to Roberts et al. (1996) and Bonaquist (2008), the confining pressure was selected to be 137 kPa (20 psi). However, specimens tested under confining pressures did not fail during the 10,000 cycles (second) of loading time, and the correct F_N and F_T could not be calculated. For the rest of the 17 mixes, confining pressure was not applied.

The F_T test is similar to the F_N test; however, instead of the repeated compressive load, a static compressive load is used. The loading process was terminated at a maximum of 10,000

29

seconds, or when a deformation of 50,000 microstrain was reached. Data acquisition and calculation were performed automatically by the integrated flow testing software. Figure 3.10 shows specimens before and after the flow test.

Figure 3.10 Specimens before and after the flow test

3.4 Rutting Test

Rutting is the permanent deformation of pavement along the wheel path; it can be defined as the accumulation of small amounts of unrecoverable strain resulting from applied wheel loads to the pavement. Rutting is usually caused by the consolidation or plastic flow, or both, of asphalt mixture under wheel loads (Brown et al., 2009). Rutting not only decreases the service life of pavement, but also creates a safety problem for motorists. Generally, rutting in excess of 0.25 in. (6 mm) is considered to be a hydroplaning safety hazard by state DOTs (Jacksona and Baldwina, 2000). The Long-term Pavement Performance (LTPP) manual suggests that rutting depths between 6 mm and 12 mm are considered moderate severity, and any rutting depth greater than 12 mm is considered high severity.

An asphalt pavement analyzer (APA) was used to evaluate the rutting susceptibility of the 21 HMAs and to develop a database of rutting depth to identify the most critical factors and their influencing potential. In addition, the correlation between rutting depth and F_N/F_T was investigated.

3.4.1 Testing Apparatus

Figure 3.11 shows the APA used to evaluate the rutting susceptibility of the mixtures. The original version of the APA was the Georgia Loaded Wheel Tester (GLWT), developed during the mid-1980s through a cooperative research study between the Georgia DOT and the Georgia Institute of Technology. The APA (a modification of the GLWT) was first manufactured in 1996 by Pavement Technology, Inc. The APA follows a similar rut-testing procedure as the

GLWT and features controllable wheel load and contact pressure that are representative of actual field conditions; thus, it has been widely used by many DOTs and transportation agencies in the U.S. A wheel is loaded onto a pressurized linear hose and tracked back and forth over a testing sample to induce rutting (Kandhal and Cooley, 2003). The tests were conducted according to AASHTO test standard T340-10.

(a) APA   (b) Sample in the tester

Figure 3.11 APA rutting susceptibility test

3.4.2 Specimen Fabrication

Cylindrical specimens 6 in. (150 mm) in diameter and 3 in. (75 mm) in height were compacted by the SGC for the APA rutting test. The air void content was controlled at 7%. Prior to testing, the air voids content of the samples were measured in accordance with AASHTO standards T166 and T329. The air voids results obtained by UAF and UTK (University of Tennessee) are summarized in Table 3.5, which shows that the air voids were around 7%.

Table 3.5 Air voids of testing specimens

Project ID	Sample ID	Air Voids, UAF (%)	Air Voids, UTK (%)	Deviation (%)
AIA	1	7.3	7.3	0.56
	2	7.4	7.5	2.08
	3	7.3	7.2	1.12
	4	7.4	7.6	2.62
CH	1	6.8	N/A	N/A
	2	6.7	N/A	N/A
	3	6.5	N/A	N/A
	4	6.5	N/A	N/A
CH2	1	7.4	7.2	2.96
	2	7.4	6.7	9.95
	3	6.7	5.4	18.24
	4	7	6.5	6.69
CO	1	7.2	7.1	1.3
	2	7.4	7.3	1.37
	3	7.4	7.4	0.04
	4	7.1	6.9	2.54
D	1	7.7	8.3	8.36
	2	7.7	8.6	11.66
	3	6.3	6.8	8.04
	4	7.4	8.2	9.73
DH	1	6.8	6.7	0.45
	2	7	6.7	3.94
	3	7.1	6.7	6.54
	4	7.1	6.9	3.53
FIA	1	7.1	N/A	N/A
	2	6.7	N/A	N/A
	3	7.1	N/A	N/A
	4	7.2	N/A	N/A
FIA64	1	7.4	7.6	2.51
	2	7.5	7.3	2.63
	3	7.4	7.5	1.02
	4	7.3	7.1	1.96
GCH	1	7.2	7.1	1.72
	2	7.1	7.2	1.6
	3	6.7	6.7	0.54
	4	6.7	6.6	1.32
GGB	1	6.9	7.3	6.31
	2	7.1	7.5	5.35
	3	7.4	7.7	3.99
	4	6.8	6.9	1.99

Project ID	Sample ID	Air Voids, UAF (%)	Air Voids, UTK (%)	Deviation (%)
GH	1	9.2	9.2	0.84
	2	9	8.8	1.9
	3	9	8.7	3.14
	4	9	9.1	0.9
GPP	1	6.9	6.9	0.27
	2	6.9	6.7	1.95
	3	7.2	7.3	0.49
	4	6.8	6.6	2.64
HNS	1	6.7	6.6	1.76
	2	6.7	6.7	1.16
	3	7	6.5	7.02
	4	6.5	7.1	9.74
M	1	7.2	6.9	4.04
	2	6.7	6.8	2.02
	3	6.9	6.9	0.17
	4	6.8	6.9	2.03
N	1	7.4	7.2	2.74
	2	7.5	7.6	0.94
	3	6.5	6.3	3.35
	4	6.6	6.6	0.53
NPI	1	6.8	6.6	3.48
	2	7.1	6.7	5.09
	3	7.1	6.9	2.74
	4	6.9	6.7	3.04
OGP	1	7.4	7.4	0.78
	2	7.1	7.1	0.37
	3	7.1	7	0.8
	4	6.9	7	0.26
TOK	1	7.1	7.1	0.49
	2	7.5	7.5	0.83
	3	7.1	6.8	4.53
	4	7	6.9	1.91
UNK	1	7.2	7.8	8.18
	2	7.5	7.6	1.3
	3	7.3	6.6	9.2
	4	7.2	6.3	12.28
PW	1	7.4	N/A	N/A
	2	7.1	N/A	N/A
	3	7.2	N/A	N/A
	4	7.1	N/A	N/A

3.4.3 APA Procedure

All APA tests were conducted in accordance with procedures specified in the AASHTO T340-10. The fabricated specimens were placed in the testing chamber and conditioned to 120°F (58°C), which is the testing temperature. The tubes were pressurized to 100 psi, and the wheel load was 100 lb. The test consisted of oscillating the loaded grooved wheel over a pressurized rubber hose that rested on the test specimen up to 8000 times (Bhasin et al., 2005). One full back-and-forth motion is considered one loading cycle. The test frequency is 1 Hz. Rutting depth measurements were obtained at a seating load of 10 cycles and intermediate loadings of 25, 4000, and 8000 cycles.

Four specimens were tested for each mixture. As shown in Figure 3.12, samples No. 1 and 2 were placed on the left wheel track, and samples No. 3 and 4 were placed on the center wheel track of the APA. Data from each pair were recorded to one channel. Figure 3.13 shows a typical rut depth versus loading cycle curve. The rut depth measured at the 8000th cycle was used to evaluate the rutting resistance of HMA.

(a) Samples before testing   (b) Samples after testing
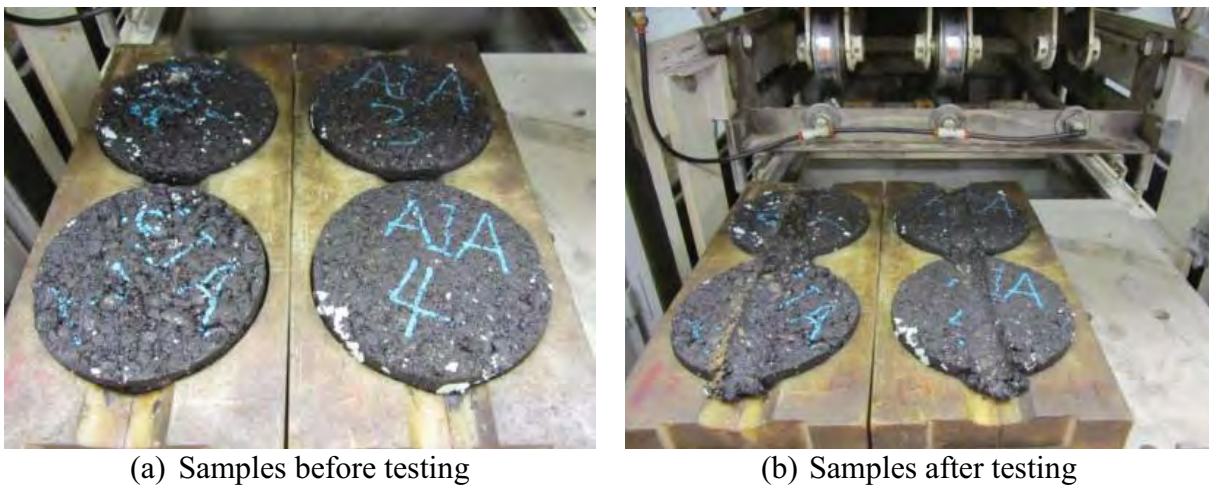
Figure 3.12 APA samples before and after rutting test (58°C)
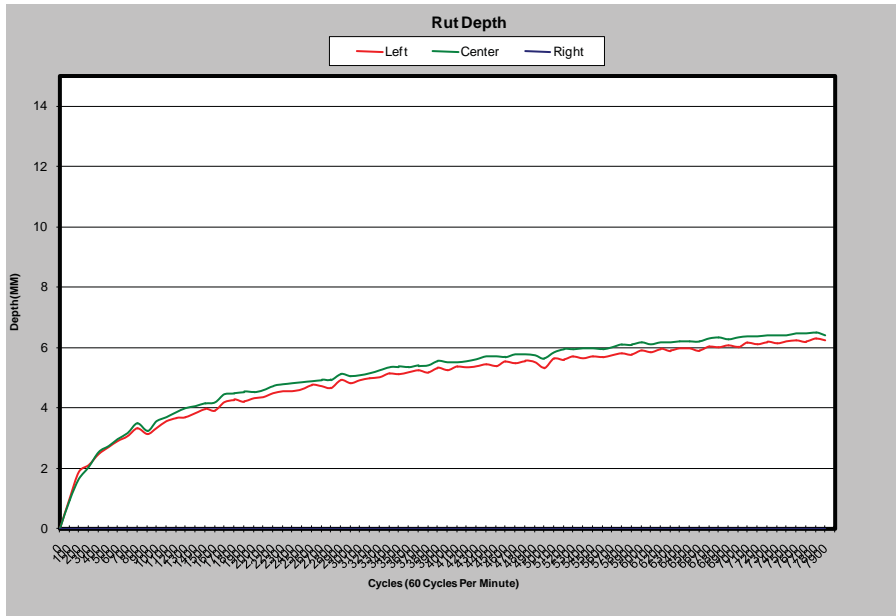
Figure 3.13 Rut depth vs. loading cycle, APA test

CHAPTER 4 TEST RESULTS AND DATA ANALYSIS

Testing results are presented and analyzed in this chapter. The SPT tests including $|E^*|$, F_N, and F_T tests were performed on 19 HMA mixtures. The APA tests were performed on all 21 mixtures. The $|E^*|$ master curves were constructed from measured $|E^*|$, and optimization techniques were applied during the process. Predictive models were verified at two levels, which correspond to input Level 2 and Level 3 specified in the MEPDG. In Level 2, the $|E^*|$ was calculated based on both measured binder and mix volumetric properties. In Level 3, the $|E^*|$ was calculated based on mix volumetric properties and default binder properties, which were determined according to the binder's PG. The results of flow tests and APA tests were summarized, and the effects of potential influencing factors were analyzed. The correlations between measured rutting depth and F_N/F_T were investigated.

4.1 Dynamic Modulus Test

4.1.1 Dynamic Modulus

The $|E^*|$ test was performed over eight loading frequencies (i.e., 25, 20, 10, 5, 2, 1, 0.5, and 0.1 Hz) and four temperatures (i.e., 4, 21.1, 37.8, and 54°C). Three replicates were tested for each mixture, and the results were the average of the three. Figures 4.1 to 4.4 present $|E^*|$ at four different temperatures. Each figure contains $|E^*|$ measured on compacted HMA for nineteen sources at eight frequencies. The values were plotted in the logarithm scale. Generally, $|E^*|$ increases as loading frequency increases and temperature drops. At 4°C, $|E^*|$ was in the range of 20,000 to 2000 MPa. The highest modulus was observed on material collected from the Old Glenn Highway paving project (OGP); the lowest modulus was observed at the Palmer-Wasilla Highway project (PW). At 21°C, the range of $|E^*|$ was 9000 to 200 MPa, and the modulus decreased to the range of 1000 to 30 MPa at 54°C. The detailed testing results of $|E^*|$ at eight loading frequencies and four temperatures for nineteen mixtures are summarized in Appendix A.
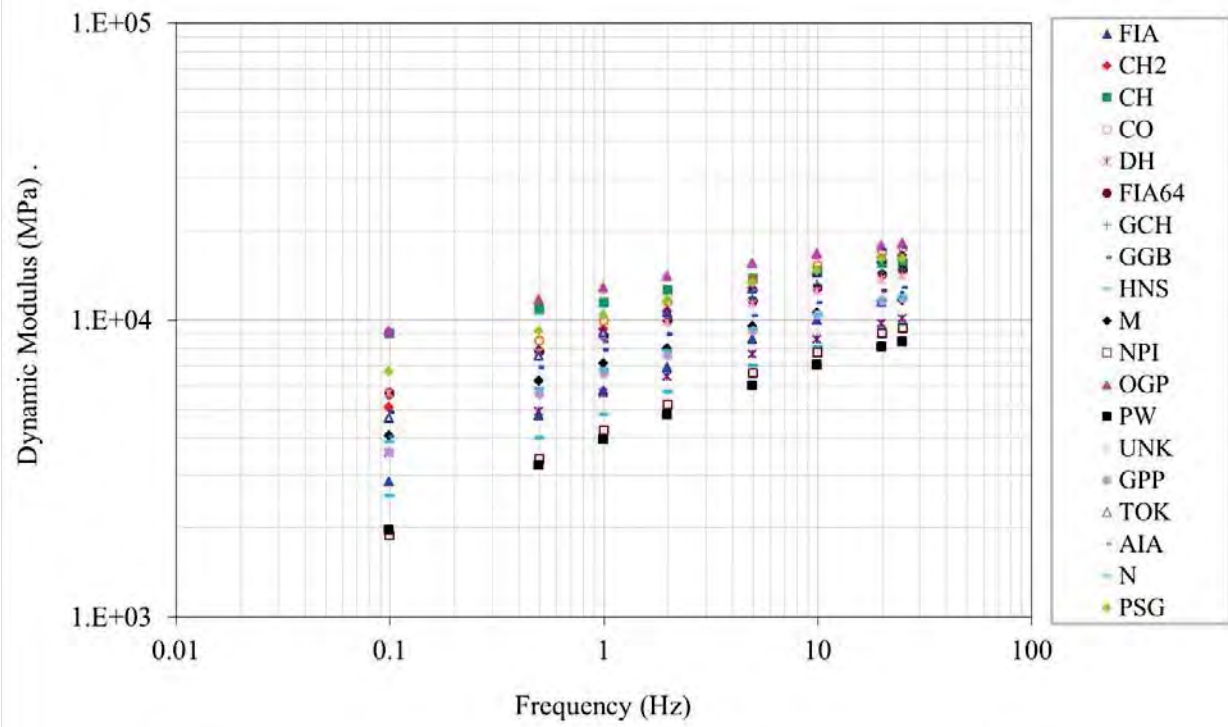
Figure 4.1 Summary of dynamic modulus at 4°C
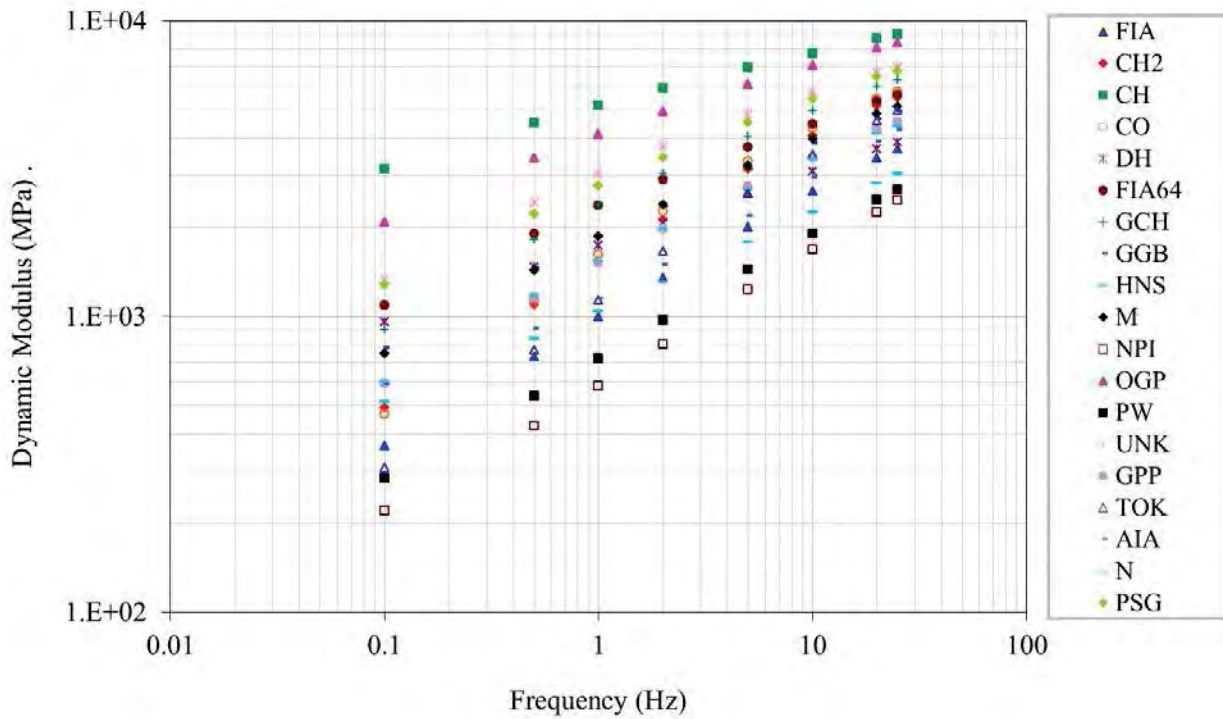
Figure 4.2 Summary of dynamic modulus at 21°C
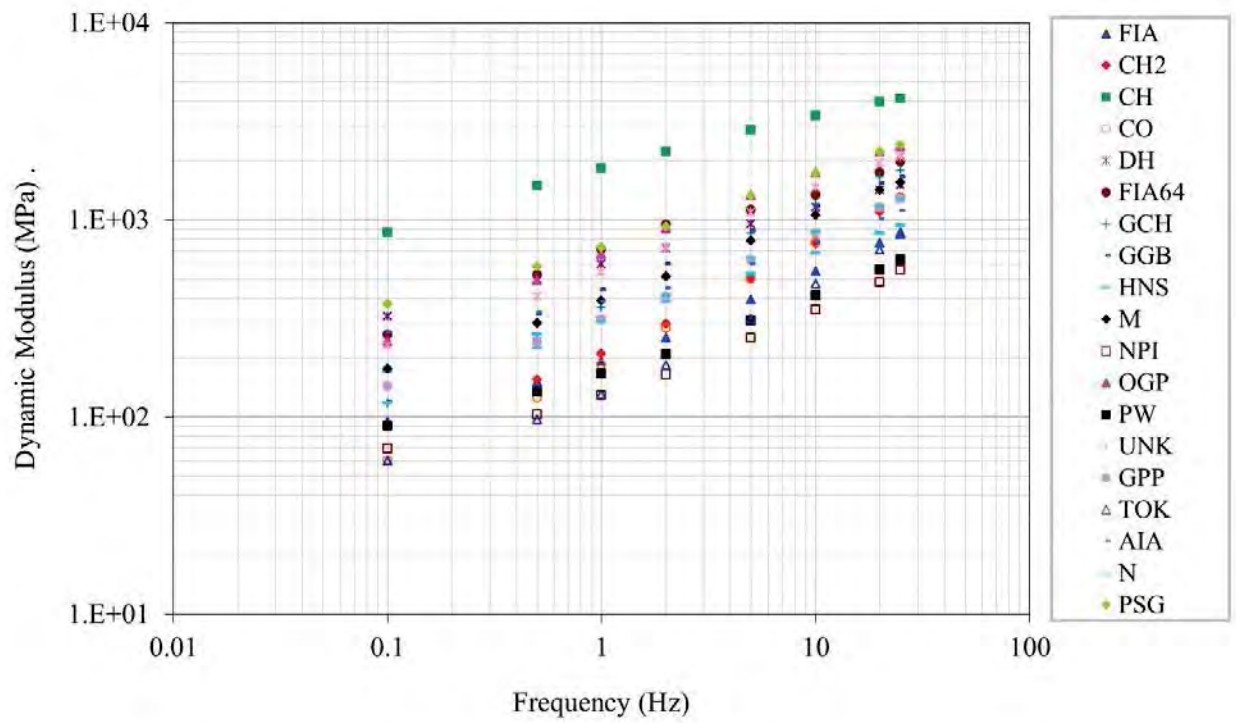
Figure 4.3 Summary of dynamic modulus at 37°C
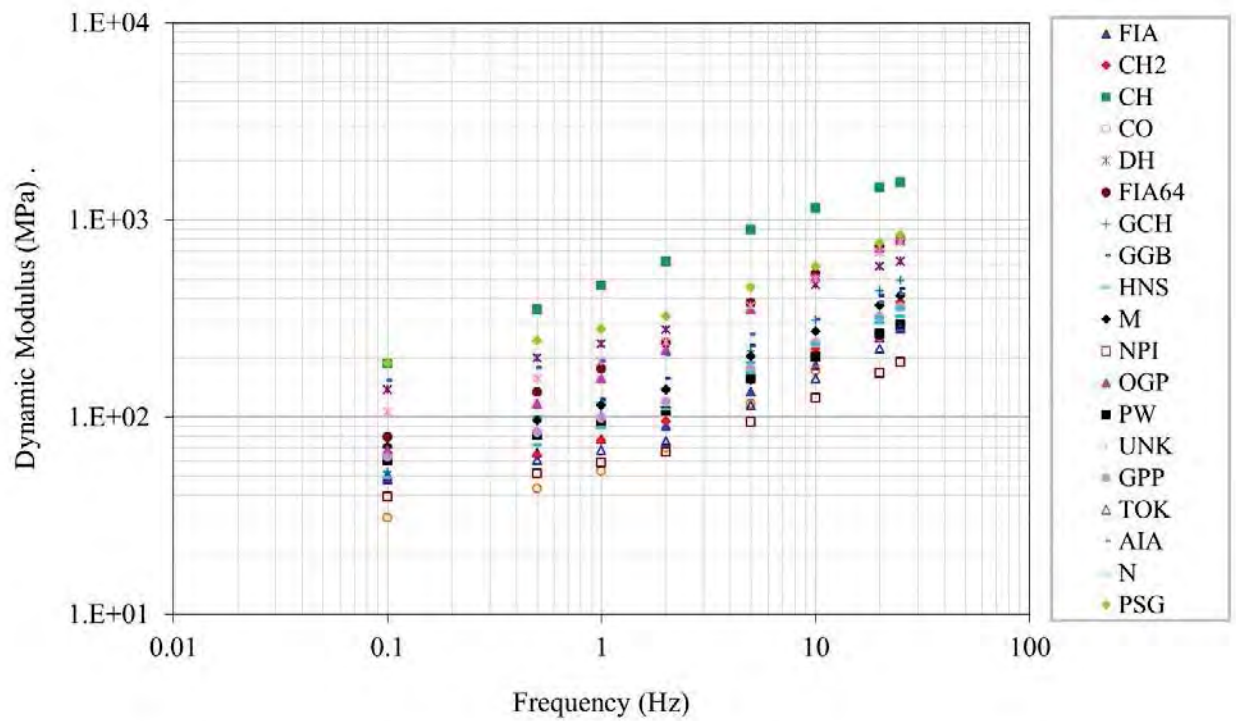
Figure 4.4 Summary of dynamic modulus at 54°C

4.1.2 Master Curves

The rheological properties of HMA mixtures, such as |E*|, depend on both temperature and loading frequency. It has been found that the time-temperature superposition principle can be applied to an asphalt mixture, since asphalt is a linear viscoelastic material, which means that the modulus measured at the higher temperature and lower loading frequency is equal to the one measured at the lower temperature and higher frequency. Therefore, usually, the |E*| of HMA is characterized over a wide range of loading time or frequency (10^{-4} to 10^4 s or Hz). However, due to the practical limitation of the machine's capacity, the loading frequency applied during a test only goes up to 25 Hz. This limited range of loading frequency is extended by using the time-temperature superposition principle. The |E*| values measured over a range of temperatures and loading frequencies can be shifted with respect to frequency/time axis to form a smooth *S*-shape curve at a reference temperature (usually 20°C). This curve is called master curve of |E*|. The |E*| master curve is used in the MEPDG for structural analysis and to account for temperature and frequency effects of asphalt mixtures at all analysis levels.

Figure 4.5 uses the data from mixture collected from the Minnesota Dr. Resurfacing Project (M) as an example to illustrate the process of developing a master curve. Dynamic modulus, measured at four temperatures and eight frequencies, is plotted in log-log scale (Figure 4.5a). Each individual curve represented |E*| measured at a single temperature over eight frequencies. The curve obtained at 20°C was selected as the reference curve, and other individual curves were shifted along the time axis to merge with the reference curve and to form a single smooth curve (Figure 4.5b). A shift factor was used to characterize the amount of horizontal shift, and it was calculated by Eq. 4.1. The shift factor is a function of temperature (Eq. 4.2). After shift factors at four temperatures are determined, the coefficients *a*, *b*, and *c* can be obtained through regression. Once the master curve is constructed (Figure 4.5c), a sigmoidal function (Eq. 4.3) can be used to mathematically describe it (Pellinen and Witczak 2002).

$$a(T) = \frac{f}{f_R} \tag{4.1}$$

$$a(T) = 10^{aT^2 + bT + c} \tag{4.2}$$

$$\log_{10}|E*| = \delta + \frac{\alpha}{1 + e^{\beta + \gamma \cdot \log(f_R)}} \tag{4.3}$$

where
a(T) = shift factor as a function of temperature,
f = loading frequency, Hz,
f$_R$ = reduced loading frequency at a reference temperature of 20°C, Hz,

T = temperature, °C,

$|E^*|$ = dynamic modulus of HMA, MPa, and

$\delta, \alpha, \beta, \gamma, a, b, c$ = regression constants.

    The optimization technique was used to determine the regression constants δ, α, β, γ, and shift factors at the same time using the least square method. Then the shift factors were fitted using Eq. 4.2. The final master curve function consists of seven coefficients—δ, α, β, γ, a, b, c— which are the same as the coefficients used in MEPDG. Figure 4.6 summarizes the master curve of the HMA collected from 19 projects. The individual master curves and coefficients for each mix are summarized in Appendix A.
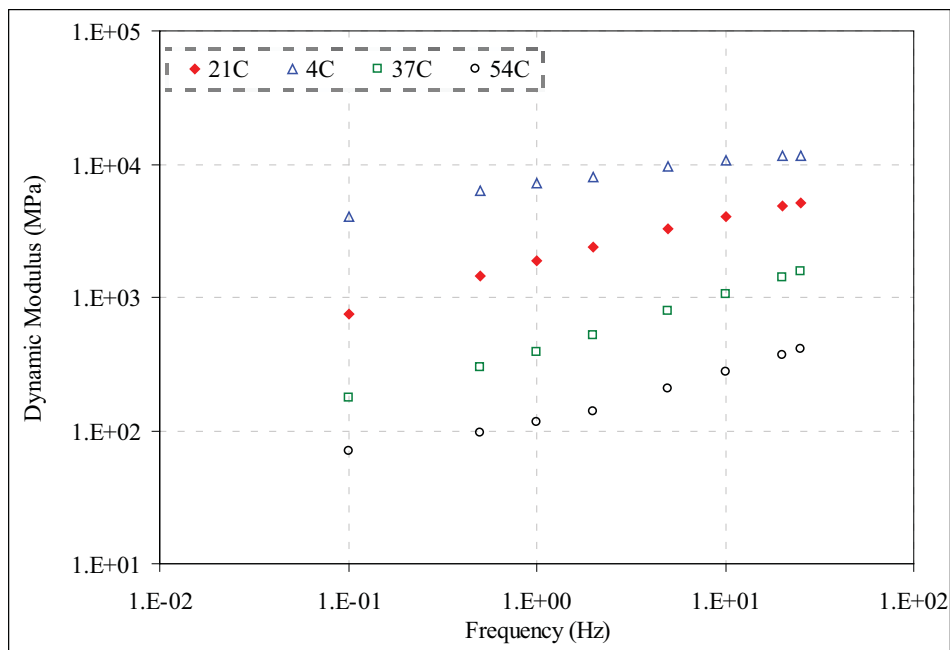
a) Measured |E*| at different temperatures and frequencies
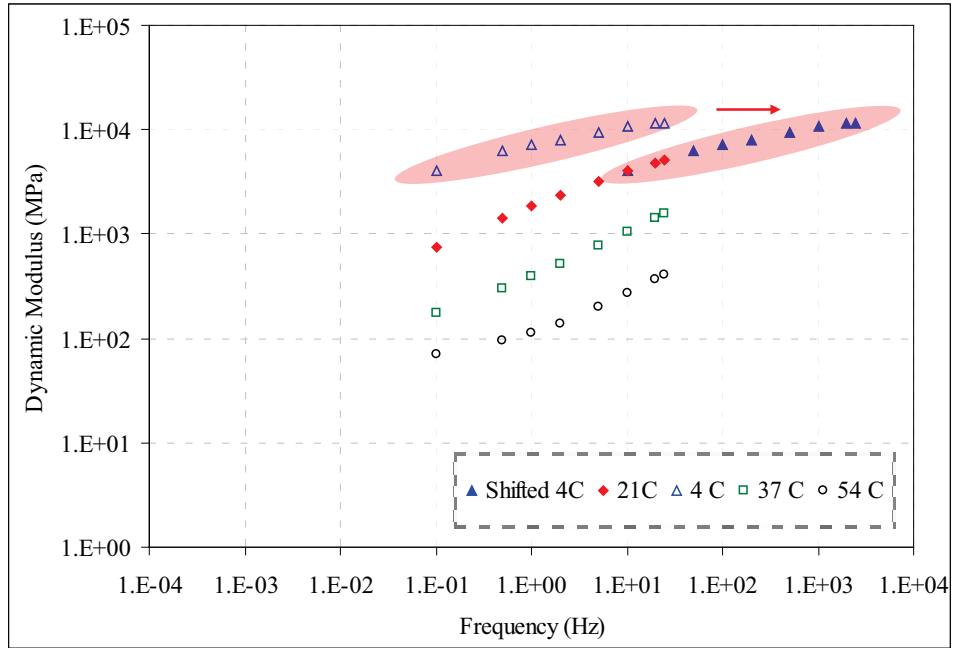
b) Shifting
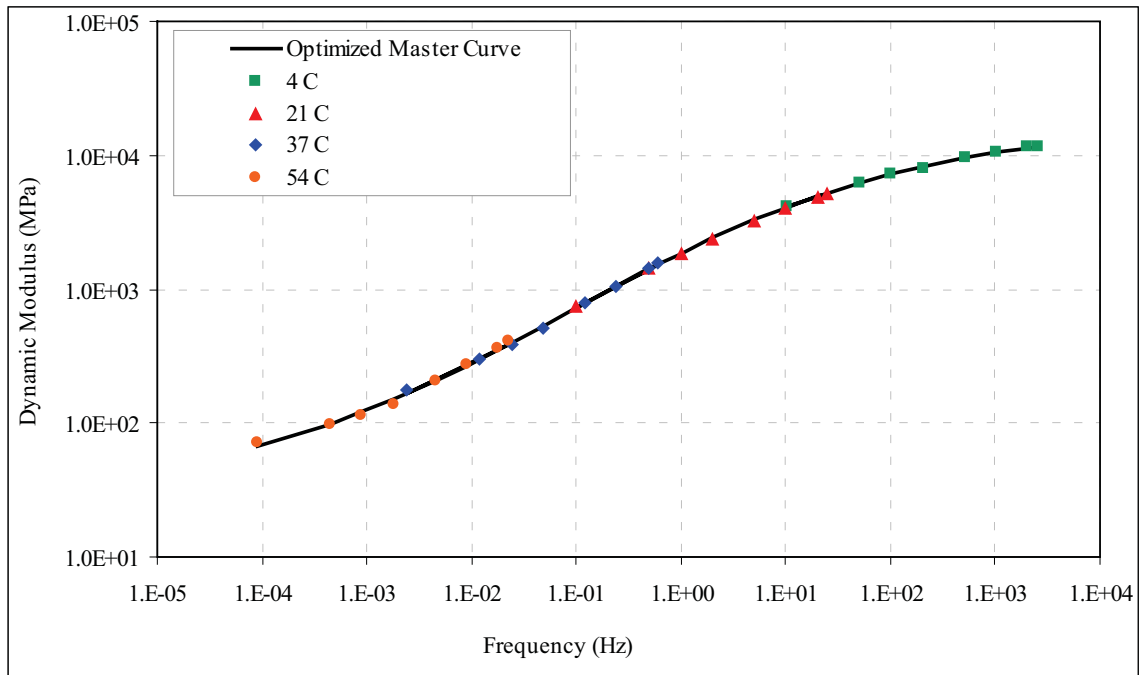
c) Final master curve

Figure 4.5 Example of developing a master curve (Minnesota Dr. resurfacing, M)
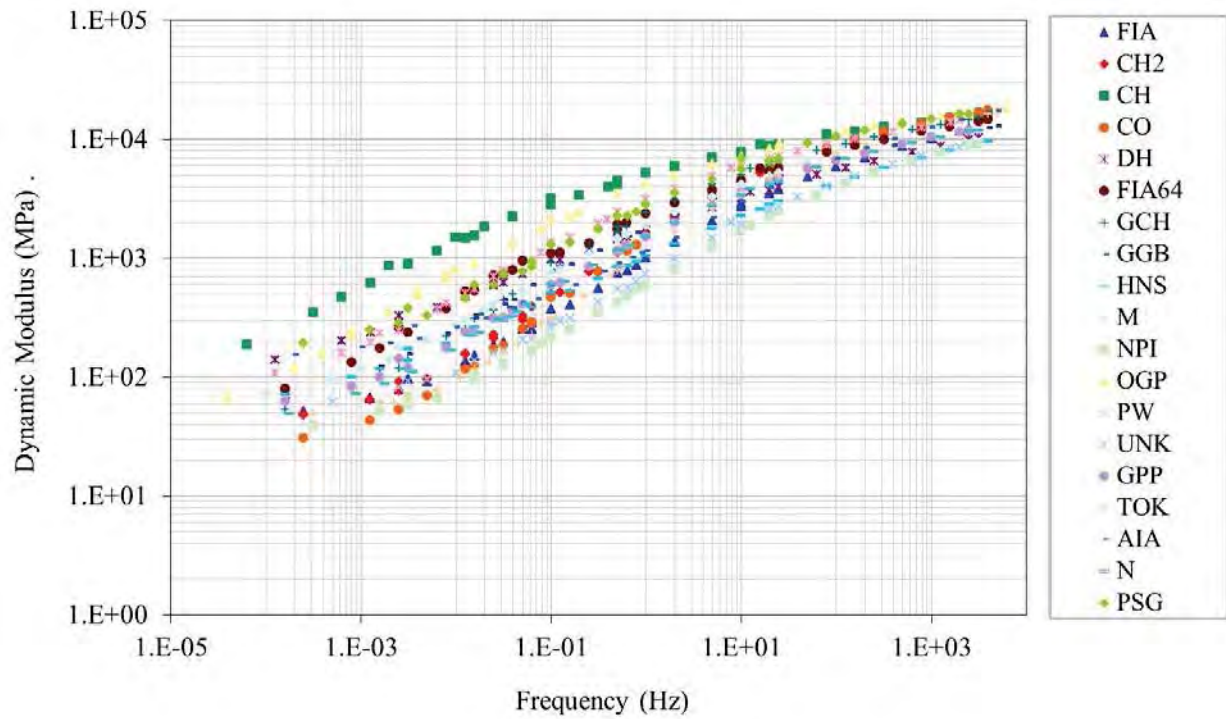
Figure 4.6 Summary of master curves (20°C reference temperature)

4.1.3 Phase Angle

The phase angle, φ, is the angle by which strain lags behind stress; it represents the viscous properties of the material being evaluated. A pure elastic material has a 0° phase angle, which means that no lag occurs between strain and stress, and a purely viscous material exhibits a 90° lag. The mathematical expression of phase angle is expressed by Eq. 4.4.

$$\varphi = \frac{t_i}{t_p} \cdot 360 \tag{4.4}$$

where

t_i = time lag between peaks of stress and strain, s, and

t_p = time of loading cycle, s.

The phase angle measured during |E*| tests for all materials are plotted against loading frequency in Figures 4.7 to 4.10 at four temperatures (i.e., 4, 21, 37, 54°C). Generally, the phase angle ranged between 9° and 50°. At 4° and 21°C, the phase angle decreased as loading frequency increased. However, at 37° and 54°C, the trend reversed, showing that phase angle increased as loading frequency increased. The results are consistent with the findings reported by previous studies (Pellinen and Witczak, 2002; Zhang, 2005; Obulareddy, 2006). At lower

42

temperature (e.g., lower than 37°C), the phase angle of asphalt mixtures is primarily affected by the asphalt binder. As a type of viscoelastic material, the asphalt binder exhibits a more elastic response under higher loading frequencies. At higher temperature, the effect of asphalt binder on the overall behavior of HMA becomes insignificant. The increase of loading frequency amplifies the effect of asphalt binder and, therefore, leads to the increase of phase angle.
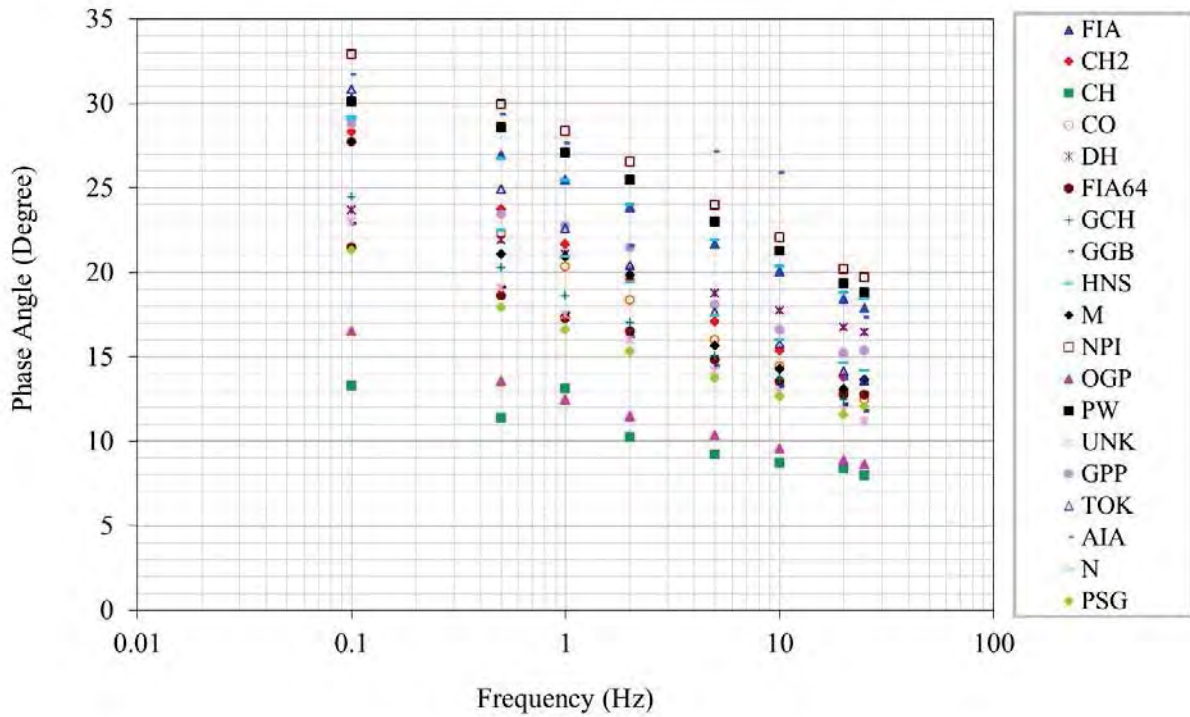
Figure 4.7 Summary of phase angle at 4°C
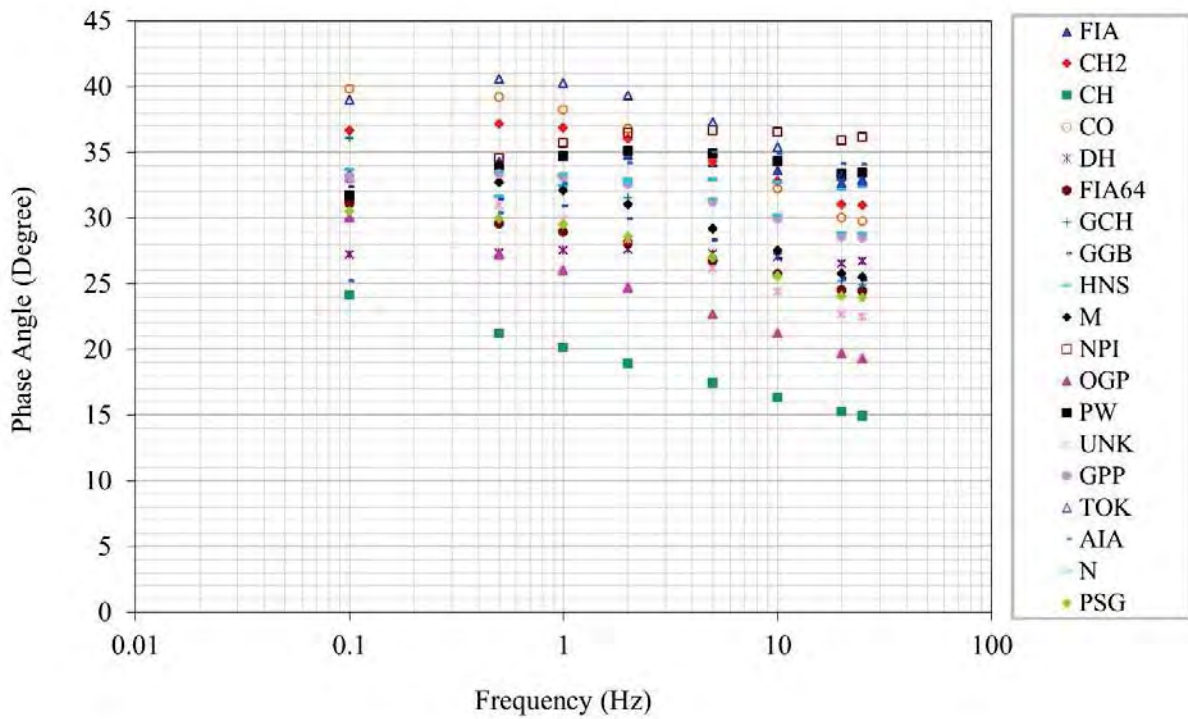
Figure 4.8 Summary of phase angle at 21°C
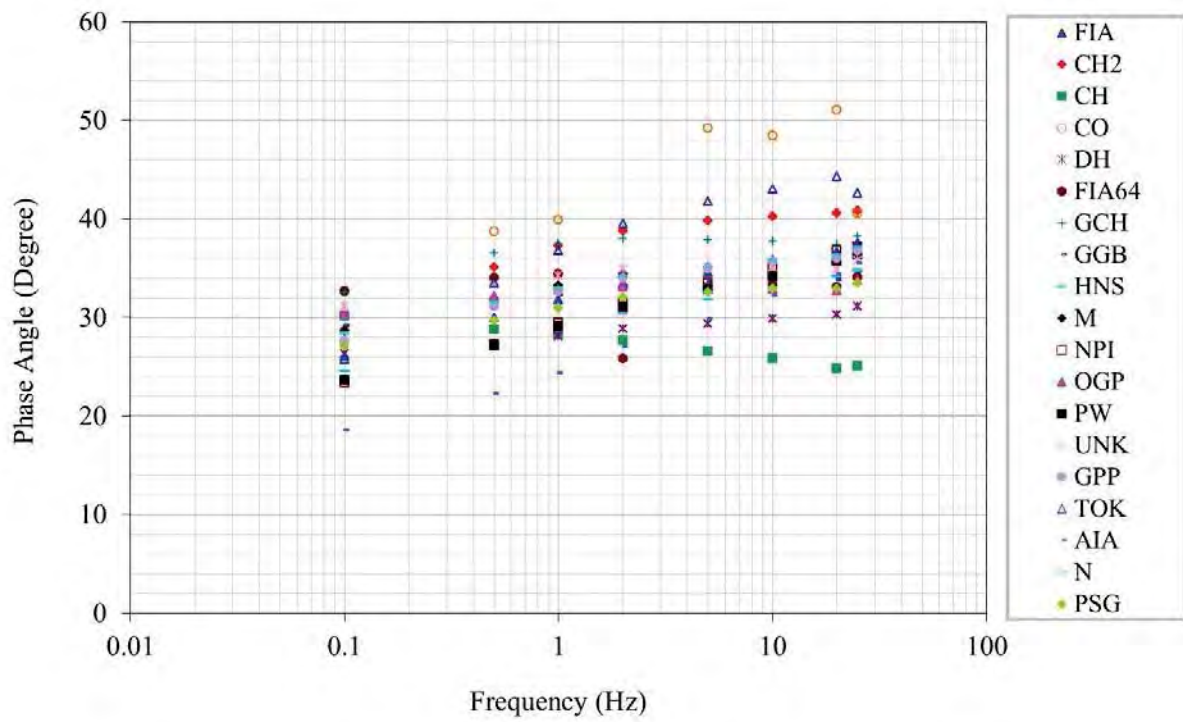
Figure 4.9 Summary of phase angle at 37°C
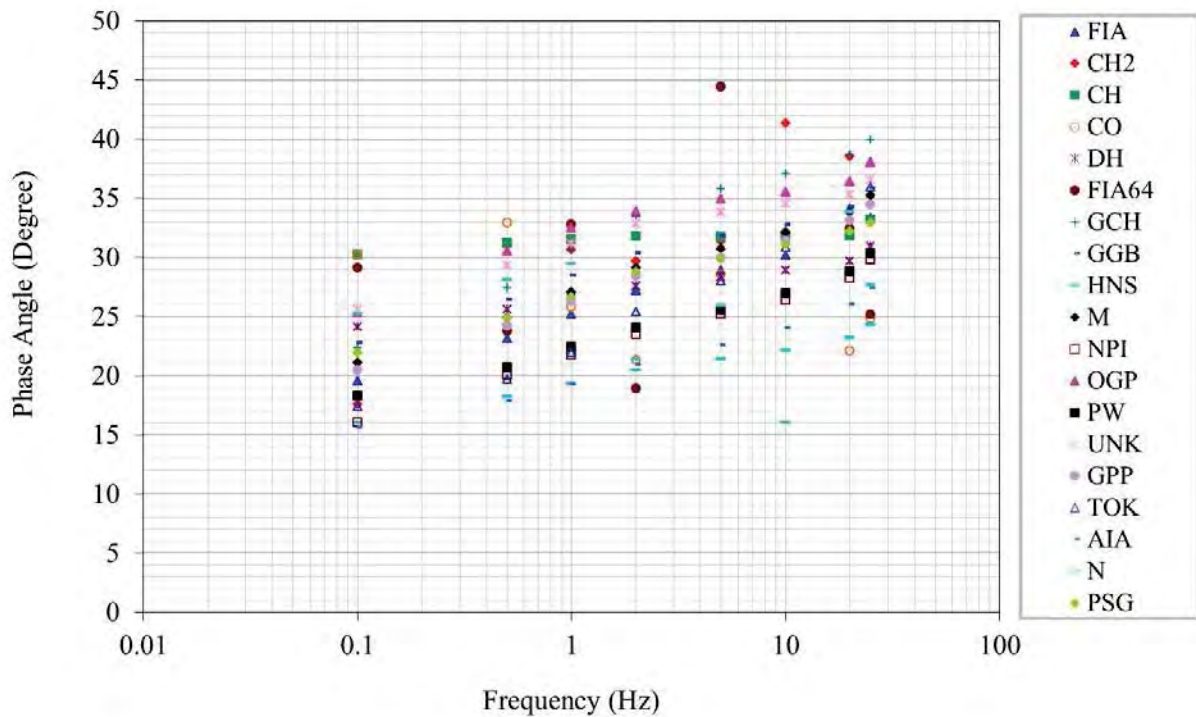
Figure 4.10 Summary of phase angle at 54°C

The effect of temperature on phase angle is illustrated in Figure 4.11. The phase angles measured at 1 Hz loading frequency were plotted versus temperature for all materials collected. The plot exhibited a parabolic shape, and the maximum values of phase angle were expected to be in the range of 21° and 37°C based on the trend observed in Figure 4.11. As mentioned before, the phase angle of the asphalt mixtures is primarily affected by the asphalt binder at lower temperature. Under the same loading frequency, as temperature increases, the asphalt binder becomes more viscous, which leads to the increase of phase angle on both asphalt binder and HMA. At the higher temperature, the behavior of HMA is dominated by aggregate properties, such as skeleton and angularity. The decrease of phase angle as temperature increases indicates that the effects of asphalt binder on the overall behavior of HMA become insignificant.
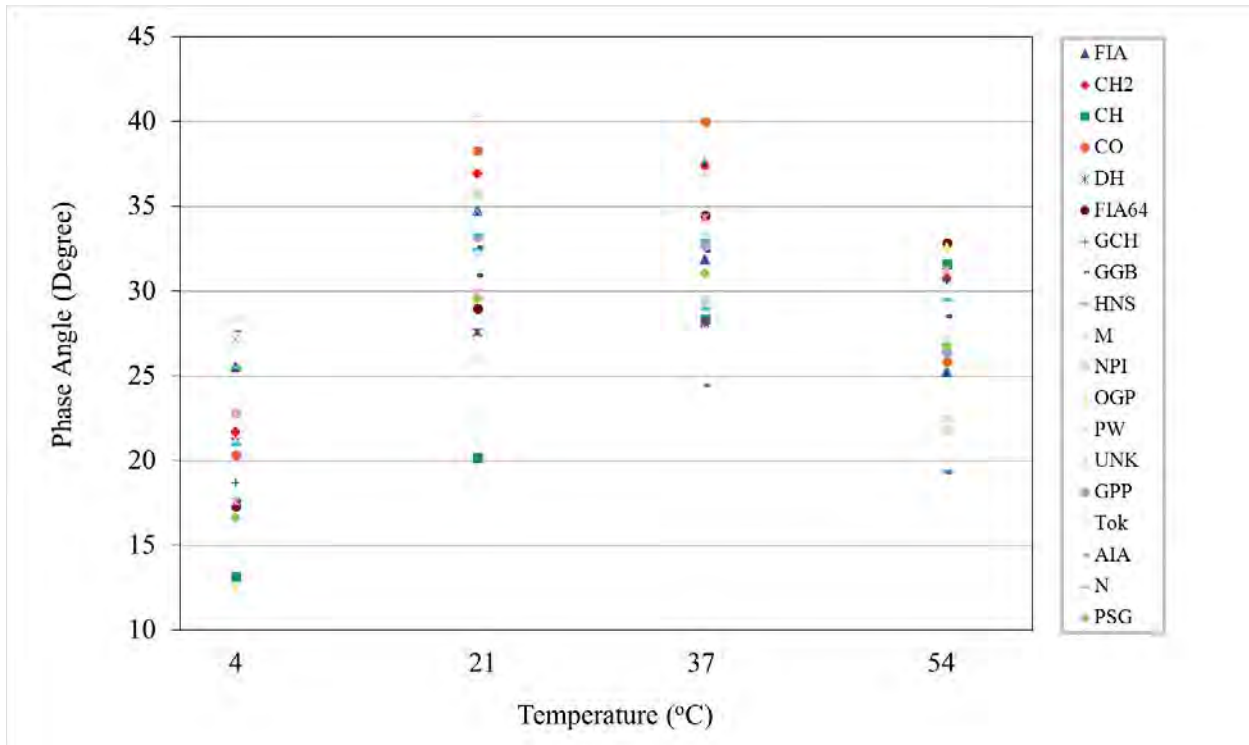
Figure 4.11 Phase angle at four temperatures (1 Hz loading frequency)

Following the same procedure used for |E*|, a master curve can be constructed for phase angle. Figure 4.12 shows the phase angle master curves of all mixes investigated in this study at the reference temperature of 20°C. The master curves also exhibited a parabolic shape and the maximum value of phase angle was observed when the loading frequency ranged from 0.1 to 1 Hz.
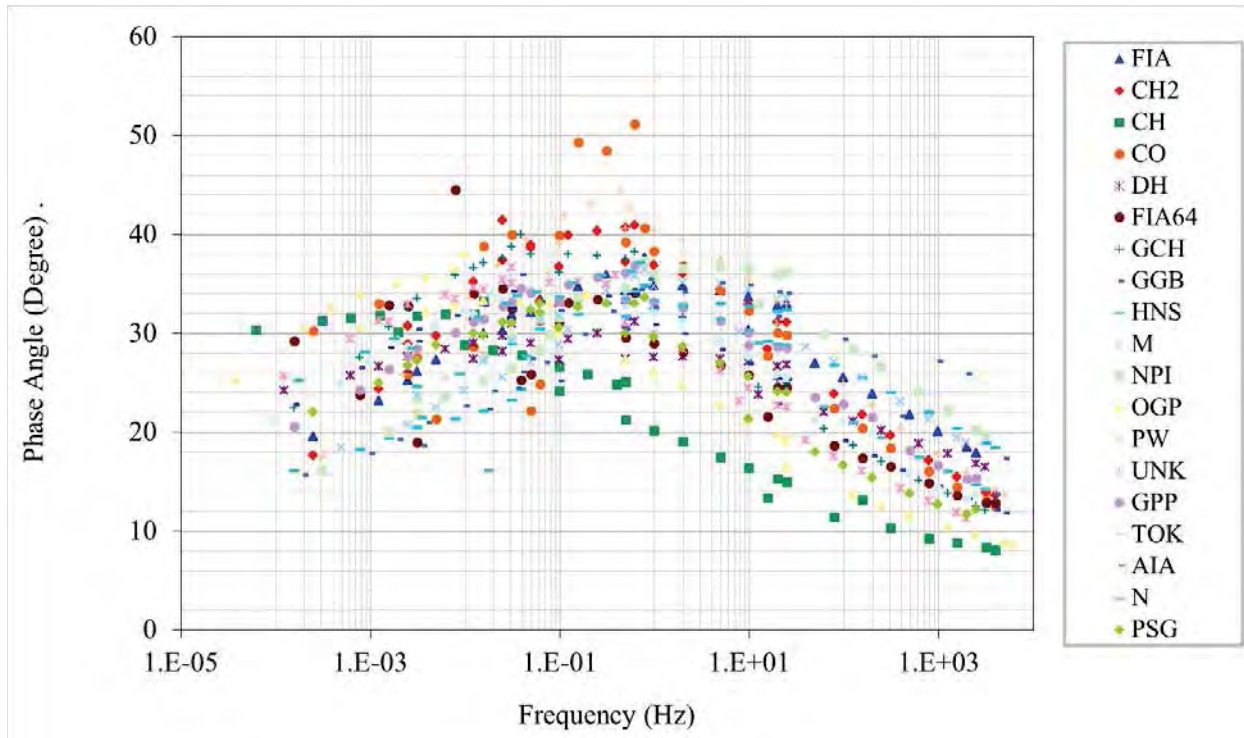
Figure 4.12 Summary of phase angle master curve for Alaska mixes
(reference temperature 20°C)

4.1.4 Verification of Predictive Models

According to the MEPDG, there are three input levels for |E*|. Level 1 uses measured |E*|. Levels 2 and 3 use predicted |E*|. In Level 2, |E*| is calculated based on both measured binder and mix volumetric properties, and in Level 3, |E*| is calculated based on mix volumetric properties and default binder properties, which are determined according to the binder PG. In this study, three predictive models were verified at both Levels 2 and 3.

Level 2 Model Verification

The Level 2 model verifications were performed for the original Witczak model (Eq. 2.3), modified Witczak model (Eq. 2.4), and Hirsch model (Eq. 2.5). At Level 2, all predictive models require rheological properties measured on short-term (RTFO) aged binder and HMA volumetric properties. The required data inputs for each predictive model are summarized in Table 4.1. The original Witczak model requires laboratory-measured viscosity (η). Since this parameter is no longer a routine measurement for the PG binder grading system, a conversion (Eq. 4.5) is used to transfer |G*| and δ to viscosity (η) (ARA, Inc., 2004). This equation can be applied for G* and δ obtained from the DSR test conducted at a 10 Hz loading frequency. The modified Witczak model requires G* and δ , and the Hirsch model requires G*. The available rheological properties are listed in Table 4.2 for each project (except the HNS project). In the HNS project,

47

the DSR testing results were reported in the value of G*·sinδ. Therefore, the viscosity cannot be converted by using Eq. 4.5.

$$\eta = \frac{G*}{10}(\frac{1}{Sin\delta})^{4.8628}$$ (4.5)

where

η   = viscosity, cP, (Pα.s)
G*   = binder complex shear modulus, Pa, and
δ   = binder phase angle, degree.

Table 4.1 Required inputs for |E*| predictive models at Level 2

Parameters		Description	Units	Required Inputs		
				Original Witczak	Modified Witczak	Hirsch
Binder Properties	η	Binder Viscosity	10^6 Poise	√		
	f	Loading Rate	Hz	√		
	|G*|	Dynamic Shear Modulus	psi		√	√
	δ	Phase Angle	Degree		√	
Mix Volumetric Properties	V_{beff}	Effective Binder Content by Volume	%	√	√	
	V_a	Air Void Content	%	√	√	
	VMA	Voids in Mineral Aggregate	%			√
	VFA	Voids filled with Asphalt	%			√
	$\rho_{3/4}$	Cumulative Percent Retained on ¾″ Sieve	%	√	√	
	$\rho_{3/8}$	Cumulative Percent Retained on ⅜″ Sieve	%	√	√	
	ρ_4	Cumulative Percent Retained on #4 Sieve	%	√	√	
	ρ_{200}	Percent Passing #200. Sieve	%	√	√	

Table 4.2 Summary of binder rheological properties

No.	Mix	PG	Temperature (°C)	DSR (RTFO)		Converted η (10^6 P)
				$\|G^*\|$ (KPa)	Phase Angle (degree)	
1	AIA	64-34	64	3.73	51.5	1.23E-02
2	CH	52-28	52	3.14	86.5	3.17E-03
3	CH2	52-28	52	3.14	86.5	3.17E-03
4	CO	52-28	52	3.10	83.1	3.21E-03
5	D	64-34	64	1.68	50.2	6.06E-03
6	DH	52-40	52	2.82	53.3	8.27E-03
7	FIA	52-34	52	4.24	68.7	5.99E-03
8	FIA64	64-34	64	2.75	58.6	5.95E-03
9	GCH	52-28	52	2.56	86.9	2.58E-03
10	GGB	64-34	64	2.08	63.1	3.64E-03
11	GH	64-34	64	1.80	52.6	5.52E-03
12	GPP	64-34	64	1.89	62.3	3.42E-03
13	HNS	58-28	58	3.54 (G* sinδ)		n/a
14	M	64-34	64	2.15	63.4	3.71E-03
15	N	52-34	52	3.79	67.5	5.58E-03
16	NPI	64-34	64	2.13	50.1	7.74E-03
17	OGP	52-28	52	2.59	86.9	2.61E-03
18	PSG	58-28	58	4.13	73.2	5.11E-03
19	PW	64-34	64	1.92	52.9	5.78E-03
20	TOK	52-28	52	3.14	86.7	3.17E-03
21	UNK	52-28	52	3.43	85.6	3.48E-03

The original Witczak model (Eq. 2.3) can be used to calculate the |E*| of HMA at various temperatures and loading frequencies. The effects of temperature and loading frequency are represented by the parameter of viscosity (η) and frequency (*f*) in Eq. 2.3. The viscosity at various temperatures is calculated based on the ASTM viscosity temperature relationship defined by Eq. 4.6 (ASTM D341, ARA, Inc., 2004). The MEPDG requires viscosity (η) (or G* and δ) measured at a minimum of three temperatures to calculate the regression constants A and VTS. However, in routine practice, G* and δ are only measured at the temperature at the higher end of PG. Therefore, the verification of the original Witczak model was only performed at temperatures specified in the high end of PG at 10 Hz loading frequency. Based on the measured binder viscosity and mix volumetric properties listed in Table 3.2, predicted and measured |E*| are plotted in Figure 4.13. It can be seen that, generally, at higher temperature, the modified Witczak model over-predicts |E*|. The measured moduli varied from 100 to 500 MPa, whereas the predicted values ranged from 350 to 700 MPa.

$$\log\log\eta = A + VTS\log T_R \tag{4.6}$$

where

T_R = temperature (in Rankine at which the viscosity was estimated), and

A,VTS = regression parameters
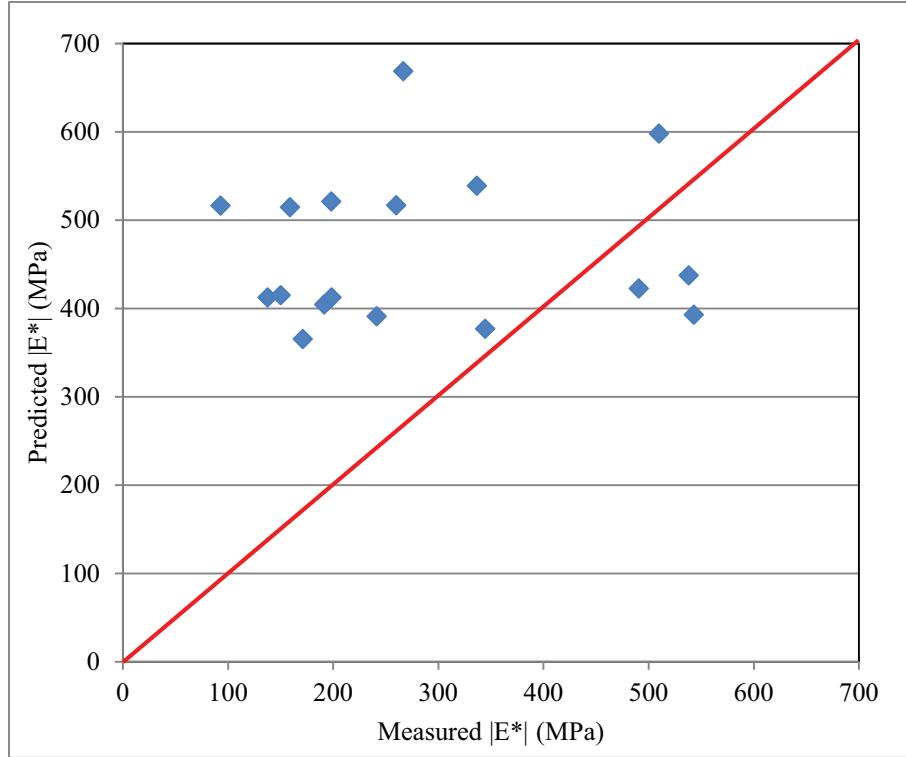
Figure 4.13 Predicted vs. measured |E*| for all mixes (original Witczak model, Level 2)

Following the same strategy, verification of Level 2 input was also performed for the modified Witczak model (Eq. 2.4). The predicted values were based on measured G* and δ at temperatures at the higher end of PG at a loading frequency of 10 Hz. As specified in the modified Witczak model, the frequencies between shear mode and compression mode were converted by Eq. 4.7. Predicted and measured |E*| are plotted in Figure 4.14. Predicted |E*| is scattered on both sides of the equality line. The scattered data of predicted |E*| with varied mix volumetric and binder rheological properties are in a data band between 500 and 800 MPa. Meanwhile, measured |E*| is in a wide range from 200 to 1200 MPa, indicating that the predictive model is not sensitive to change in the mix volumetric or binder rheological properties.

$$f_s = \frac{f_c}{2\pi} \qquad (4.7)$$

where

f_s = loading frequency in shear mode, Hz, and

f_c = loading frequency in compression mode, Hz.
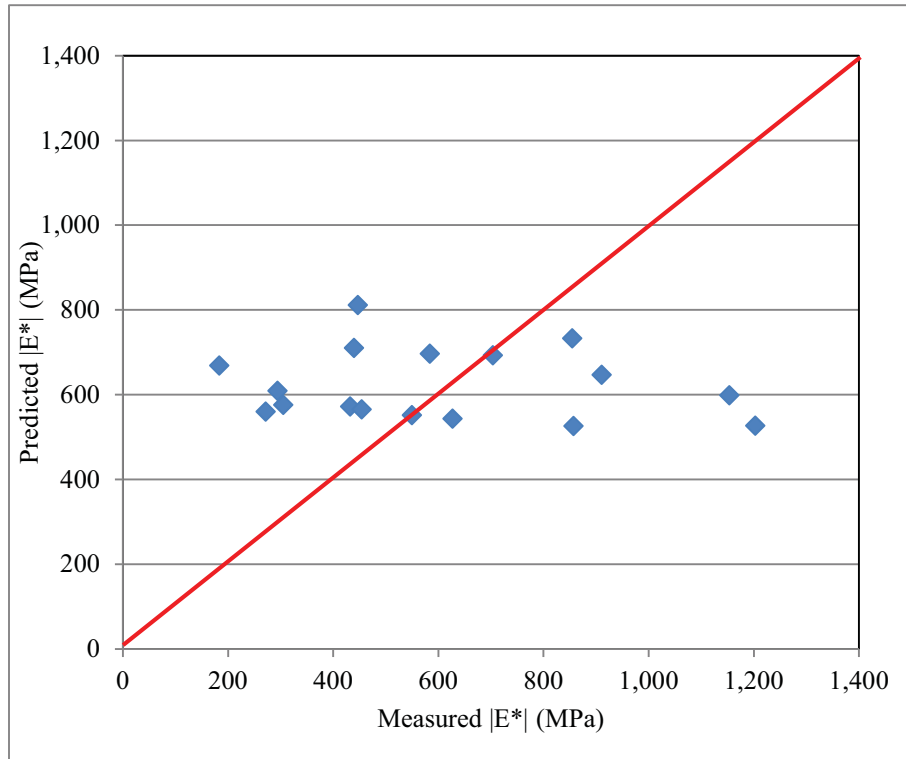
Figure 4.14 Predicted vs. measured |E*| for all mixes (modified Witczak model, Level 2)

The Hirsch model only contains three parameters: VFA, VMA, and $|G^*|_b$ (see Eq. 2.5 to 2.7). Predicted and measured |E*| are illustrated in Figure 4.15. The predicted |E*| was about 250 MPa for all mixtures. The data band of predicted |E*| was even narrower compared with the modified Witczak model. The measured moduli varied from 100 to 550 MPa, while the predicted values consistently equaled approximately 250 MPa regardless of material properties. Compared with the modified Witczak model, the Hirsch model was even more insensitive to volumetric and rheological properties.
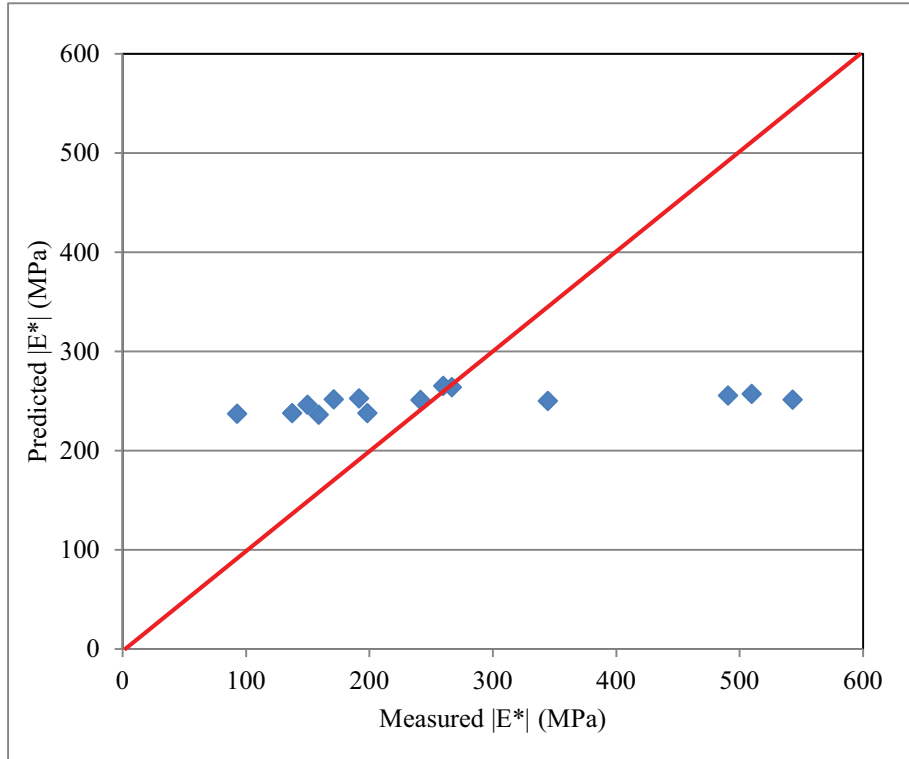
Figure 4.15 Predicted vs. measured |E*| for all mixes (Hirsch model, Level 2)

Verification of Level 3 Inputs

The verification of Level 3 was conducted using measured mix volumetric properties and default rheological properties, the estimation based on the PG of the binder. Table 4.3 summarizes the required inputs for each model. In the original Witczak model, the viscosity was calculated according to the ASTM viscosity temperature relationship (Eq. 4.6) (ASTM D341, ARA, Inc., 2004). Instead of using calculated A and VTS based on regression analysis for Level 2 verification, the default values of A and VTS for the RTFO aged binder based on PG were used, as listed in Table 4.4. The table includes all binder grades investigated in this study, and these default values were recommended by MEPDG. The parameter VTS represents the temperature sensitivity of the asphalt binder. As the span between the higher and lower end of PG increases, the absolute value of VTS decreases. The parameter A is the intercept. As the low end of PG decreases, the value of A decreases. The mix volumetric properties are listed in Table 3.2.

Table 4.3 Required inputs for |E*| predictive models at Level 3

Parameters		Description	Units	Required Inputs		
				Original Witczak	Modified Witczak	Hirsch
Binder Properties	PG	Binder Grade		√	√	√ *
Mix Volumetric Properties	V_{beff}	Effective Binder Content by Volume	%	√	√	
	V_a	Air Void Content	%	√	√	
	VMA	Voids in Mineral Aggregate	%			√
	VFA	Voids filled with Asphalt	%			√
	$\rho_{¾}$	Cumulative Percent Retained on ¾″ Sieve	%	√	√	
	$\rho_{⅜}$	Cumulative Percent Retained on ⅜″ Sieve	%	√	√	
	ρ_4	Cumulative Percent Retained on #4 Sieve	%	√	√	
	ρ_{200}	Percent Passing #200. Sieve	%	√	√	

* The Hirsch model does not contain a predictive model for G* based on the binder's PG. The G* predictive model integrated in the modified Witczak model was used to calculate the G* as an input for Hirsch model.

Table 4.4 Defaults values of A and VTS based on asphalt PG (ARA, Inc., 2004)

PG	A	VTS
52-28	11.84	-4.012
58-28	11.01	-3.701
52-34	10.707	-3.602
52-40	9.496	-3.164
64-34	9.461	-3.134

Figure 4.16 illustrates measured |E*| versus predicted |E*| by the original Witczak model. The results show that the predicted |E*| obtained from the original Witczak model is close to measured moduli in a wide range of temperature and frequency. The correlation between measured and predicted values (R^2) was 0.84. The regressed trend line indicated that generally, the model overestimates |E*| at higher temperatures and lower loading frequencies and underestimates |E*| at lower temperatures and higher loading frequencies. The observation is consistent with previous studies reported by Mohammad et al. (2005), Dongre et al. (2005), and Ceylan et al. (2008). Appendix B includes individual mix results.
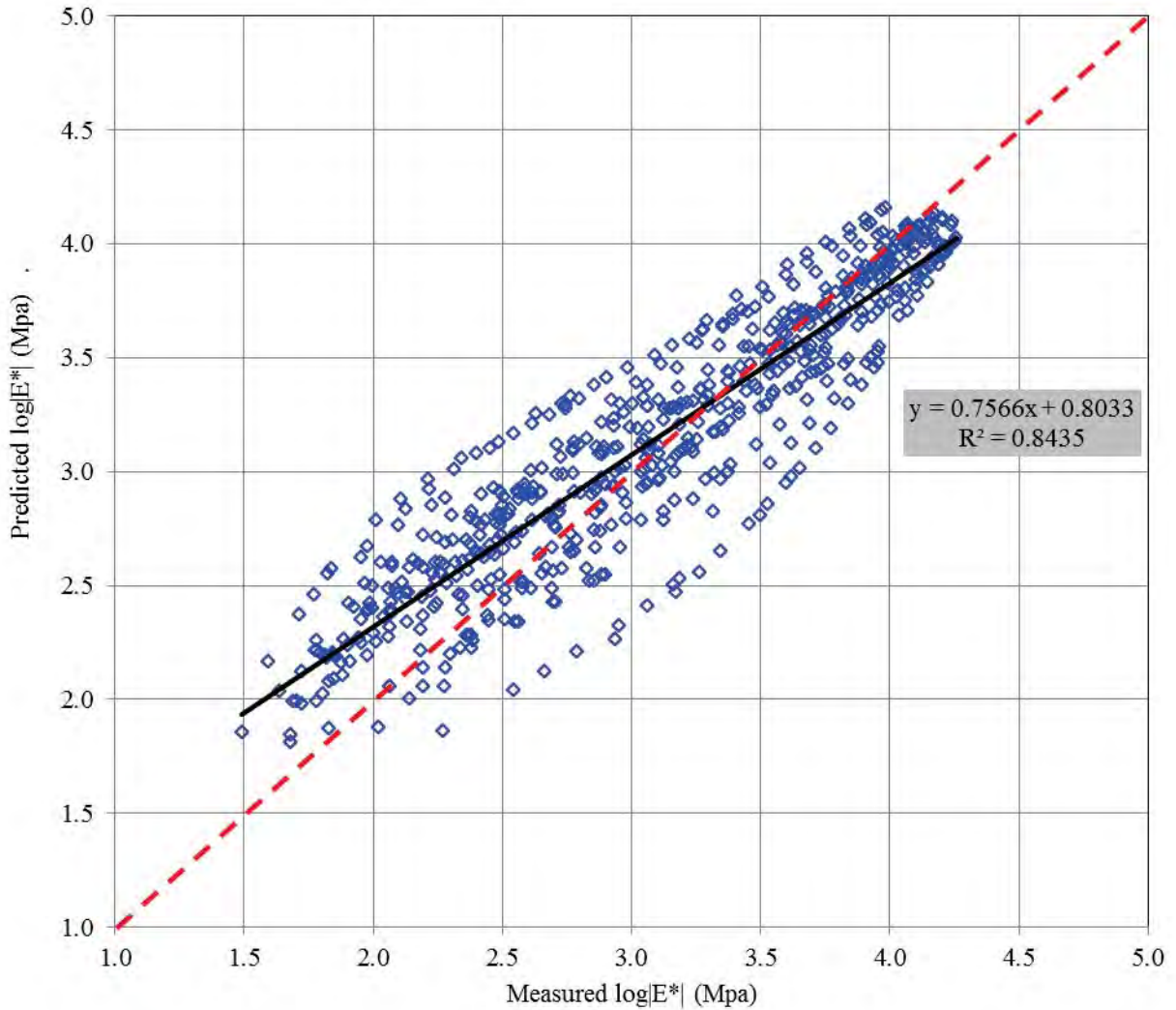
Figure 4.16 Predicted vs. measured |E*| for all mixes (original Witczak model, Level 3)

The modified Witczak models use a $|G^*|_b$-based prediction methodology. $|G^*|_b$ and δ are the primary parameters used to characterize the rheological properties of the asphalt binder in the PG system. In the Level 3 verification, $|G^*|_b$ and δ are estimated using Eqs. 4.8 to 4.12. The $|G^*|_b$ can be calculated based on viscosity, shear loading frequency, and δ (Eq. 4.8), and δ is calculated from shear loading frequency, viscosity, and adjusted A' and VTS' (Eq. 4.9). The A' and VTS' are adjusted for shear loading frequency.

$$\left|G_b*\right| = 0.0051 f_s \eta_{f_s,T}(Sin\delta_b)^{7.1542-0.4929 f_s+0.0211 f_s^2} \tag{4.8}$$

$$\delta_b = 90 + (-7.3146 - 2.6162 VTS') \times \log(f_s \times \eta_{f_s,T}) + (0.1124 + 0.2029 VTS') \times \log(f_s \times \eta_{f_s,T})^2 \tag{4.9}$$

$$\log\log\eta_{f_s,T} = A' + VTS'\log T_R \tag{4.10}$$

$$A' = 0.9699 f_s^{-0.0527} A \tag{4.11}$$

$$VTS' = 0.9668 f_s^{-0.0575} VTS \tag{4.12}$$

where

f_s	= shear loading frequency,
$\eta_{fs,T}$	= viscosity at reference shear loading frequency and temperature, cP,
A'	= adjusted A (adjusted for loading frequency), and
VTS'	= adjusted VTS (adjusted for loading frequency).

The |E*| values predicted by the modified Witczak model for Level 3 are plotted in Figure 4.17 versus the measured |E*|. The overall correlation (R^2) between measured and predicted values was 0.81, which is slightly lower than that of the original Witczak model. This observation is consistent with the findings of previous studies that the modified Witczak model does not improve the accuracy of the prediction (Garcia and Thompson, 2007; Kim et al., 2011). The model overestimated |E*| as indicated by the trend line, especially for lower frequencies and higher temperatures.
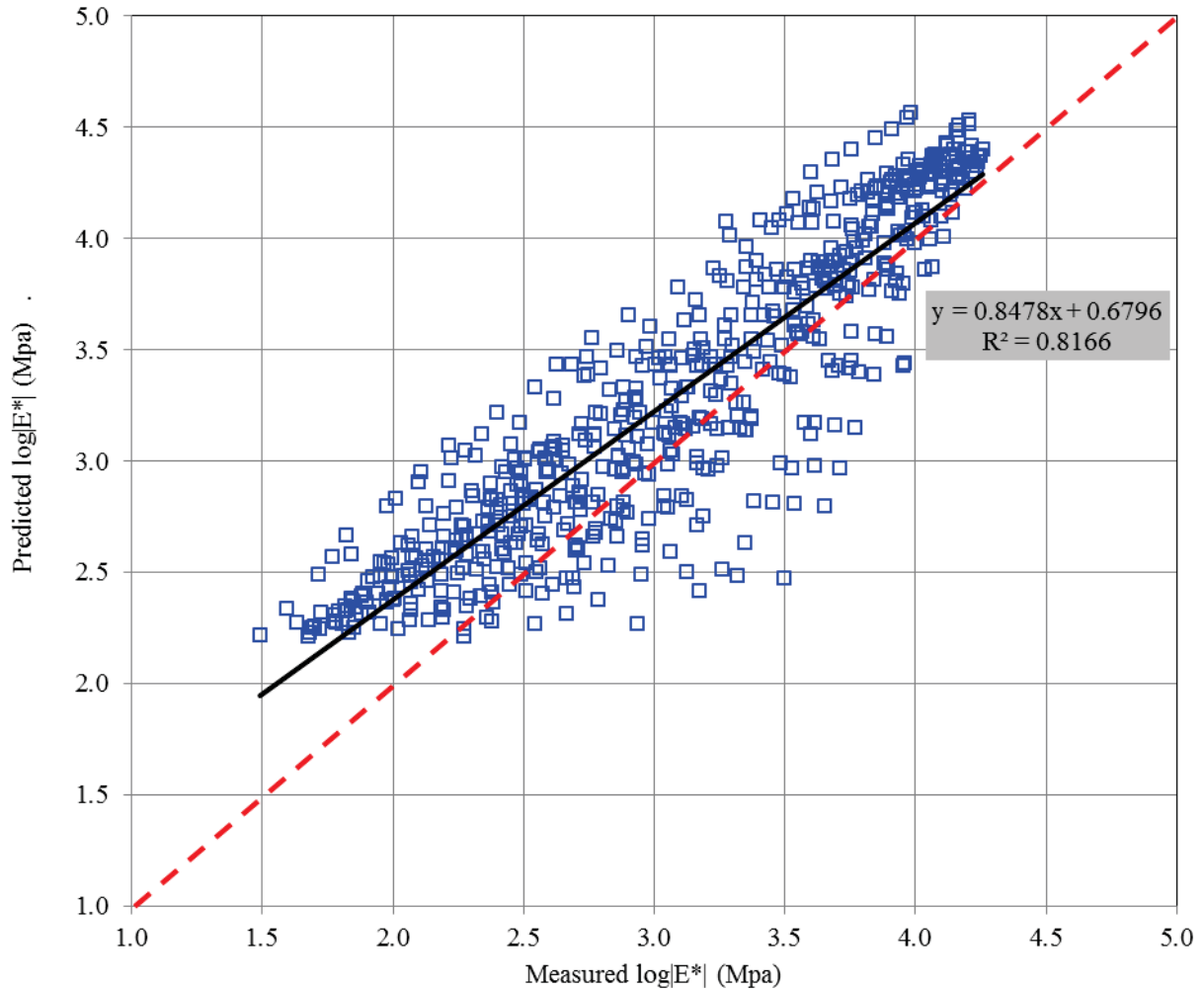
Figure 4.17 Predicted vs. measured |E*| (modified Witczak model, Level 3)

A comparison between the two versions of Witczak models was also made. See Appendix C for detailed mix results. The predicted values by two models are plotted in Figure 4.18. The figure shows a great linear correlation between the two models as indicated by the R^2 of 0.96. The |E*|s obtained from the original Witczak model had a better correlation with measured values (R^2=0.845) than those from the modified Witczak model (R^2=0.8166) The |E*|s estimated using the modified Witczak model were greater than the values obtained from the original Witczak model at the higher and lower end of the correlation curve. However, the advantage of using the modified Witczak model is that the modified model is a G*-based model, and G* is currently used in the binder PG system.
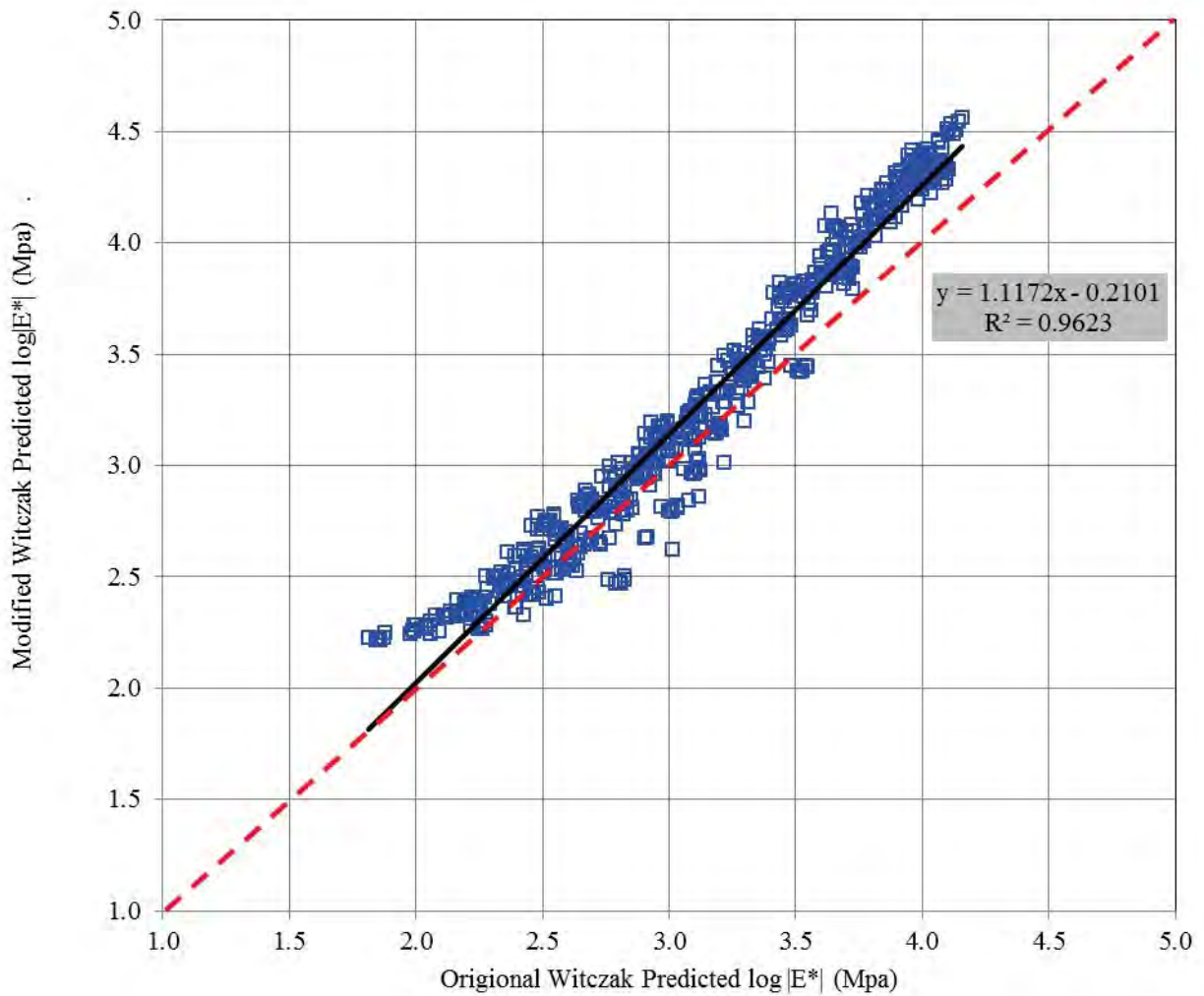
Figure 4.18 Predicted vs. measured |E*| (original vs. modified Witczak model, Level 3)

The Level 3 verification was also conducted for the Hirsch model. The |G*| of the asphalt binder was estimated using equations provided in the modified Witczak model (Eqs. 4.1 to 4.15). The results are summarized in Figure 4.19. Similar results were reported by Dongre et al. (2005) and Garcia and Thompson (2007). The R^2 of correlation between measured and predicted log(|E*|) was 0.79—lower than that of both versions of Witczak models. The model underestimated |E*| at higher loading frequency and lower temperature, and overestimated |E*| at lower frequency and higher temperature. In addition, a wide, flat bottom line can be observed from Figure 4.19, indicating a minimum value existed in the Hirsch model. Appendix D contains detailed mix results.
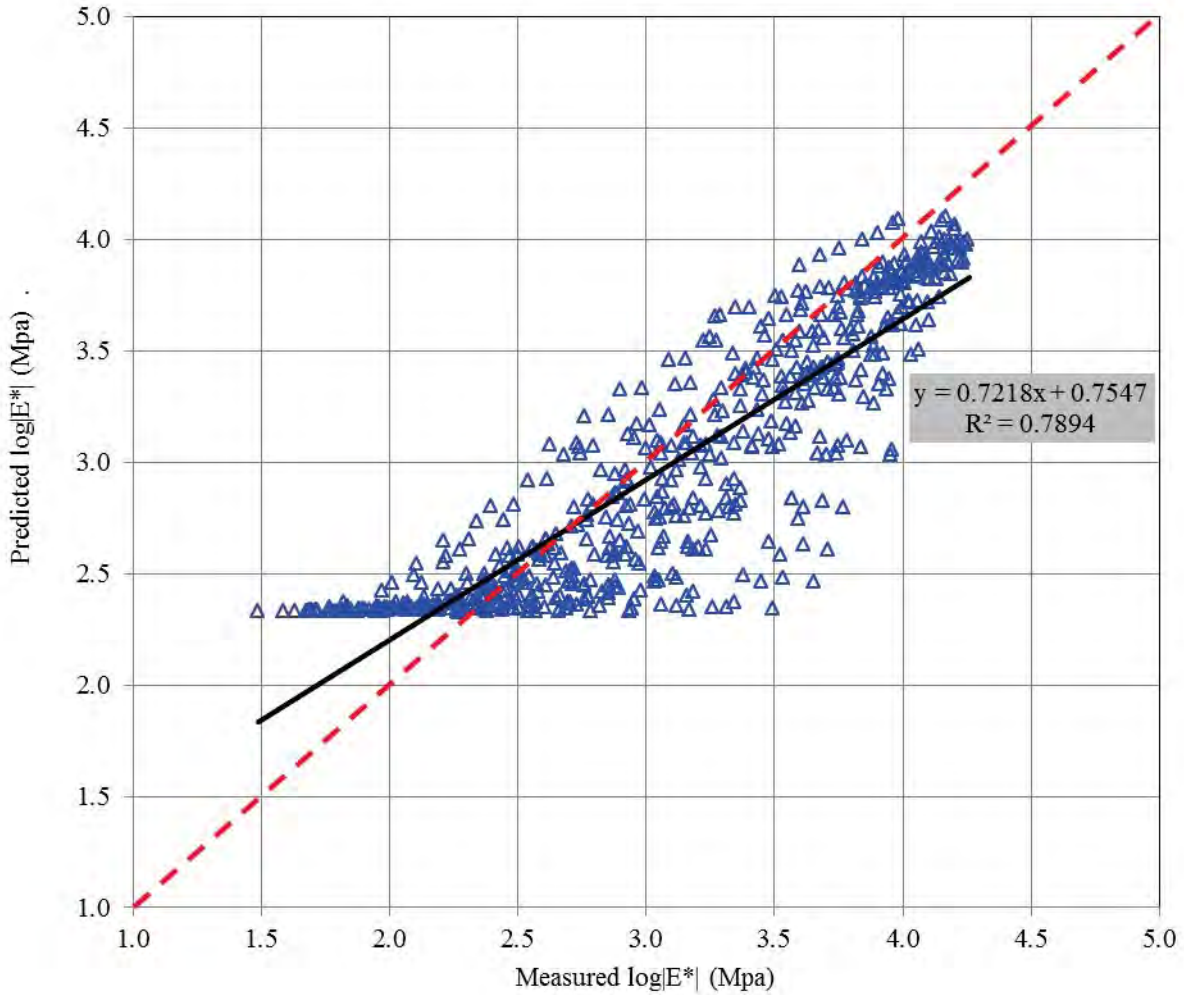
Figure 4.19 Predicted vs. measured |E*| (Hirsch model, Level 3)

Error Analysis for Level 3 Predictions

Error analysis was performed for verification of Level 3. The error was defined as the difference between the log value of predicted and measured |E*|, as shown in Eq. 4.13. The effects of variables in the predictive equations, such as |G*|, δ, V_a, VMA, etc., on the errors were investigated. The effects were graphically examined by plotting errors against parameters. The error plots were also made for log(f), Va, V_{beff}, and percentage passing the ⅜″ and #4 sieves. The error plots are summarized in Appendix E. Figure 4.20 illustrates the errors versus log(η) and percentage passing the #200 sieve for the original Witczak model. Figure 4.20b shows that as the percentage passing the #200 sieve increased, the error decreased.

$$Error = \log(Predicted\_|E*|) - \log(Measured\_|E*|) \tag{4.13}$$

58

a) Error vs. log(η)
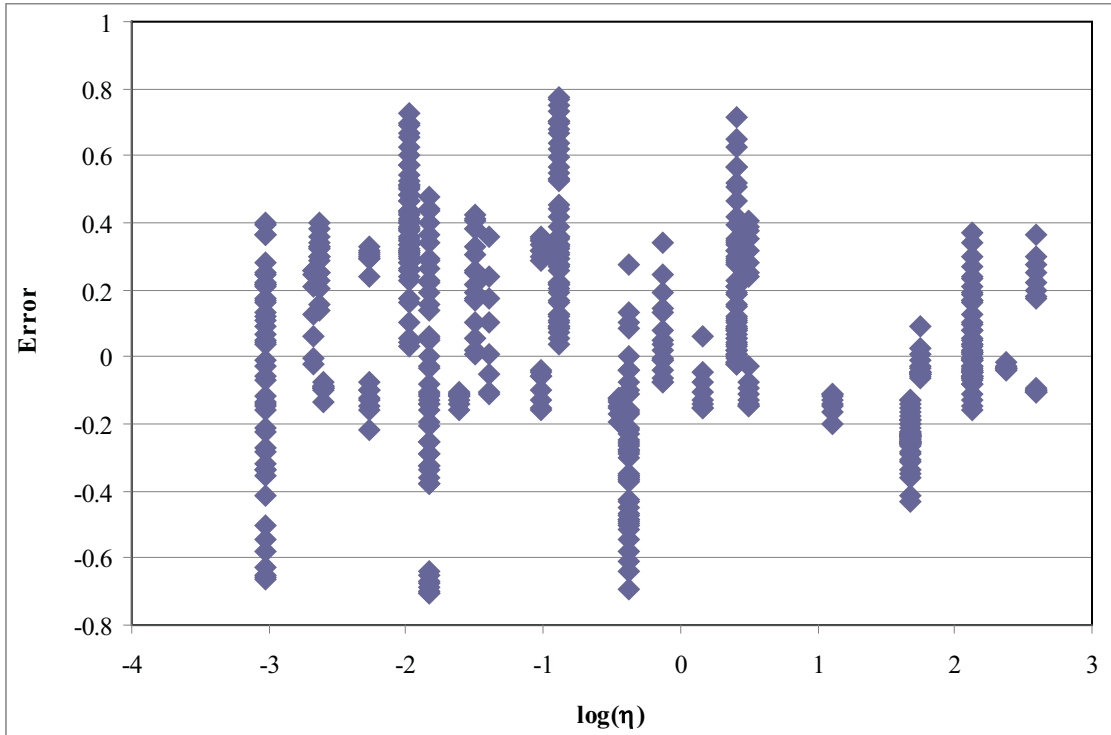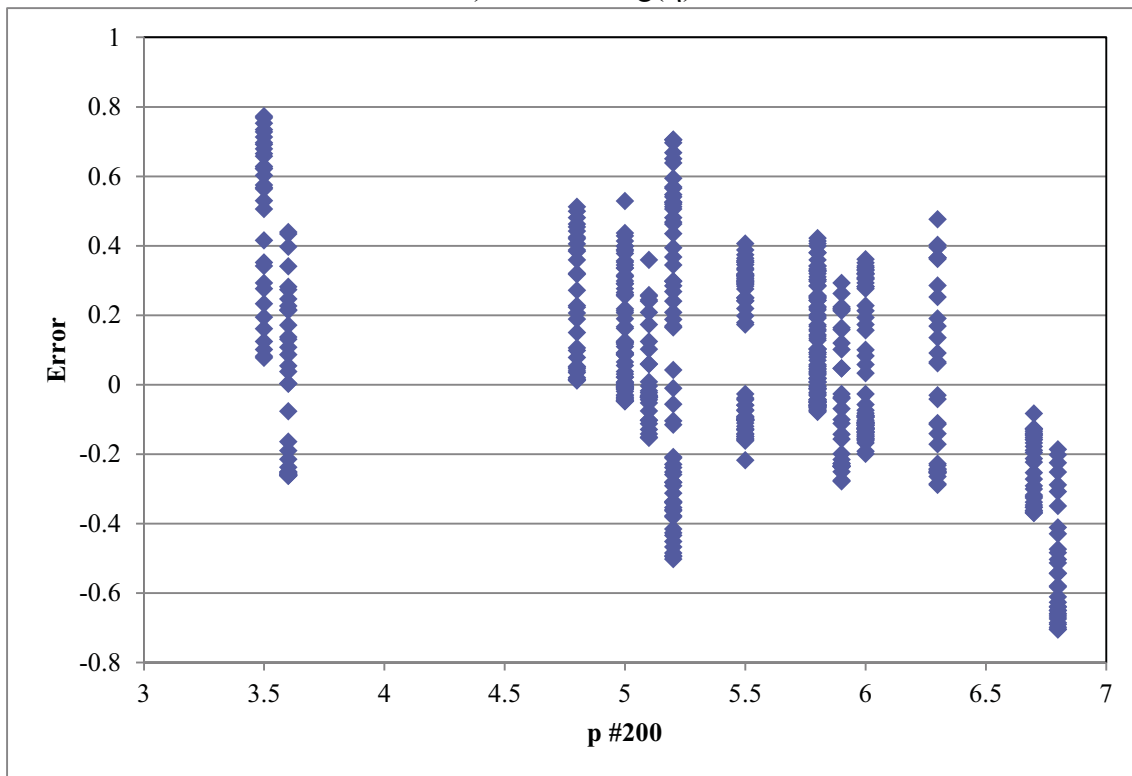
b) Error vs. percentage passing #200 sieve

Figure 4.20 Error analysis for original Witczak model – Level 3

A regression analysis was conducted to statistically examine the significance of influence on error caused by each variable. To avoid multicollinearity during the regression, which would cause considerable bias in determining the significance of the individual variable, correlations between variables were examined; the results are listed in Table 4.5. The results indicate that the percentages passing the ⅜″ sieve and #4 sieve were highly correlated to each other (R^2=0.76). Therefore, the percentage passing the ⅜″ sieve was eliminated, and the final linear regression model is expressed by Eq. 4.14.

Table 4.5 Correlations among variables used in the predictive models

	$log(\eta)$	$log(f)$	V_a	V_{beff}	$p_{⅜″}$	$p_{#4}$	$p_{#200}$
$log(\eta)$	1.0000						
$log(f)$	0.0000	1.0000					
V_a	-0.0077	0.0000	1.0000				
V_{beff}	0.0627	0.0000	0.2638	1.0000			
$p_{⅜″}$	0.0753	0.0000	-0.3119	0.3581	1.0000		
$p_{#4}$	0.0403	0.0000	-0.3805	0.2239	0.7595	1.0000	
$p_{#200}$	-0.0805	0.0000	-0.3321	-0.3198	-0.3215	-0.0365	1.0000

$$Error = A + B \cdot log(\eta) + C \cdot log(f) + D \cdot V_a + E \cdot V_{beff} + F \cdot P_{#4} + G \cdot P_{#200} + \delta \qquad (4.14)$$

The regression analysis was conducted at a 95% confidence level, and the results are summarized in Table 4.6. The P-value is used to determine if the variable has an effect on the errors of |E*|. In a 95% confidence level analysis, a P-value that is smaller than 0.05 means that, the associated variable has an effect; that is, the coefficient of the associated variable does not equal "zero." Note in Table 4.6 that all the P-values are much smaller than 0.05, indicating that all the variables had effects on the errors of |E*|. The coefficient of variable (does not include the intercept) is the slop associated with the variable, and the bigger value indicates the greater effect. The coefficients listed in Table 4.6 show that air void content and percentage passing the #200 sieve had the greatest effects among all variables.

Table 4.6 Summary of regression analysis (original Witczak model) – Level 3

	Coefficients	P-value	Lower 95%	Upper 95%
Intercept	2.3299	4.2121E-18	1.8190	2.8409
$log(\eta)$	-0.0382	2.5592E-11	-0.0492	-0.0272
$log(f)$	-0.0642	1.8875E-07	-0.0881	-0.0403
V_a	-0.2816	4.3458E-12	-0.3599	-0.2034
V_{beff}	0.0439	7.4129E-04	0.0185	0.0693
$p_{#4}$	-0.0134	2.2958E-07	-0.0185	-0.0084
$p_{#200}$	-0.1907	3.6748E-45	-0.2151	-0.1664

Using the same methodology, error analysis was performed for the modified Witczak model Level 3. The effects of variables (i.e., log(G*), Va, V_{beff}, and percentage passing the ⅜″, #4, and #200 sieves) were investigated. Figure 4.21 shows the plot of error versus log(G*) and percentage passing the #200 sieve. The error plots for Va, V_{beff}, and percentage passing the ⅜″ and #4 sieves are summarized in Appendix E. Figure 4.21a shows that as log(G*) increased, the variation of error decreased. Figure 4.21b shows that as the percentage passing the #200 sieve decreased the error decreased and moves from a positive domain to a negative domain.

The model used for regression analysis is expressed by Eq. 4.15. The variable of percentage passing the ⅜″ sieve was eliminated to avoid the multicollinearity, which causes basis on judging the significance of variables. The results are summarized in Table 4.7. All the *P*-values are smaller than 0.05, indicating that all variables affect the error of prediction. Among all variables, the log(δ) mostly influences the error indicated by the greatest value of coefficient.

$$Error = A + B \cdot \log(G^*) + C \cdot \log(\delta) + D \cdot V_a + E \cdot V_{veff} + F \cdot P_{\#4} + G \cdot P_{\#200} + \delta \qquad (4.15)$$
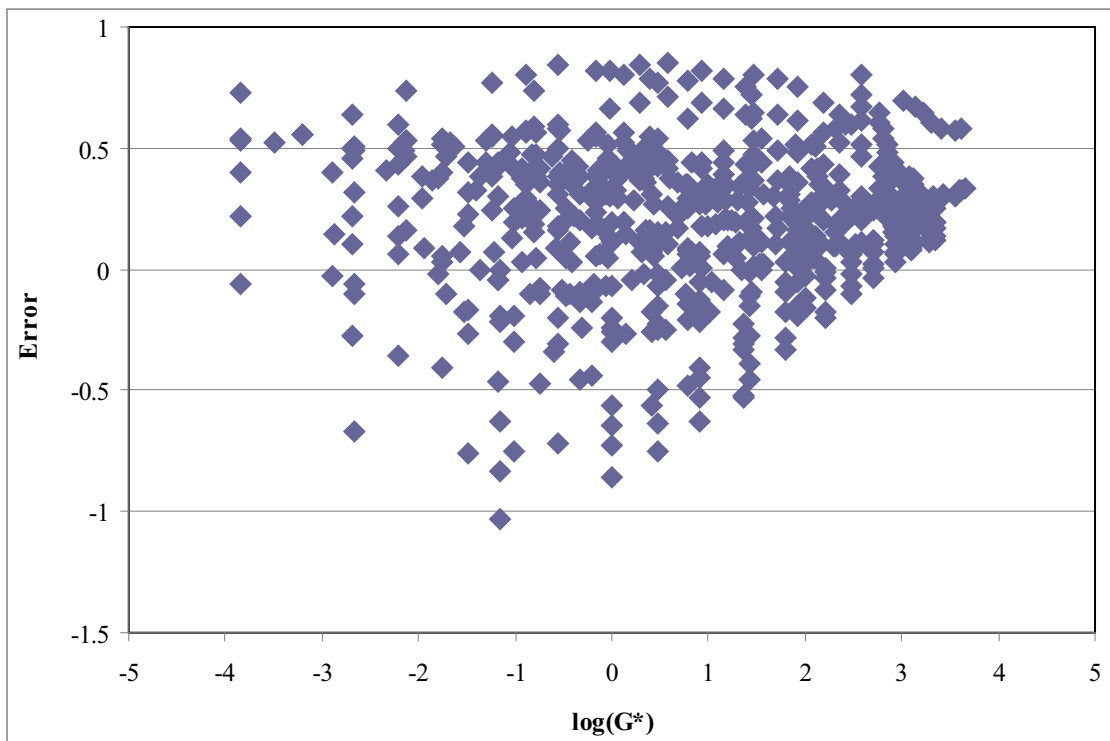
a) Error vs. log(G*)
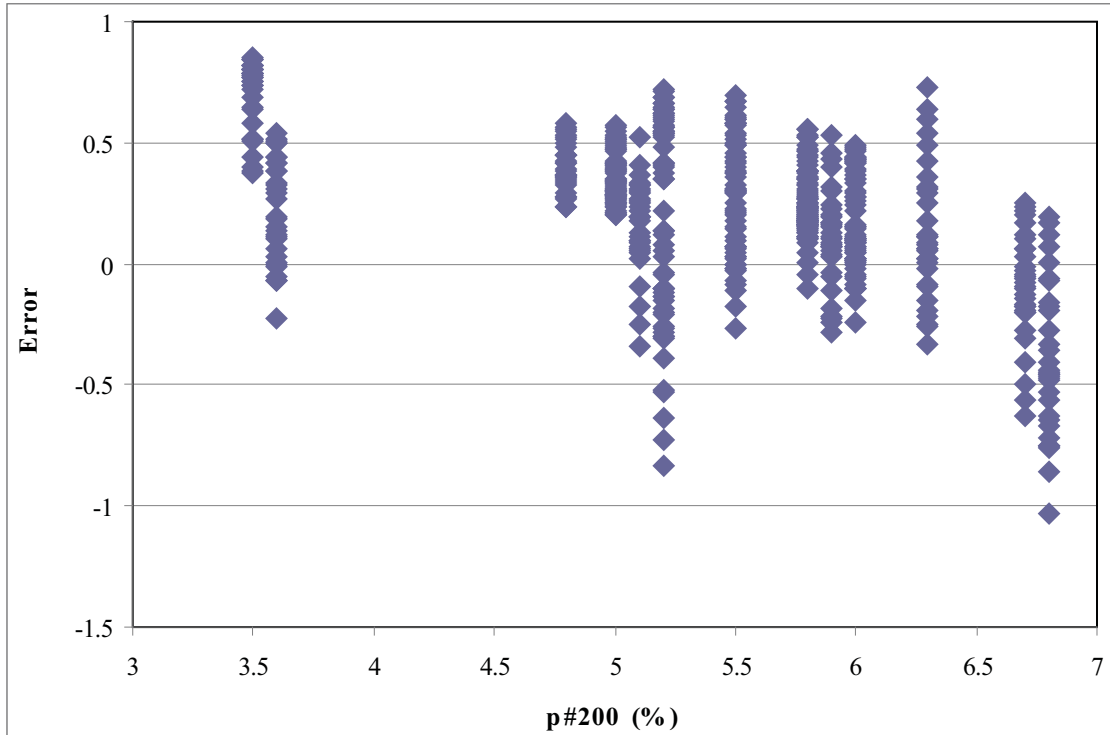
b) Error vs. P#200

Figure 4.21 Error analysis for the modified Witczak model

Table 4.7 Summary of regression analysis (modified Witczak model) – Level 3

	Coefficients	P-value	Lower 95%	Upper 95%
Intercept	3.8363	6.2696E-24	3.1212	4.5515
log (G*)	-0.0496	1.3786E-07	-0.0678	-0.0313
Log(δ)	-0.8691	2.6257E-11	-1.1203	-0.6178
V_a	-0.2514	5.5038E-09	-0.3348	-0.1679
V_{beff}	0.0424	2.1749E-03	0.0154	0.0695
p #4	-0.0079	4.0316E-03	-0.0133	-0.0025
p #200	-0.1981	2.7801E-43	-0.2241	-0.1721

The error plot of log(G*) for the Hirsch model Level 3 is shown in Figure 4.22. The variation of error reduced as log(G*) increased. The error plots of VMA and VFA are listed in Appendix E. The regression equation used for error in the Hirsch model is shown in Eq. 4.16. The findings (Table 4.8) obtained from regression analysis confirmed the observation from graphical analysis, that variables did not have any obvious effects on the error. The P-value of the VFA indicated that VFA is not a significant factor for the error of prediction. Even though the P-values of log(G*) and VMA were smaller than 0.05, the absolute values of associated coefficients were close to "zero," indicating weak effects.

$$Error = A + B \cdot \log(G^*) + C \cdot VFA + D \cdot VMA + \delta \qquad (4.16)$$
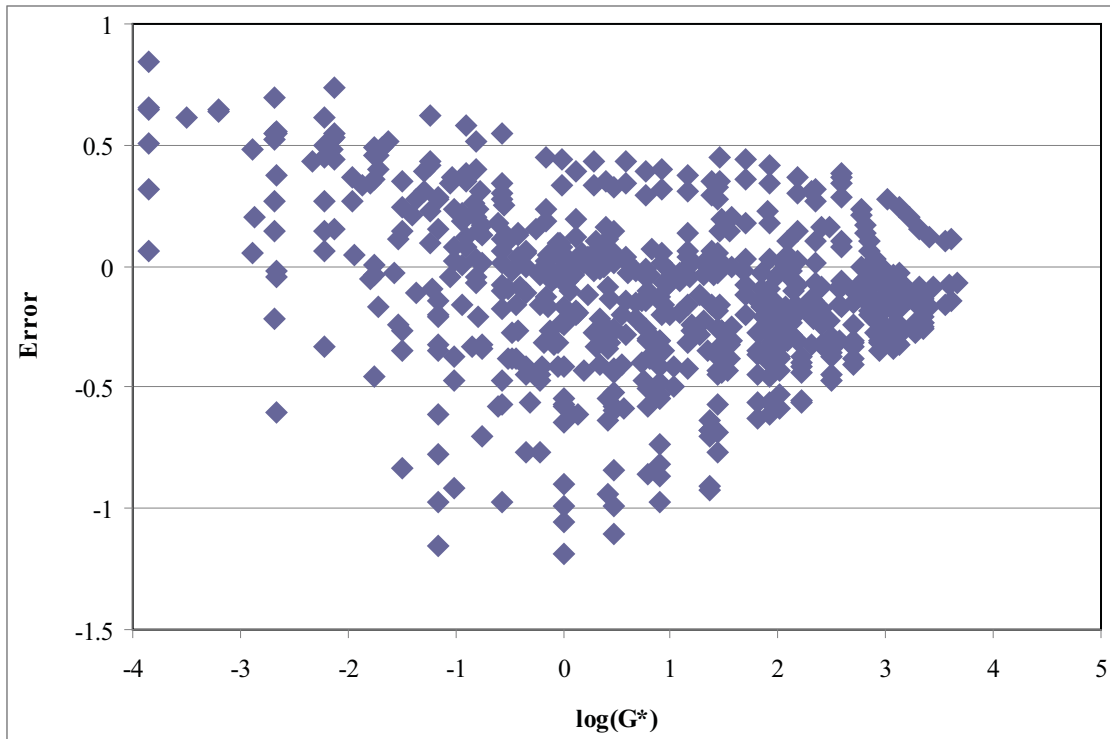
Figure 4.22 Error analysis for Hirsh model (error vs. log(G*)) – Level 3

Table 4.8 Summary of regression analysis (Hirsch model) – Level 3

	Coefficients	*P-value*	*Lower 95%*	*Upper 95%*
Intercept	-0.6538	2.9442E-01	-1.8777	0.5700
log (G)*	-0.0602	9.8229E-12	-0.0771	-0.0432
VFA	-0.0040	6.3387E-01	-0.0205	0.0125
VMA	0.0603	7.8433E-04	0.0252	0.0953

4.2 Flow Number (F_N) and Flow Time (F_T) Tests

The F_N and F_T tests were performed to evaluate the rutting resistance of HMA collected from 19 sources. The testing results were also used to investigate the correlations between F_N/F_T and rutting depth measured from an APA. The correlation analysis is presented at the end of this chapter.

Flow number and flow time tests can be performed with or without confining pressure. The application of confining pressure simulates the real stress conditions of field pavement, and the results correlate to field distress observation better than the non-confined flow test (Brown et al., 2009). In this study, confined flow tests were performed on 2 mixes: the Anchorage

International Airport project (AIA) and the Parks Highway project (N). However, specimens tested under confining pressures did not fail (break) during the 10,000 cycles (second) of loading time, and the correct F_N and F_T could not be calculated. The remaining 17 mixes were tested without confining pressure.

Figure 4.23 presents the F_T of unconfined tests. The results were grouped according to the mix design method; the F_Ts of most mixes were less than 50. The maximum F_T was observed for mixtures collected from the Dalton Highway project (DH in the figure). The results of F_N tests are plotted in Figure 4.24. Flow numbers of mixtures designed according to the Marshall method were less than 400 and among these mixtures. Maximum F_Ns were also obtained from the Dalton Highway project (DH in the figure). Flow numbers of mixtures designed according to the Superpave method clearly were higher than the mixtures designed by the Marshall method. During the mix design process, a higher compaction effort was used in the Superpave mix design. Based on the specimen fabrication experience from this study, approximately 20 SGC gyrations provided the same compaction effort as produced by 75 Marshall hammer blows. In other words, for the same asphalt mixture, 20 SGC gyrations and 75 Marshall hammer blows produced specimens with the same bulk specific gravity (G_{mb}) and air voids. During the Superpave mix design, 75 gyrations were applied for each specimen. High compaction effort leads to better rutting resistance.
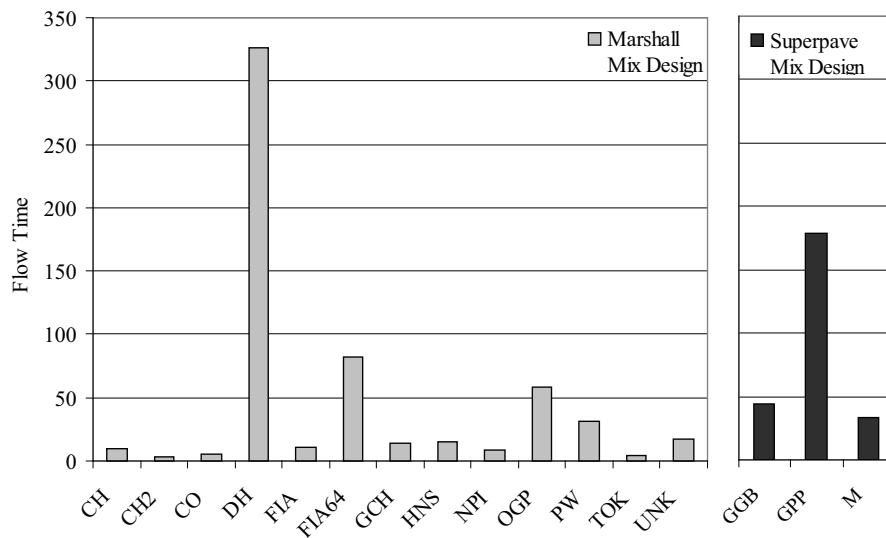
Figure 4.23 Summary of flow time (unconfined test)
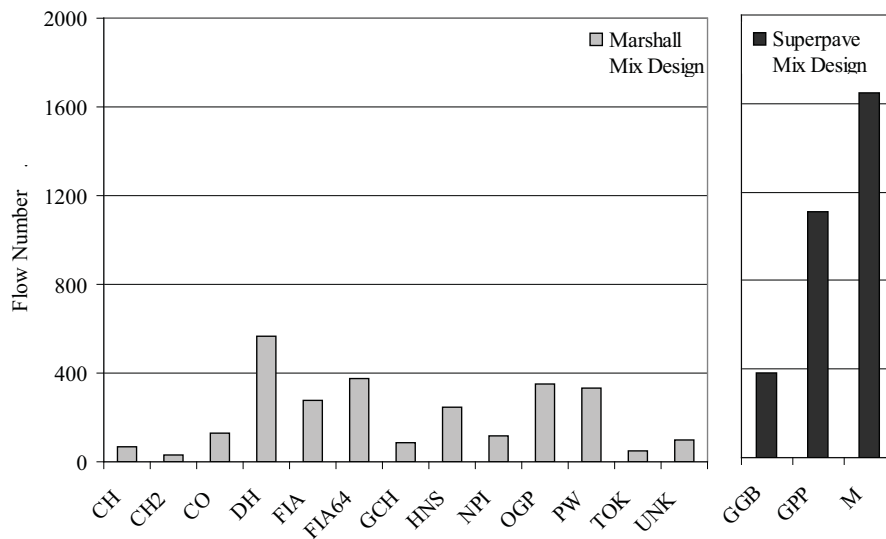
Figure 4.24 Summary of flow number (unconfined test)

Statistical analysis was performed to investigate the influencing factors of F_N/F_T. The potential influencing factors considered were design method, higher end of PG (PG H), lower end of PG (PG L), binder content, air voids, VFA, VMA, and gradation. The correlation between each potential factor and F_N was calculated. The correlation is represented by a value between -100% and 100%. A higher positive value indicates a stronger positive correlation; a lower negative value indicates a stronger negative correlation. The correlations between potential influencing factors and F_T are summarized in Figure 4.25. The plot indicated that temperature at the low end of PG correlated well with F_T, the correlation was about 70%. A good correlation was also observed on VFA with the value of 50%.

The correlations between potential influencing factors and F_N are summarized in Figure 4.26. The results indicate that F_N correlates well with the mix design method and temperatures at the higher and lower end of the PG. In addition, F_N negatively correlates with the percentage passing of all sieve sizes, but the corelation is not strong. The lower percentage passing of sieves means a coarser gradation. This might indicate that mixtures with coarse gradation would have higher F_N.
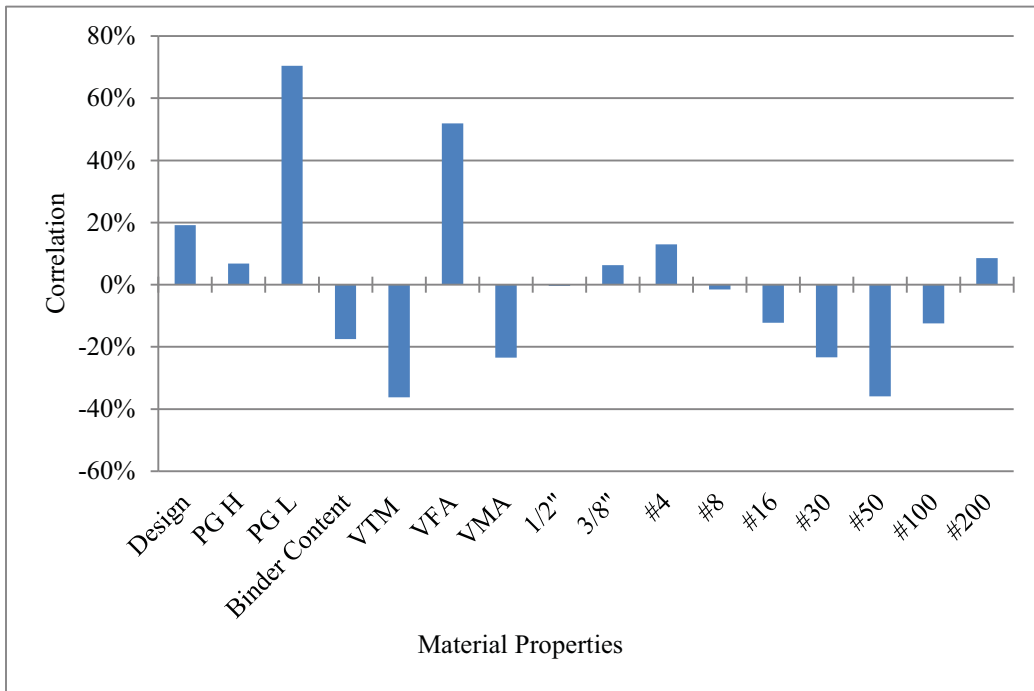
Figure 4.25 Correlations between influencing factors and flow time
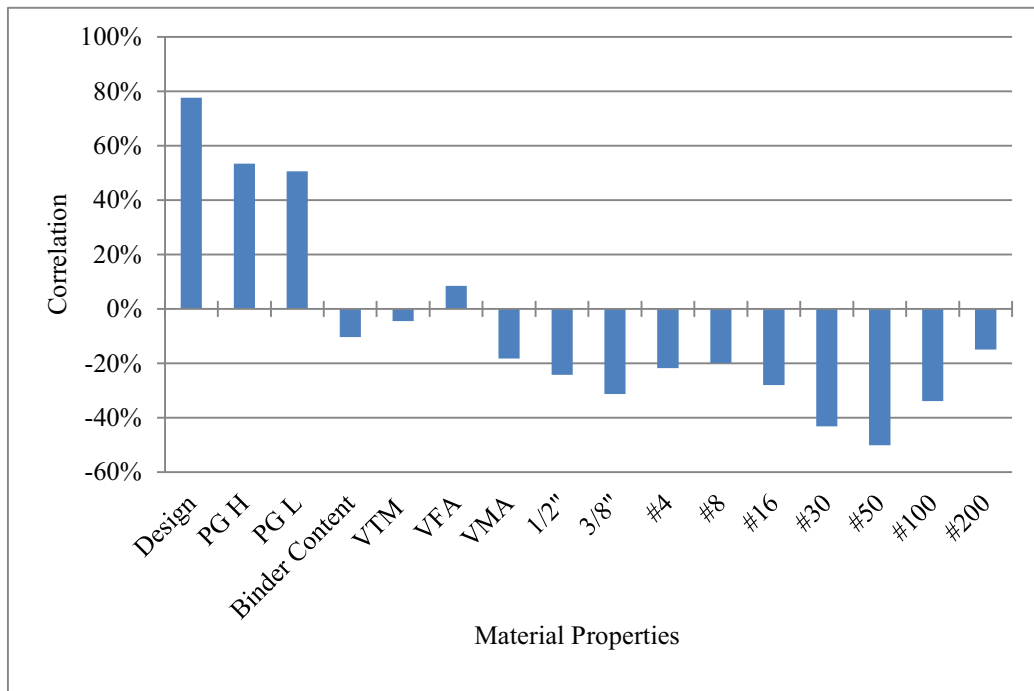
Figure 4.26 Correlations between influencing factors and flow number

4.3 Laboratory Rutting Test

Figure 4.27 shows the APA rutting depth test results of different mixtures. Note that 11 out of 21 mixtures had a final rutting depth of less than 6 mm. The M mixture had the lowest rutting depth, followed by FIA, GPP, PSG, AIA, GGB, FIA64, CH, DH, PW, and HNS.
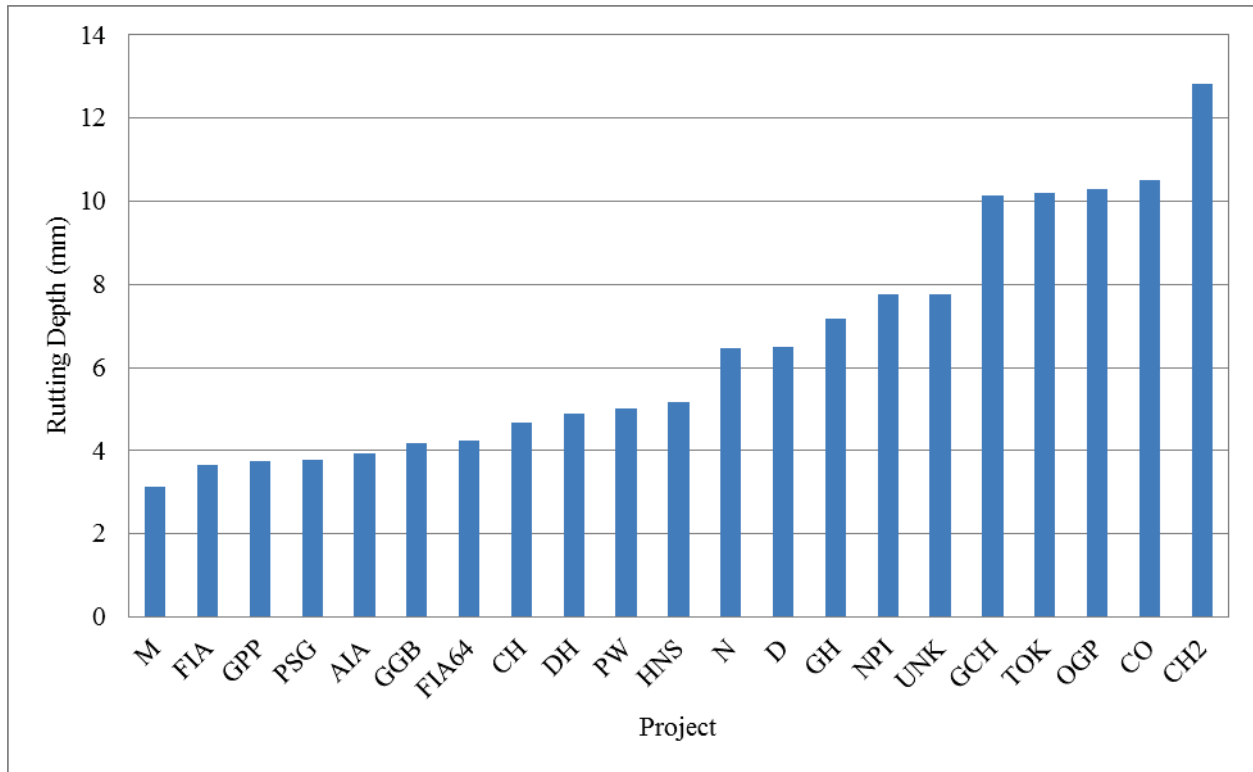
Figure 4.27 APA rutting depth test results for different mixtures

The binder and aggregate gradation information of those mixtures collected from the plant were used for influence analysis. The multiple regression model, as shown in Eq. 4.17, was built to analyze the influence of different factors (X_i) on rutting depth (Y). The parameters were estimated by the ordinal least square method.

$$Y = \beta_0 + \beta_1 X_1 + \cdots + \beta_i X_i + \cdots + \beta_k X_k + \varepsilon \tag{4.17}$$

where

$\beta_0, \beta_1, \ldots, \beta_i, \ldots, \beta_k$ = partial regression coefficients or estimates of the regression parameters, β_i is the magnitude and direction change in response with each one-unit increase in predictor i, provided other predictors are held constant.

ε = random error term.

The data were examined to select potential representative independent variables. Figure 4.28 shows the scatter plot of the aggregate gradation data. Note that there are two groups of correlations among the passing percentages of different sieves. One group is the correlation among the sieves that ranged from ½″ to #50. The other group is the correlation among #100, #200, and the dust-to-asphalt ratio. Thus, two variables—the passing percent of ½″ and the dust-to-asphalt ratio—were included in the multiple regression analysis as indicators of aggregate gradation. The passing percent of ½″ indicates the skeleton of the aggregate gradation, whereas the dust-to-asphalt ratio indicates the mineral filler content.
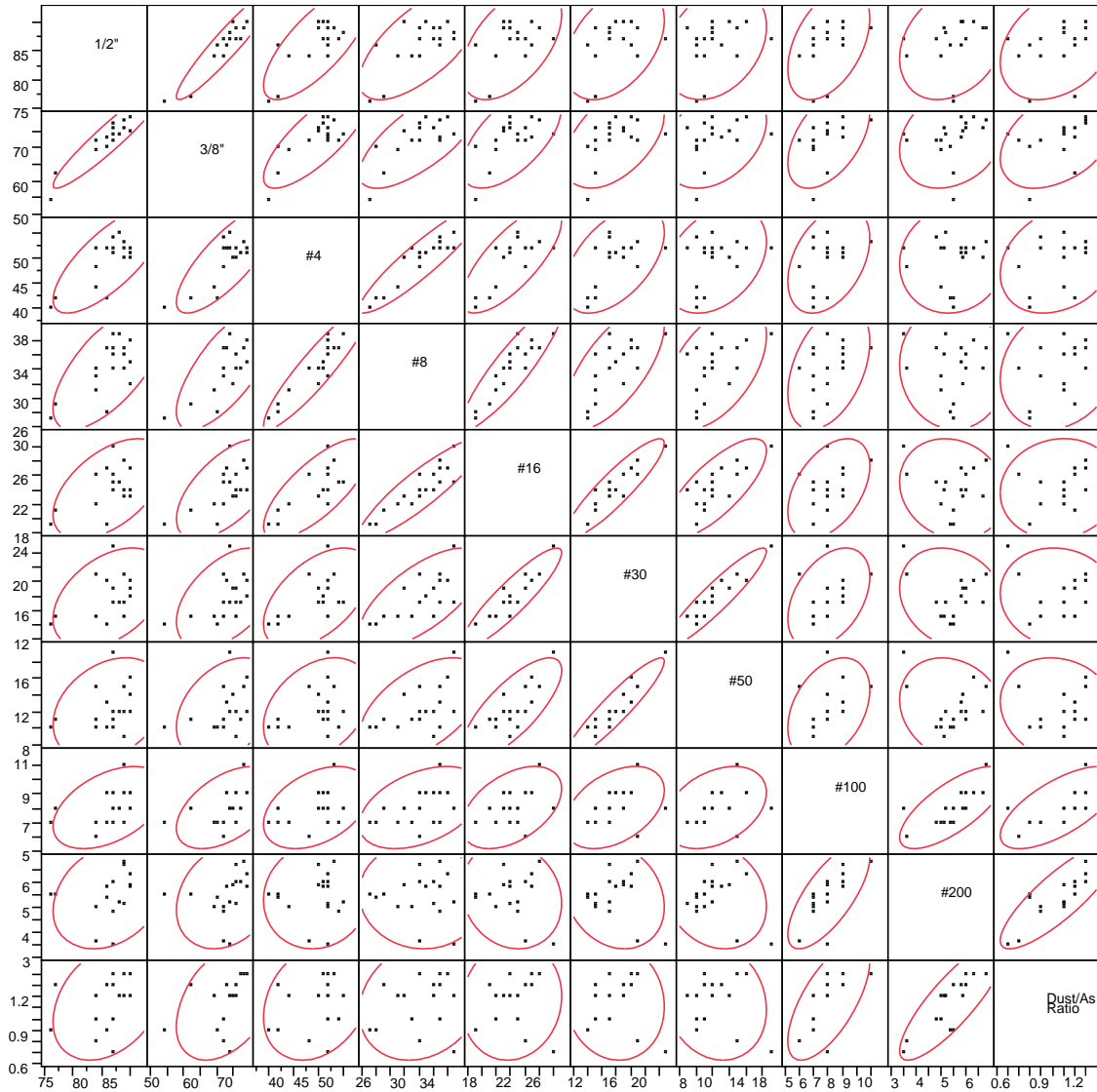
Figure 4.28 Scatter plots of aggregate gradation data of the mixtures

Figure 4.29 show the scatter plot of other potential factors. Note that clear correlations exist among the binder content, VFA and VMA. In addition, VFA and VMA also correlate with

VA and a passing percent of ½″ sieve. The VFA, VA, and VMA were not included in the multiple regression analysis. In total, seven independent variables were included in the multiple regression analysis. Figure 4.30 shows the distribution of the dependent and independent variables.
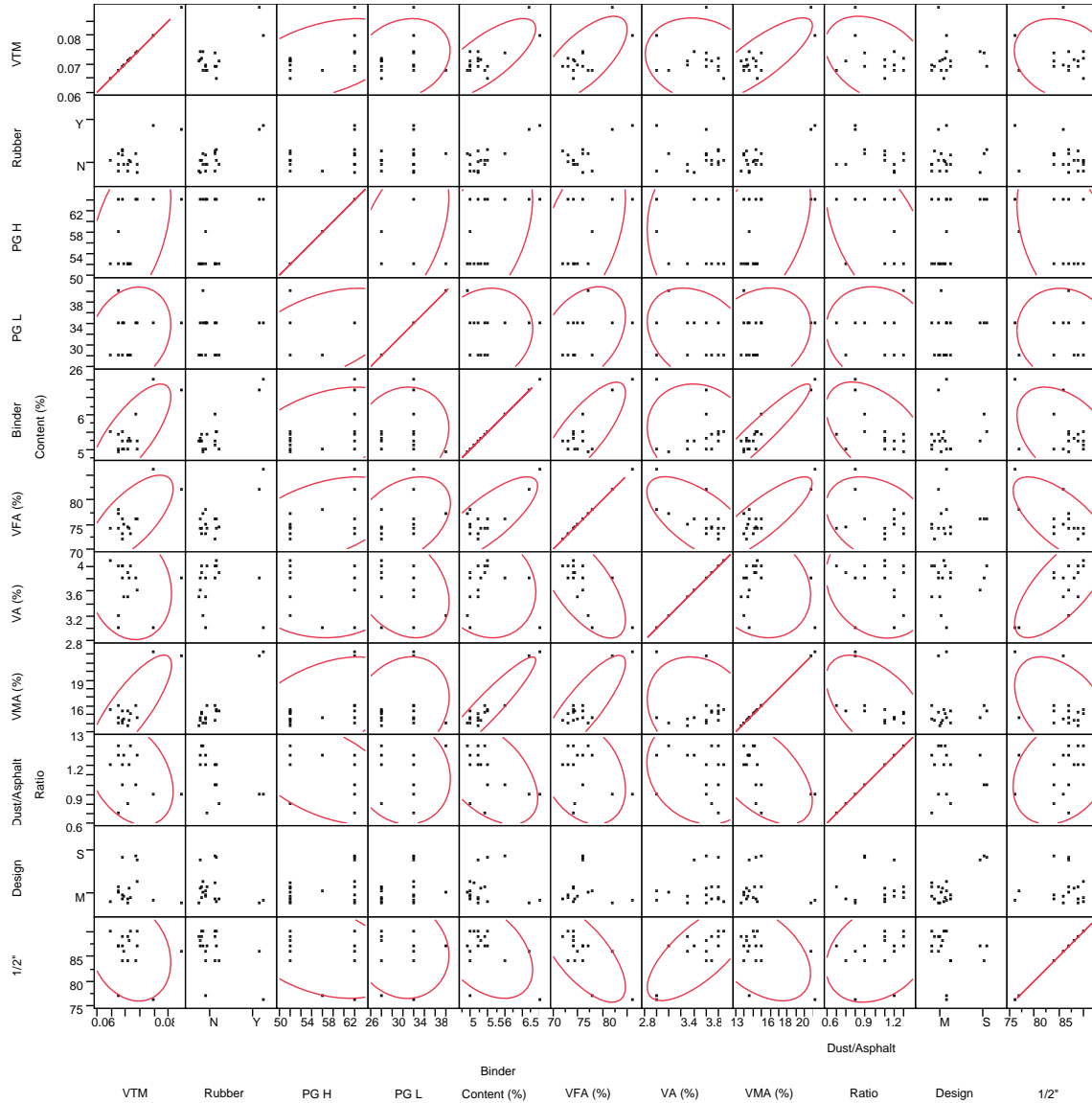
Figure 4.29 Scatter plots of other independent variables

(a) Depth (mm)

(b) VTM

(c) Binder content (%)

(d) High temperature grade

(e) Low temperature grade

(f) Dust/asphalt ratio

(f) ½″

(g) Design

(h) Rubber
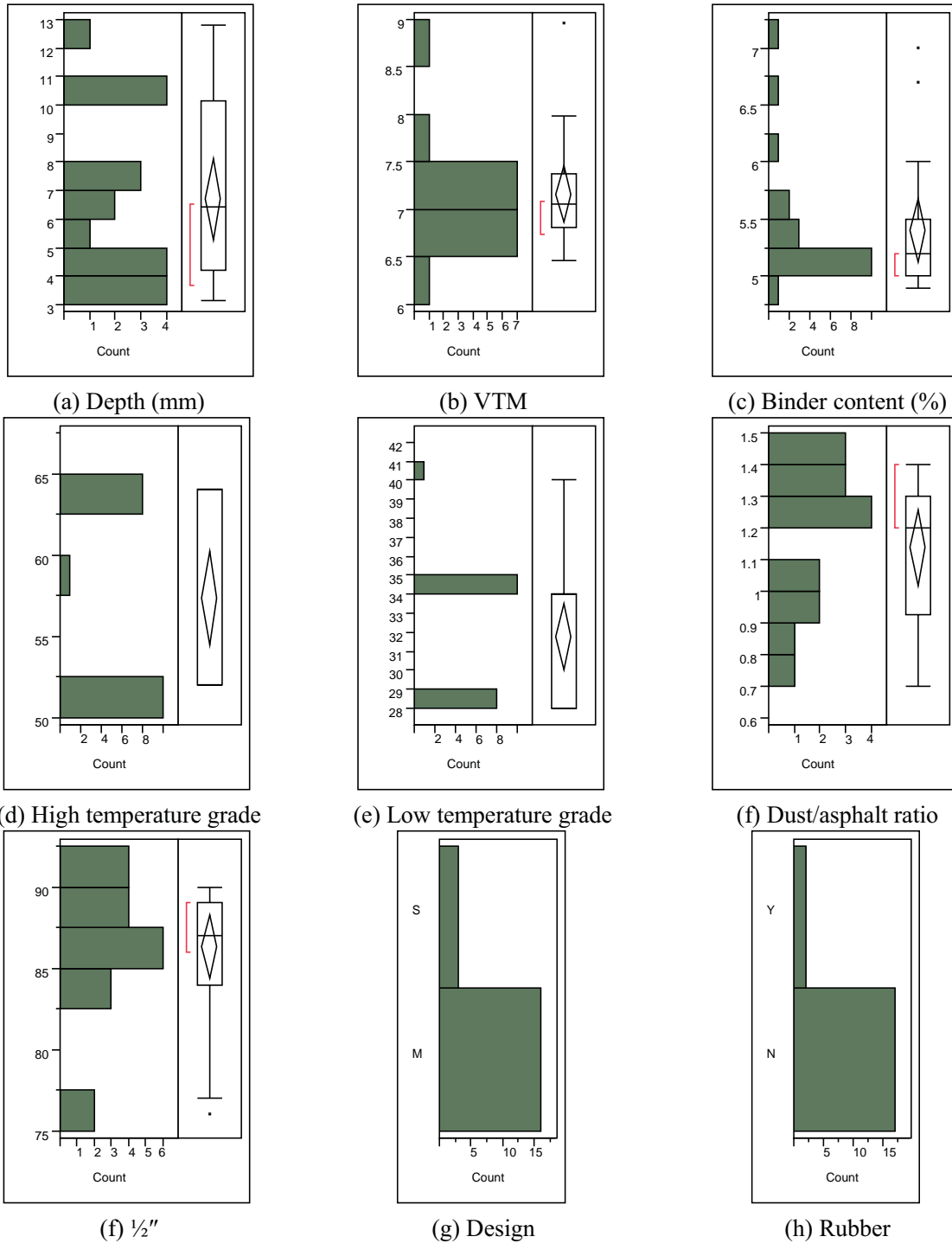
Figure 4.30 Distribution of the dependent and independent variables

Figure 4.31 shows the multiple model including all seven factors. The partial t-test results are presented to show the significance of each predictor by testing the significant increase in explained variation by adding that predictor to the reduced model. The null hypothesis of the partial t-tests is H$_0$: $\beta_i = 0 \mid \beta_0, \beta_1, \ldots, \beta_{i-1}, \beta_{i+1}, \ldots, \beta_k$. The significance level was 0.05, meaning

70

that the probability of getting this result by chance is less than 5%. Note that not all the factors were significant. Potential significant factors included the binder's PG, dust-to-asphalt ratio, and percentage passing the ½″ sieve, whose *p*-values were lower or close to 0.05. The insignificant factors were then dropped to build a new model. As the number of factors in the model changed, the *p*-values of each factor changed. After several trials, a final model with only significant factors was built, as shown in Figure 4.32.
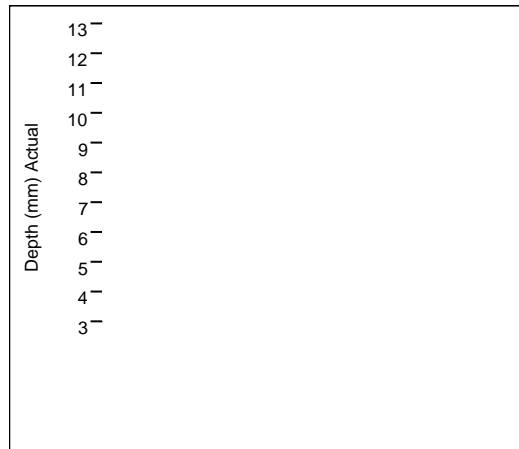
Term	Estimate	Std Error	t Ratio	P value
Intercept	8.1761484	14.27938	0.57	0.5877
VTM	-122.0665	99.10601	-1.23	0.2641
Rubber[N]	-0.558544	1.674627	-0.33	0.7501
PG H	-0.247498	0.068585	-3.61	**0.0112***
PG L	-0.375704	0.078147	-4.81	**0.0030***
Binder Content (%)	2.1315183	1.235229	1.73	0.1352
Dust/Asphalt Ratio	-3.105986	1.352835	-2.30	**0.0614***
Design[M]	0.7740454	0.54671	1.42	0.2066
½″	0.3022412	0.072972	4.14	**0.0061***

Figure 4.31 Multiple regression model for rut depth with all factors

Figure 4.32 includes the predictor profiler of the model, which shows the predicted response as one predictor is changed while the others are held constant, and thus the influence of each predictor on the response can be clearly illustrated. It can be seen that the high temperature grade of the binder and the dust/asphalt ratio were significant factors for the rutting resistance of those mixtures. The low temperature grade of the binder, incorporating crumb rubber, different design method (Marshall vs. Superpave), binder content, and percentage passing the ½″ sieve, was not significant. Mixtures with higher high-temperature grade and dust-to-asphalt ratios showed a tendency to have lower rutting depth or higher rutting resistance.
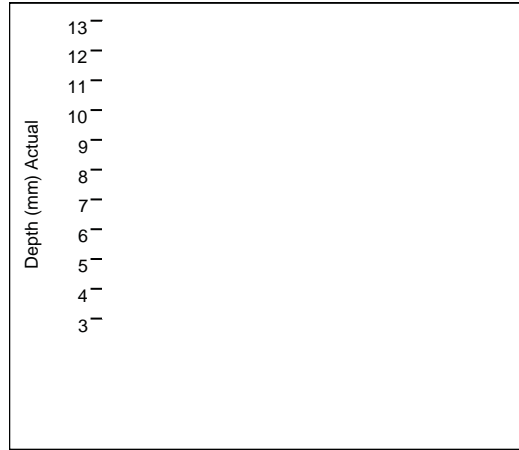
Term	Estimate	Std Error	t Ratio	Prob>|t|
Intercept	42.093762	8.049849	5.23	0.0002*
PG H	-0.454476	0.103121	-4.41	0.0007*
Dust/Asphalt Ratio	-7.865686	2.747546	-2.86	0.0133*

Prediction Profiler

Figure 4.32 Multiple regression model for rut depth with only significant factors

4.4 Correlation between Flow Time (Number) and APA Rutting Depth

In the plot of cumulative permanent strain versus the number of loading cycles from the SPT test, the "flow number" is the cycle number at which tertiary flow starts. In a typical relationship between the calculated total compliance and loading time from a triaxial static creep test, the "flow time" is defined as the starting time of tertiary deformation (Witczak et al., 2002b). The flow time indicates the beginning of shear deformation under constant volume (Bhasin et al., 2004). Figures 4.33 and 4.34 show the relationship between the test results of rutting resistance and the test results of F_N and F_T. Note that F_N correlated to rutting depth better than F_T did, as indicated by a higher R^2 value. Generally, higher rutting depth correlates with lower F_N and F_T, indicating lower rutting resistance. In addition, when F_N was greater than 400 or F_T was greater

than 40, the asphalt mixture would have good rutting resistance indicated by a rutting depth less than 5 mm. However, when F_N was less than 400 or F_T was less than 40, the results were mixed. Such mixes would have a wide range of rutting depth, between 3 and 13 mm.
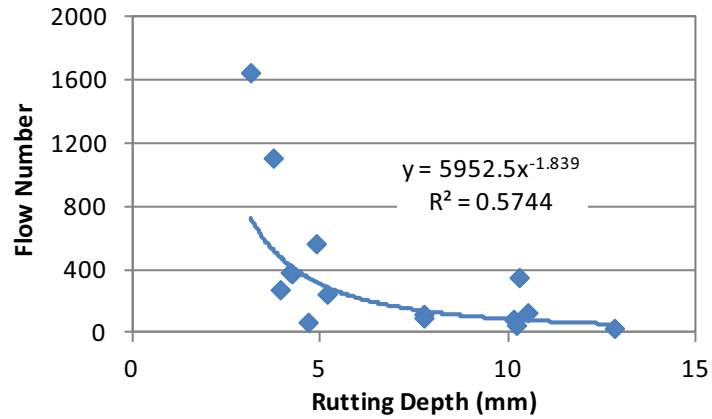

Figure 4.33 Relationship between flow number and rutting depth
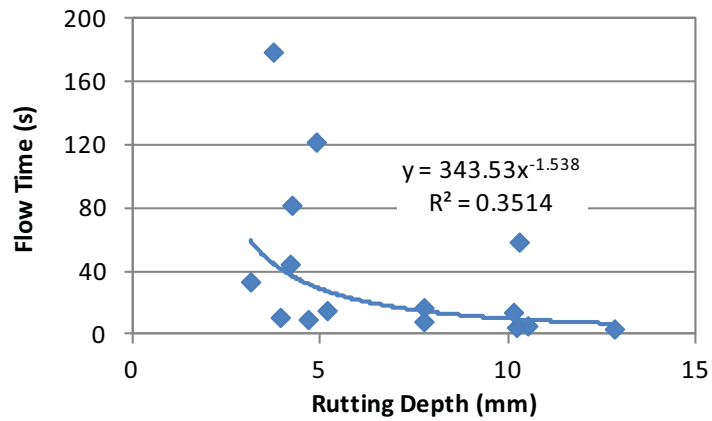
Figure 4.34 Relationship between flow time and rutting depth

CHAPTER 5 SUMMARY, CONCLUSIONS AND RECOMMENDATIONS

Summary

The focus of this study was the characterization of an Alaskan HMA mixture using the asphalt mixture performance tester (AMPT). Simple performance tests (SPT) were performed on 19 asphalt mixtures using the AMPT. Rutting depths were measured for 21 asphalt mixtures using the asphalt pavement analyzer (APA). This chapter presents the conclusions obtained from laboratory tests and data analysis, as well as recommendations

Conclusions

The dynamic modulus ($|E^*|$) was measured according to AASHTO TP62 at 4 temperatures and 8 frequencies for 19 asphalt mixtures collected from 3 ADOT&PF regions. Optimization techniques were applied to develop the master curve for each mixture. Testing results and master curve coefficients for each mixture are listed in Appendix A.

Predictive models for $|E^*|$ (i.e., Witczak model – η based, modified Witczak model – G^* based, and Hirsch model) were verified at Levels 2 and 3, as specified in the MEPDG. Because the rheological binder information collected was limited, Level 2 verifications were only performed for $|E^*|$ at a single reference temperature and loading frequency. The high temperature end of the performance grade (PG) was selected as the reference temperature for measuring G^*. The reference frequency was determined according to DSR testing at 10 Hz frequency. None of the three models accurately predicted $|E^*|$ at high temperature. Measured $|E^*|$s vary in a wider range than predicted values, indicating that predictive models are relatively insensitive to the changes of HMA volumetric properties, especially the Hirsch model, which approximately predicts the same $|E^*|$ for all mixtures at temperatures in the higher end of the PG (Figure 4.11). The Witczak model (η based) over-predicts $|E^*|$ at high temperature in most instances (Figure 4.9). Among the three predictive models, the modified Witczak model (G^* based) provided the most accurate estimation of $|E^*|$ at Level 2 input.

At Level 3 input, the most accurate estimations of $|E^*|$ were obtained from the original Witczak model (η based), and the correlation between predicted values and measured $|E^*|$ had a R^2 of 0.8435. The modified Witczak model (G^* based) and Hirsch model have R^2 values of 0.8166 and 0.7894, respectively.

The results obtained from flow tests indicated that confining pressure greatly increased F_N and F_T. To accomplish a confined flow test within 10,000 loading cycles/second, the confining pressure needs to be much less than 137 kPa or the compressive stress needs to be increased. The results also indicated that F_N correlates well with the mix design method and PG. Hot mix asphalt designed by the Superpave mix method had higher F_N values due to the higher compaction effort applied during specimen fabrication. Mixtures with coarse aggregate gradation had higher F_N values.

Measured rutting depths from APA tests at 58°C showed that 11 out of 21 mixtures had a final rutting depth of less than 6 mm. The M mixture had the lowest rutting depth, followed by FIA, GPP, PSG, AIA, GGB, FIA64, CH, DH, PW, and HNS. Through statistical analysis, it was found that the high temperature grade of the binder and the dust/asphalt ratio were significant factors in the rutting resistance of the asphalt mixtures investigated. Mixtures with higher high-temperature grades and dust/asphalt ratios tend to have lower rutting depth or higher rutting resistance.

Correlations between the F_N/F_T and rutting depth obtained from APA tests were statistically analyzed as well. Flow number correlates with rutting depth better than F_T does, as indicated by a higher R^2 value. Generally, higher rutting depth correlates with lower F_N and F_T. In addition, when F_N is greater than 400 or when F_T is greater than 40, the asphalt mixture has good rutting resistance, as indicated by a rutting depth less than 5 mm. However, when F_N is less than 400 or when F_T is less than 40, the results are mixed. Such mixes had a wide range of rutting depth, between 3 and 13 mm.

Recommendations

A preliminary local database was developed, which contains measured |E*| and regression coefficients of the master curve for typical Alaskan HMA mixtures. The database can be used for further implementation of |E*| into an Alaskan flexible pavement design or adoption of the MEPDG. If measured G* is available for Level 2 input, the modified Witczak model (G* based) is recommended for predicting |E*| of the asphalt mixture in the MEPDG. If default inputs of binder properties, which are based on PG, are used (Level 3 input according to the MEPDG), the Witczak model (η based) is recommended.

Alternatively, if any mixture collected in this study is close to the mixture that will be used in a future paving project, field engineers could directly choose a measured |E*| or master curve coefficient from the Appendix. The input can be implemented through Level 1 input in the MEPDG.

To increase rutting resistance, the Superpave mix design method and a binder that has a higher high-temperature grade are recommended. Additional cautions should be taken when using a higher dust/asphalt ratio and coarse gradation to increase rutting resistance, because extreme values would sacrifice the water susceptibility and cracking resistance of HMA. Flow number is recommended when characterizing the rutting resistance of HMA among SPTs, because F_N has a higher correlation to rutting depth than F_T has. However, when F_N is less than 400, the indication of rutting resistance becomes insignificant.

REFERENCES

AASHTO, 2008. "Determining Dynamic Modulus of Hot Mix Asphalt Concrete Mixtures, TP 62-07." Washington, DC.

AASHTO T342-11, 2011. "Standard Method of Test for Determining Dynamic Modulus of Hot-Mix Asphalt Concrete Mixtures." Washington, DC.

Ahmed, M.J., 2007. "Analysis of Rutting for Anchorage Pavements." Master's thesis, University of Alaska Fairbanks, Fairbanks, AK.

Al-Khateeb, G., Shenoy, A., Gibson, N., and Harman, T., 2006. "A new simplistic model for dynamic modulus." *Journal of the Association of Asphalt Paving Technologists*, 75: 1254–1293.

Apeagyei, A.K., 2011. "Rutting as a function of dynamic modulus and gradation." *Journal of Materials in Civil Engineering,* 23(9).

Apeagyei, A.K., and Diefenderfer, S.D., 2011. "Asphalt Material Design Inputs for Use with the Mechanistic-Empirical Pavement Design Guide in Virginia." FHWA/VCTIR 12-R6.

ARA, Inc., ERES Consultants Division, 2004. "Guide for Mechanistic-Empirical Design of New and Rehabilitated Pavement Structures." Final Report.

Archilla, A.R., and Diaz, L.G., 2008. "Using permanent deformation tests and the MEPDG to quantify permanent deformation improvements from modified binders (with discussion)." *Journal of the Association of Asphalt Paving Technologists*, 77.

Azari, H., Al-Khateeb, G., Shenoy, A., and Gibson, H., 2007. "Comparison of simple performance test |E*| of accelerated loading facility mixtures and prediction |E*|: Use of NCHRP 1-37A and Witczak's new equations." *Transportation Research Record: Journal of the Transportation Research Board*, Issue 1998.

Bari, J., 2005. "Development of a New Revised Version of the Witczak E* Predictive Models for Hot Mix Asphalt Mixtures." Ph.D. Dissertation, Arizona State University, Phoenix, AZ.

Bari, J., and Witczak, M.W., 2006. "Development of a new revised version of the Witczak E* predictive model for hot mix asphalt mixtures." *Journal of the Association of Asphalt Paving Technologists*, 75: 381–423.

Bausano, J., and Williams, R.C., 2009. "Transitioning from AASHTO T283 to the simple performance test using moisture conditioning." *Journal of Materials in Civil Engineering*, 21(2).

Bausano, J., Kvasnak, A., and Williams, R.C., 2006. "Development of Simple Performance Tests Using Laboratory Test Procedures to Illustrate the Effects of Moisture Damage on Hot Mix Asphalt." RC-1521, Federal Highway Administration, Washington, DC.

Bhasin, A., Button, J.W., and Chowdhury, A., 2004. "Evaluation of simple performance tests on hot-mix asphalt mixtures from South Central United States." *Transportation Research Record: Journal of the Transportation Research Board*, Issue 1891: 174–181.

Bhasin, A., Button, J.W., and Chowdhury, A., 2005. "Evaluation of Selected Laboratory Procedures and Development of Databases for HMA." FHWA/TX-05/0-4203-3 Texas Department of Transportation, Texas Transportation Institute.

Biligiri, K.P., Kaloush, K.E., Mamlouk, M.S., and Witczak, M.W., 2007. "Rational modeling of tertiary flow for asphalt mixtures." *Transportation Research Record: Journal of the Transportation Research Board*, Issue 2001.

Blankenship, P.B., and Anderson, R.M., 2010. "Laboratory Investigation of HMA modulus, flow number and flexural fatigue on samples of varying density." *Journal of the Association of Asphalt Paving Technologists*, 79.

Bonaquist, R., 2008. "Refining the Simple Performance Tester for Use in Routine Practice." *NCHRP Report 614*, Transportation Research Board, National Research Council, Washington, D. C.

Bonaquist, R., 2009. "Wisconsin Mixture Characterization Using the Asphalt Mixture Performance Tester (AMPT) on Historical Aggregate Structures." WHRP 09-03, Wisconsin Department of Transportation, Madison, WI.

Brown, E.R., Kandhal, P.S., and Zhang, J., 2004. "Performance Testing for Hot-Mix Asphalt, Transportation Research E-Circular E-C068." Transportation Research Record, National Research Council, Washington, DC.

Brown, E.R., Kandhal, P.S., Roberts, F.L. Kim, Y.R., Lee, D., and Kennedy, T.W., 2009. "Hot Mix Asphalt Materials, Mixture Design, and Construction, Third Edition." NAPA Research and Education Foundation, Lanham, MD.

Ceylan, H., Gopalakrishnan, K., and Kim, S., 2008. "Advanced approaches to hot-mix asphalt dynamic modulus prediction," *Can. J. Civ. Eng.*, 35(7): 699–707.

Christensen, Jr., D.W., Pellinen, T.K., and Bonaquist, R.F., 2003. "Hirsch model for estimating the modulus of asphalt concrete." *Journal of the Association of Asphalt Paving Technologists*, 72: 97–121.

Cominsky, R.J., Killingsworth, B.M. Anderson, R.M. Anderson, D.A., and Crockford, W.W., 1998. "Quality Control and Acceptance of Superpave-Designed Hot Mix Asphalt." *NCHRP Report 409*, Transportation Research Board, National Research Council, Washington, DC.

Cooley, L.A., Kandhal, P.S., Buchanan, M.S., Fee, F., and Epps, A., 2004. "Loaded Wheel Testers in the United States: State of the Practice." National Center for Asphalt Technology. *Report 00-04*, Auburn, AL.

Dongre, R., Myers, L., D'Angelo, J., Paugh, C., and Gudimettla, J., 2005. "Field evaluation of Witczak and Hirsch models for predicting dynamic modulus of hot-mix asphalt." *Journal of the Association of Asphalt Paving Technologists*, 74: 381–442.

Dongre, R.N., D'Angelo, J.A., and Copeland, A., 2009. "Refinement of flow number as determined by asphalt mixture performance tester: Use in routine quality control–quality assurance practice." *Transportation Research Record: Journal of the Transportation Research Board*, Issue 2127.

Fonseca, O.S., and Witczak, M.W., 1996. "A prediction methodology for the dynamic modulus of in-place aged asphalt mixtures (with discussion)." *Journal of the Association of Asphalt Paving Technologists*, 65.

Garcia, G., and Thompson, M., 2007. "HMA Dynamic Modulus–Temperature Relations." FHWA-ICT-07-006, Illinois Center for Transportation, Urbana, IL.

Gedafa, D.S., Hossain, M.R., and Romanoschi, S.A., 2009. "Field Verification of KDOT's Superpave Mixture Properties to Be Used as Inputs in the NCHRP Mechanistic-Empirical Pavement Design Guide." Kansas Department of Transportation, Topeka, KS.

Goh, S.W., You, Z., Wang, H., Mills-Beale, J., and Ji, J., 2011. "Determination of flow number in asphalt mixtures from deformation rate during secondary state." *Transportation Research Record: Journal of the Transportation Research Board*, Issue 2210.

Hajj, E.Y., Ulloa Calderon, A.E., Siddharthan, R.V., and Sebaaly, P.E., 2010. "Characteristics of the loading pulse for the flow number performance test." *Journal of the Association of Asphalt Paving Technologists*, 79.

Huang, B., Shu, X., and Bass, J., 2008. "Investigation of simple performance characteristics of plant-produced asphalt mixtures in Tennessee." *Transportation Research Record: Journal of the Transportation Research Board*, Issue 2057.

Jacksona, N.M., and Baldwina, C.D., 2000. "Assessing the relative rutting susceptibility of HMA in the laboratory with the asphalt pavement analyzer." *International Journal of Pavement Engineering*, 1(3): 203–217.

Kaloush, K.E., and Witczak, M.W., 2002. "Tertiary flow characteristics of asphalt mixtures (with discussion and closure)." *Journal of the Association of Asphalt Paving Technologists*, 71.

Kandhal, P.S., and Parker, Jr., F., 1998. "Aggregate Tests Related to Asphalt Concrete Performance in Pavements." *NCHRP Report 405*, Transportation Research Board, National Research Council, Washington, DC.

Kandhal, P.S., and Cooley, L.A., 2003. "Accelerated Laboratory Rutting Tests: Evaluation of the Asphalt Pavement Analyzer." *NCHRP Report 508*, Transportation Research Board, National Research Council, Washington, DC.

Kim, Y.R., and King, M., 2005. "Typical Dynamic Moduli for North Carolina Asphalt Concrete Mixes." FHWA/NC/2005-03, Federal Highway Administration, Washington, DC.

Kim, Y.R., Seo, Y., King, M., and Momen, M., 2004. "Dynamic modulus testing of asphalt concrete in indirect tension mode." *Transportation Research Record: Journal of the Transportation Research Board*, Issue 1891.

Kim, Y.R., Underwood, B., Sakhaei, M.F., Jackson, N., and Puccinelli, J., 2011. "LTPP Computed Parameter: Dynamic Modulus." FHWA-HRT-10-035, Turner-Fairbank Highway Research Center, McLean, VA.

Liu, J., and Connor, B., 2008. "Simple Performance Test of Barrow Airport Mixes." ADOT&PF Report, University of Alaska Fairbanks, Fairbanks, AK.

Liu, J., and Li, P., 2012. "Low temperature performance of Sasobit-modified warm mix asphalt." *ASCE Journal of Materials in Civil Engineering*, 24(1): 57–63.

Liu, J., Saboundjian, S., Li, P., Connor, B., and Brunette, B., 2011. "Laboratory evaluation of Sasobit modified warm mix asphalt for Alaskan conditions." *ASCE Journal of Materials in Civil Engineering*, 23(11): 1498–1505.

Loulizi, A., Flintsch, G.W., Al-Qadi, I.L., and Mokarem D.W., 2006. "Comparing resilient modulus and dynamic modulus of hot-mix asphalt as material properties for flexible pavement design." *Transportation Research Record: Journal of the Transportation Research Board*, Issue 1970.

Mogawer, W.S., Austerman, A.J., Daniel, J.S., Zhou, F., and Bennert, T., 2011. "Evaluation of the effects of hot mix asphalt density on mixture fatigue performance, rutting performance and MEPDG distress predictions." *International Journal of Pavement Engineering*, 12(2).

Mohammad, L.N., Wu, Z., Myers, L., Cooper, S., Abadie, C., Chehab, G., and Davis, R., 2005. "A practical look at the simple performance tests: Louisiana's experience." *Journal of the Association of Asphalt Paving Technologists*, 74.

Mohammad, L.N., Wu, Z., Obulareddy, S., Cooper, S., and Abadie, C.D., 2006. "Permanent deformation analysis of hot-mix asphalt mixtures using simple performance tests and

2002 Mechanistic-Empirical Pavement Design software." *Transportation Research Record: Journal of the Transportation Research Board*, Issue 1970: 133–142.

Nadkarni, A.A., Kaloush, K.E., Zeiada, W.A., and Biligiri, K.P., 2009. "Using dynamic modulus test to evaluate moisture susceptibility of asphalt mixtures." *Transportation Research Record: Journal of the Transportation Research Board*, Issue 2127.

Obulareddy, S., 2006. "Fundamental Characterization of Louisiana HMA Mixtures for the 2002 Mechanistic-Empirical Design Guide." Thesis, B.E., Andhra University, India.

Oscarsson, E., 2011. "Modeling flow rutting in in-service asphalt pavements using the mechanistic empirical pavement design guide. *Road Materials and Pavement Design*, 12(1).

Pellinen, T.K., 2001. Investigation of the use of dynamic modulus as an indicator of hot-mix asphalt performance. Ph.D. thesis, Arizona State University, Tempe, AZ.

Pellinen, T.K., and Witczak, M.W., 2002. "Stress dependent master curve construction for dynamic (complex) modulus." *Journal of the Association of Asphalt Paving Technologists*, 71.

Solaimanian, M., Fedor, D., Bonaquist, R., Soltani, A., and Tandon, V., 2006. "Simple performance test for moisture damage prediction in asphalt concrete (with discussion)." *Journal of the Association of Asphalt Paving Technologists*, 75.

Sotil, A., Kaloush, K.E., and Witczak, M.W., 2004. "Reduced confined dynamic modulus testing protocol for asphalt mixtures." *Transportation Research Record: Journal of the Transportation Research Board*, Issue 1891.

Stuart, K.D., and Izzo, R.P., 1995. "Correlation of G* / Sin Delta with rutting susceptibility from laboratory mixture tests." *Transportation Research Record: Journal of the Transportation Research Board*, Issue 1492: 176–183.

Tashman, L., and Elangovan, M.A., 2008. "Dynamic Modulus Test – Laboratory Investigation and Future Implementation in the State of Washington." Final Research Report, Washington State Transportation Center, Seattle, WA.

Tran, N.H., and Hall, K.D., 2006. "Evaluation of testing protocols for dynamic modulus of hot-mix asphalt." *Transportation Research Record: Journal of the Transportation Research Board*, Issue 1970.

Vallerga, B.A., and Lovering, W.R., 1985. "Evolution of the Hveem stabilometer method of designing asphalt paving mixtures." *Journal of the Association of Asphalt Paving Technologists*, 54.

Williams, R.C., and Prowell, B.D., 1999. "Comparison of laboratory wheel-tracking test results with Wes Track Performance." *Transportation Research Record: Journal of Transportation Research Board*, No.1681, 121–128.

Williams, R.C., Robinette, C.J., Bausano, J., and Breakah, T., 2007. "Testing Wisconsin Asphalt Mixtures for the AASHTO 2002 Mechanistic Design Procedure," WHRP 0092-04-07.

Witczak, M.W., 2007. "Specification Criteria for Simple Performance Tests for Rutting: Volume I: Dynamic Modulus (E*) and Volume II: Flow Number and Flow Time," *NCHRP Report 580*, Transportation Research Board, National Research Council, Washington, DC.

Witczak, M.W., Kaloush, K., Pellinen, T., El-Basyouny, M., and Vonquintus, H., 2002a. "Simple Performance Test for Superpave Mix Design." *NCHRP Report 465*, Transportation Research Board, National Research Council, Washington, DC.

Witczak, M.W., Kaloush, K.E., and Vonquintus, H., 2002b. "Pursuit of the simple performance test for asphalt mixture rutting." *Journal of the Association of Asphalt Paving Technologists*, 71.

Witczak, M.W., Pellinen, T.K., and El-Basyouny, M.M., 2002c. "Pursuit of the simple performance test for asphalt concrete fracture/cracking." *Journal of the Association of Asphalt Paving Technologists*, 71.

Zhang, C., 2005. "Comparative Study of the Physical and Mechanistic Properties of HMA Mixture: Field vs. Laboratory." Thesis, Louisiana State University, LA.

Zhou, F., and Scullion, T., 2003. "Preliminary field validation of simple performance tests for permanent deformation: Case study." *Transportation Research Record: Journal of the Transportation Research Board*, Issue 1832, National Research Council, Washington, DC.

Zhou, F., Scullion, T., and Sun, L., 2004. "Verification and modeling of three-stage permanent deformation behavior of asphalt mixes." *Journal of Transportation Engineering*, 130(4).

APPENDIX A: Summary of |E*| and Master Curve

Master curve

$$\log_{10}|E*| = \delta + \frac{\alpha}{1 + e^{\beta + \lambda \times \log(f_R)}}$$

$$f_R = f(aT^2 + bT + C)$$

Where:

$|E*|$ = Dynamic modulus of HMA, MPa,

f_R = Reduced loading frequency at reference temperature of 20°C, Hz,

f = Loading frequency, Hz, and

$\delta, \alpha, \beta, \gamma, a, b, c$ = Regression constants.
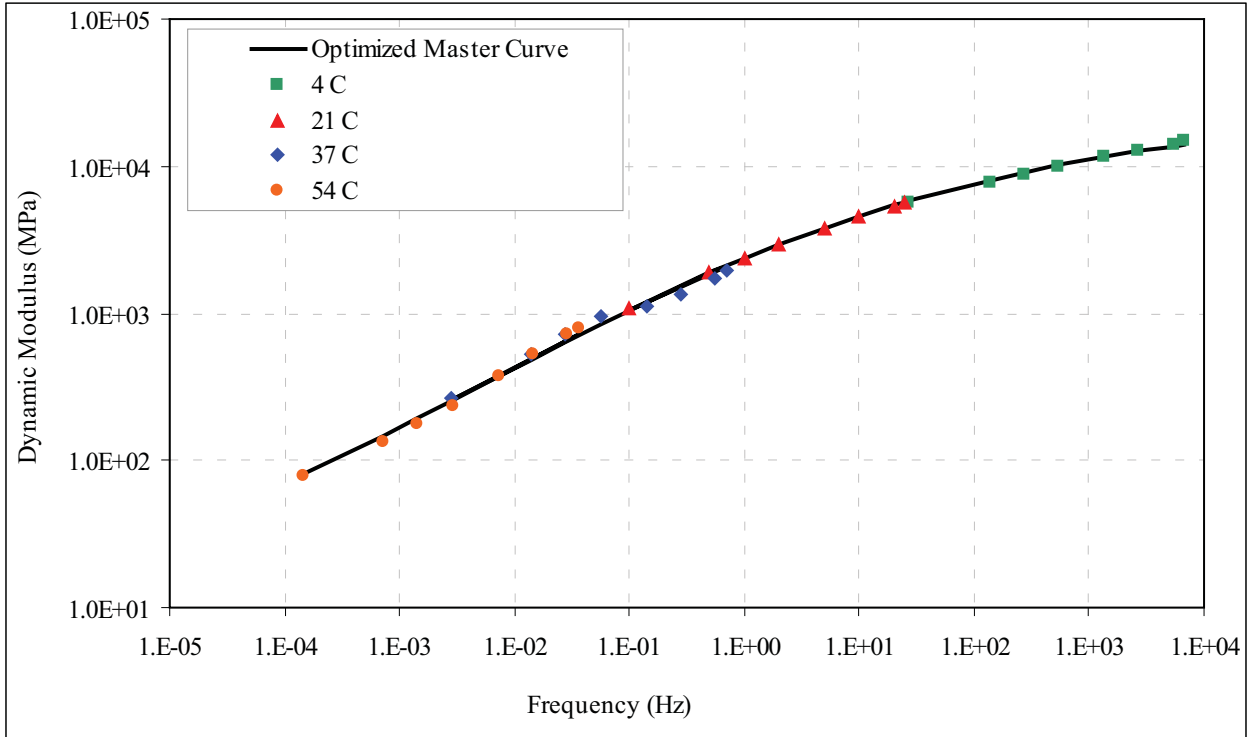
Figure A.1 Optimized Master Curve
(Project: FIA Runway 1L_19R stage 3 (64-34))

Table A.1 Summary of Measured |E*| and Master curve Coefficients
(Project: FIA Runway 1L_19R stage 3 (64-34))

Temperature (ºC)	Measured Dynamic Modulus (Mpa)							
	25 Hz	20 Hz	10 Hz	5 Hz	2 Hz	1 Hz	0.5 Hz	0.1 Hz
4	14678	14176	12815	11575	10005	8837	7803	5675
21	5630	5339	4490	3748	2902	2367	1910	1092
37	1981	1736	1335	1121	943	710	527	262
54	797	729	530	378	237	175	134	80

Master Curve Coefficients							R^2 (Logarithmic)	R^2 (Arithmetic)
δ	α	β	γ	a	b	c		
6.32140E-01	3.75909E+00	-9.88409E-01	4.31771E-01	-1.02307E-03	1.64006E-01	-3.05425E+00	0.99794	0.99764
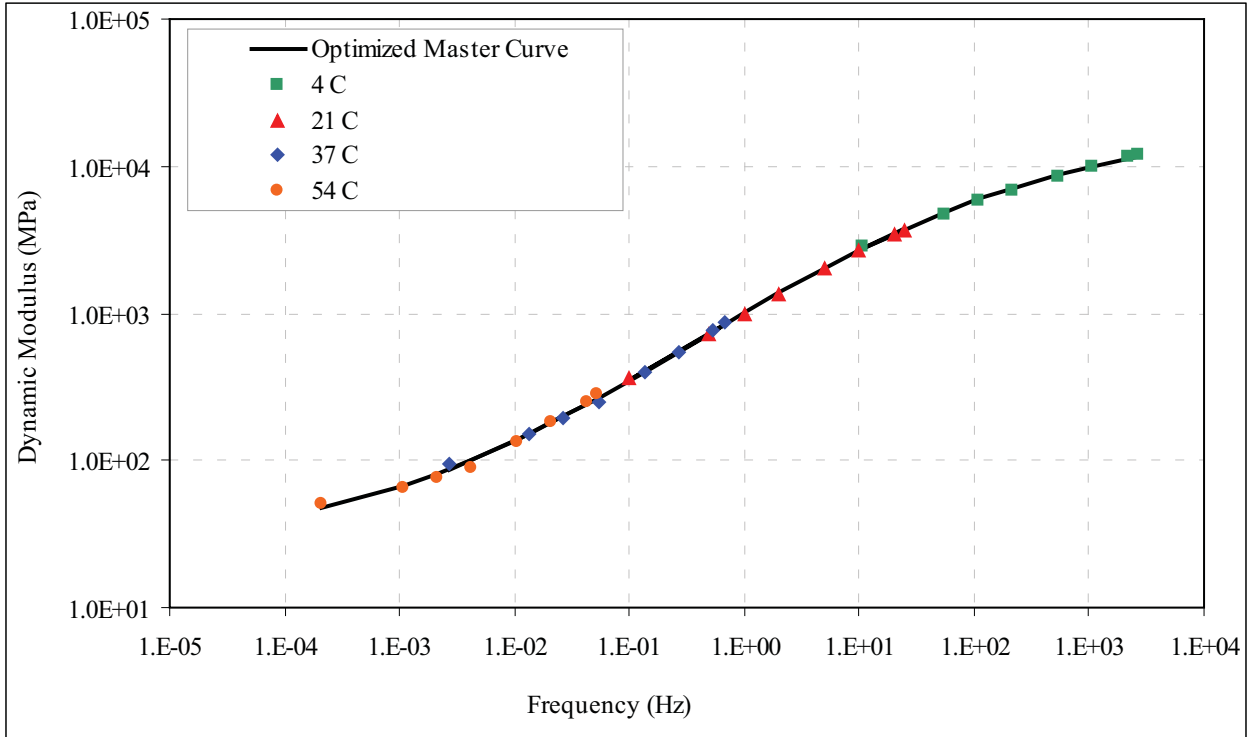
Figure A.2 Optimized Master Curve
(Project: FIA Runway 1L_19R stage 3 (52-34))

Table A.2 Summary of Measured |E*| and Master curve Coefficients
(Project: FIA Runway 1L_19R stage 3 (52-34))

Temperature (ºC)	Measured Dynamic Modulus (Mpa)							
	25 Hz	20 Hz	10 Hz	5 Hz	2 Hz	1 Hz	0.5 Hz	0.1 Hz
4	12067	11479	9981	8585	6913	5781	4763	2853
21	3693	3434	2648	2008	1354	994	731	365
37	860	764	548	395	251	191	150	95
54	285	251	183	134	90	77	66	51

Master Curve Coefficients							R^2 (Logarithmic)	R^2 (Arithmetic)
δ	α	β	γ	a	b	c		
1.32356E+00	3.00269E+00	-2.34476E-01	6.16108E-01	-8.29047E-04	1.42623E-01	-2.60062E+00	0.99943	0.99881
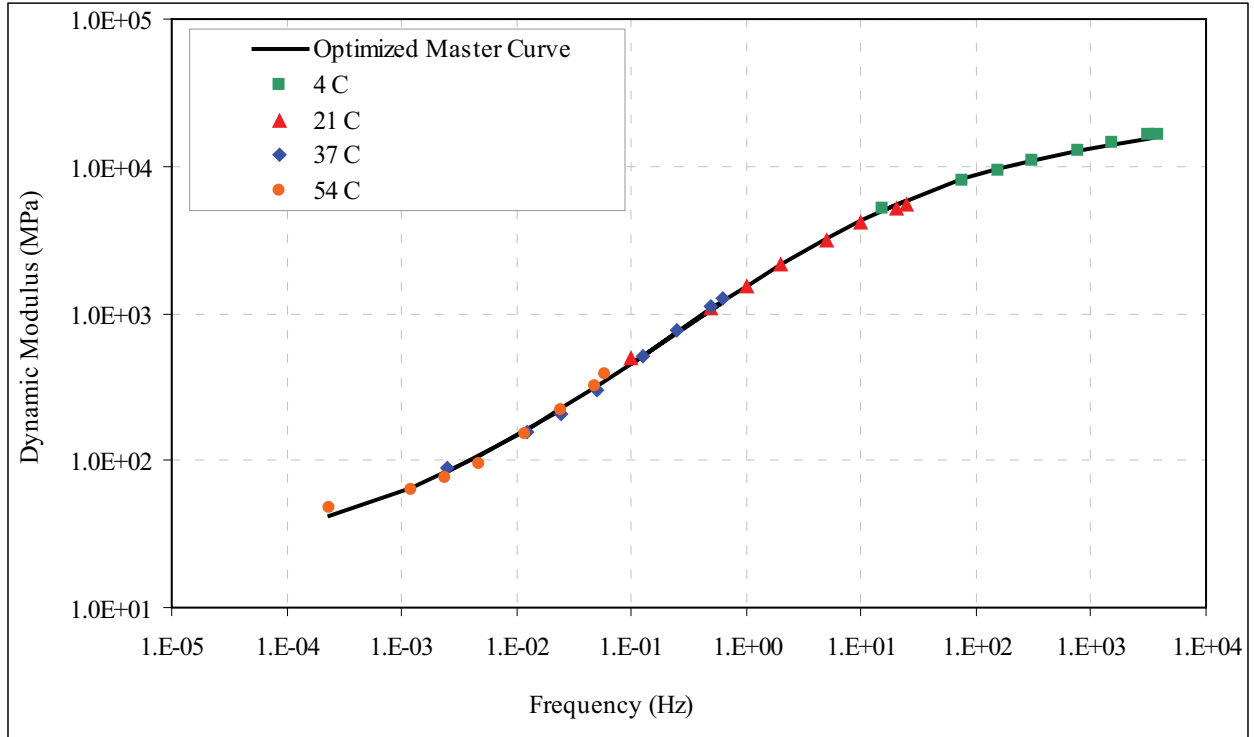
Figure A.3 Optimized Master Curve
(Project: Project: Chena Hot Springs Rd, MD-1)

Table A.3 Summary of Measured |E*| and Master curve Coefficients
(Project: Chena Hot Springs Rd, MD-1)

Temperature (ºC)	Measured Dynamic Modulus (Mpa)							
	25 Hz	20 Hz	10 Hz	5 Hz	2 Hz	1 Hz	0.5 Hz	0.1 Hz
4	16443	16165	14404	12787	10745	9277	7896	5099
21	5521	5181	4094	3147	2132	1538	1095	491
37	1269	1105	755	507	297	210	154	90
54	382	324	223	153	95	76	64	48

Master Curve Coefficients							R^2 (Logarithmic)	R^2 (Arithmetic)
δ	α	β	γ	a	b	c		
1.26214E+00	3.08184E+00	-5.02978E-01	6.91294E-01	-1.04618E-03	1.57244E-01	-2.81071E+00	0.99917	0.99750
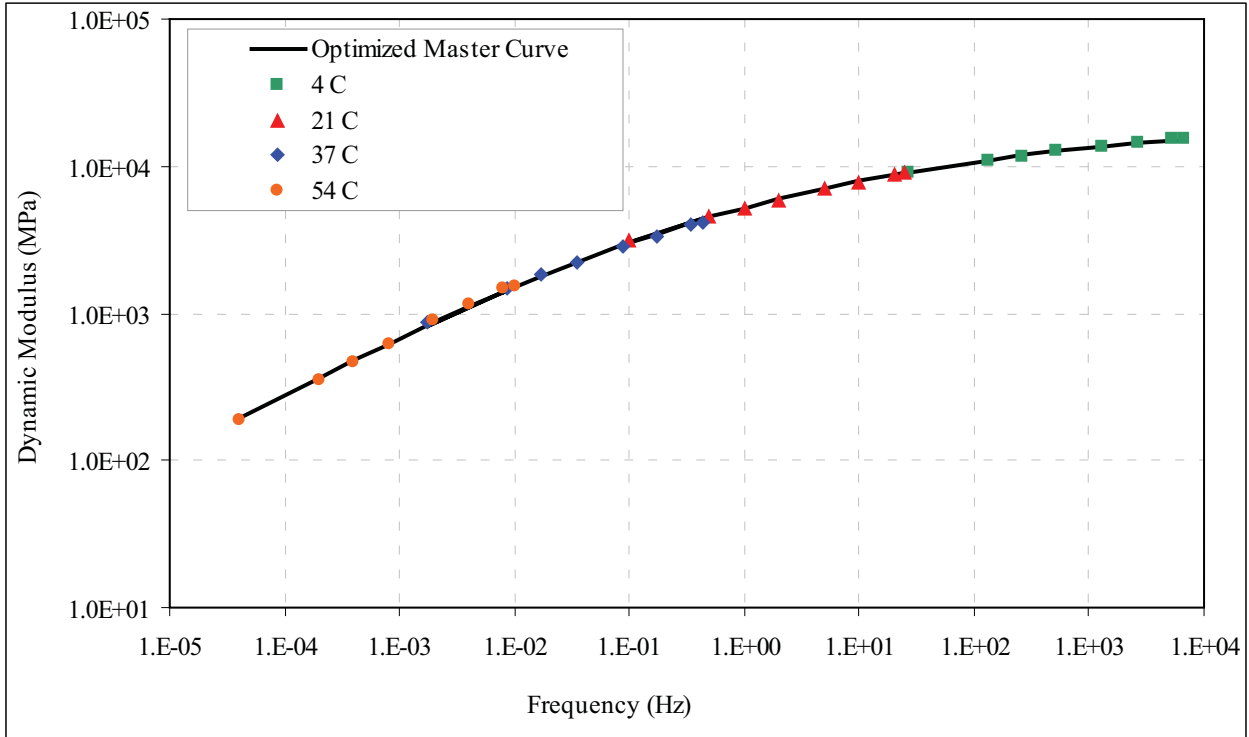
Figure A.4 Optimized Master Curve
(Project: Chena Hot Springs Rd MD-3)

Table A.4 Summary of Measured |E*| and Master curve Coefficients
(Project: Chena Hot Springs Rd MD-3)

Temperature (ºC)	Measured Dynamic Modulus (Mpa)							
	25 Hz	20 Hz	10 Hz	5 Hz	2 Hz	1 Hz	0.5 Hz	0.1 Hz
4	15545	15541	14620	13745	12572	11444	10861	9012
21	8992	8702	7792	6947	5902	5179	4519	3157
37	4145	3977	3374	2845	2224	1828	1489	865
54	1544	1459	1151	891	613	464	351	187

Master Curve Coefficients							R^2 (Logarithmic)	R^2 (Arithmetic)
δ	α	β	γ	a	b	c		
6.32140E-01	3.68417E+00	-1.64125E+00	4.17929E-01	-6.98378E-04	1.56302E-01	-3.02077E+00	0.99939	0.99826

86
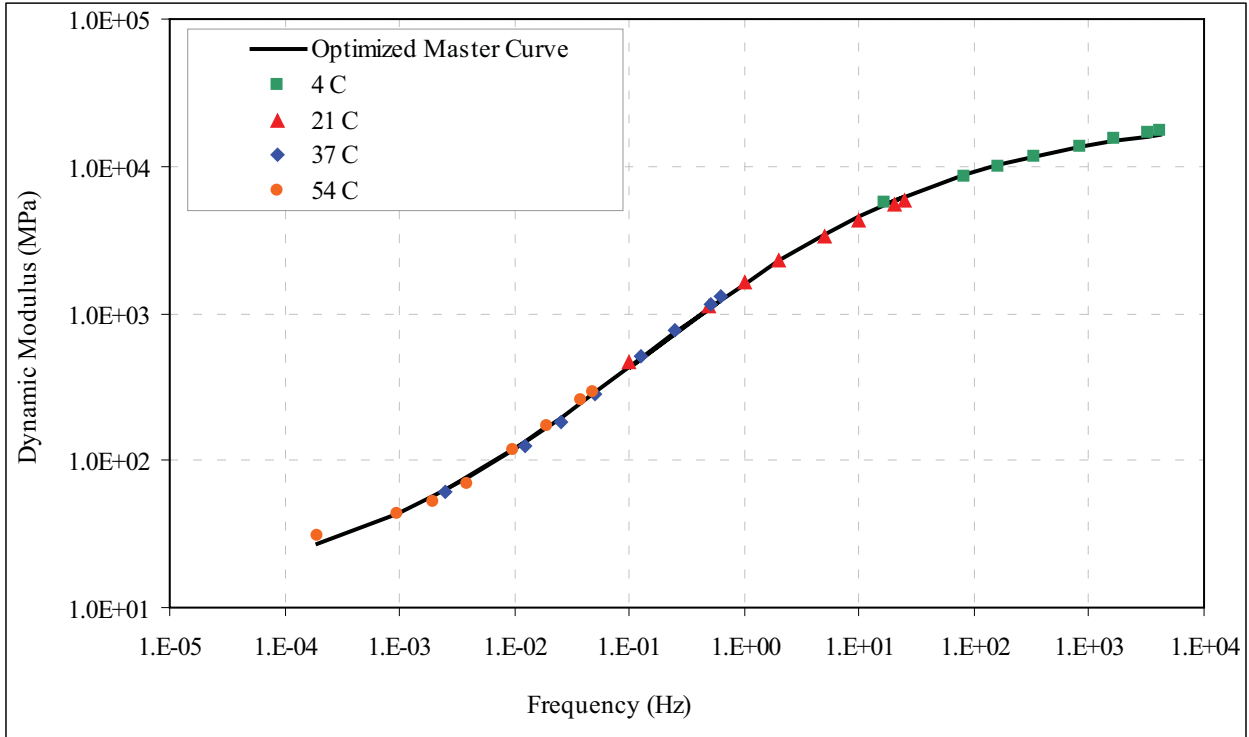
Figure A.5 Optimized Master Curve
(Project: Fairbanks Cowles Street Upgrade)

Table A.5 Summary of Measured |E*| and Master curve Coefficients
(Project: Fairbanks Cowles Street Upgrade)

Temperature (ºC)	Measured Dynamic Modulus (Mpa)							
	25 Hz	20 Hz	10 Hz	5 Hz	2 Hz	1 Hz	0.5 Hz	0.1 Hz
4	17411	16884	15223	13585	11465	9929	8496	5584
21	5783	5437	4330	3346	2264	1617	1128	466
37	1296	1141	767	503	284	185	125	60
54	288	254	173	117	70	53	43	31

Master Curve Coefficients							R^2 (Logarithmic)	R^2 (Arithmetic)
δ	α	β	γ	a	b	c		
1.02628E+00	3.31607E+00	-6.43023E-01	7.04611E-01	-9.83274E-04	1.55817E-01	-2.82873E+00	0.99931	0.99641
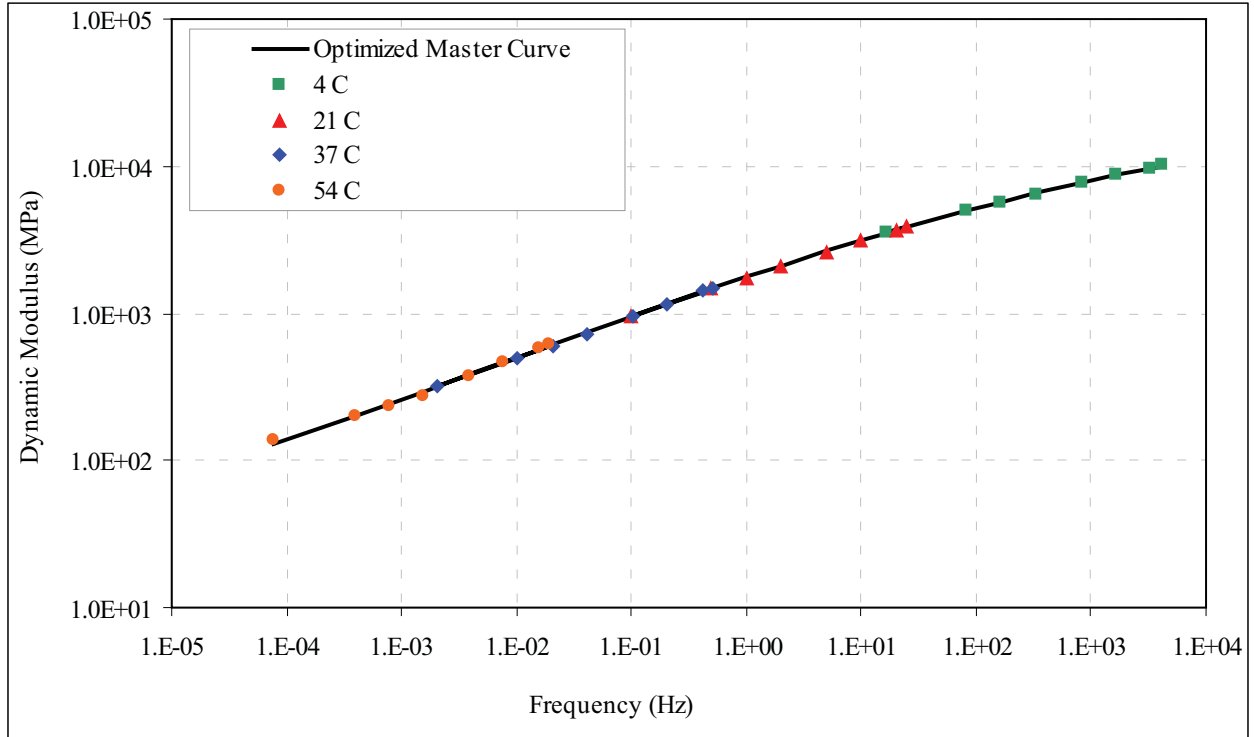
Figure A.6 Optimized Master Curve
(Project: Dalton Hwy. MP 175-197 Rehabilitation)

Table A.6 Summary of Measured |E*| and Master curve Coefficients
(Project: Dalton Hwy. MP 175-197 Rehabilitation)

Temperature (ºC)	Measured Dynamic Modulus (Mpa)							
	25 Hz	20 Hz	10 Hz	5 Hz	2 Hz	1 Hz	0.5 Hz	0.1 Hz
4	10081	9697	8636	7646	6459	5654	4935	3573
21	3890	3688	3105	2616	2070	1740	1466	959
37	1497	1417	1161	952	721	600	499	324
54	615	578	468	377	277	234	198	138

Master Curve Coefficients							R² (Logarithmic)	R² (Arithmetic)
δ	α	β	γ	a	b	c		
7.06449E-01	3.93672E+00	-5.96808E-01	2.87615E-01	-7.10035E-04	1.47593E-01	-2.79477E+00	0.99973	0.99990
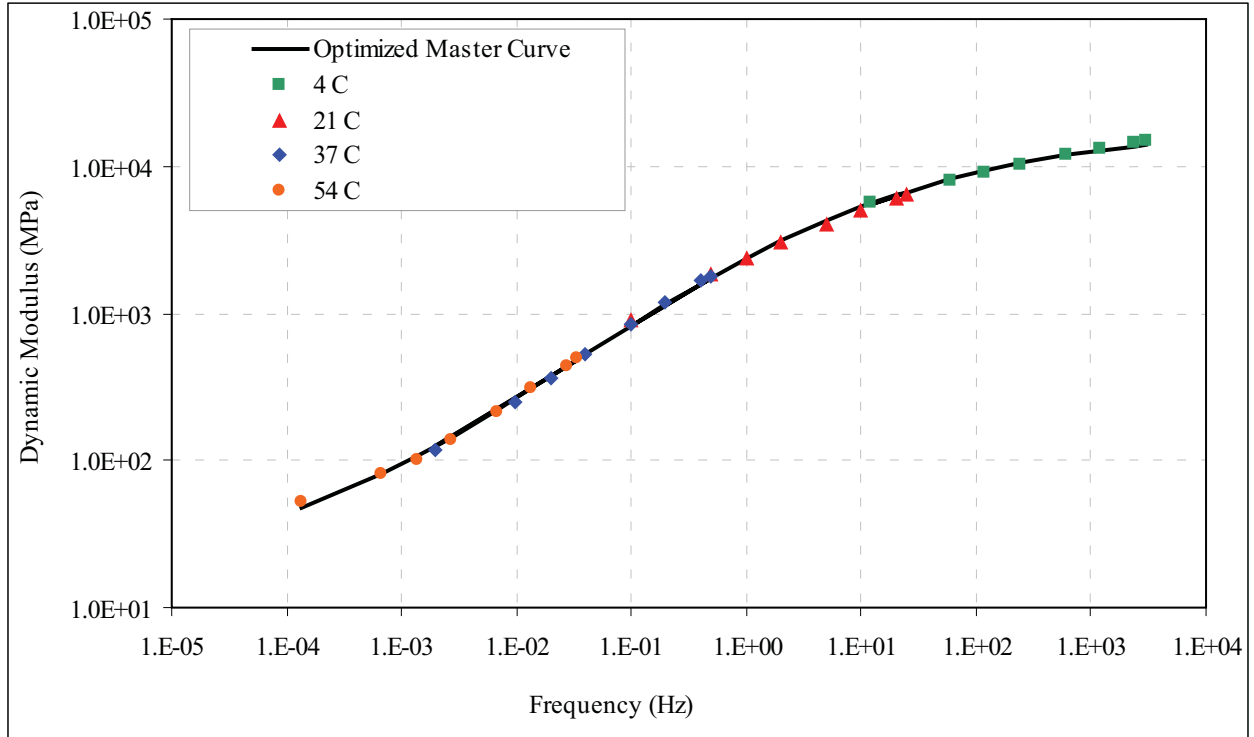
Figure A.7 Optimized Master Curve
(Project: Glen Why MP 92-97 Cascade to Hicks Creek)

Table A.7 Summary of Measured |E*| and Master curve Coefficients
(Project: Glen Why MP 92-97 Cascade to Hicks Creek)

Temperature (ºC)	Measured Dynamic Modulus (Mpa)							
	25 Hz	20 Hz	10 Hz	5 Hz	2 Hz	1 Hz	0.5 Hz	0.1 Hz
4	14794	14408	13132	11867	10231	9043	7909	5573
21	6319	5978	4976	4073	3035	2373	1818	905
37	1798	1649	1203	852	522	360	250	117
54	492	439	309	216	136	102	81	53

Master Curve Coefficients							R^2 (Logarithmic)	R^2 (Arithmetic)
δ	α	β	γ	a	b	c		
1.10977E+00	3.17159E+00	-9.09684E-01	6.28708E-01	-8.10628E-04	1.46638E-01	-2.66778E+00	0.99931	0.99700

89
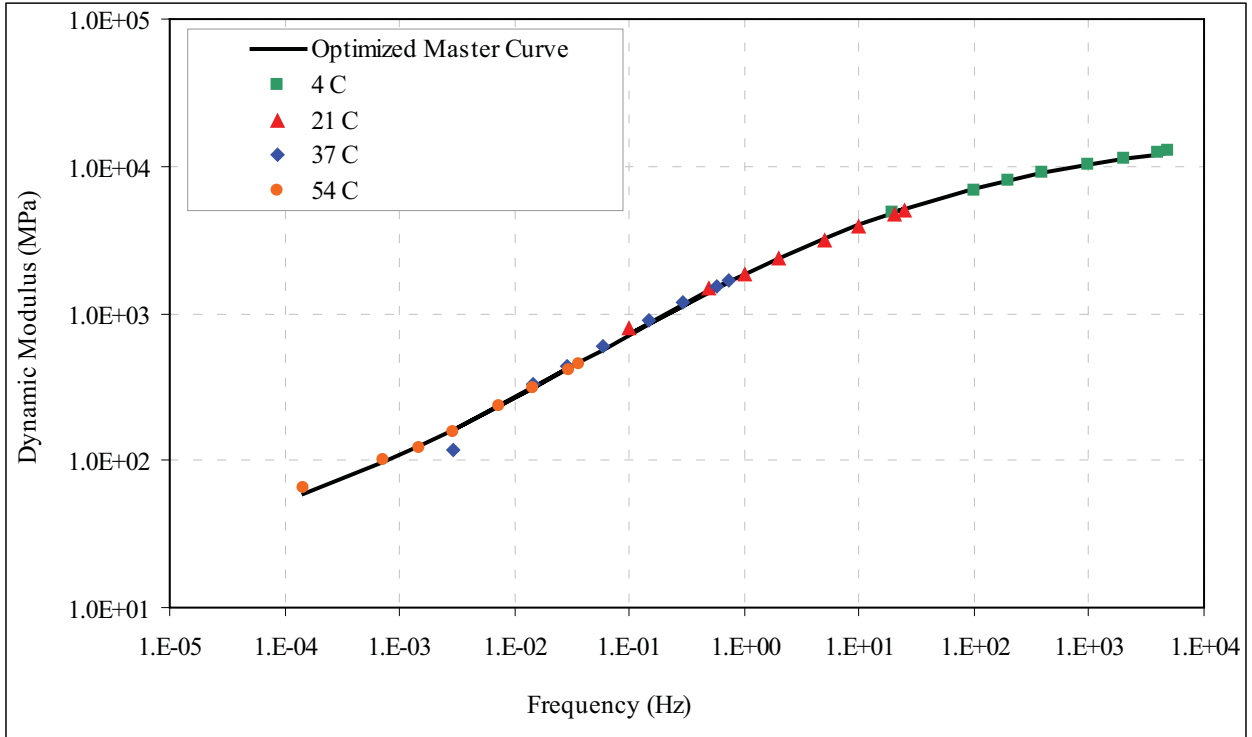
Figure A.8 Optimized Master Curve
(Project: Glenn Highway Gambell to airport MP 0-1.5)

Table A.8 Summary of Measured |E*| and Master curve Coefficients
(Project: Glenn Highway Gambell to airport MP 0-1.5)

Temperature (ºC)	Measured Dynamic Modulus (Mpa)							
	25 Hz	20 Hz	10 Hz	5 Hz	2 Hz	1 Hz	0.5 Hz	0.1 Hz
4	12827	12501	11414	10329	8930	7910	6923	4889
21	4945	4658	3855	3155	2361	1865	1456	785
37	1651	1529	1172	883	595	444	334	119
54	448	413	311	231	157	123	100	65

Master Curve Coefficients							R^2 (Logarithmic)	R^2 (Arithmetic)
δ	α	β	γ	a	b	c		
1.16608E+00	3.09460E+00	-7.49970E-01	5.65058E-01	-8.90361E-04	1.53629E-01	-2.88205E+00	0.99823	0.99843

90
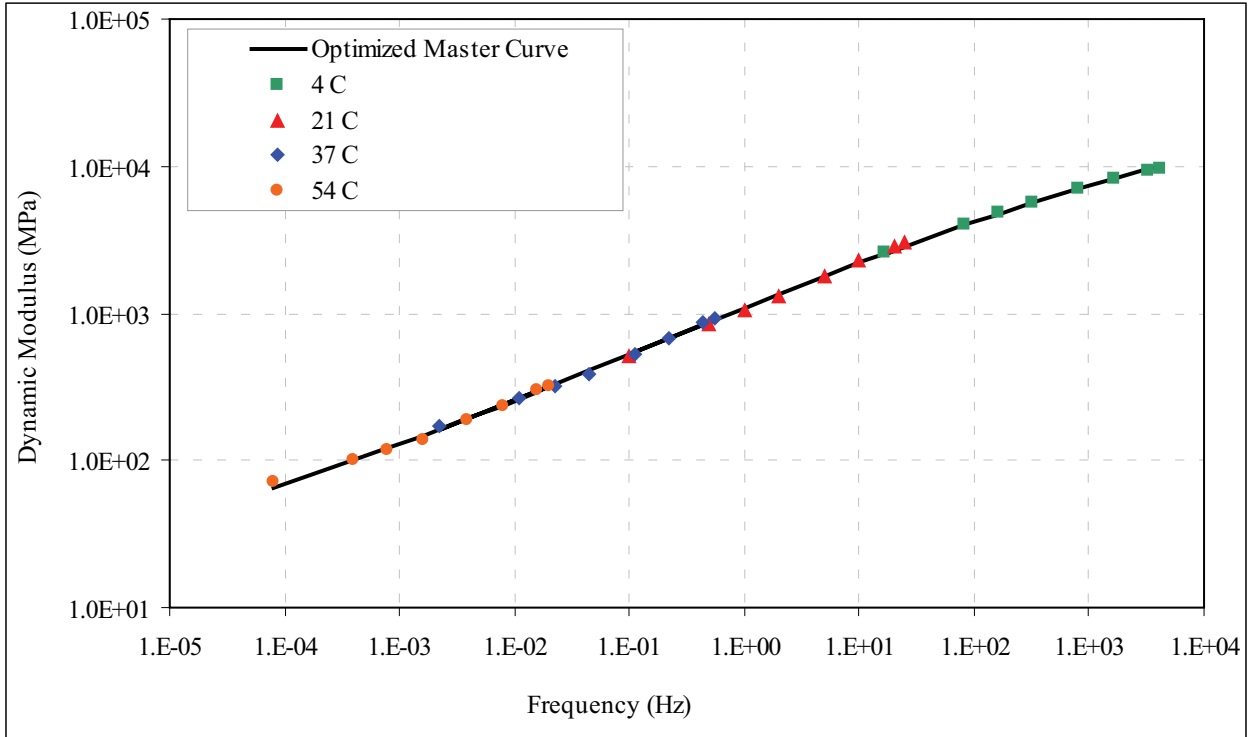
Figure A.9 Optimized Master Curve
(Project HNS Ferry Terminal to Union Street)

Table A.9 Summary of Measured |E*| and Master curve Coefficients
(Project HNS Ferry Terminal to Union Street)

Temperature (°C)	Measured Dynamic Modulus (Mpa)							
	25 Hz	20 Hz	10 Hz	5 Hz	2 Hz	1 Hz	0.5 Hz	0.1 Hz
4	9662	9274	8115	7024	5701	4806	4013	2559
21	3033	2830	2254	1789	1310	1045	842	516
37	933	857	675	532	386	317	262	171
54	322	298	237	189	138	117	100	71

Master Curve Coefficients							R^2 (Logarithmic)	R^2 (Arithmetic)
δ	α	β	γ	a	b	c		
6.89061E-01	4.17165E+00	-2.51985E-01	3.04215E-01	-6.80722E-04	1.45492E-01	-2.77615E+00	0.99945	0.99864

91
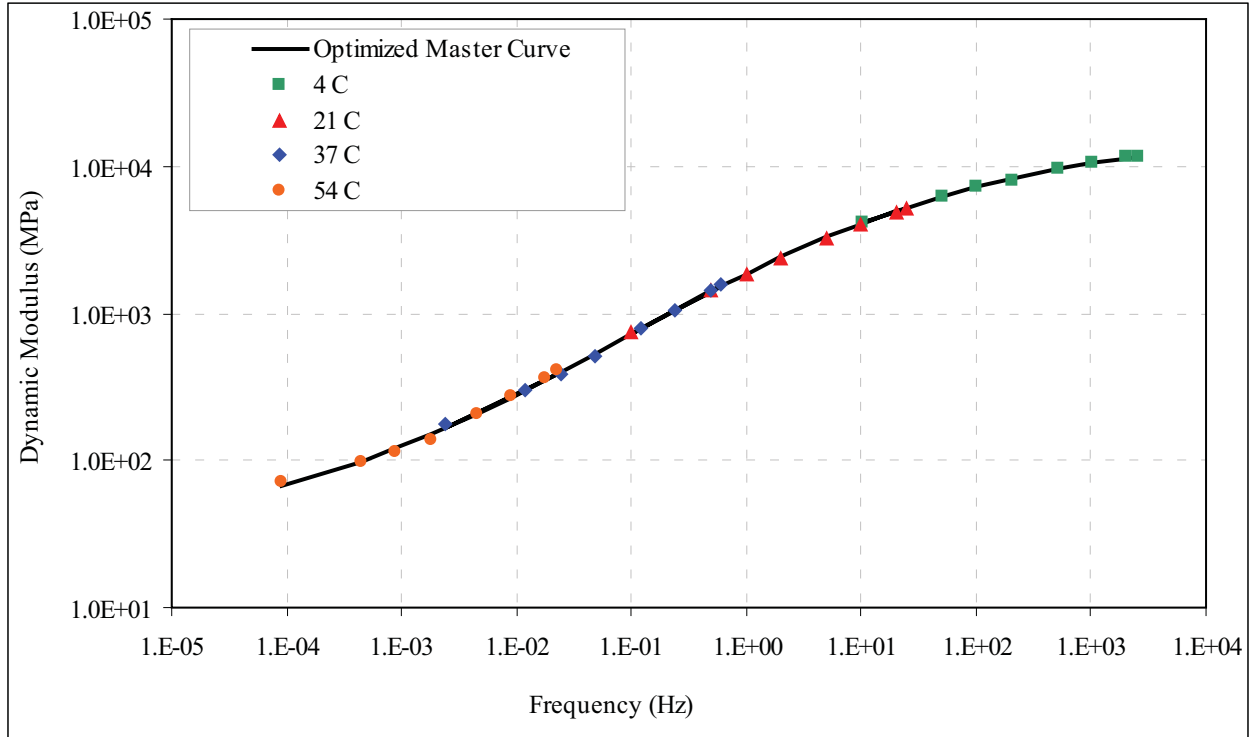
Figure A.10 Optimized Master Curve
(Project: Minnesota Dr Resurfacing: Int'l Airport Rd to 13th)

Table A.10 Summary of Measured |E*| and Master curve Coefficients
(Project: Minnesota Dr Resurfacing: Int'l Airport Rd to 13th)

Temperature (°C)	Measured Dynamic Modulus (Mpa)							
	25 Hz	20 Hz	10 Hz	5 Hz	2 Hz	1 Hz	0.5 Hz	0.1 Hz
4	11648	11594	10602	9567	8034	7164	6228	4079
21	5146	4840	3993	3243	2396	1863	1431	748
37	1550	1416	1055	780	517	389	299	175
54	413	366	272	204	138	114	96	71

Master Curve Coefficients							R^2 (Logarithmic)	R^2 (Arithmetic)
δ	α	β	γ	a	b	c		
1.40356E+00	2.84657E+00	-6.42023E-01	5.93089E-01	-5.17571E-04	1.31174E-01	-2.52647E+00	0.99964	0.99964

92
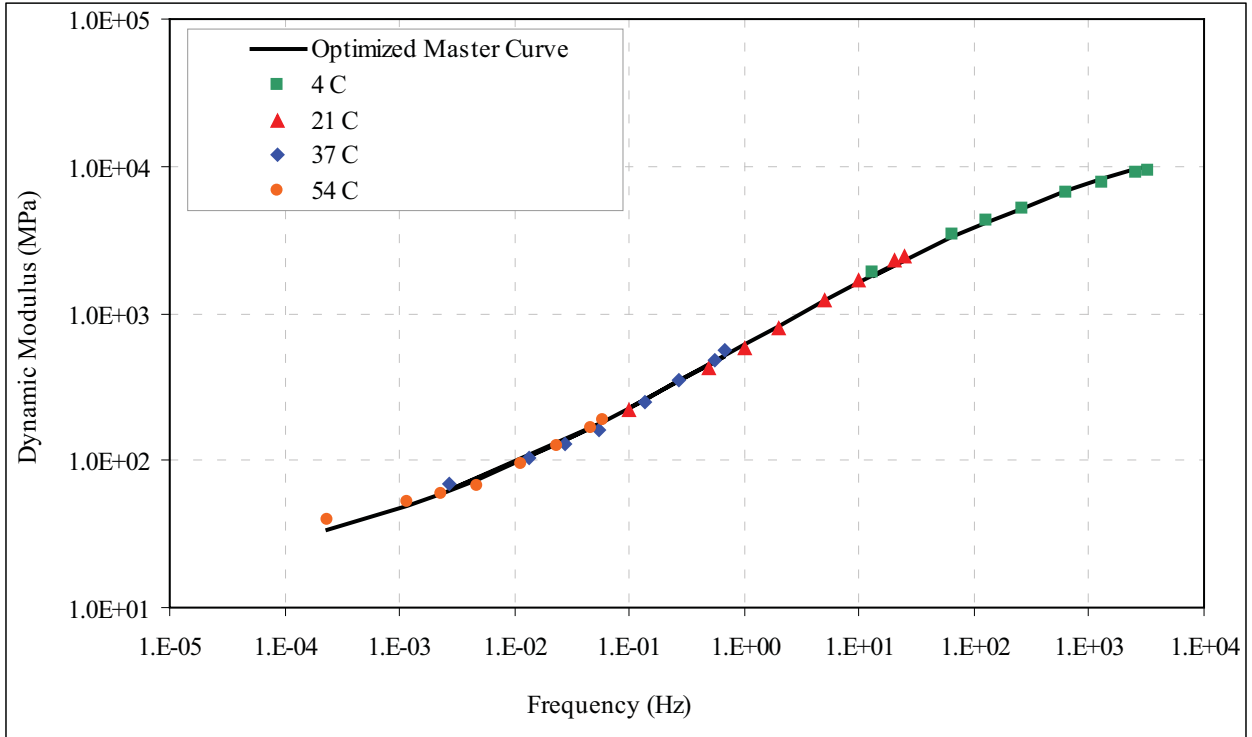
Figure A.11 Optimized Master Curve
(Project: Rich Hwy North Pole Interchange)

Table A.11 Summary of Measured |E*| and Master curve Coefficients
(Project: Rich Hwy North Pole Interchange)

Temperature (ºC)	Measured Dynamic Modulus (Mpa)							
	25 Hz	20 Hz	10 Hz	5 Hz	2 Hz	1 Hz	0.5 Hz	0.1 Hz
4	9383	8993	7767	6608	5196	4240	3398	1883
21	2463	2259	1686	1238	803	582	426	220
37	556	484	350	252	163	128	103	69
54	191	168	125	95	67	59	52	39

| Master Curve Coefficients							R^2 (Logarithmic)	R^2 (Arithmetic)
δ	α	β	γ	a	b	c		
1.03731E+00	3.46885E+00	-1.35457E-02	5.00471E-01	-9.28423E-04	1.48969E-01	-2.69739E+00	0.99888	0.99615

93
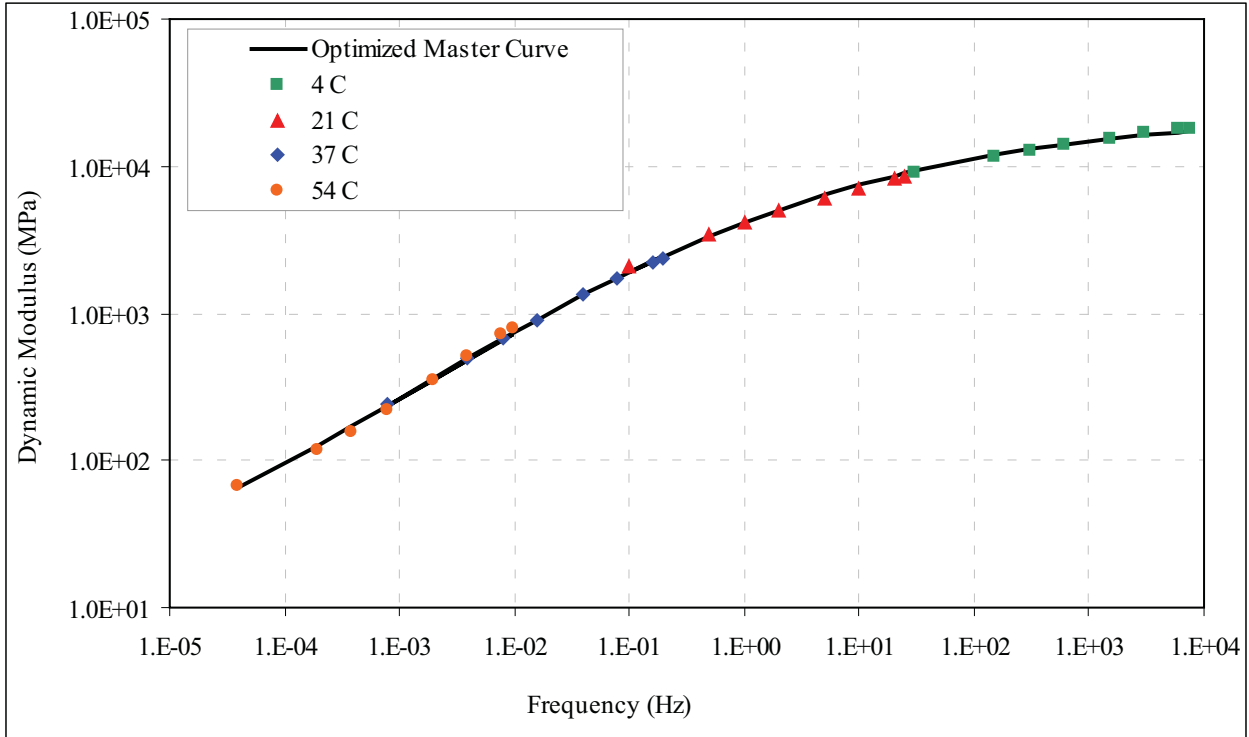
Figure A.12 Optimized Master Curve
(Project: Old Glenn Hwy.: MP 11.5-18)

Table A.12 Summary of Measured |E*| and Master curve Coefficients
(Project: Old Glenn Hwy.: MP 11.5-18)

Temperature (ºC)	Measured Dynamic Modulus (Mpa)							
	25 Hz	20 Hz	10 Hz	5 Hz	2 Hz	1 Hz	0.5 Hz	0.1 Hz
4	18105	17823	16653	15507	13994	12839	11701	9160
21	8464	8139	7078	6103	4927	4144	3441	2085
37	2361	2226	1739	1332	906	670	493	241
54	795	720	511	354	218	156	116	68

Master Curve Coefficients							R^2 (Logarithmic)	R^2 (Arithmetic)
δ	α	β	γ	a	b	c		
6.32225E-01	3.74607E+00	-1.36729E+00	4.86128E-01	-1.04493E-03	1.79727E-01	-3.21425E+00	0.99926	0.99817

94
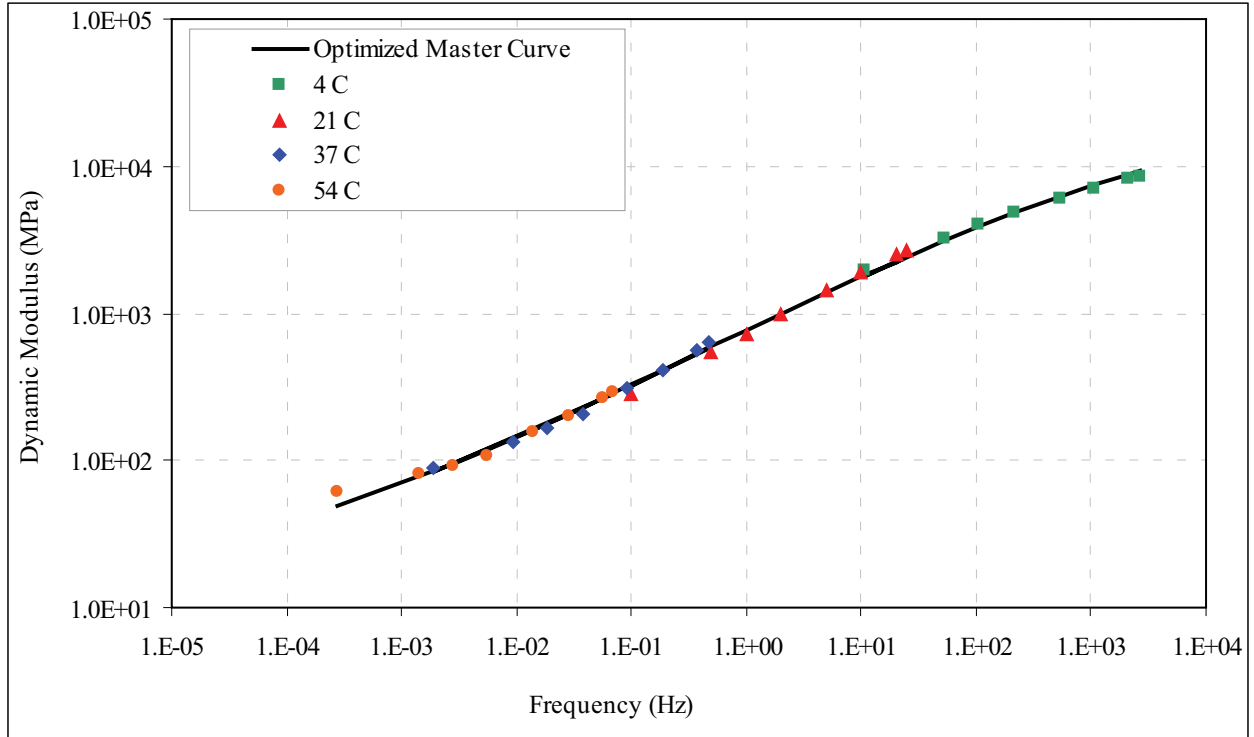
Figure A.13 Optimized Master Curve
(Project: Palmer-Wasilla Highway Phase II)

Table A.13 Summary of Measured |E*| and Master curve Coefficients
(Project: Palmer-Wasilla Highway Phase II)

Temperature (ºC)	Measured Dynamic Modulus (Mpa)							
	25 Hz	20 Hz	10 Hz	5 Hz	2 Hz	1 Hz	0.5 Hz	0.1 Hz
4	8469	8138	7040	6018	4791	3962	3236	1965
21	2677	2476	1903	1442	972	722	540	283
37	626	559	415	308	207	165	134	90
54	293	263	201	156	107	93	81	60

Master Curve Coefficients							R^2 (Logarithmic)	R^2 (Arithmetic)
δ	α	β	γ	a	b	c		
7.98974E-01	3.95363E+00	-1.08345E-01	3.77080E-01	-1.07451E-03	1.55375E-01	-2.66838E+00	0.99756	0.99141

95
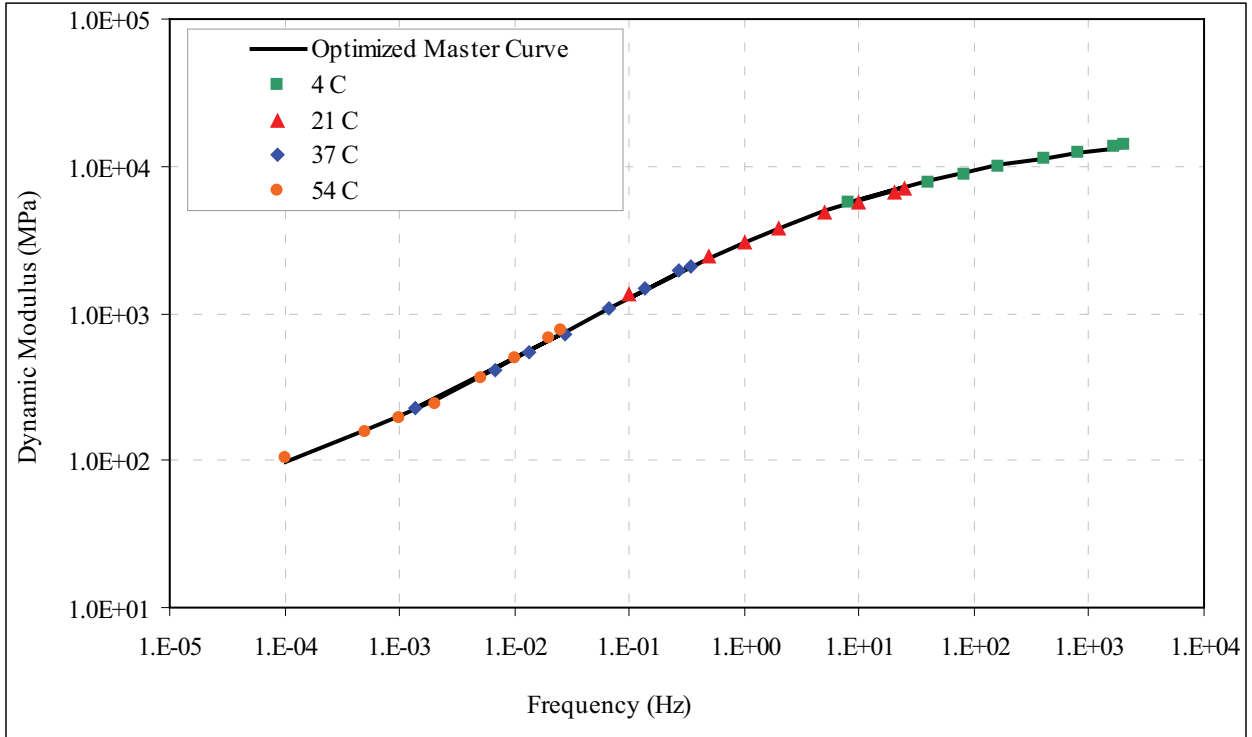
Figure A.14 Optimized Master Curve
(Project: Unalakleet Airport Paving)

Table A.14 Summary of Measured |E*| and Master curve Coefficients
(Project: Unalakleet Airport Paving)

Temperature (ºC)	Measured Dynamic Modulus (Mpa)							
	25 Hz	20 Hz	10 Hz	5 Hz	2 Hz	1 Hz	0.5 Hz	0.1 Hz
4	14039	13662	12495	11348	9878	8808	7790	5681
21	6954	6672	5714	4822	3757	3046	2428	1336
37	2088	1938	1466	1092	725	540	409	230
54	766	684	500	365	241	192	156	106

Master Curve Coefficients							R^2 (Logarithmic)	R^2 (Arithmetic)
δ	α	β	γ	a	b	c		
1.42146E+00	2.85842E+00	-9.44290E-01	5.83819E-01	-6.97673E-04	1.40284E-01	-2.50281E+00	0.99946	0.99825

96
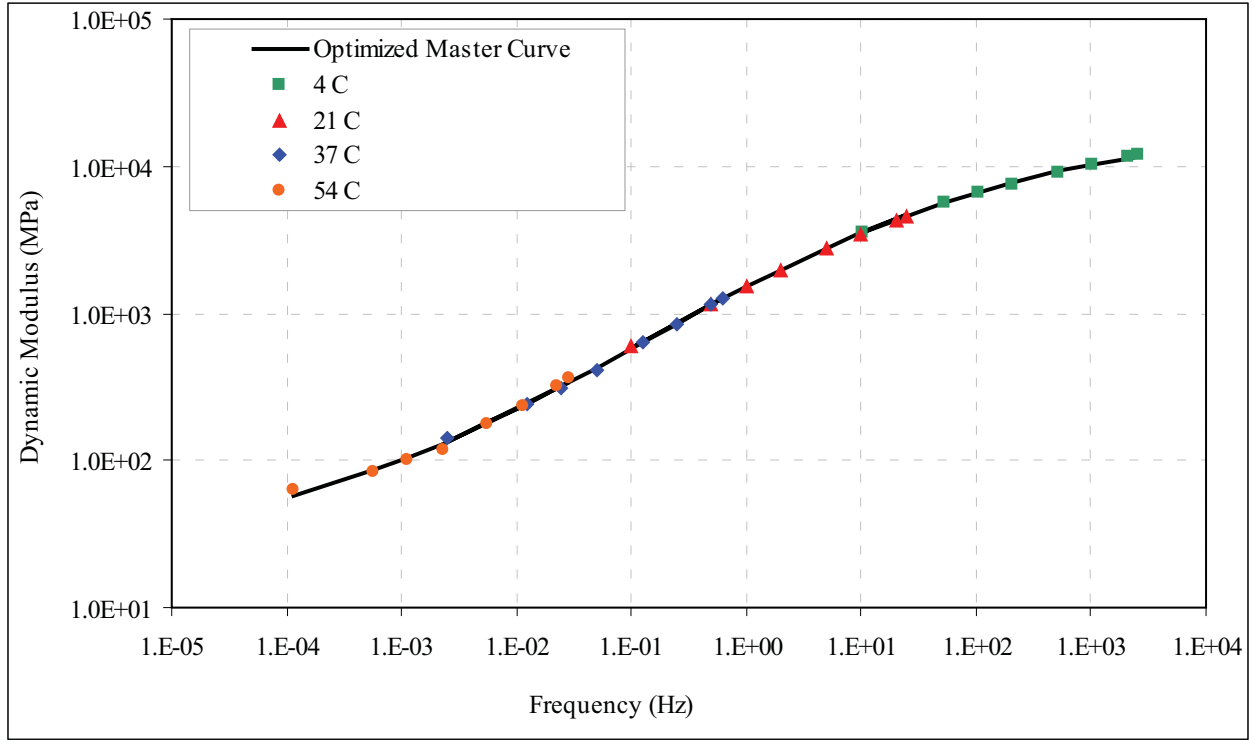
Figure A.15 Optimized Master Curve
(Project: Glenn Highway MP 34-42, parks to Palmer Resurf.)

Table A.15 Summary of Measured |E*| and Master curve Coefficients
(Project: Glenn Highway MP 34-42, parks to Palmer Resurf.)

Temperature (ºC)	Measured Dynamic Modulus (Mpa)							
	25 Hz	20 Hz	10 Hz	5 Hz	2 Hz	1 Hz	0.5 Hz	0.1 Hz
4	11815	11548	10353	9174	7585	6610	5642	3589
21	4565	4278	3455	2749	1980	1516	1151	595
37	1274	1155	852	626	411	310	239	143
54	362	320	237	176	119	99	84	63

Master Curve Coefficients							R^2 (Logarithmic)	R^2 (Arithmetic)
δ	α	β	γ	a	b	c		
1.34579E+00	2.94491E+00	-5.01107E-01	5.81627E-01	-6.01926E-04	1.34246E-01	-2.54652E+00	0.99956	0.99956

97
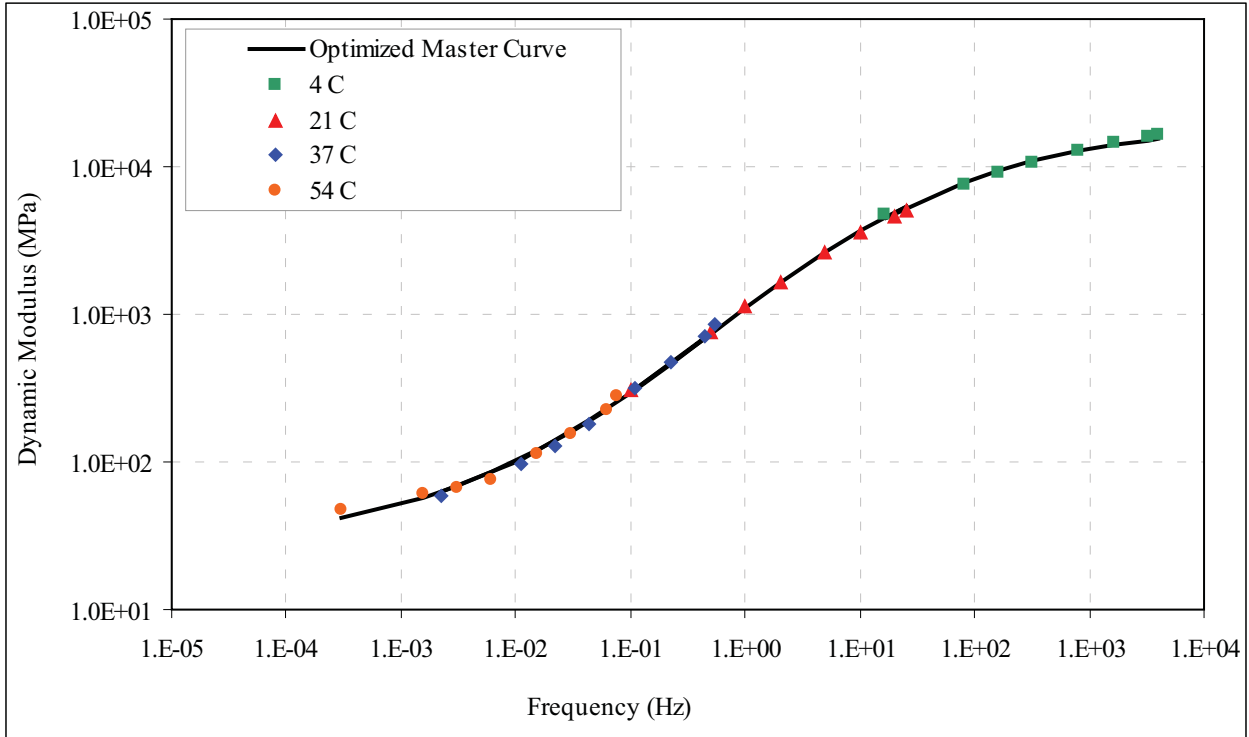
Figure A.16 Optimized Master Curve
(Project: Alaska Hwy MP 1267-1314)

Table A.16 Summary of Measured |E*| and Master curve Coefficients
(Project: Alaska Hwy MP 1267-1314)

Temperature (ºC)	Measured Dynamic Modulus (Mpa)							
	25 Hz	20 Hz	10 Hz	5 Hz	2 Hz	1 Hz	0.5 Hz	0.1 Hz
4	16476	16005	14388	12747	10624	9066	7593	4680
21	4971	4610	3534	2614	1660	1136	767	309
37	847	705	475	314	183	130	97	60
54	279	222	156	115	76	68	60	48

Master Curve Coefficients							R^2 (Logarithmic)	R^2 (Arithmetic)
δ	α	β	γ	a	b	c		
1.42688E+00	2.87628E+00	-2.48362E-01	8.15648E-01	-1.20508E-03	1.65208E-01	-2.87224E+00	0.99917	0.99691

98
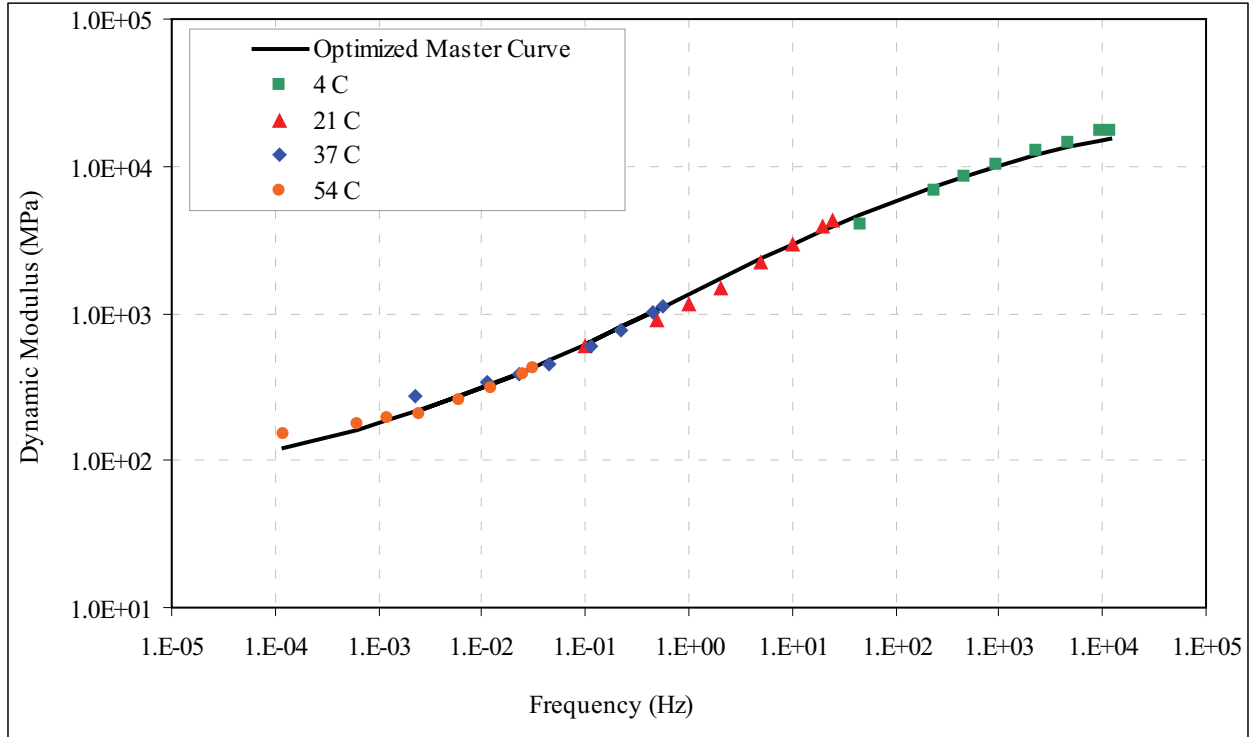
Figure A.17 Optimized Master Curve
(Project: AIA runway 7R_25L Rehab.)

Table A.17 Summary of Measured |E*| and Master curve Coefficients
(Project: AIA runway 7R_25L Rehab.)

Temperature (ºC)	Measured Dynamic Modulus (Mpa)							
	25 Hz	20 Hz	10 Hz	5 Hz	2 Hz	1 Hz	0.5 Hz	0.1 Hz
4	17482	17285	14650	12552	10119	8419	6874	4032
21	4278	3915	2949	2201	1499	1149	908	592
37	1112	1008	767	599	449	386	339	270
54	419	382	312	261	208	192	177	153

Master Curve Coefficients							R^2 (Logarithmic)	R^2 (Arithmetic)
δ	α	β	γ	a	b	c		
1.73424E+00	2.78934E+00	0.00000E+00	4.93006E-01	-1.24991E-03	1.83278E-01	-3.36018E+00	0.99593	0.98680

99
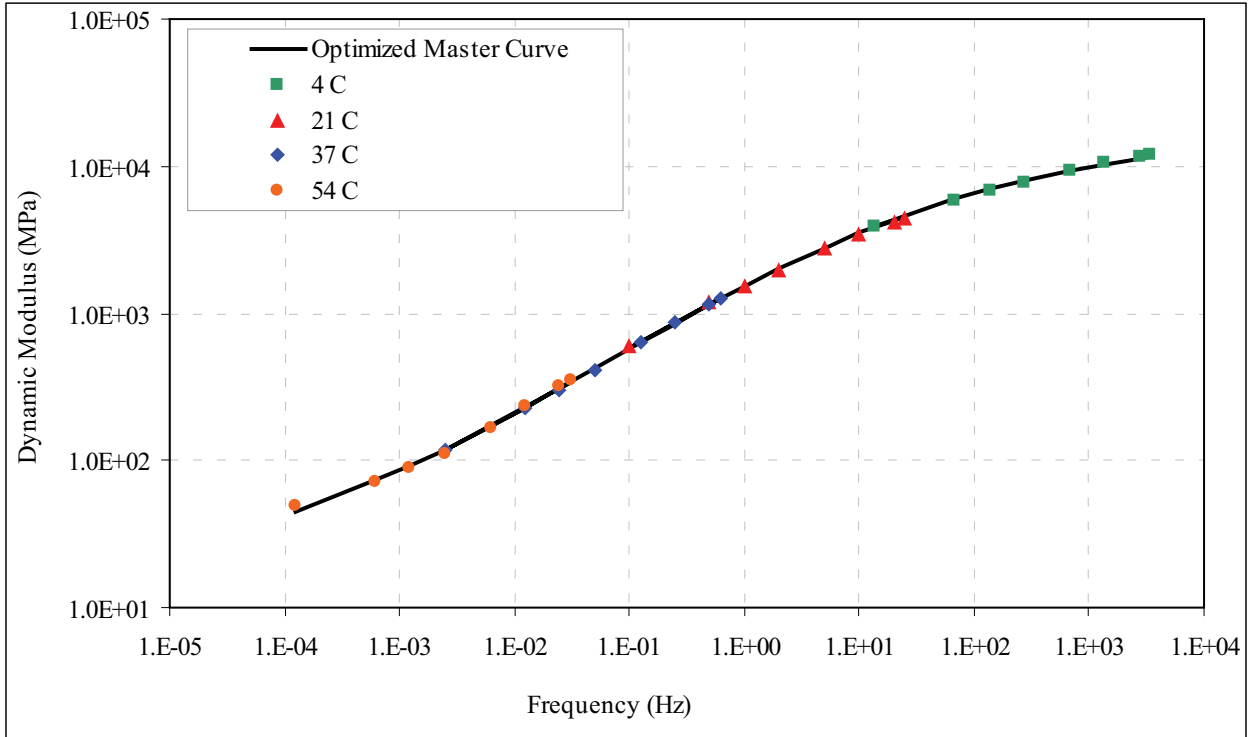
Figure A.18 Optimized Master Curve
(Project: Parks Hwy MP 287-305 Rehab.)

Table A.18 Summary of Measured |E*| and Master curve Coefficients
(Project: Parks Hwy MP 287-305 Rehab.)

Temperature (°C)	Measured Dynamic Modulus (Mpa)							
	25 Hz	20 Hz	10 Hz	5 Hz	2 Hz	1 Hz	0.5 Hz	0.1 Hz
4	11947	11647	10461	9300	7844	6816	5858	3869
21	4394	4177	3401	2727	1981	1535	1178	601
37	1273	1167	869	637	413	303	224	118
54	353	319	232	167	109	88	72	49

Master Curve Coefficients							R^2 (Logarithmic)	R^2 (Arithmetic)
δ	α	β	γ	a	b	c		
1.07428E+00	3.21272E+00	-6.46898E-01	5.51805E-01	-7.42798E-04	1.43955E-01	-2.69956E+00	0.99962	0.99915

100
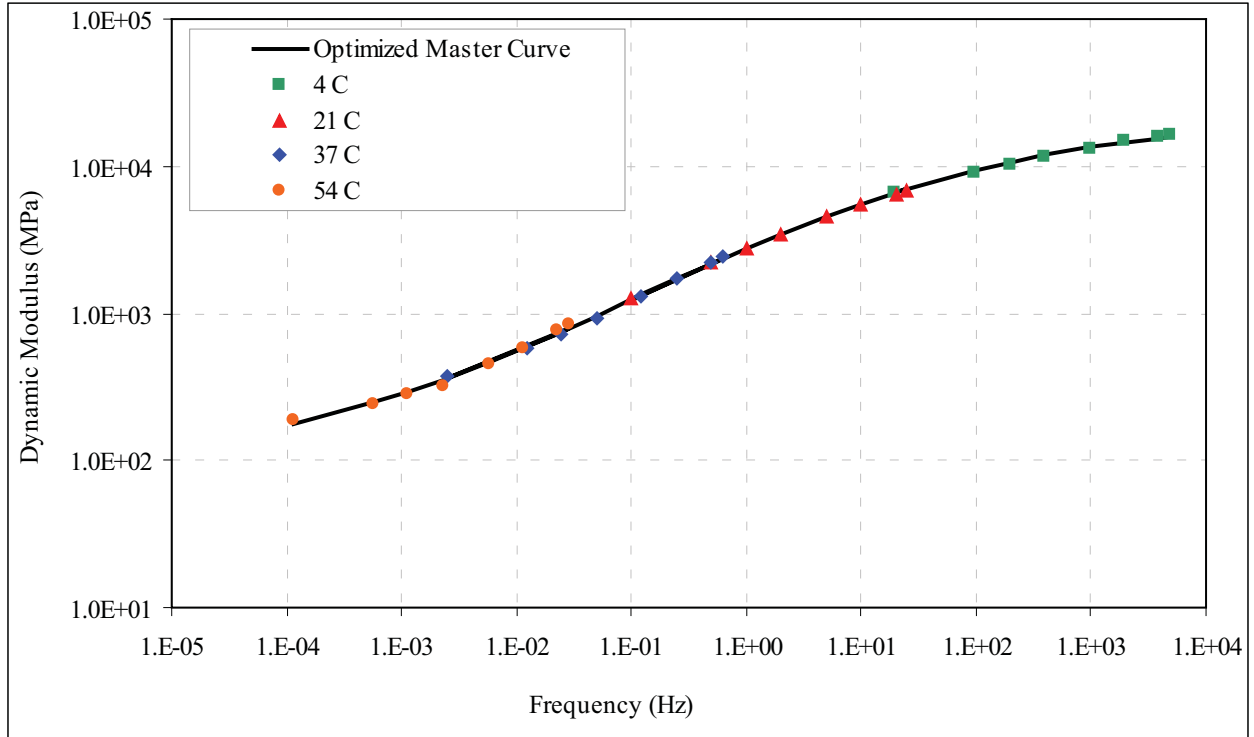
Figure A.19 Optimized Master Curve
(Project: PSG Mitkof Highway-Scow Bay to Crystal Lake Hatchery)

Table A.19 Summary of Measured |E*| and Master curve Coefficients
(Project: PSG Mitkof Highway-Scow Bay to Crystal Lake Hatchery)

Temperature (ºC)	Measured Dynamic Modulus (Mpa)							
	25 Hz	20 Hz	10 Hz	5 Hz	2 Hz	1 Hz	0.5 Hz	0.1 Hz
4	16111	16032	14660	13320	11611	10365	9168	6699
21	6781	6467	5450	4529	3465	2781	2220	1280
37	2403	2228	1722	1324	925	725	583	376
54	838	759	583	453	323	279	244	189
Master Curve Coefficients							R^2 (Logarithmic)	R^2 (Arithmetic)
δ	α	β	γ	a	b	c		
1.87310E+00	2.49071E+00	-5.30918E-01	5.75000E-01	-8.49495E-04	1.53562E-01	-2.88015E+00	0.99945	0.99925

APPENDIX B: Predicted |E*| Based on Original Witczak Model
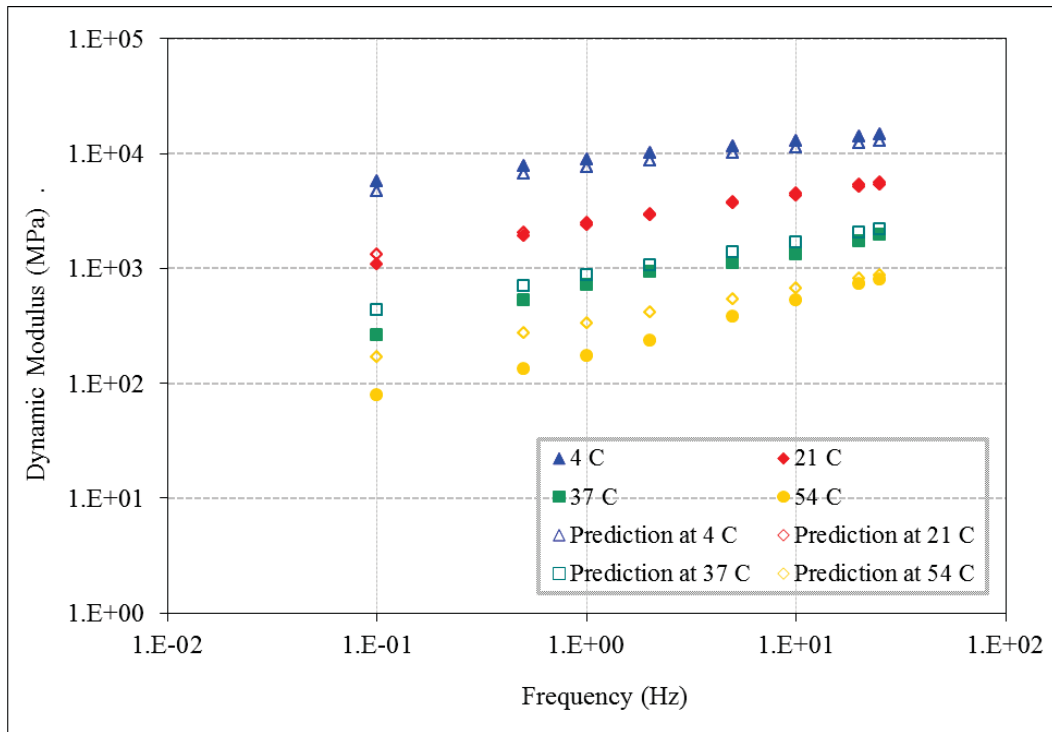
a) Measured and Predicted |E*| at Different Temperature and Frequency
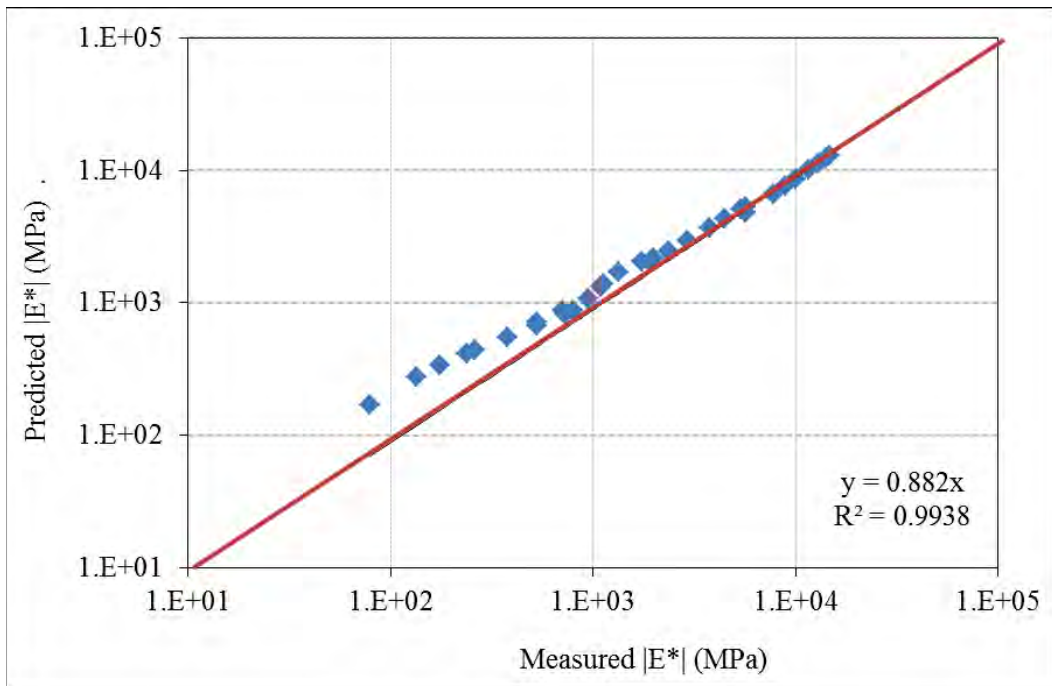
b) Measured |E*| vs. Predicted |E*|

Figure B.1 Summary of Predicted |E*| based on Original Witczak Model
(Project: FIA Runway 1L_19R stage 3 (64-34))
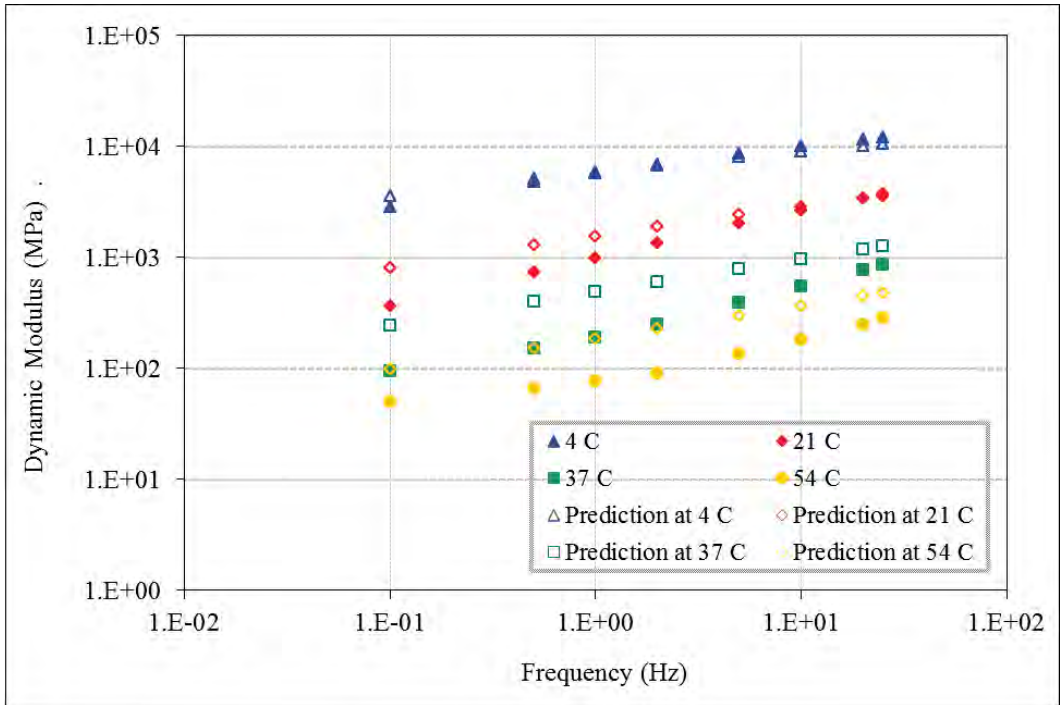
a) Measured and Predicted |E*| at Different Temperature and Frequency
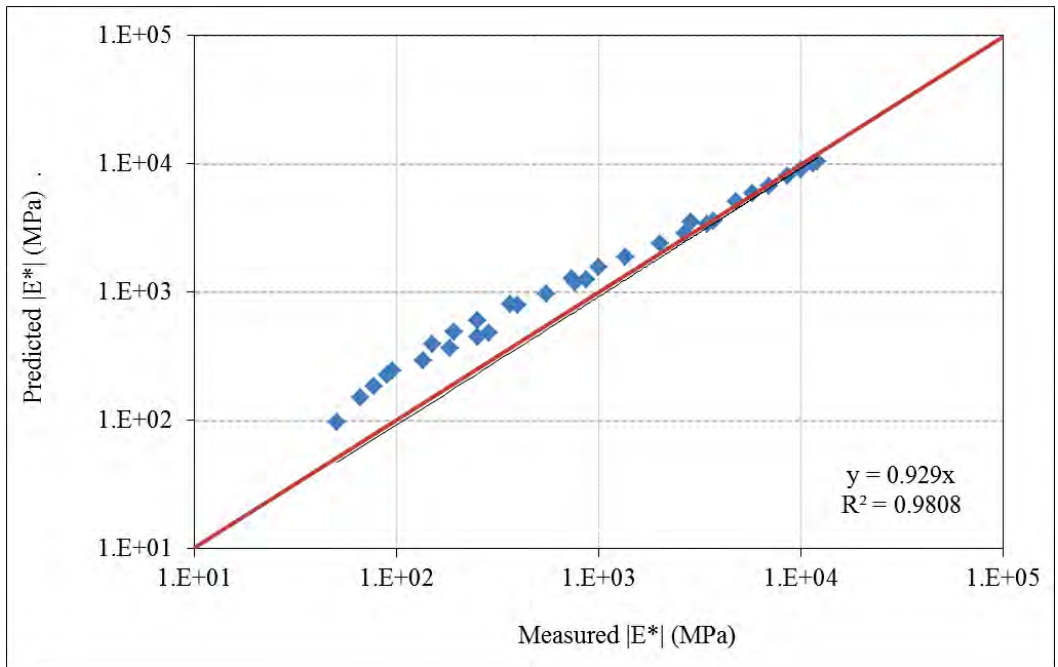
b) Measured |E*| vs. Predicted |E*|

Figure B.2 Summary of Predicted |E*| based on Original Witczak Model
(Project: FIA Runway 1L_19R stage 3 (52-34))
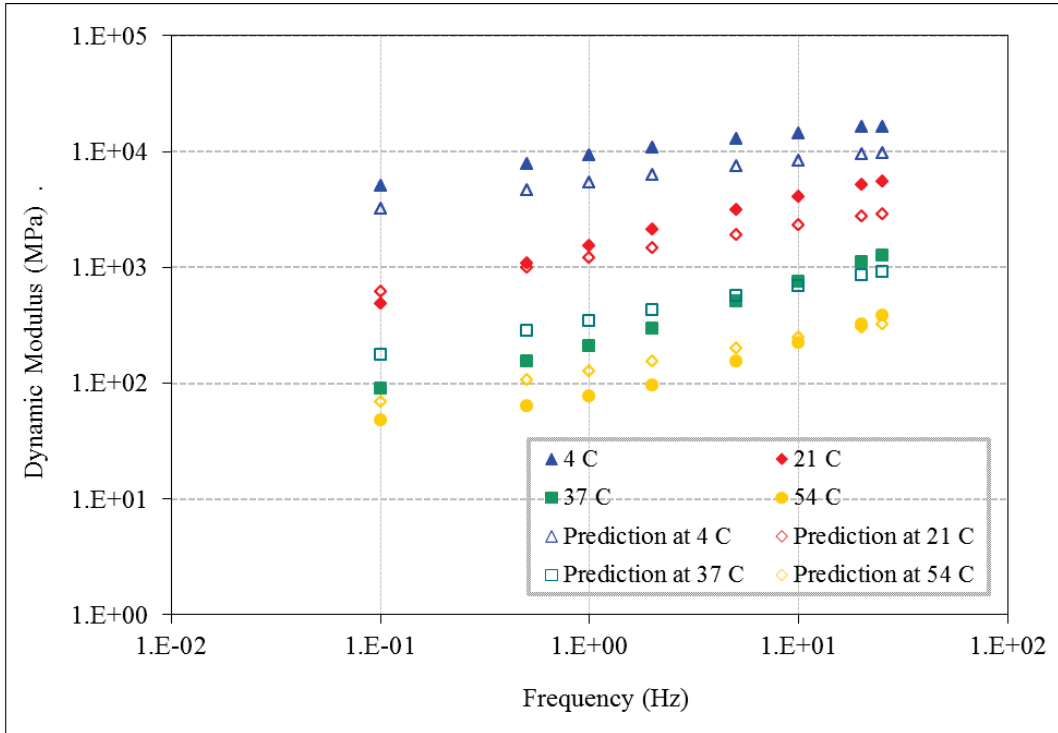
a) Measured and Predicted |E*| at Different Temperature and Frequency
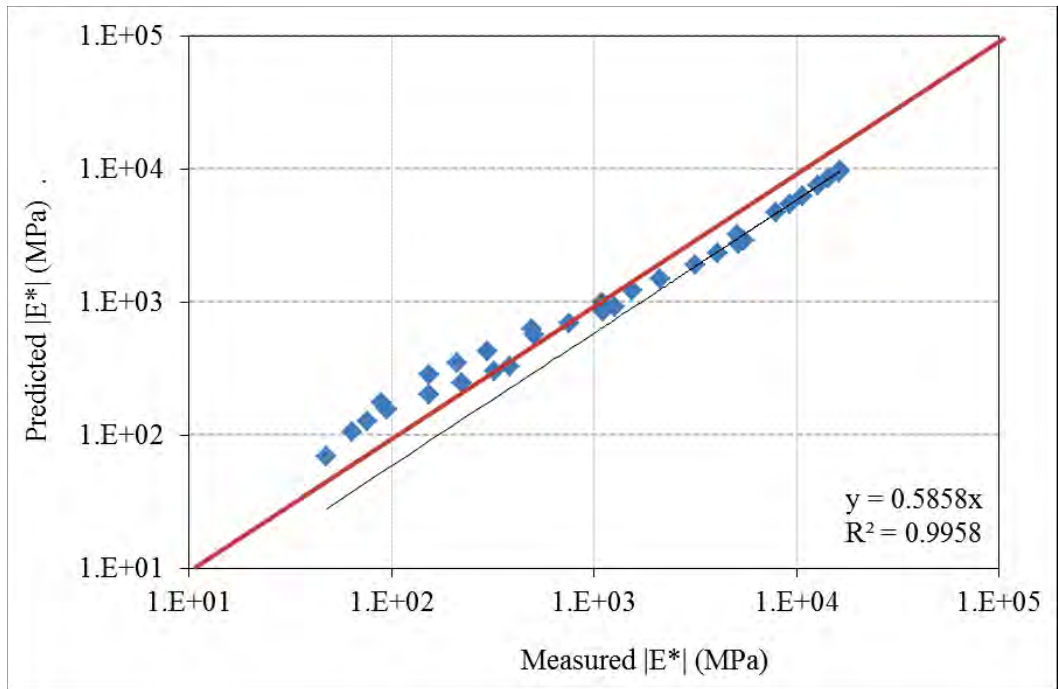
b) Measured |E*| vs. Predicted |E*|

Figure B.3 Summary of Predicted |E*| based on Original Witczak Model
(Project: Chena Hot Springs Rd, MD-1)
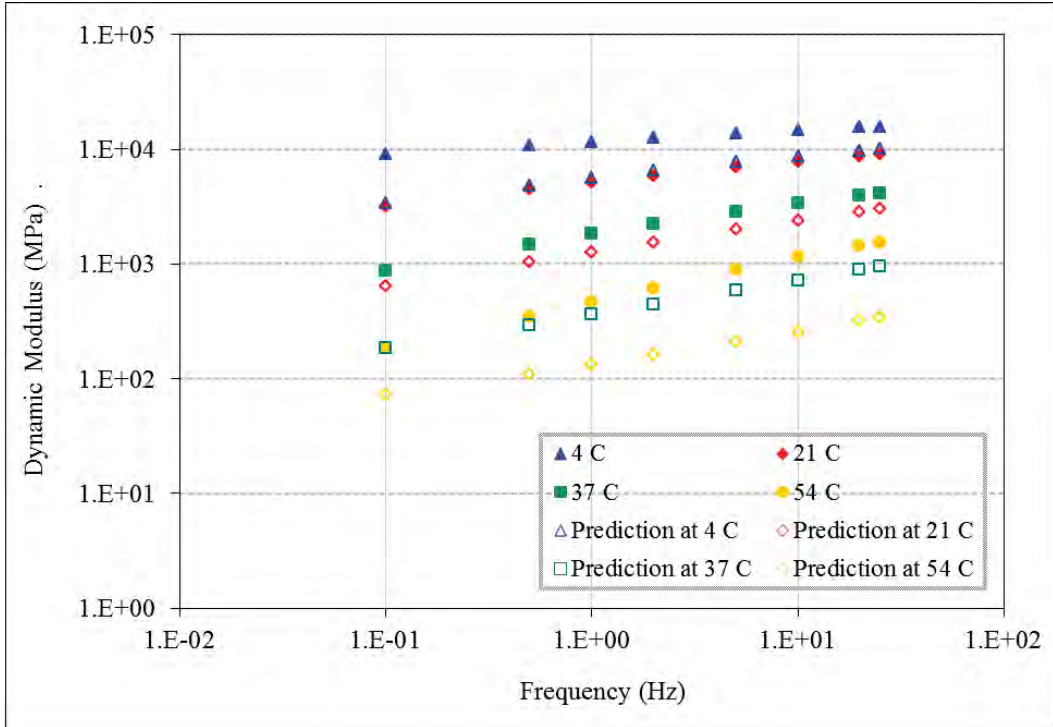
a) Measured and Predicted |E*| at Different Temperature and Frequency
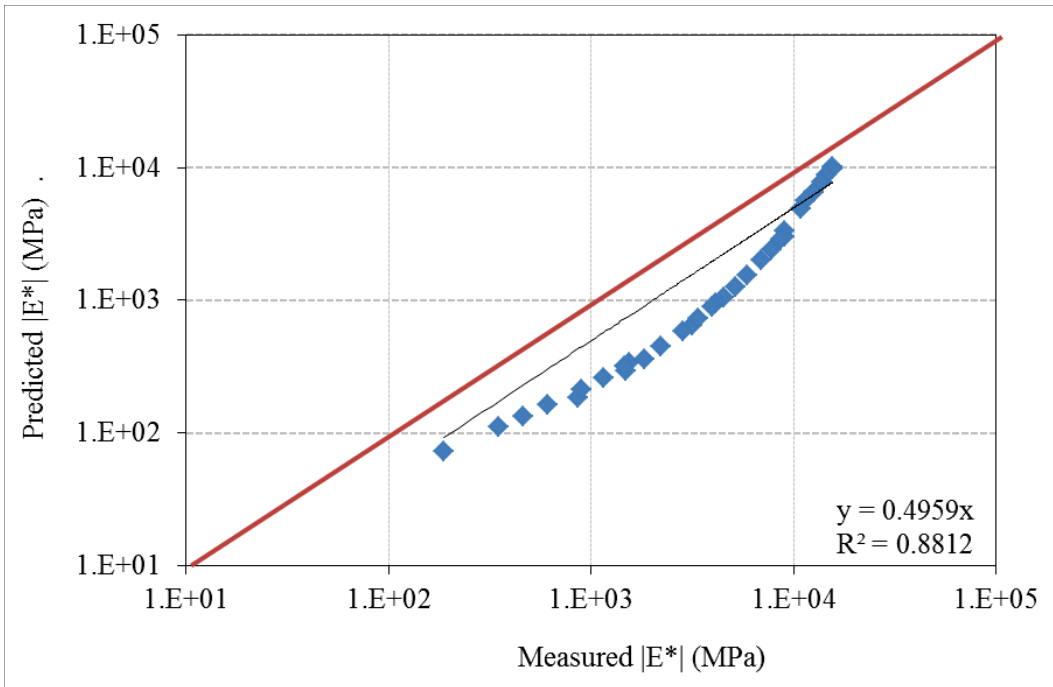
b) Measured |E*| vs. Predicted |E*|

Figure B.4 Summary of Predicted |E*| based on Original Witczak Model
(Project: Chena Hot Springs Rd MD-3)
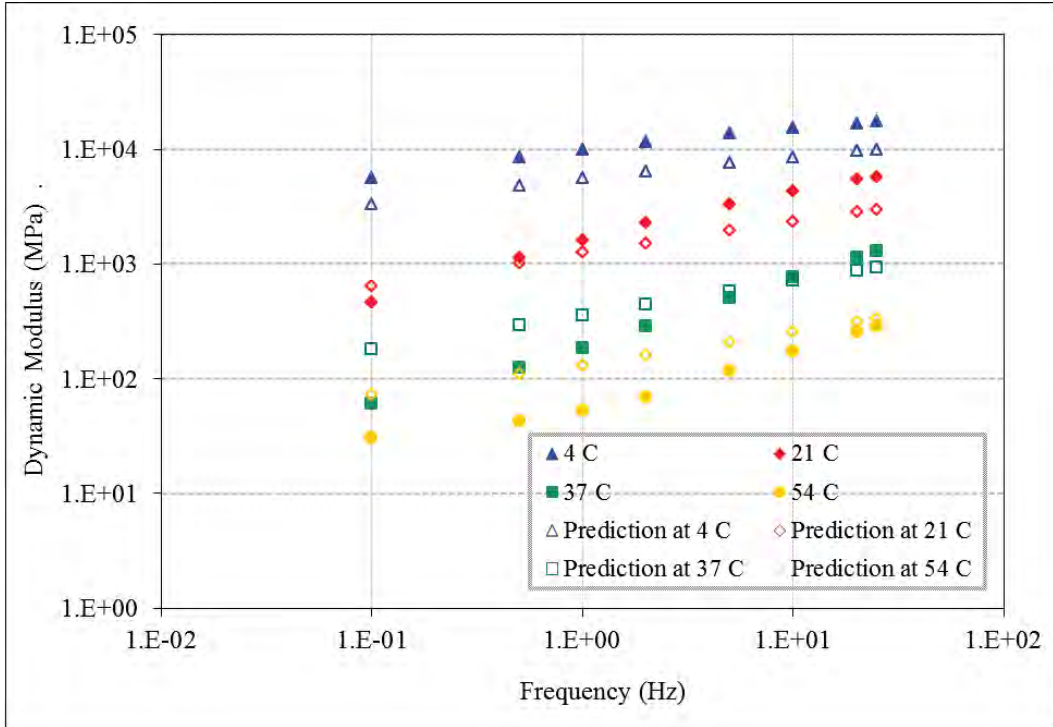
a) Measured and Predicted |E*| at Different Temperature and Frequency
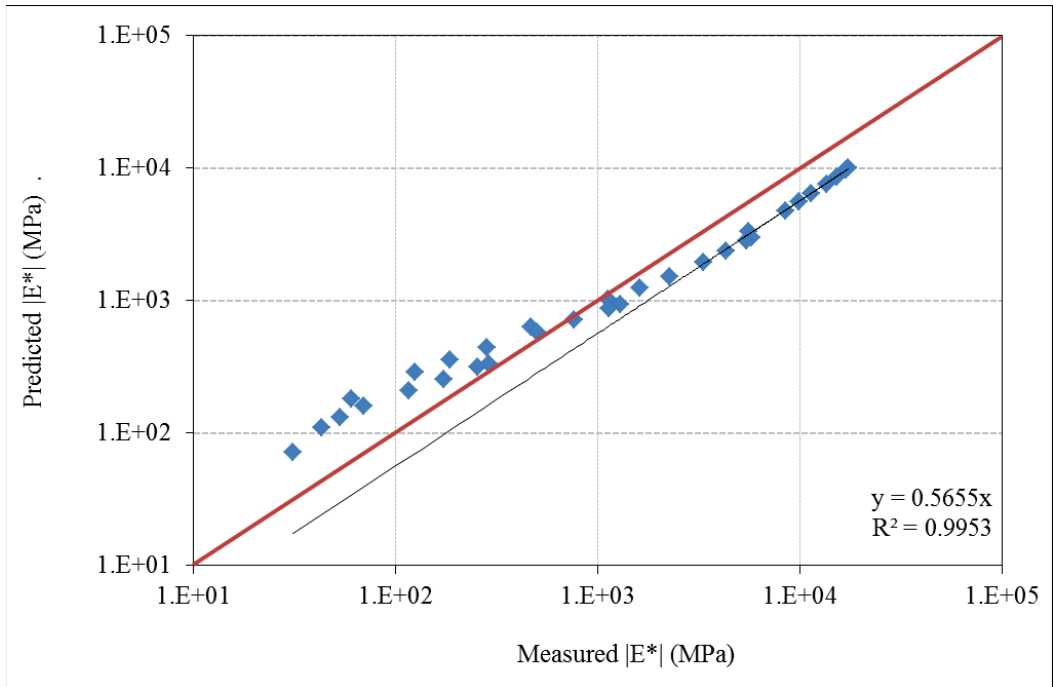
b) Measured |E*| vs. Predicted |E*|

Figure B.5 Summary of Predicted |E*| based on Original Witczak Model
(Project: Fairbanks Cowles Street Upgrade)
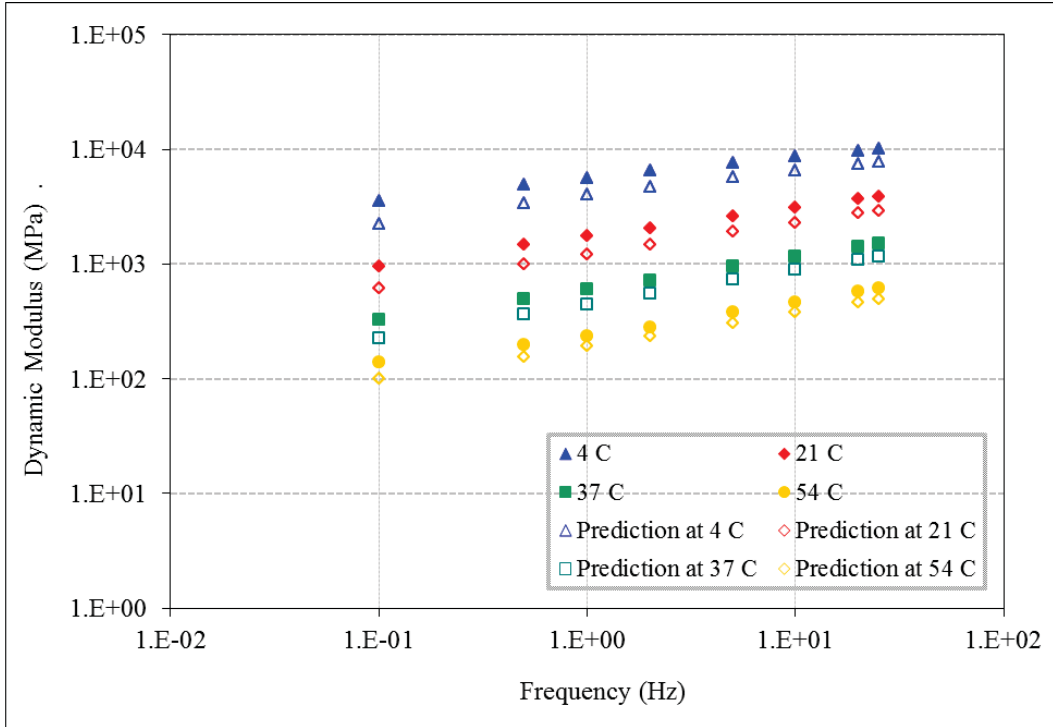
a) Measured and Predicted |E*| at Different Temperature and Frequency
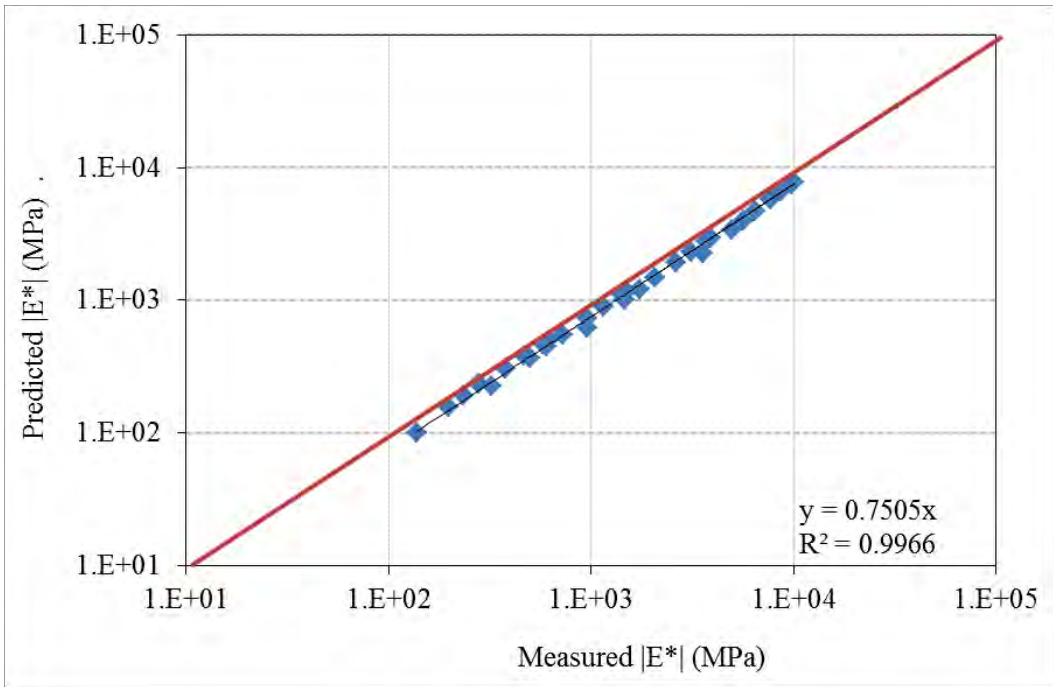
b) Measured |E*| vs. Predicted |E*|

Figure B.6 Summary of Predicted |E*| based on Original Witczak Model
(Project: Dalton Hwy. MP 175-197 Rehabilitation)
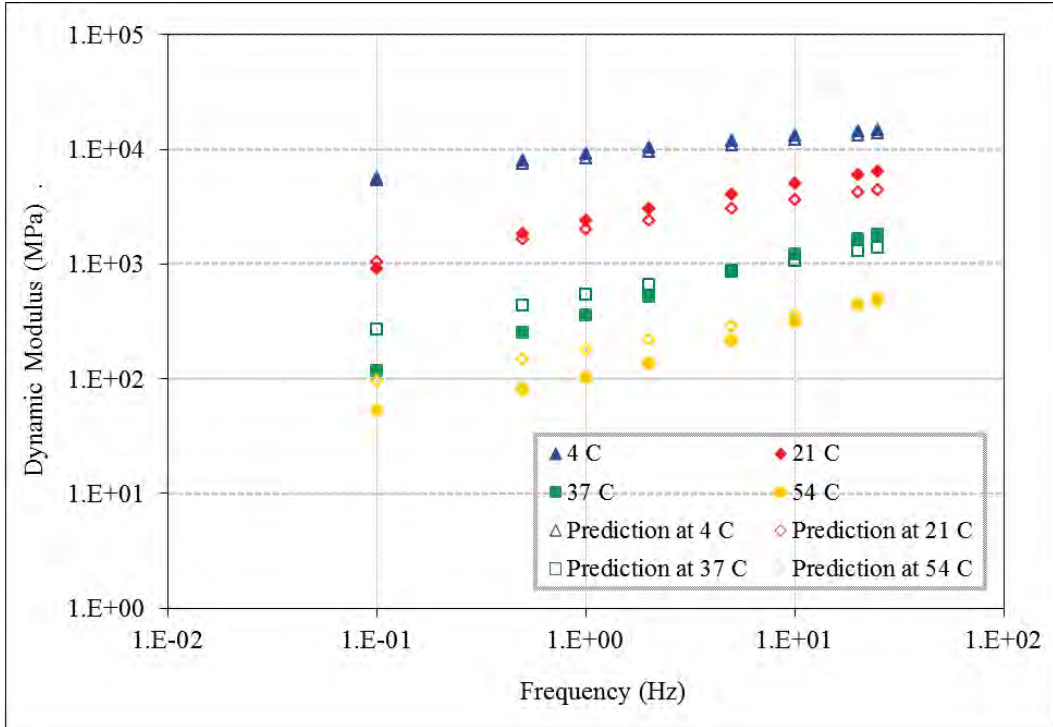
a) Measured and Predicted |E*| at Different Temperature and Frequency
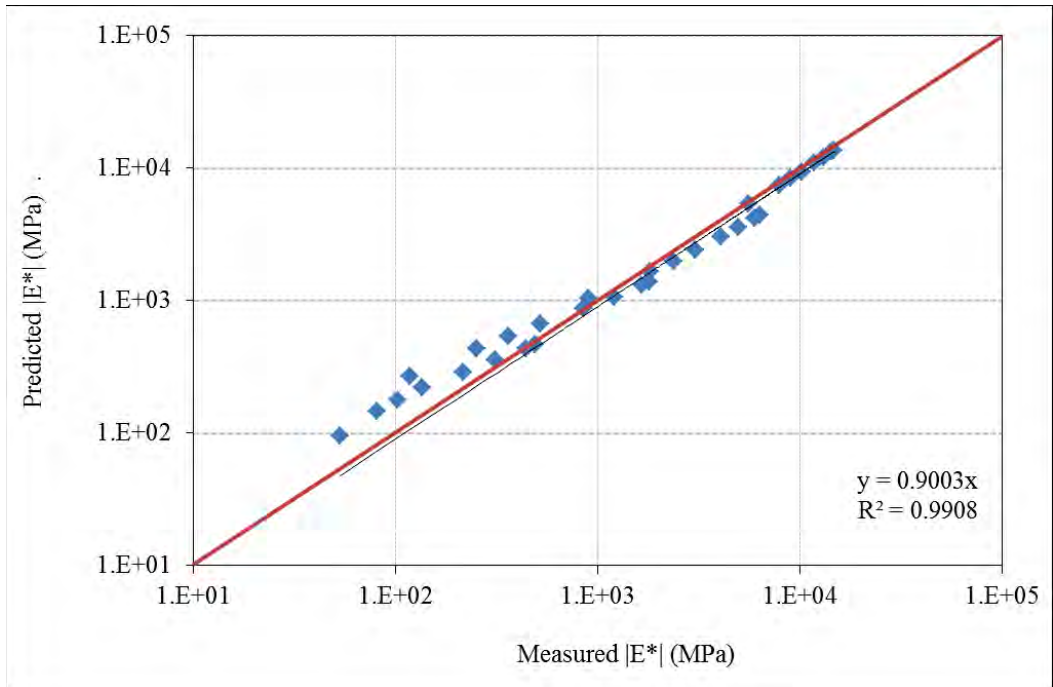
b) Measured |E*| vs. Predicted |E*|

Figure B.7 Summary of Predicted |E*| based on Original Witczak Model
(Project: Glen Why MP 92-97 Cascade to Hicks Creek)
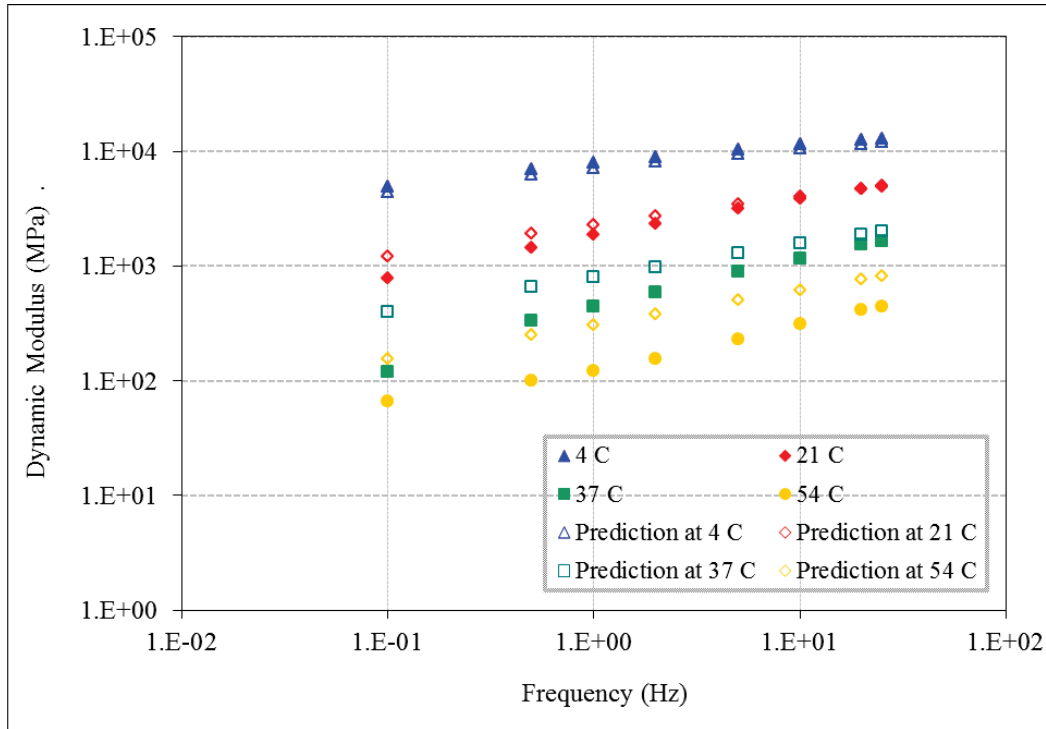
a) Measured and Predicted |E*| at Different Temperature and Frequency
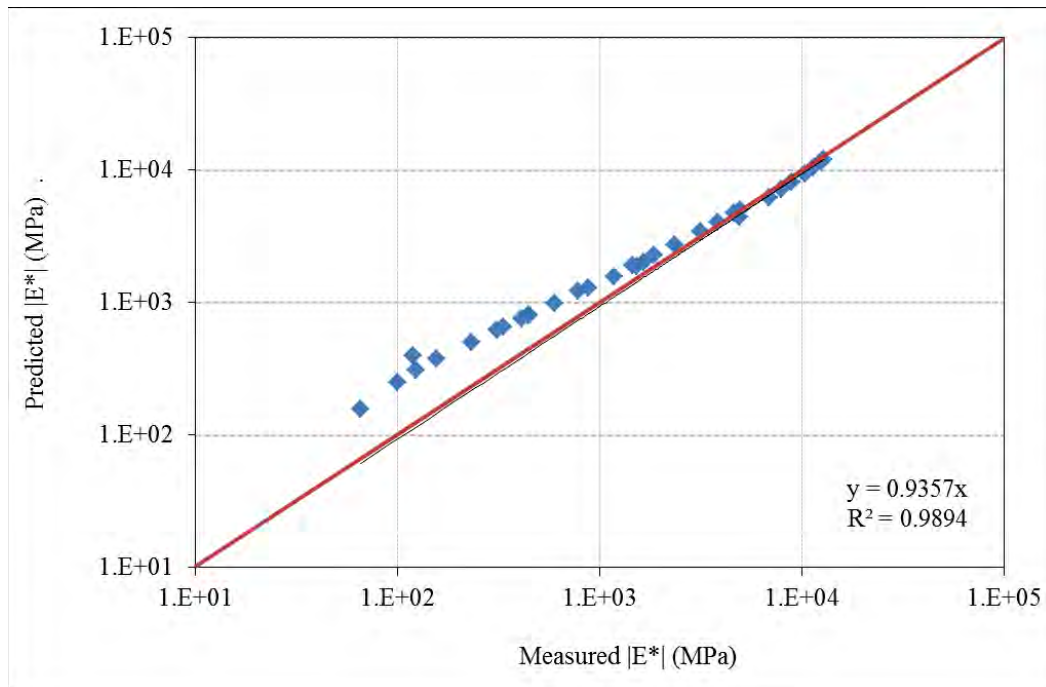
b) Measured |E*| vs. Predicted |E*|

Figure B.8 Summary of Predicted |E*| based on Original Witczak Model
(Project: Glenn Highway Gambell to airport MP 0-1.5)
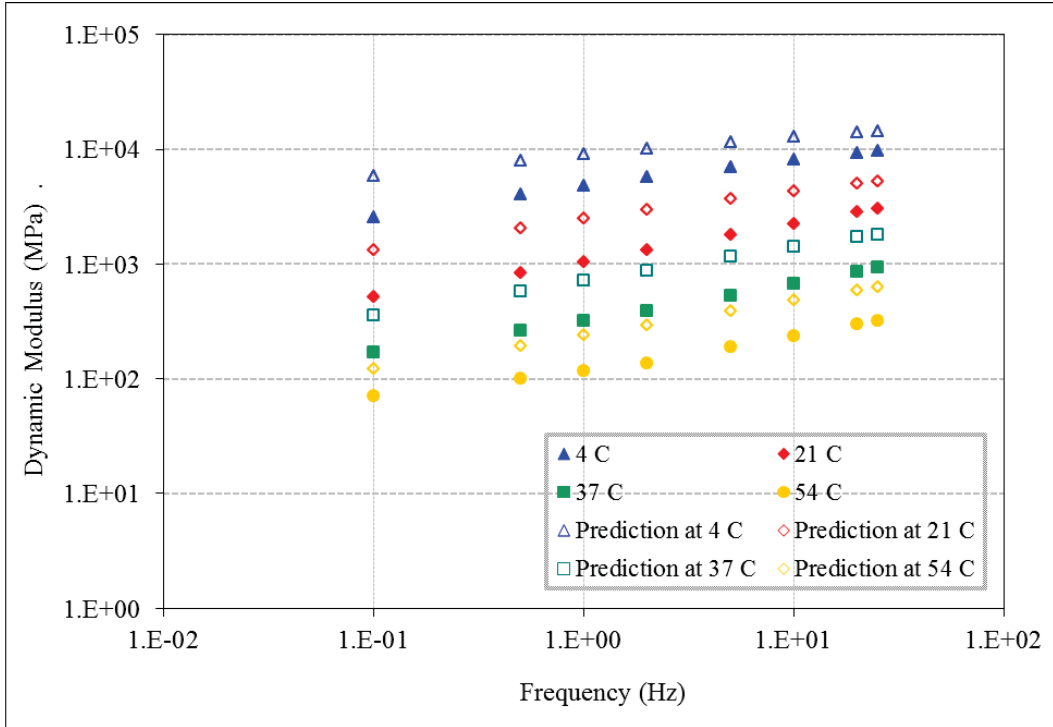
a) Measured and Predicted |E*| at Different Temperature and Frequency
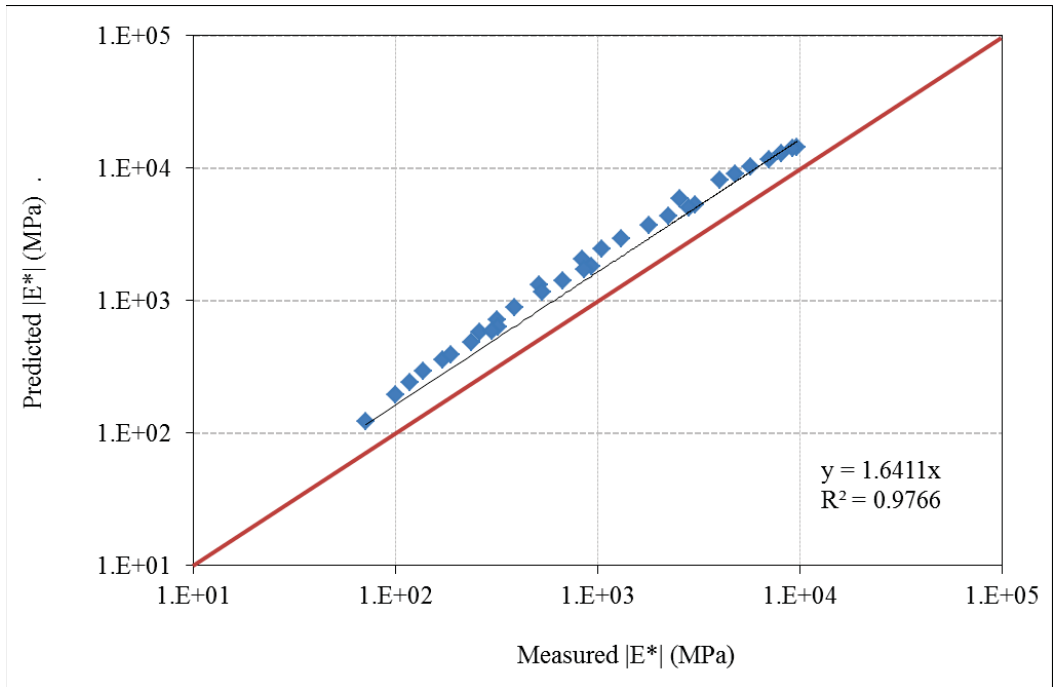
b) Measured |E*| vs. Predicted |E*|

Figure B.9 Summary of Predicted |E*| based on Original Witczak Model
(Project HNS Ferry Terminal to Union Street)
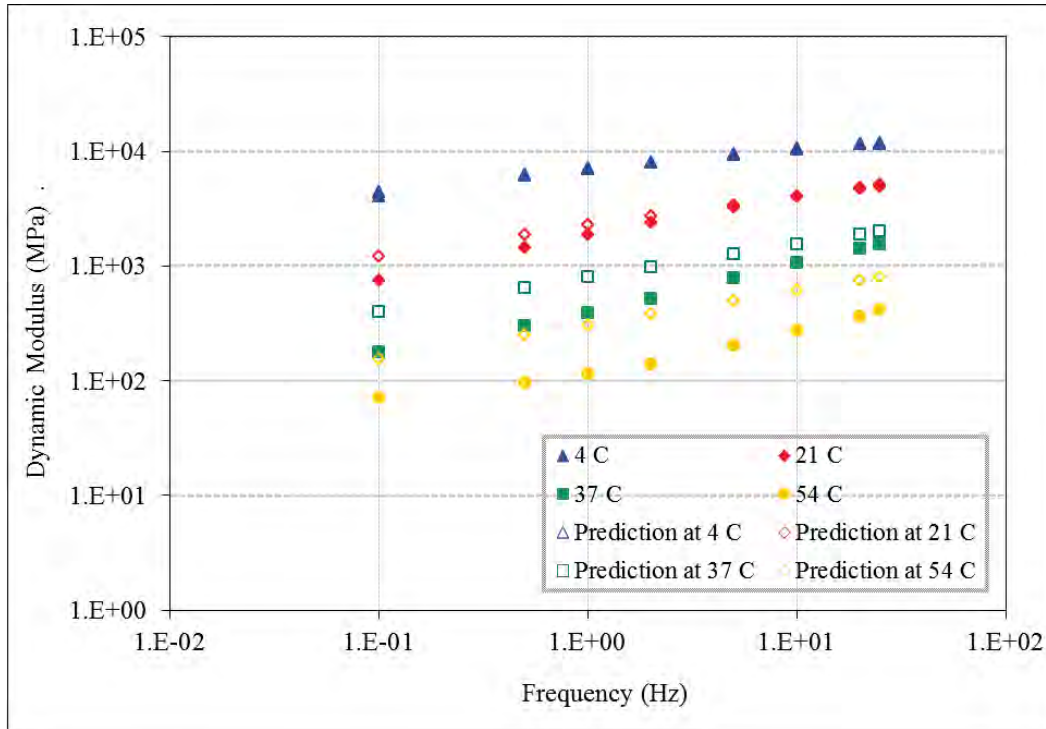
a) Measured and Predicted |E*| at Different Temperature and Frequency
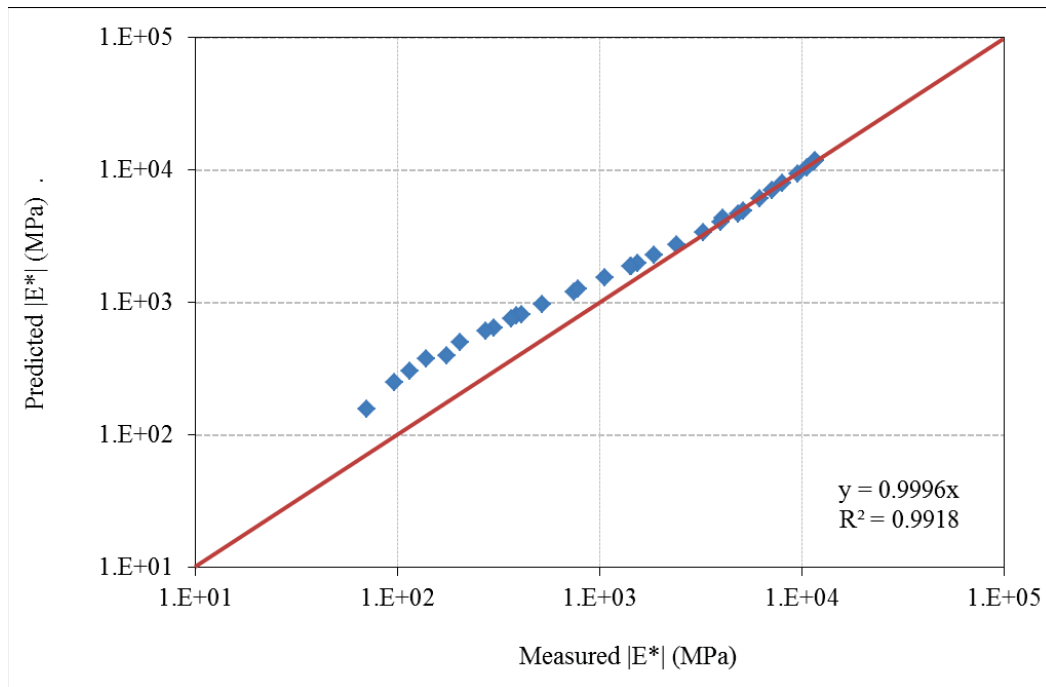
b) Measured |E*| vs. Predicted |E*|

Figure B.10 Summary of Predicted |E*| based on Original Witczak Model
(Project: Minnesota Dr Resurfacing: Int'l Airport Rd to 13th)
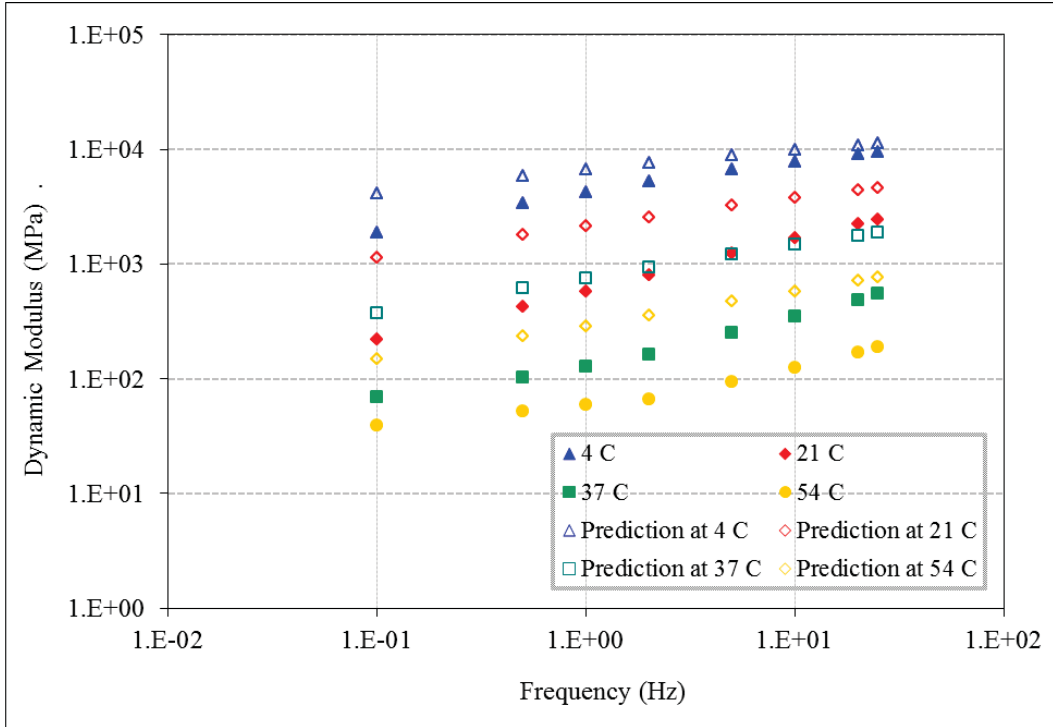
a) Measured and Predicted |E*| at Different Temperature and Frequency
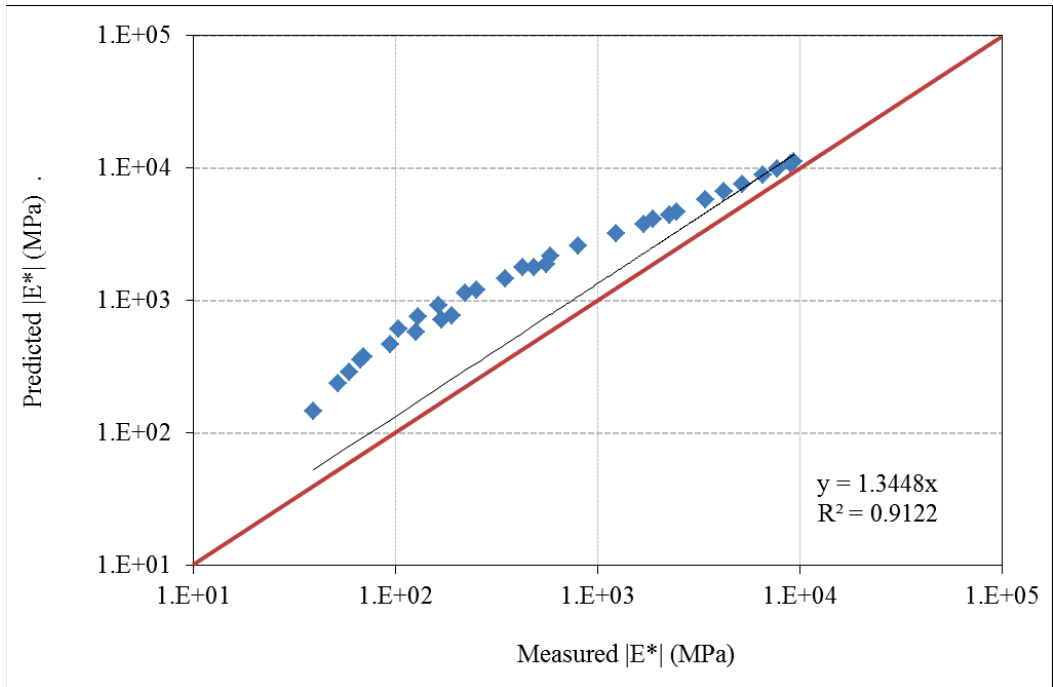
b) Measured |E*| vs. Predicted |E*|

Figure B.11 Summary of Predicted |E*| based on Original Witczak Model
(Project: Rich Hwy North Pole Interchange)
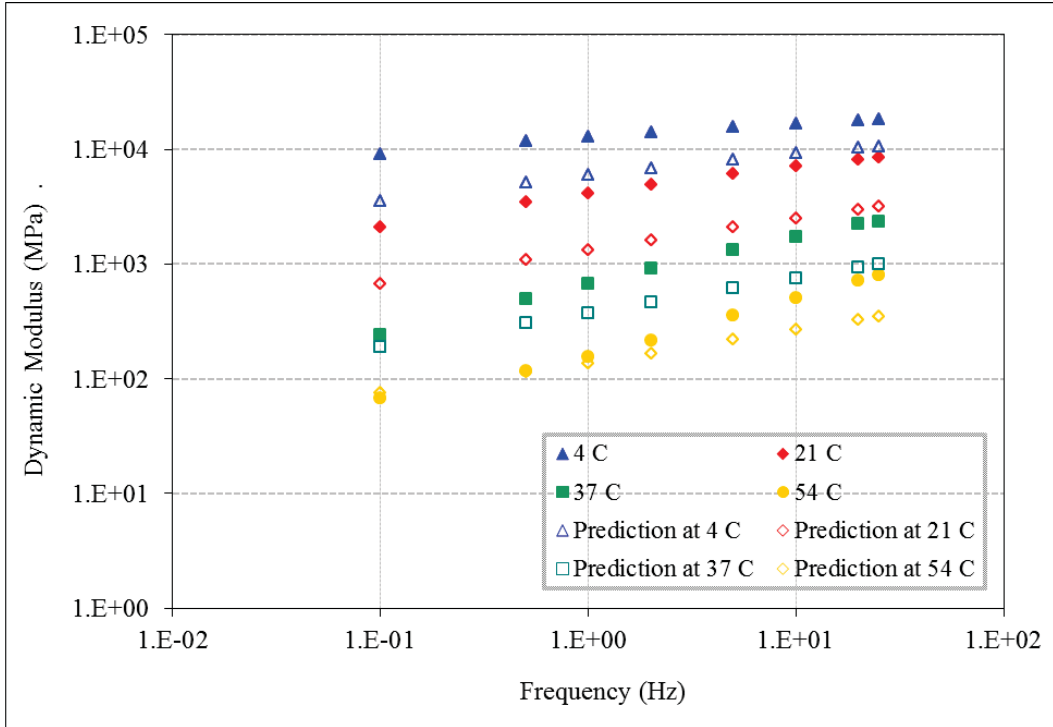
a) Measured and Predicted |E*| at Different Temperature and Frequency
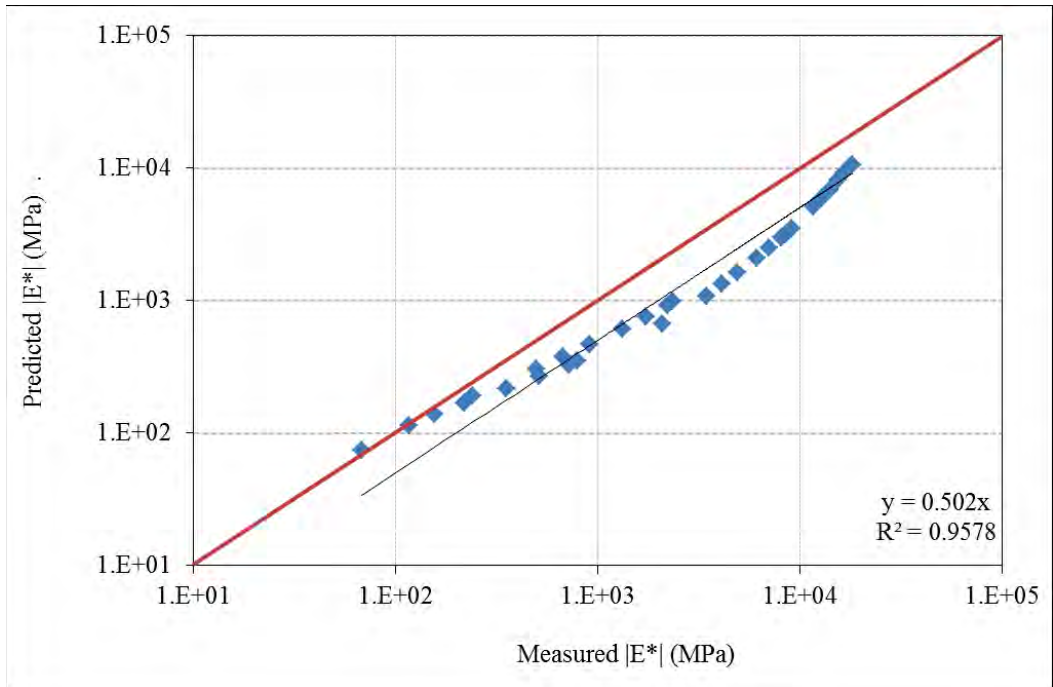
b) Measured |E*| vs. Predicted |E*|

Figure B.12 Summary of Predicted |E*| based on Original Witczak Model
(Project: Old Glenn Hwy.: MP 11.5-18)
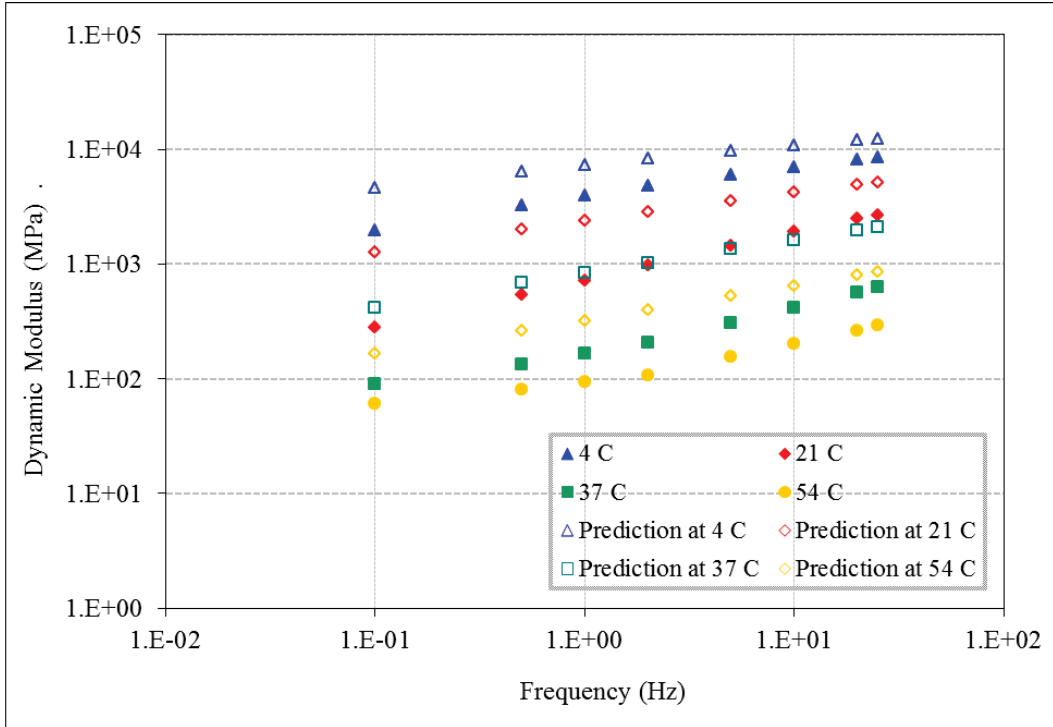
113

a) Measured and Predicted |E*| at Different Temperature and Frequency
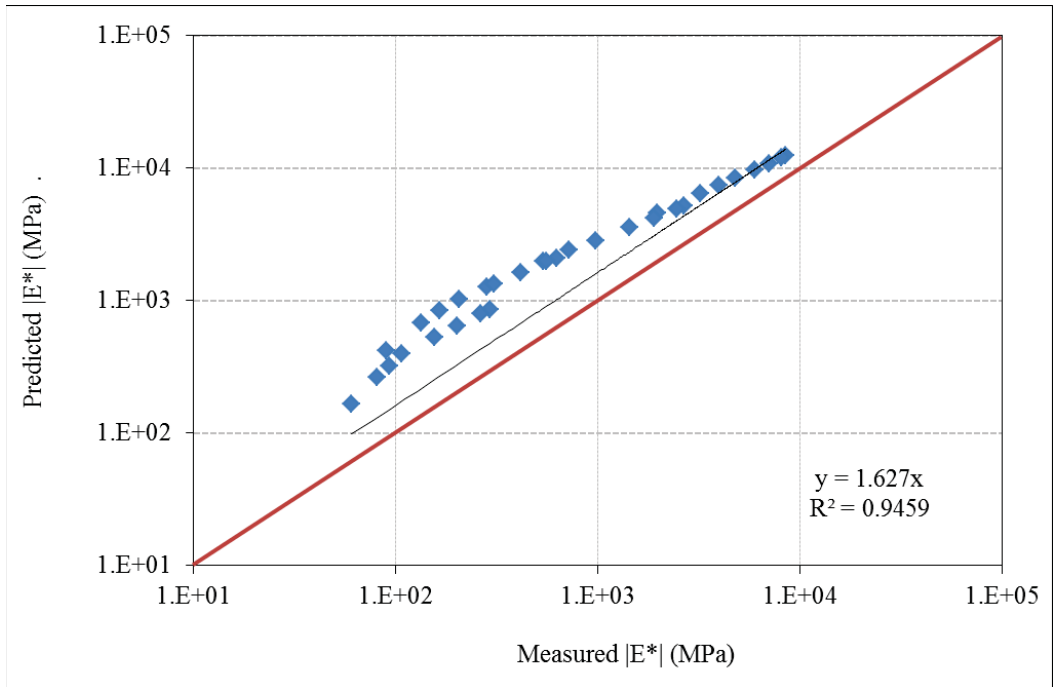
b) Measured |E*| vs. Predicted |E*|

Figure B.13 Summary of Predicted |E*| based on Original Witczak Model
(Project: Palmer-Wasilla Highway Phase II)
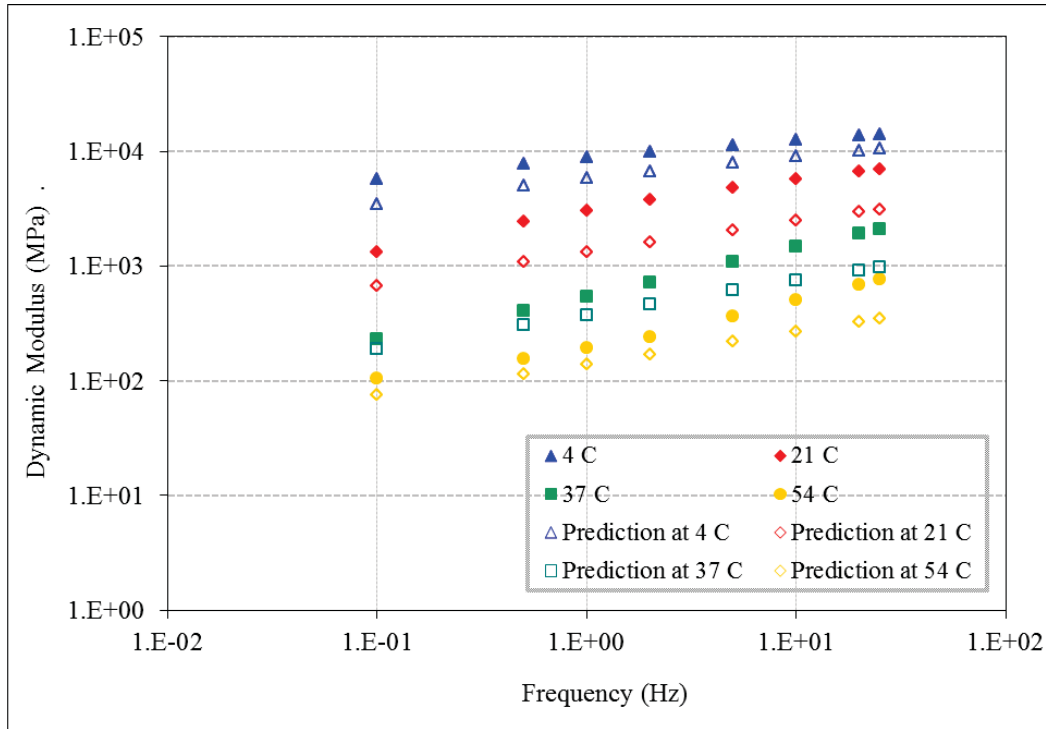
a) Measured and Predicted |E*| at Different Temperature and Frequency
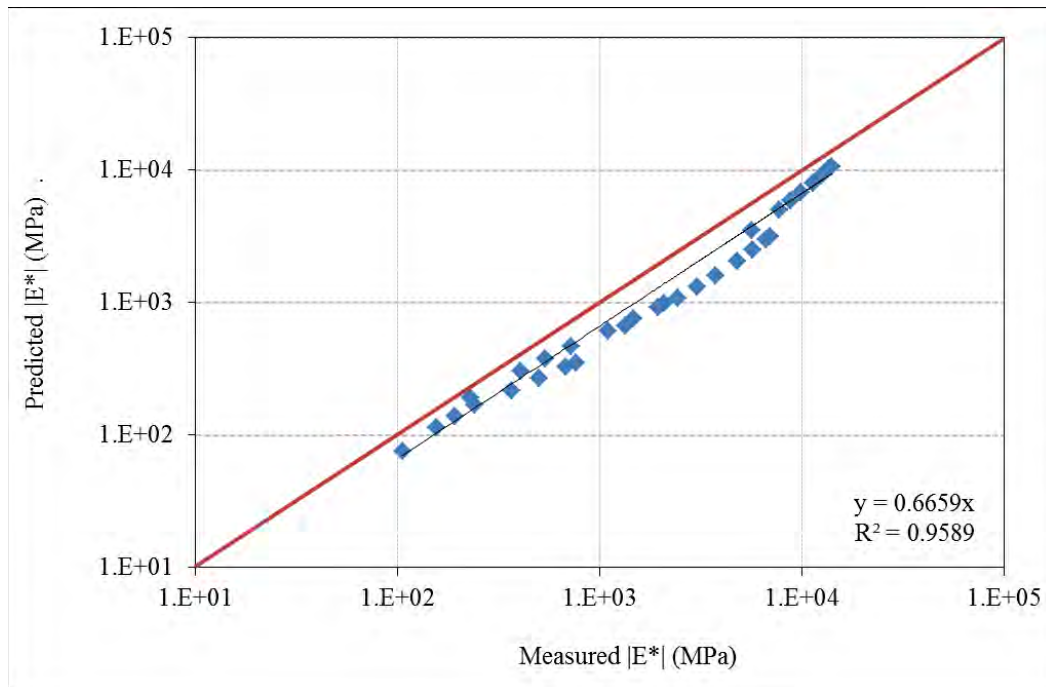
b) Measured |E*| vs. Predicted |E*|

Figure B.14 Summary of Predicted |E*| based on Original Witczak Model
(Project: Unalakleet Airport Paving)
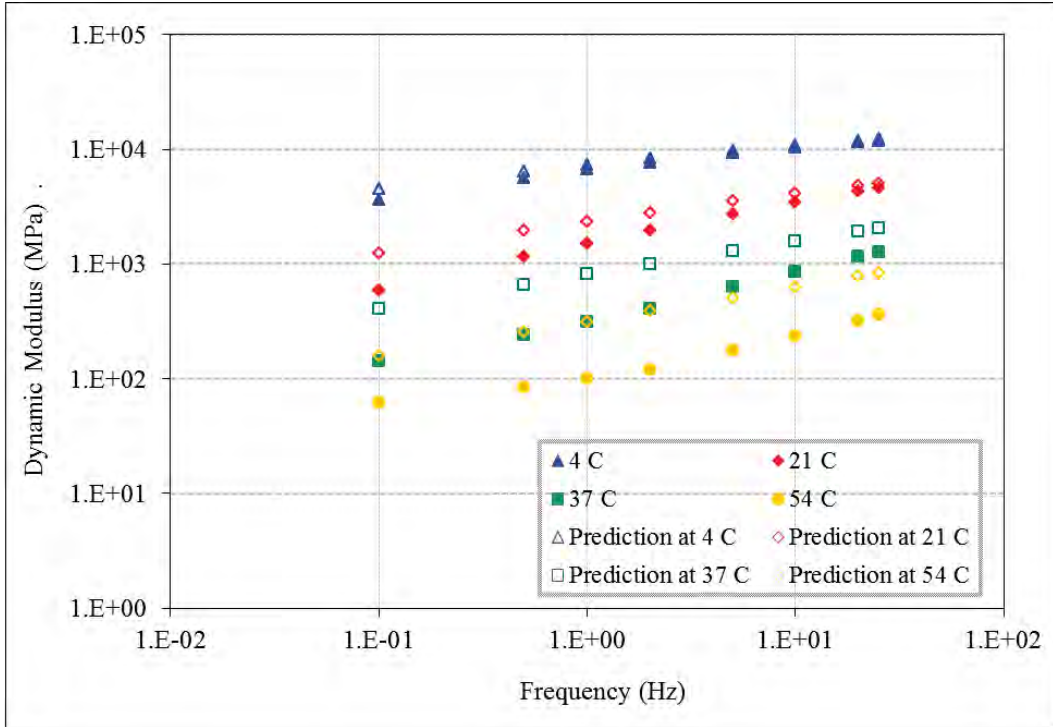
a) Measured and Predicted |E*| at Different Temperature and Frequency
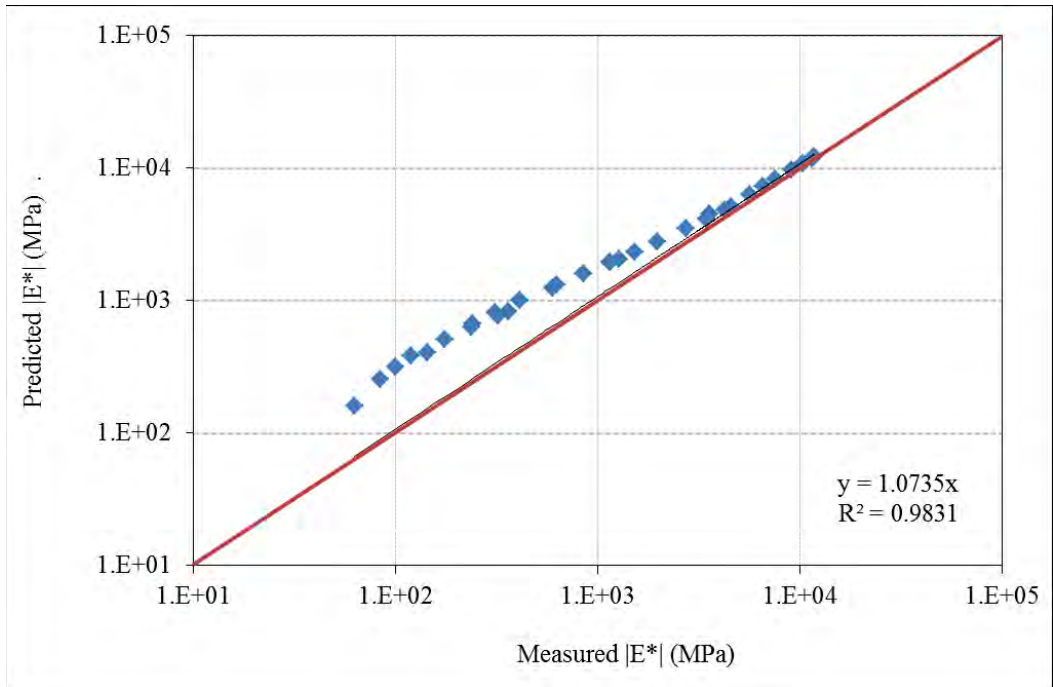
b) Measured |E*| vs. Predicted |E*|

Figure B.15 Summary of Predicted |E*| based on Original Witczak Model
(Project: Glenn Highway MP 34-42, parks to Palmer Resurf.)

116
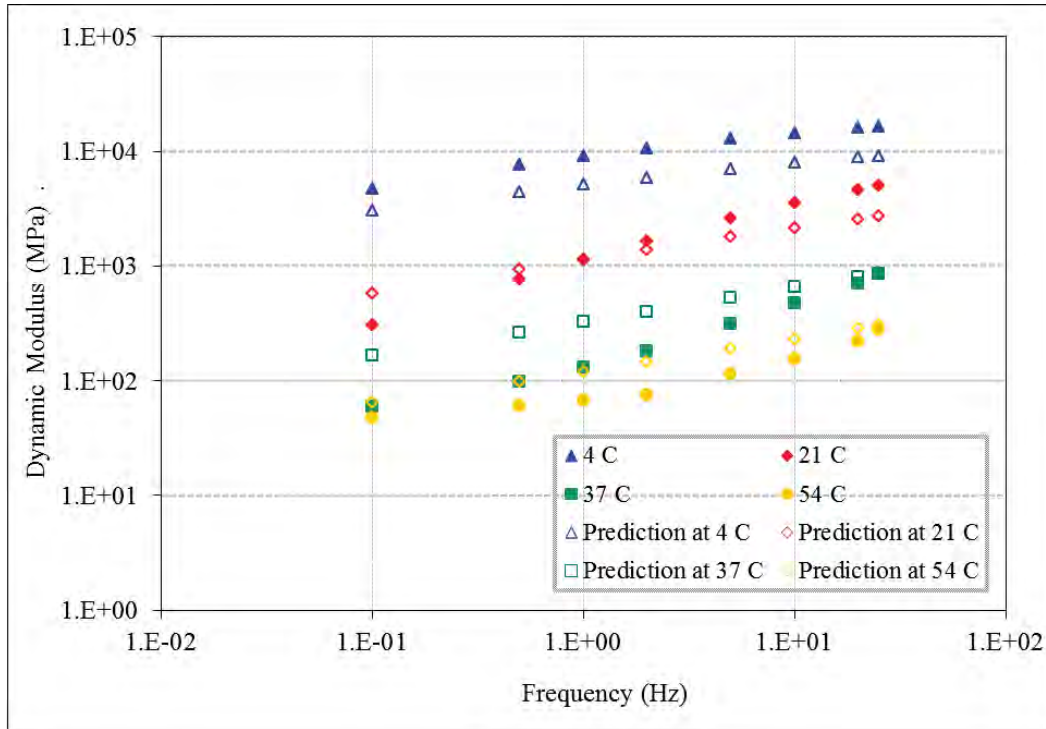
a) Measured and Predicted |E*| at Different Temperature and Frequency
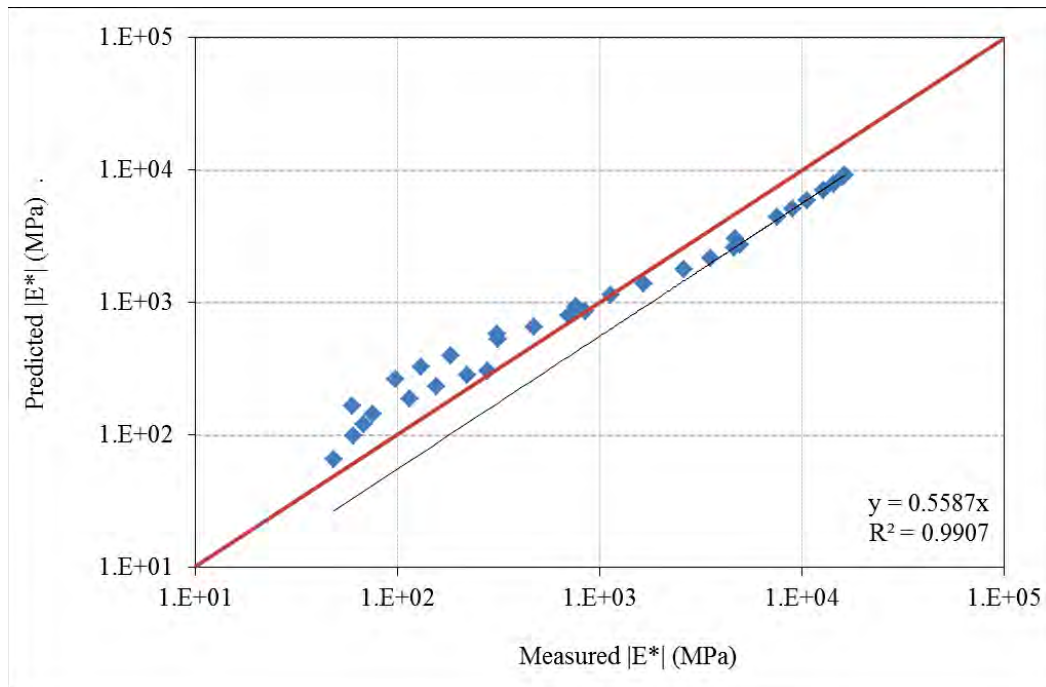
b) Measured |E*| vs. Predicted |E*|

Figure B.16 Summary of Predicted |E*| based on Original Witczak Model
(Project: Alaska Hwy MP 1267-1314)
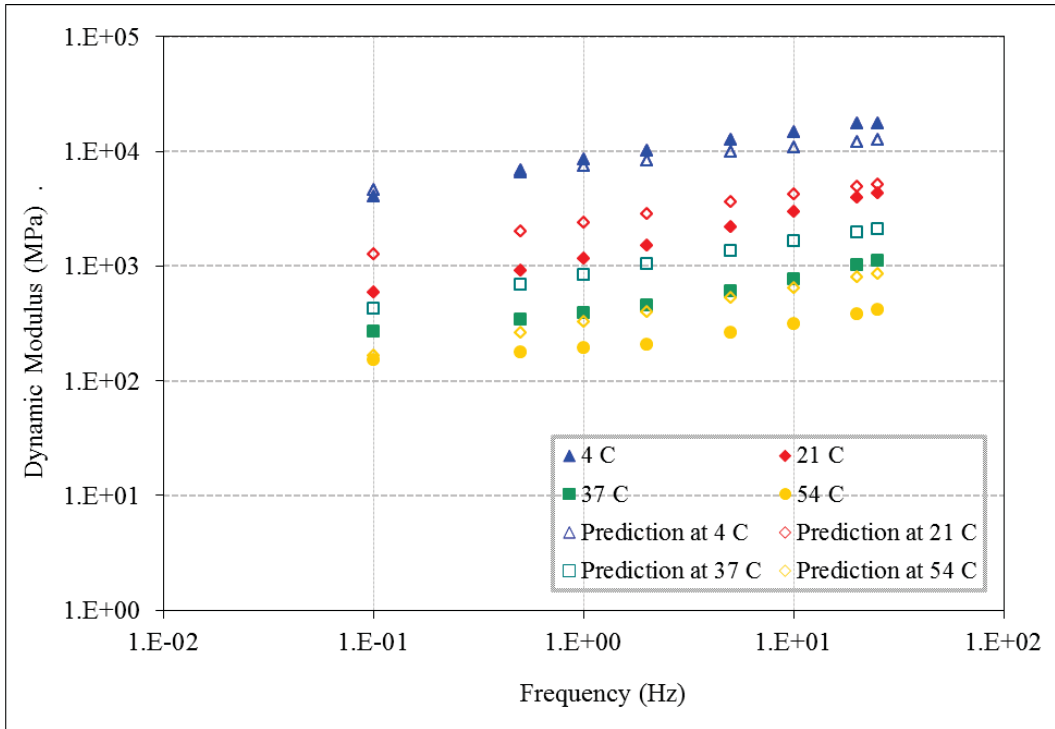
a) Measured and Predicted |E*| at Different Temperature and Frequency
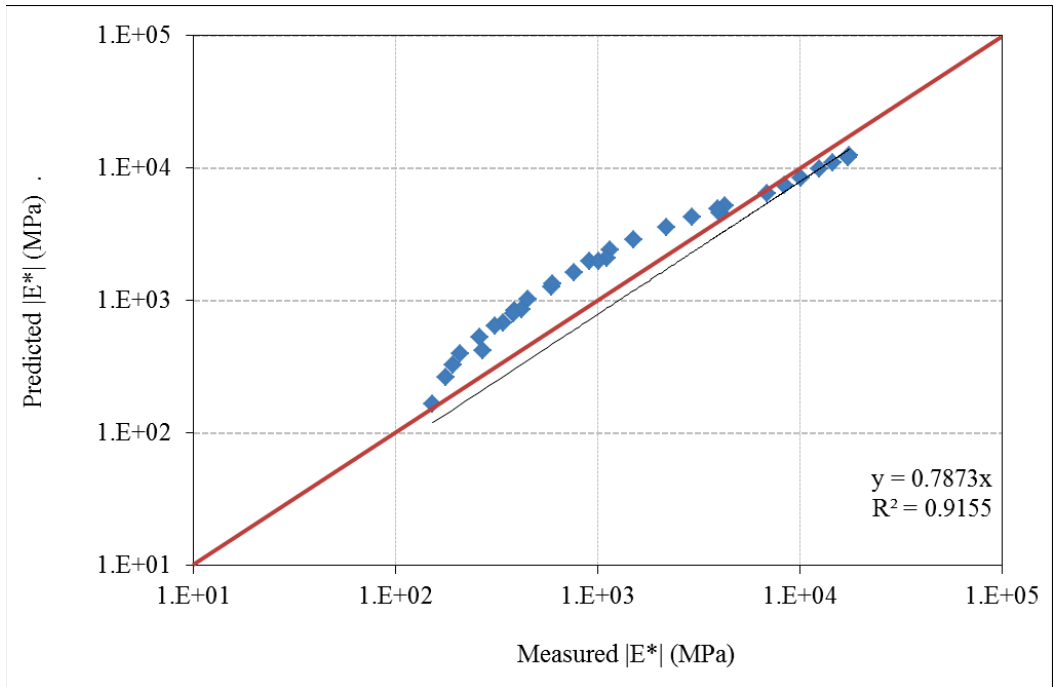
b) Measured |E*| vs. Predicted |E*|

Figure B.17 Summary of Predicted |E*| based on Original Witczak Model
(Project: AIA runway 7R_25L Rehab.)
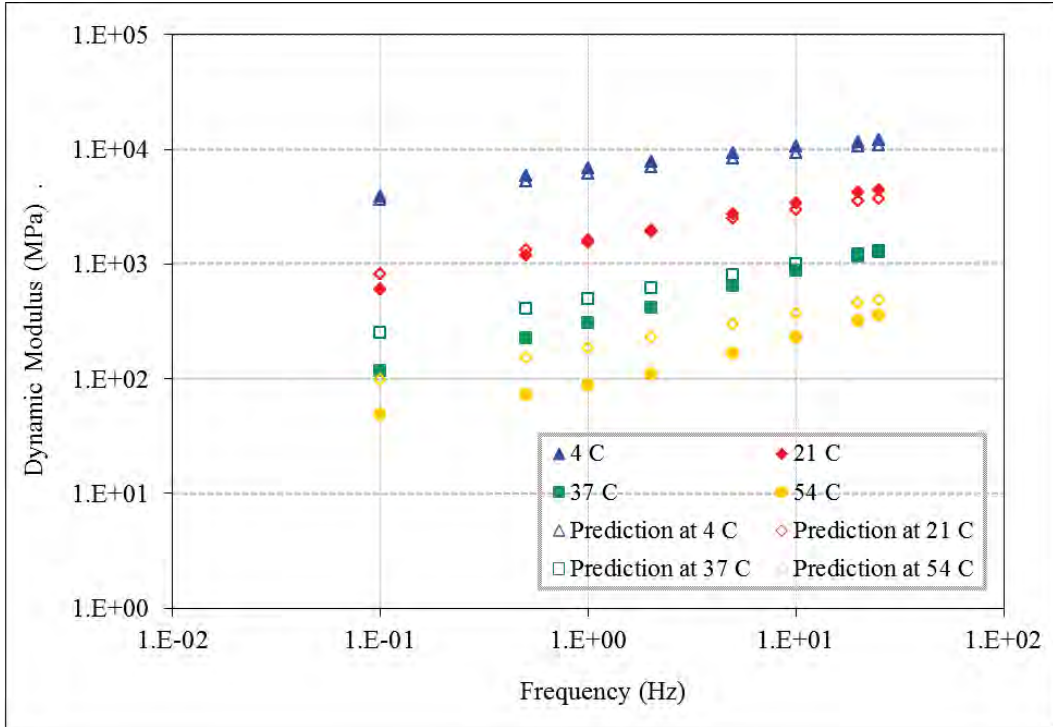
a) Measured and Predicted |E*| at Different Temperature and Frequency
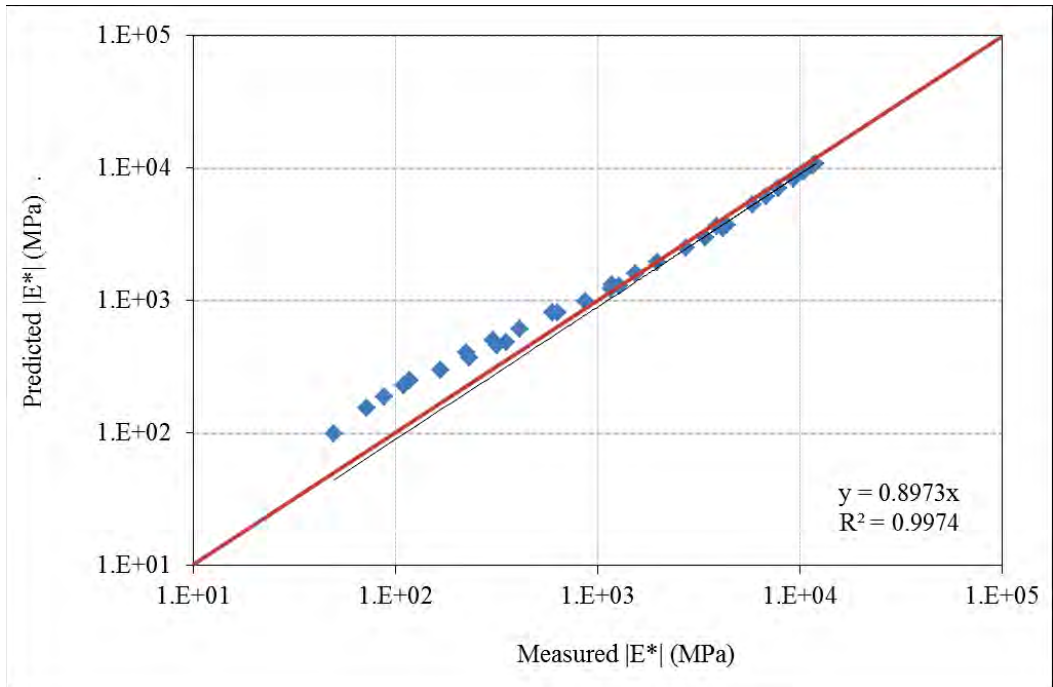
b) Measured |E*| vs. Predicted |E*|

Figure B.18 Summary of Predicted |E*| based on Original Witczak Model
(Project: Parks Hwy MP 287-305 Rehab.)
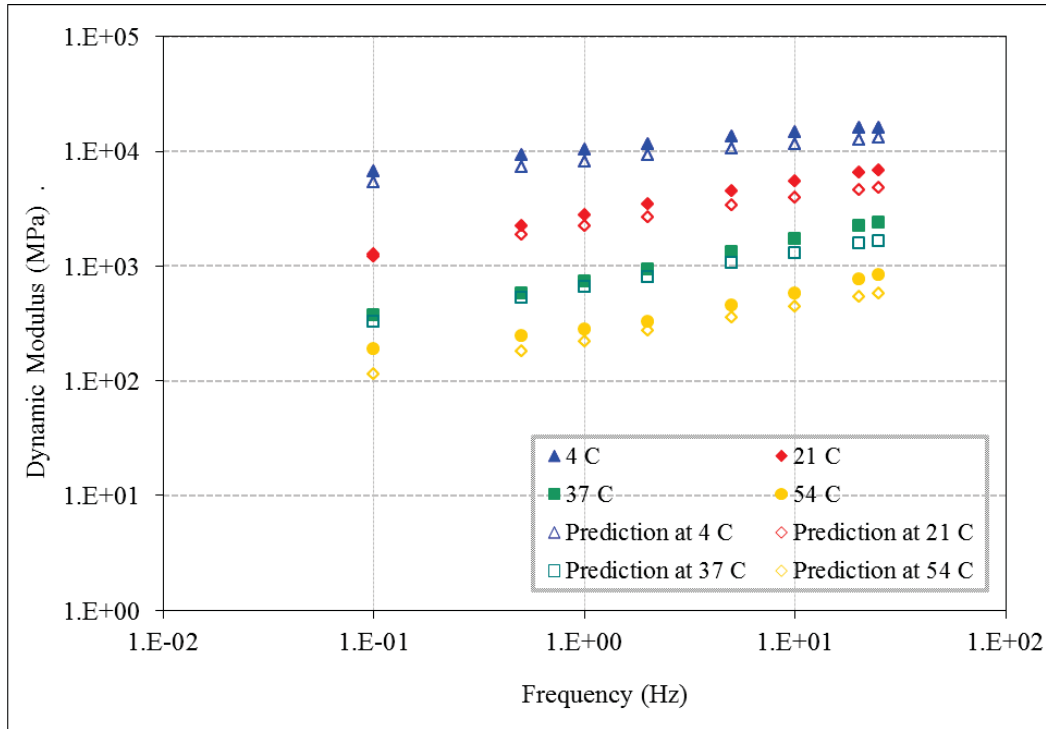
a) Measured and Predicted |E*| at Different Temperature and Frequency
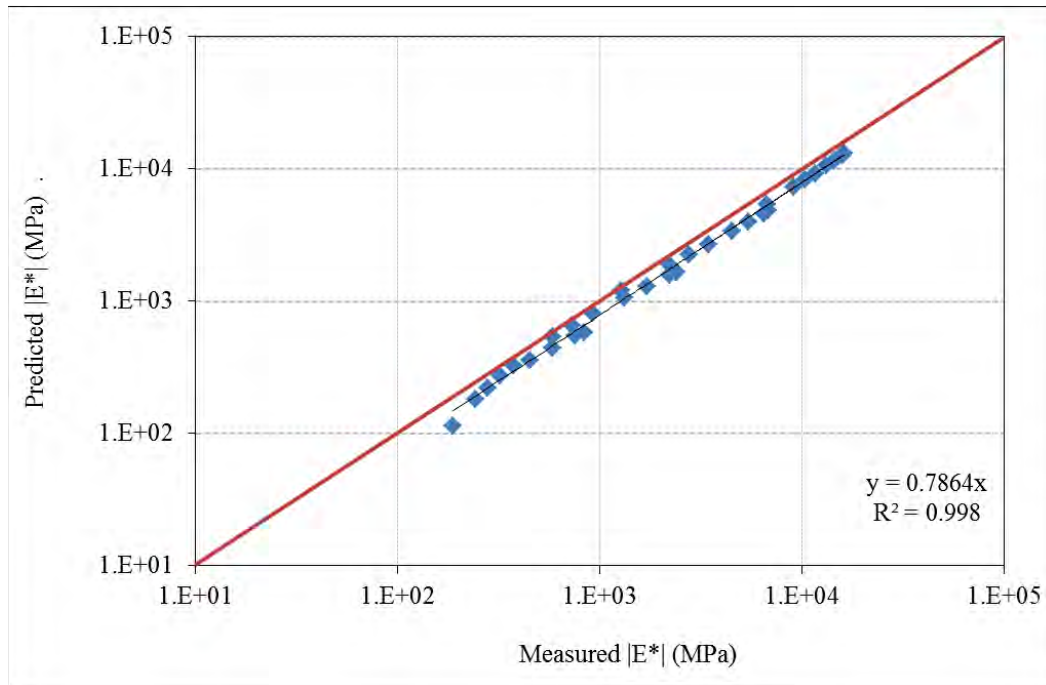
b) Measured |E*| vs. Predicted |E*|

Figure B.19 Summary of Predicted |E*| based on Original Witczak Model
(Project: PSG Mitkof Highway-Scow Bay to Crystal Lake Hatchery)

APPENDIX C: Predicted |E*| Based on Modified Witczak Model
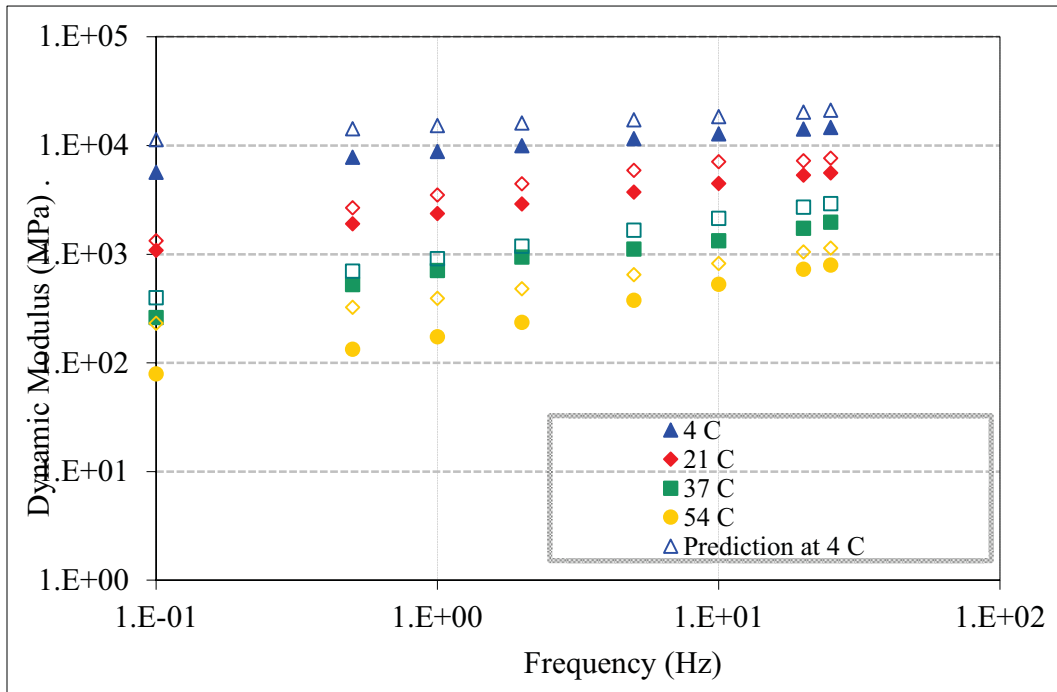
a) Measured and Predicted |E*| at Different Temperature and Frequency
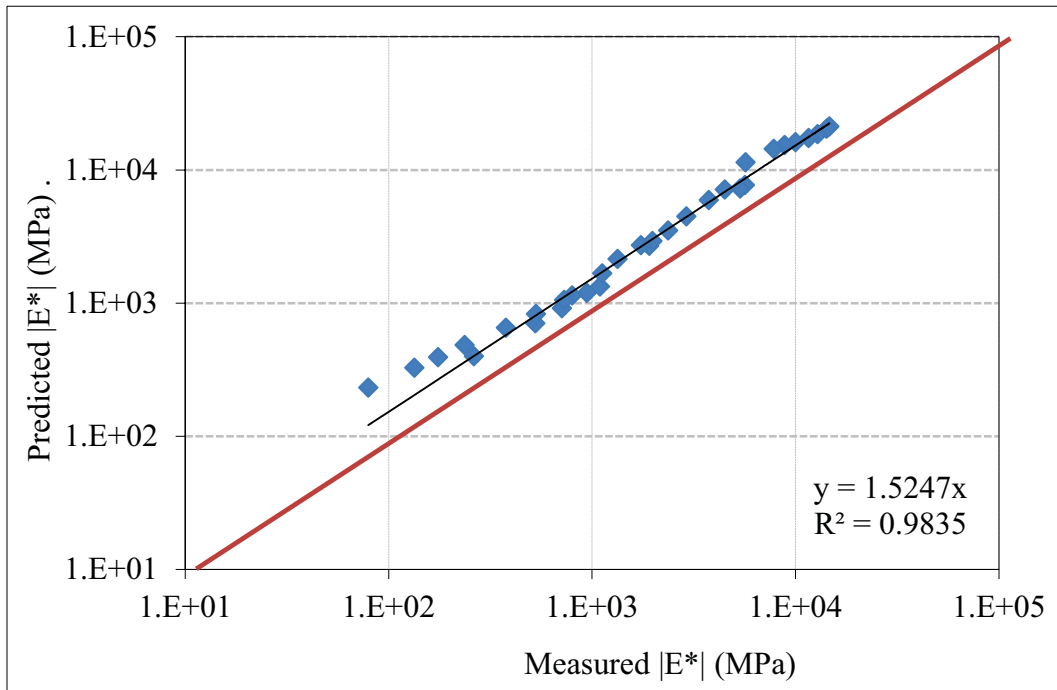
b) Measured |E*| vs. Predicted |E*|

Figure C.1 Summary of Predicted |E*| based on Modified Witczak Model
(Project: FIA Runway 1L_19R stage 3 (64-34))
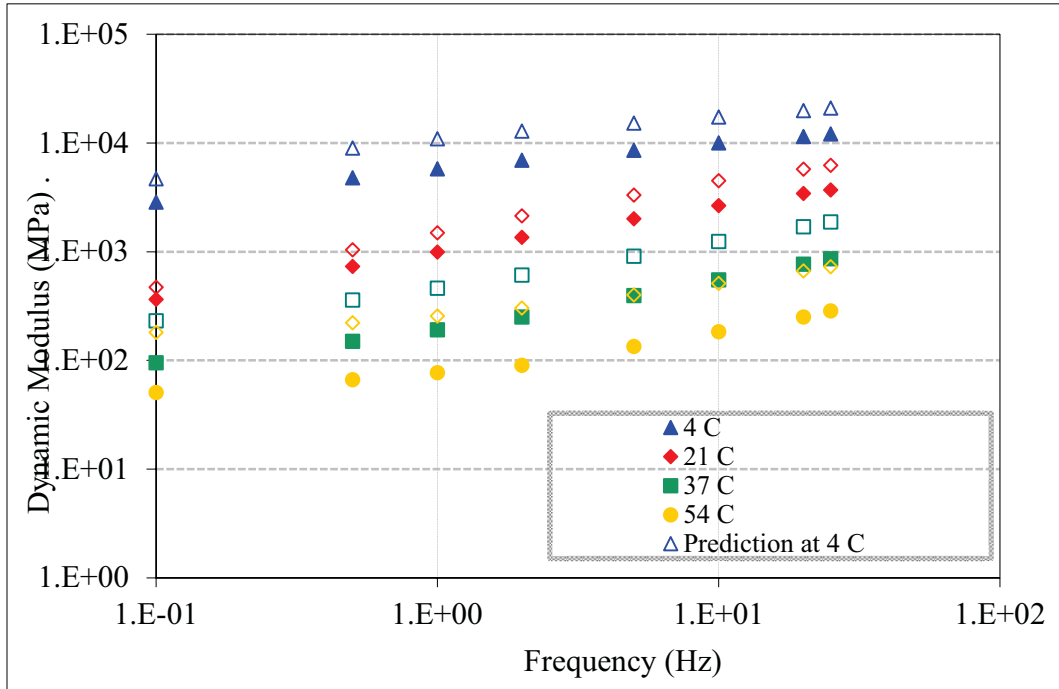
a) Measured and Predicted |E*| at Different Temperature and Frequency
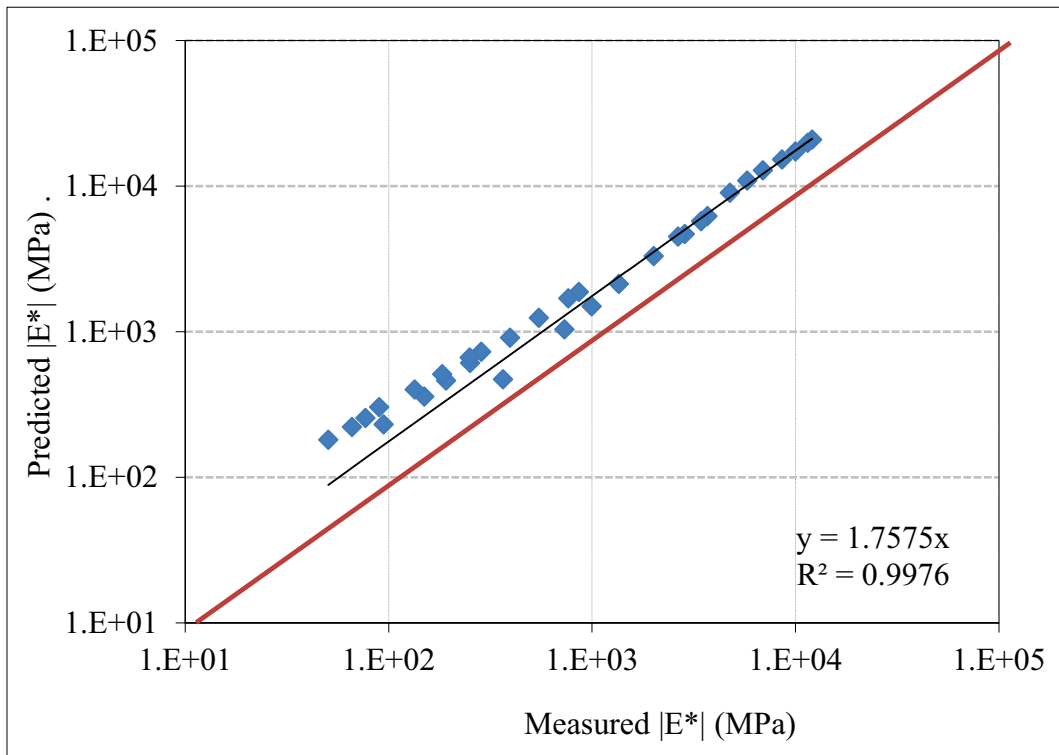
b) Measured |E*| vs. Predicted |E*|

Figure C.2 Summary of Predicted |E*| based on Modified Witczak Model
(Project: FIA Runway 1L_19R stage 3 (52-34))
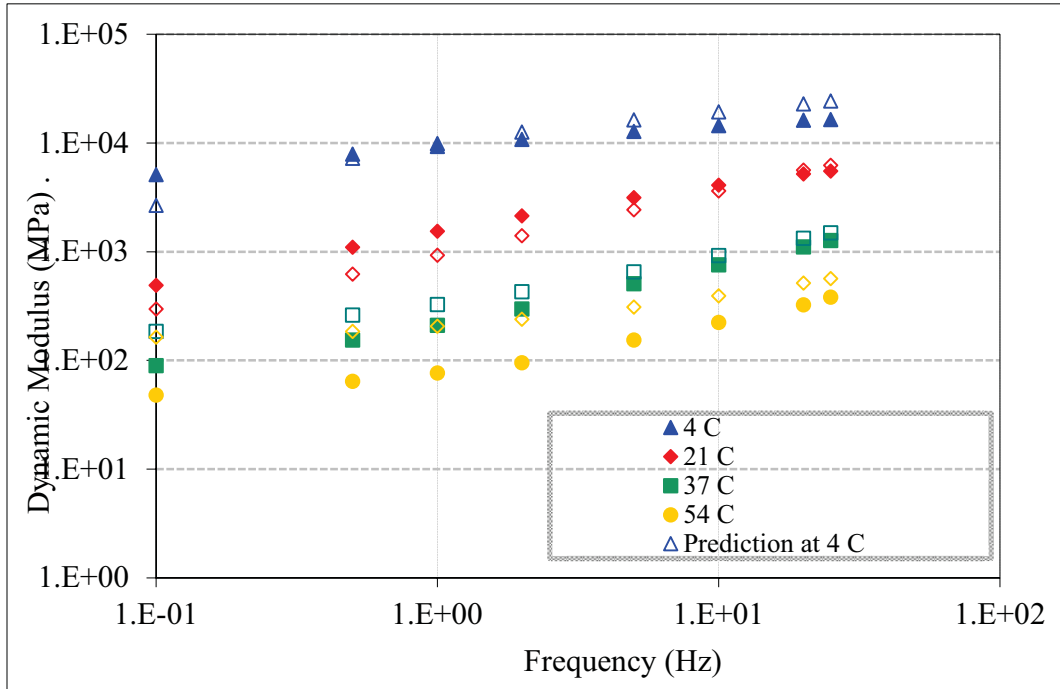
a) Measured and Predicted |E*| at Different Temperature and Frequency
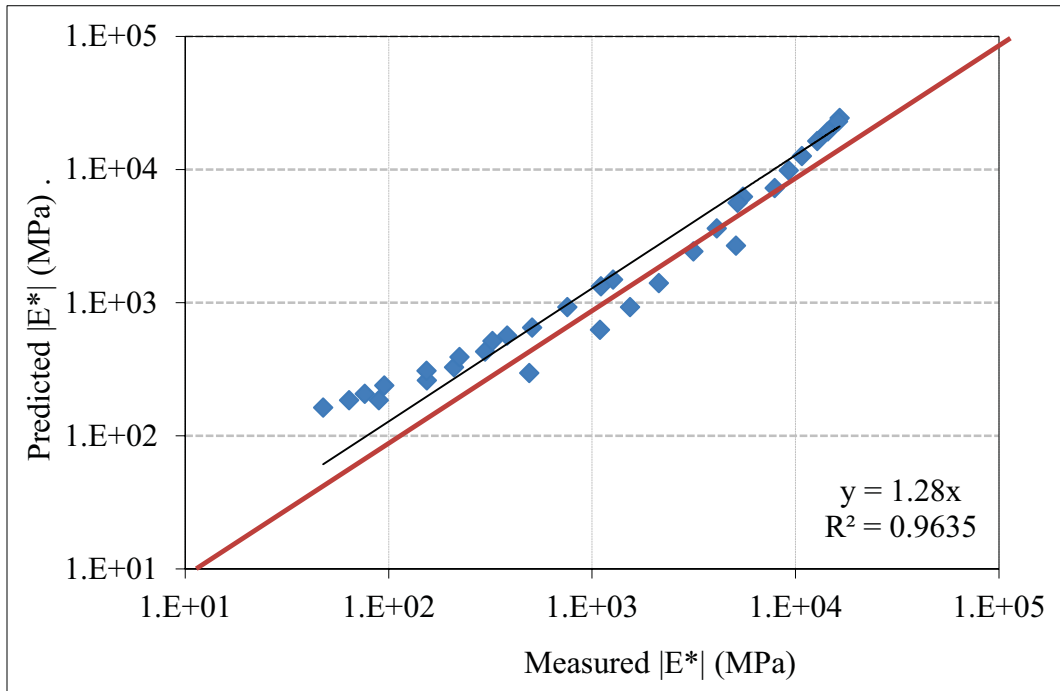
b) Measured |E*| vs. Predicted |E*|

Figure C.3 Summary of Predicted |E*| based on Modified Witczak Model
(Project: Chena Hot Springs Rd, MD-1)
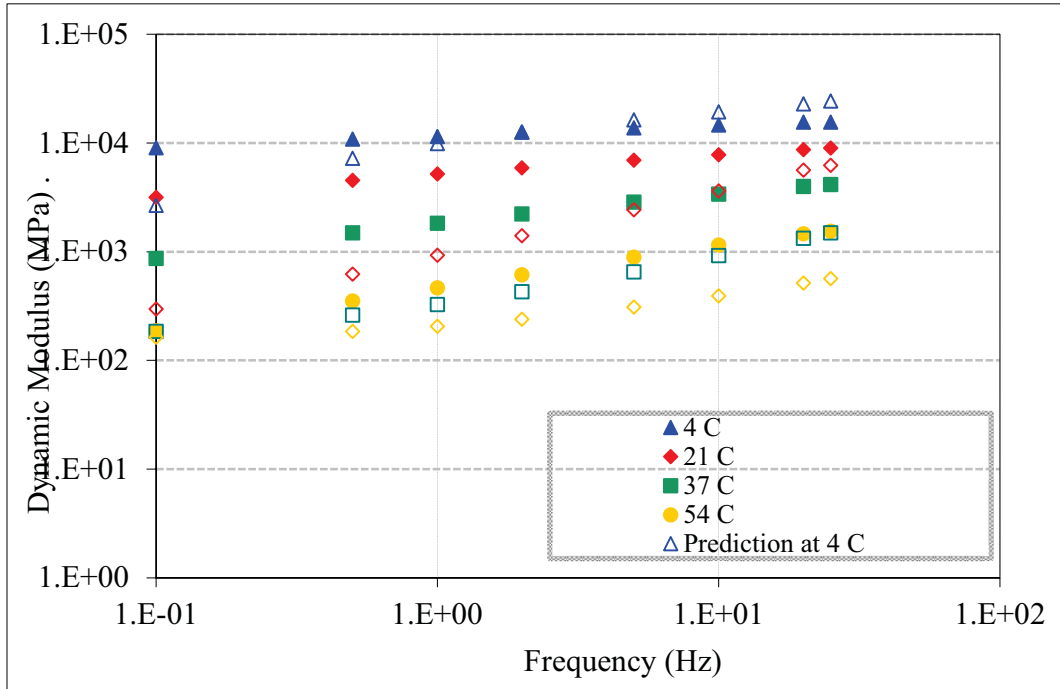
a) Measured and Predicted |E*| at Different Temperature and Frequency
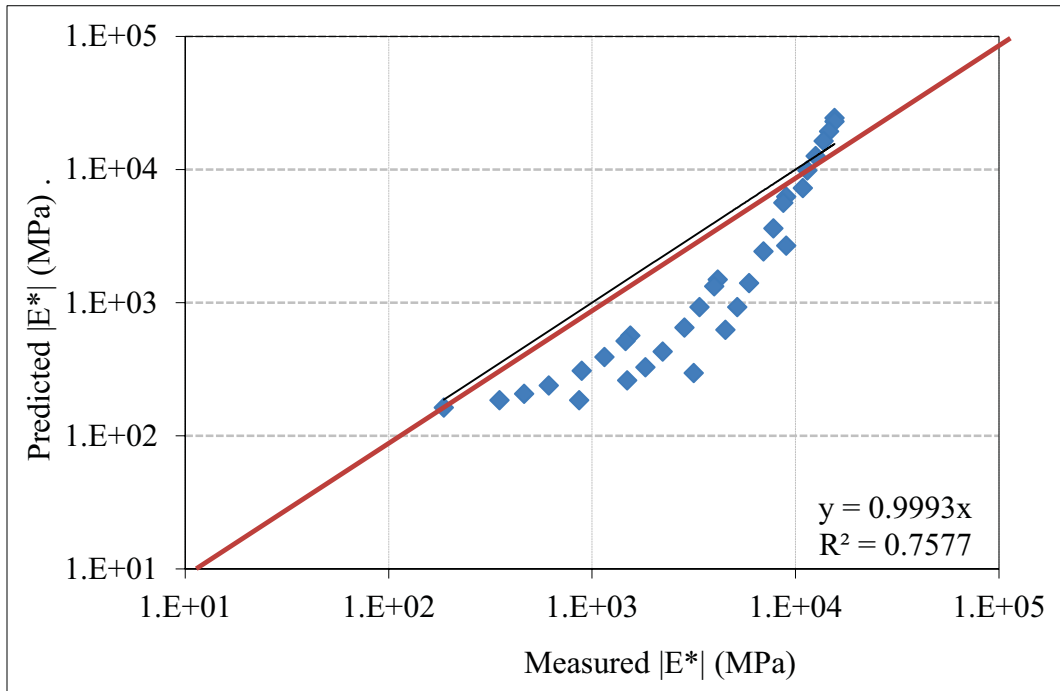
b) Measured |E*| vs. Predicted |E*|

Figure C.4 Summary of Predicted |E*| based on Modified Witczak Model
(Project: Chena Hot Springs Rd MD-3)
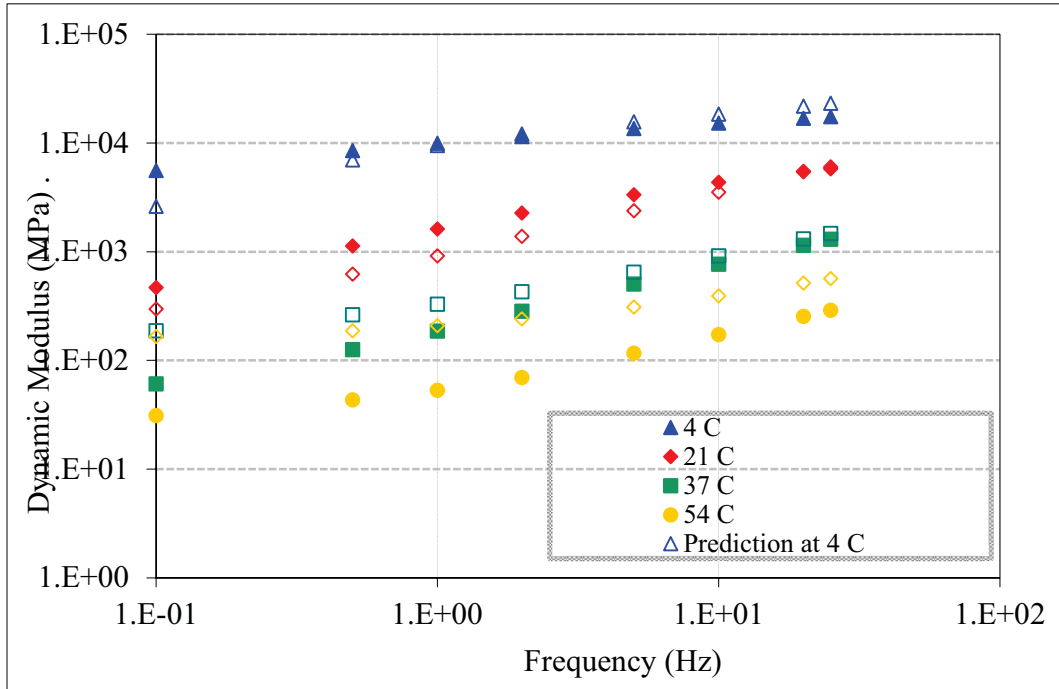
a) Measured and Predicted |E*| at Different Temperature and Frequency
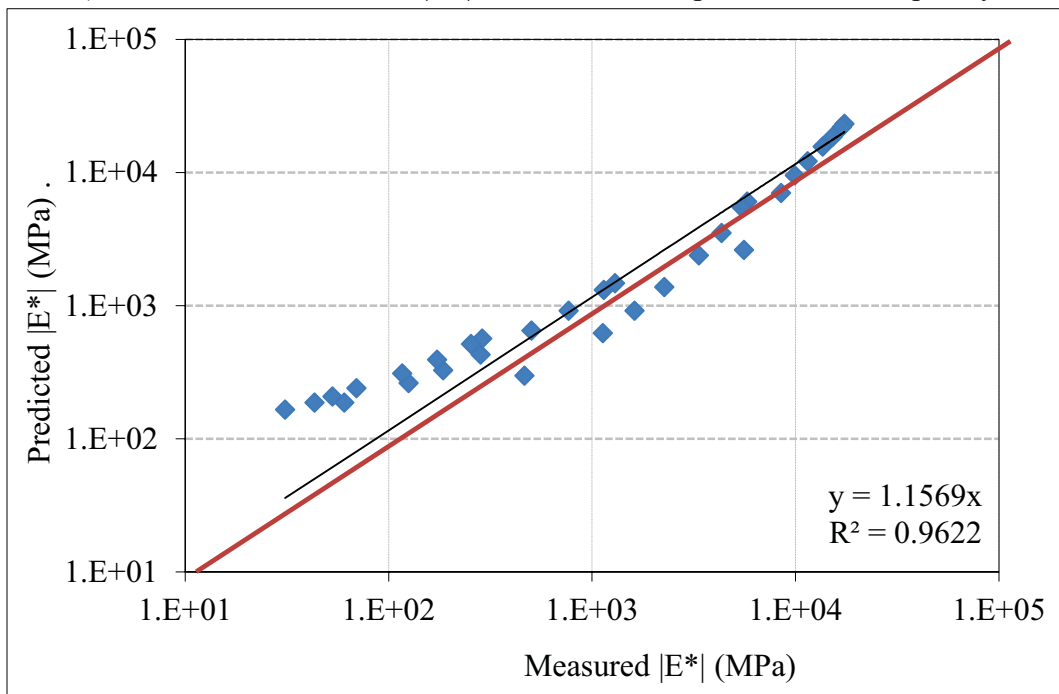
b) Measured |E*| vs. Predicted |E*|

Figure C.5 Summary of Predicted |E*| based on Modified Witczak Model
(Project: Fairbanks Cowles Street Upgrade)

a) Measured and Predicted |E*| at Different Temperature and Frequency

$$y = 1.2214x$$
$$R^2 = 0.9882$$
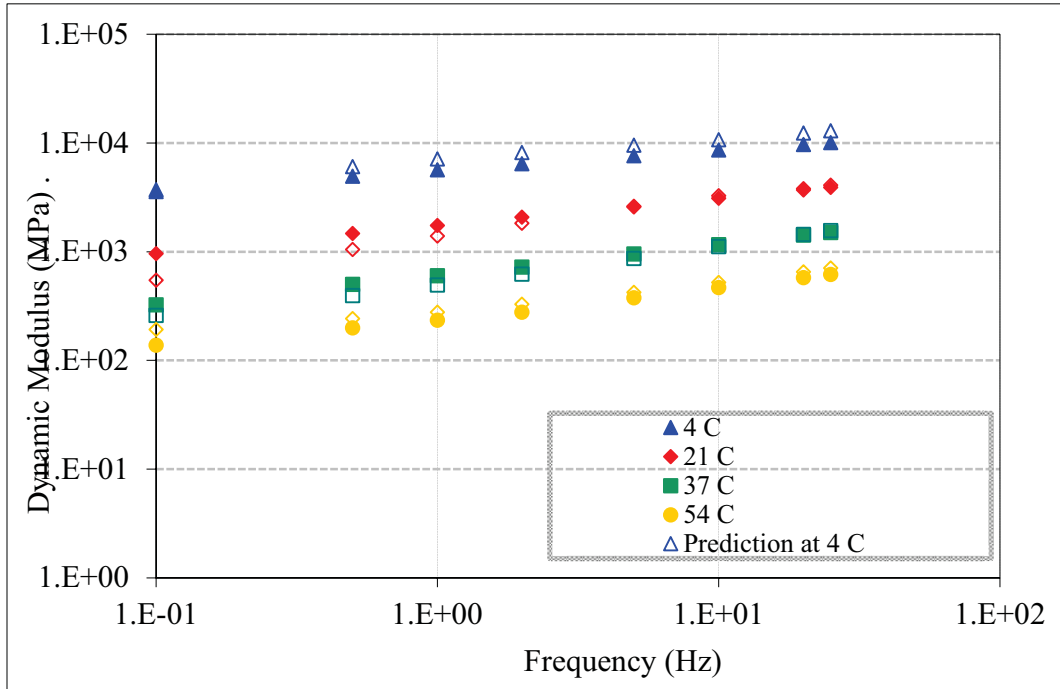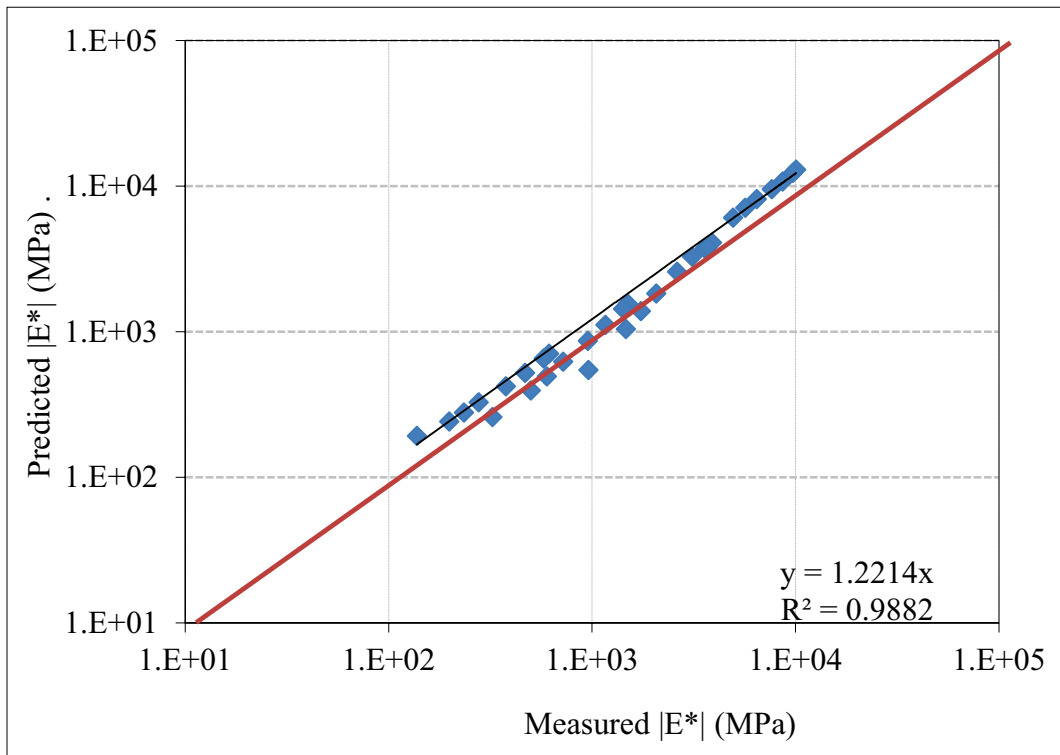
b) Measured |E*| vs. Predicted |E*|

Figure C.6 Summary of Predicted |E*| based on Modified Witczak Model
(Project: Dalton Hwy. MP 175-197 Rehabilitation)
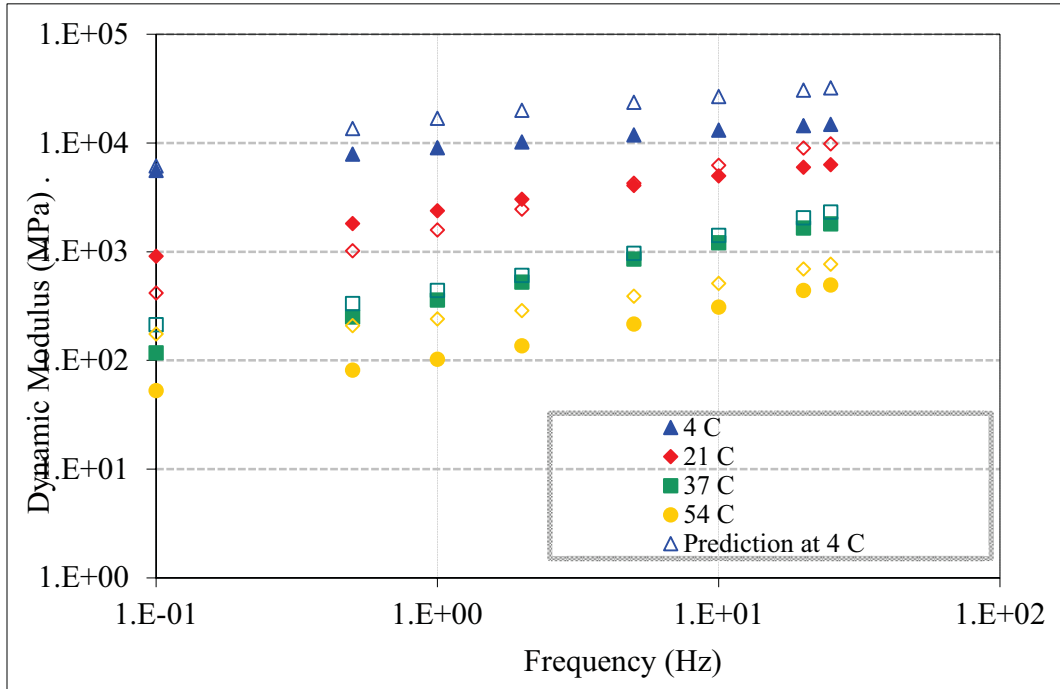
a) Measured and Predicted |E*| at Different Temperature and Frequency
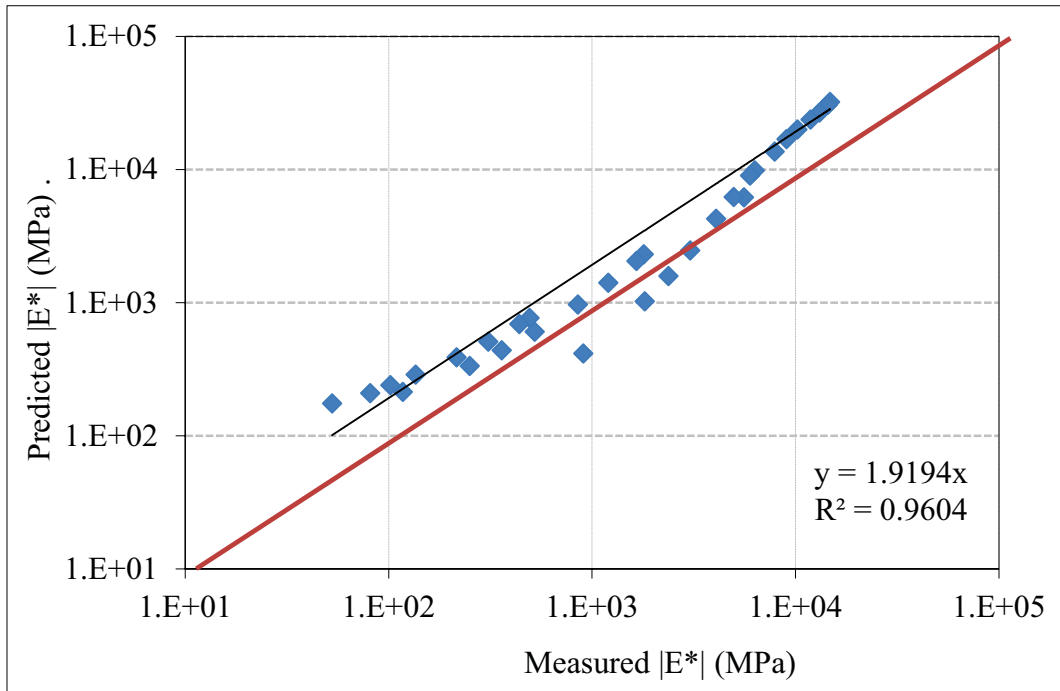
b) Measured |E*| vs. Predicted |E*|

Figure C.7 Summary of Predicted |E*| based on Modified Witczak Model
(Project: Glen Why MP 92-97 Cascade to Hicks Creek)
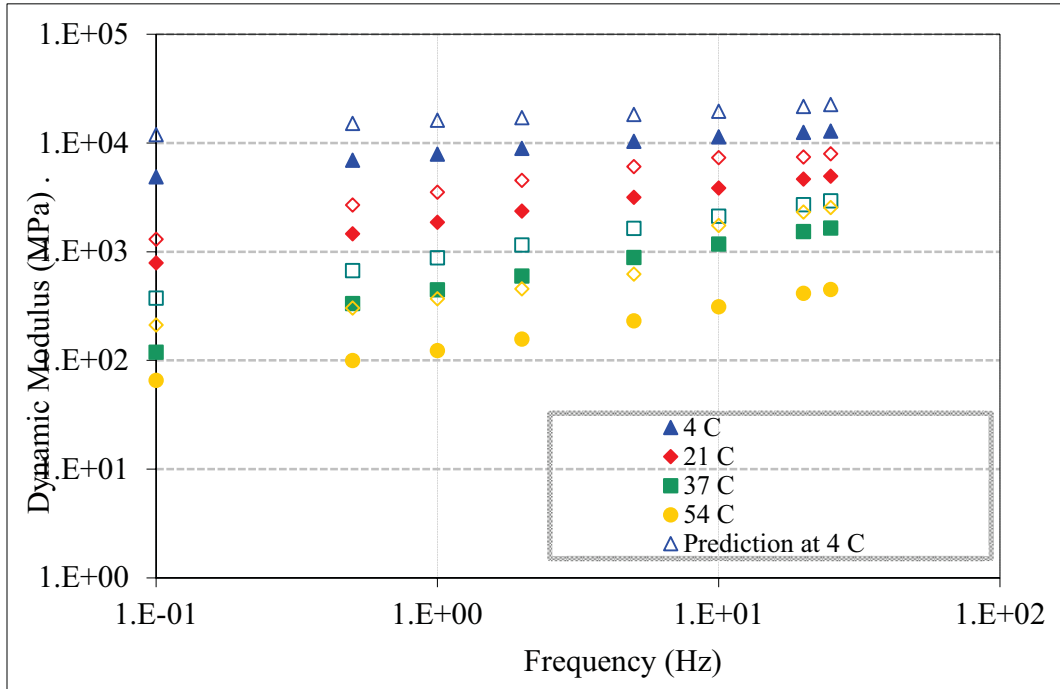
a) Measured and Predicted |E*| at Different Temperature and Frequency
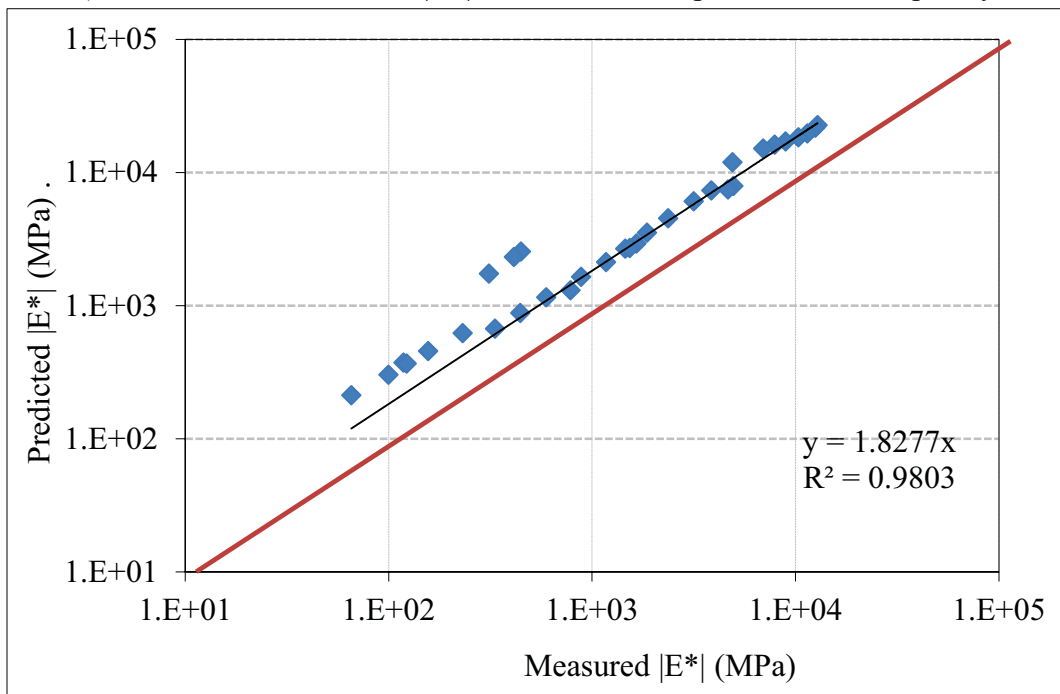
b) Measured |E*| vs. Predicted |E*|

Figure C.8 Summary of Predicted |E*| based on Modified Witczak Model
(Project: Glenn Highway Gambell to airport MP 0-1.5)
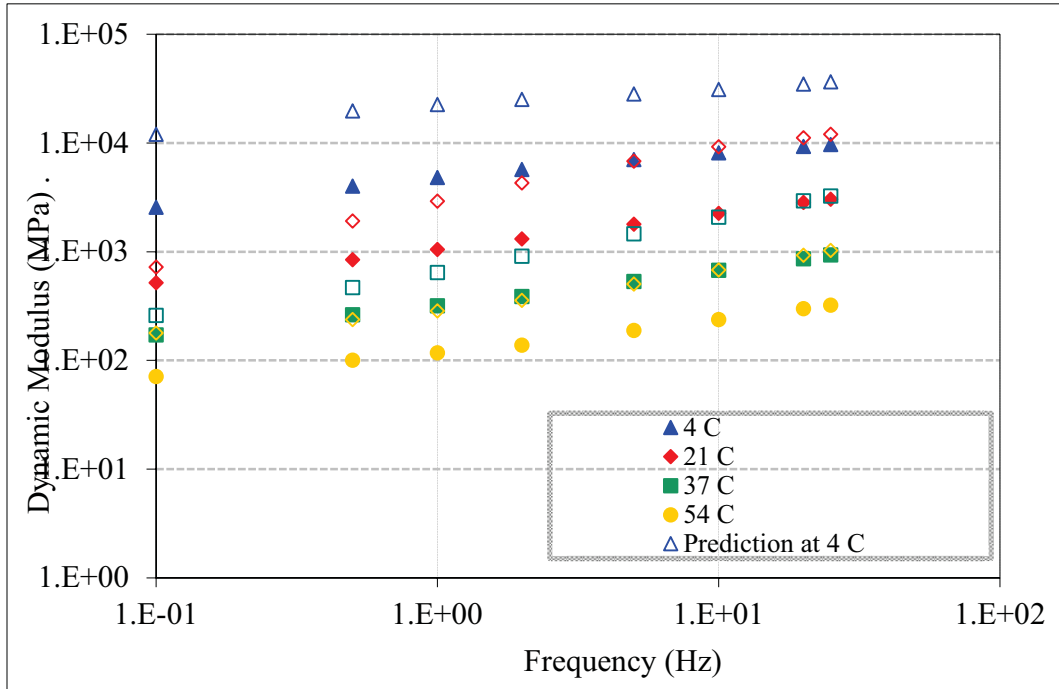
a) Measured and Predicted |E*| at Different Temperature and Frequency
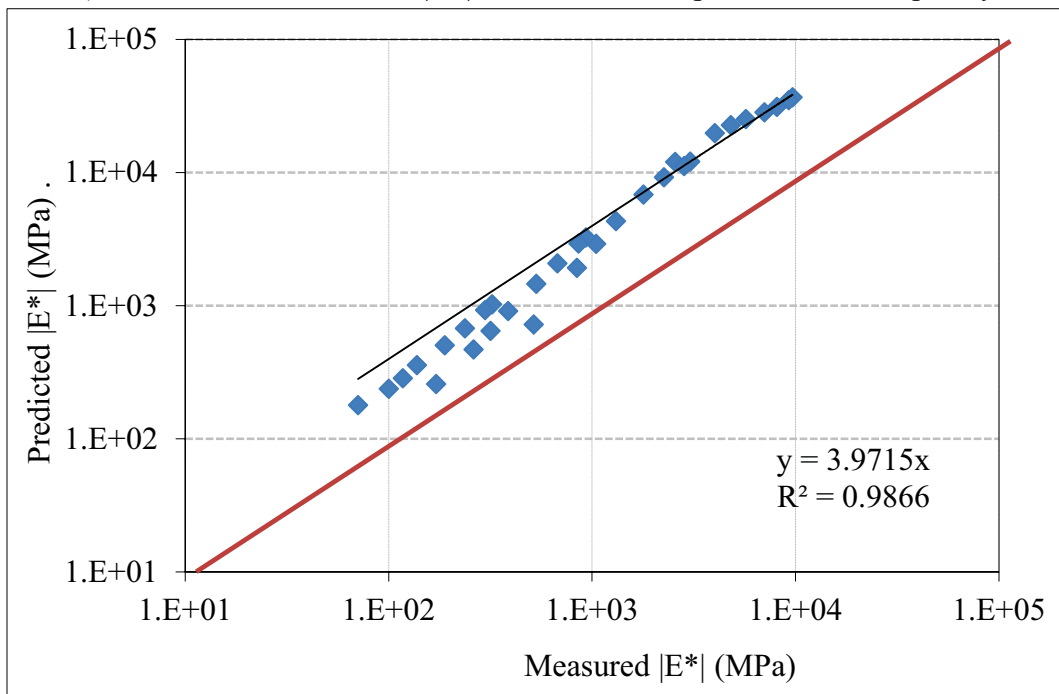
b) Measured |E*| vs. Predicted |E*|

Figure C.9 Summary of Predicted |E*| based on Modified Witczak Model
(Project HNS Ferry Terminal to Union Street)

a) Measured and Predicted |E*| at Different Temperature and Frequency

$$y = 2.0604x$$
$$R^2 = 0.9744$$
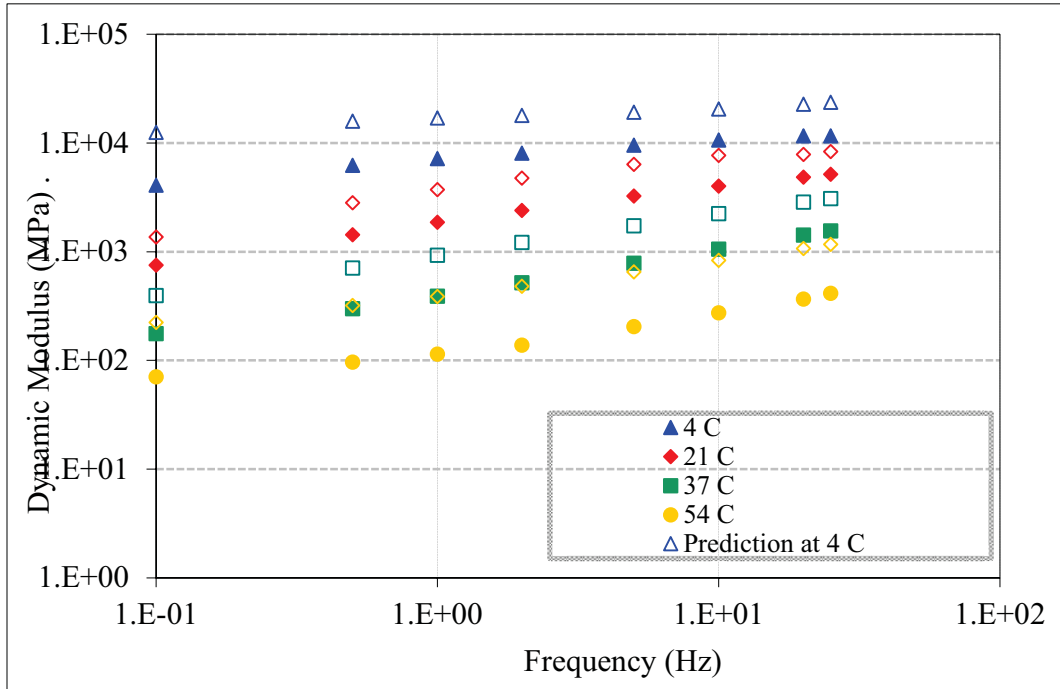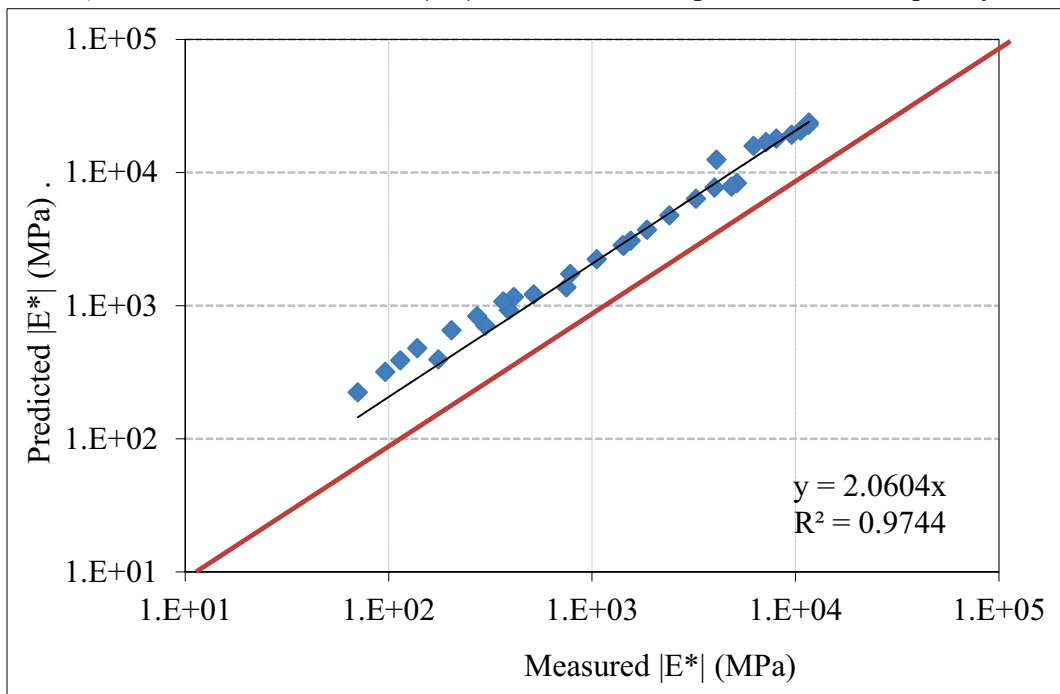
b) Measured |E*| vs. Predicted |E*|

Figure C.10 Summary of Predicted |E*| based on Modified Witczak Model
(Project: Minnesota Dr Resurfacing: Int'l Airport Rd to 13th)

130
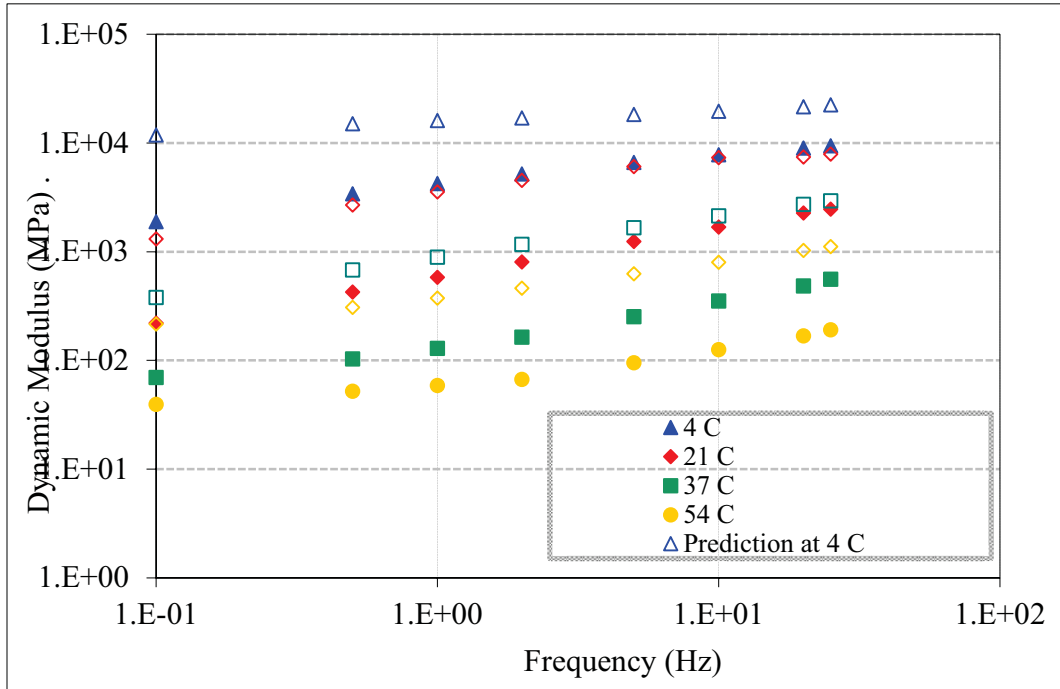
a) Measured and Predicted |E*| at Different Temperature and Frequency
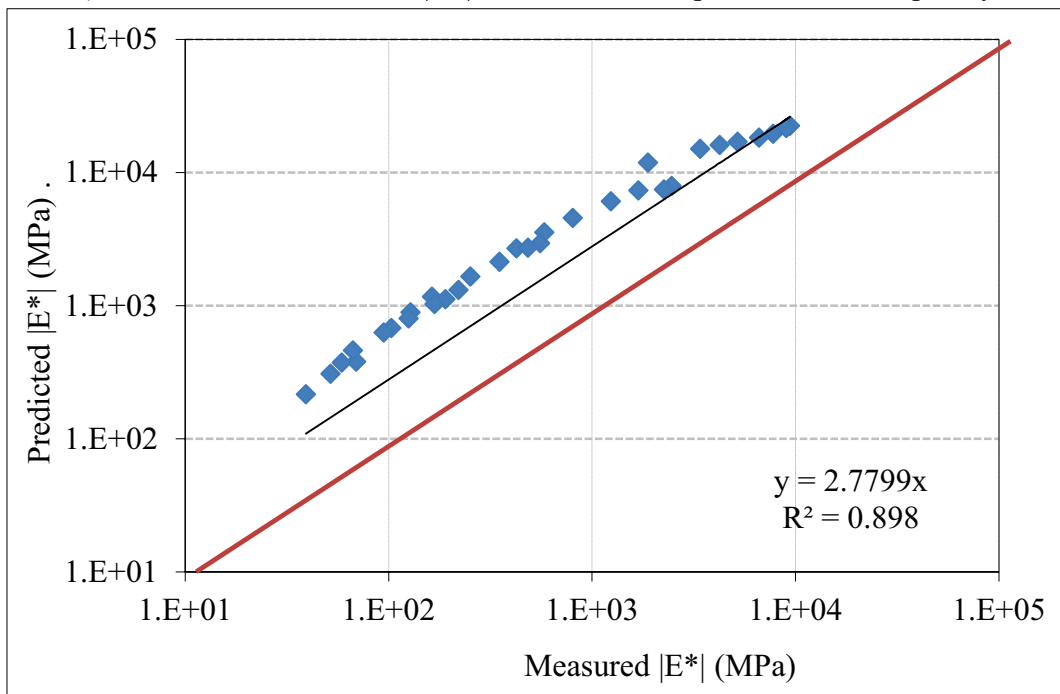
b) Measured |E*| vs. Predicted |E*|

Figure C.11 Summary of Predicted |E*| based on Modified Witczak Model
(Project: Rich Hwy North Pole Interchange)
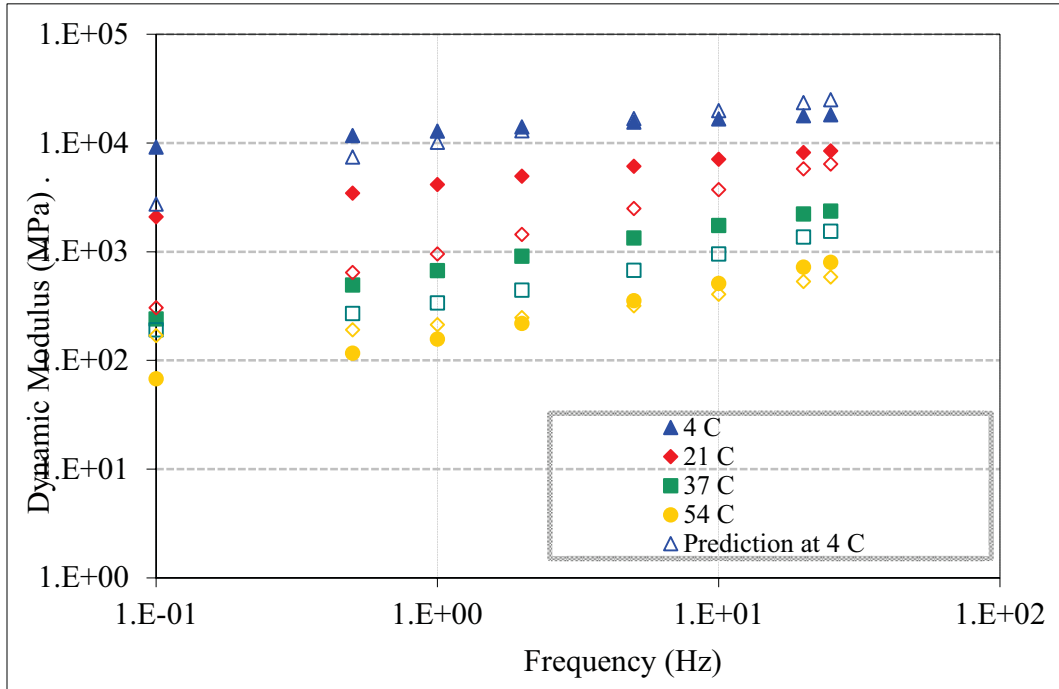
a) Measured and Predicted |E*| at Different Temperature and Frequency
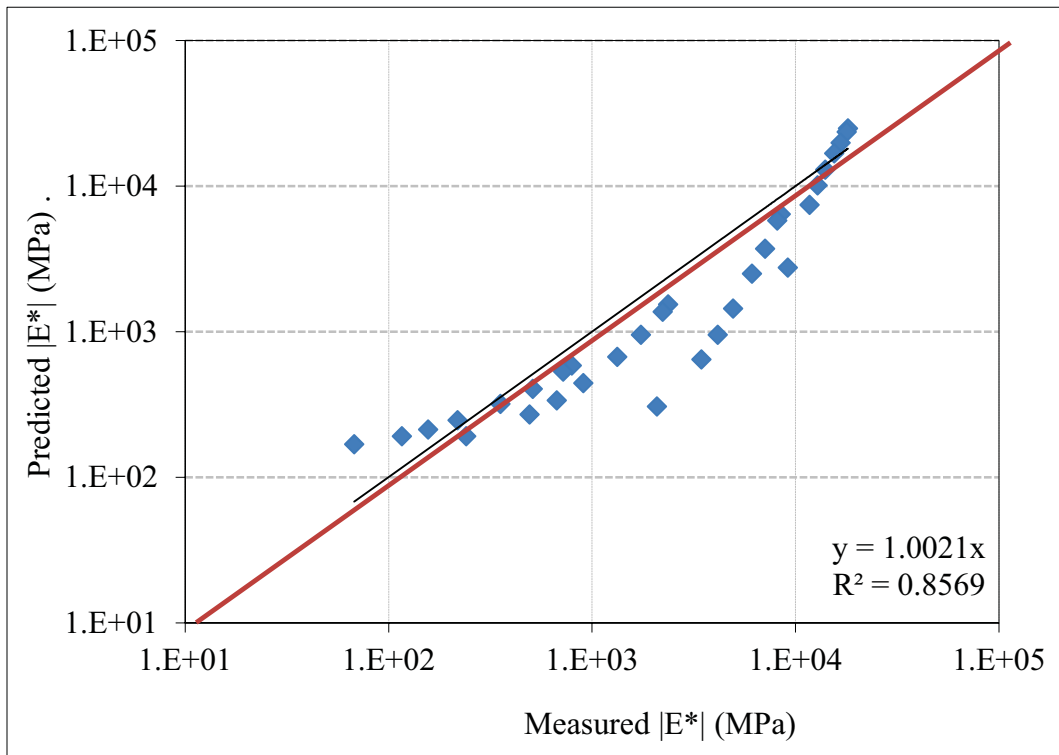
b) Measured |E*| vs. Predicted |E*|

Figure C.12 Summary of Predicted |E*| based on Modified Witczak Model
(Project: Old Glenn Hwy.: MP 11.5-18)
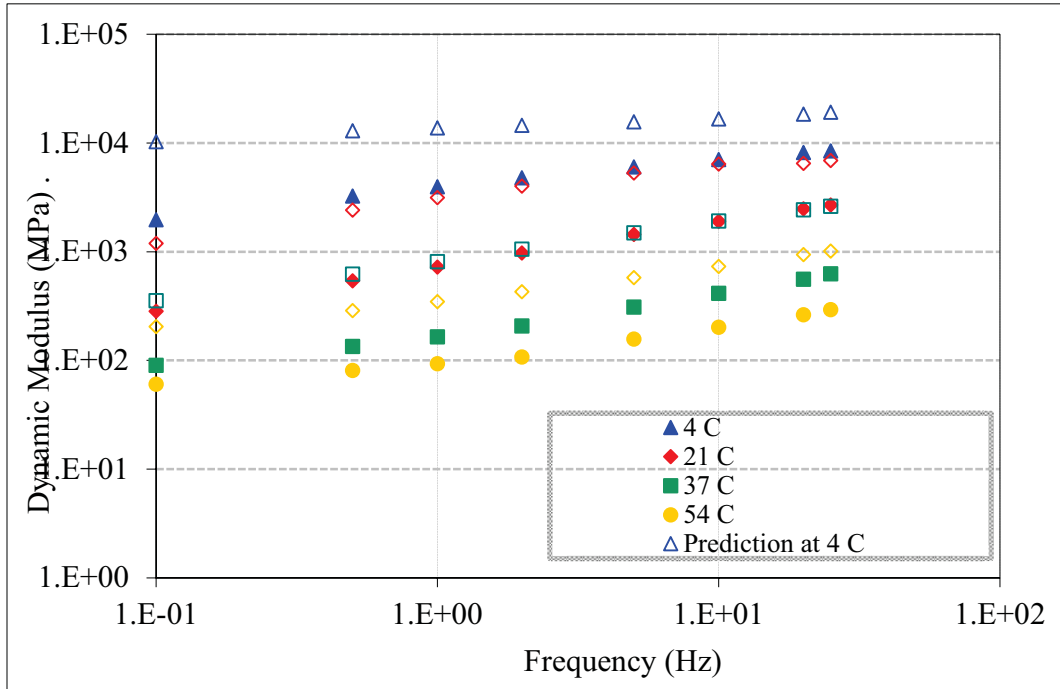
a) Measured and Predicted |E*| at Different Temperature and Frequency
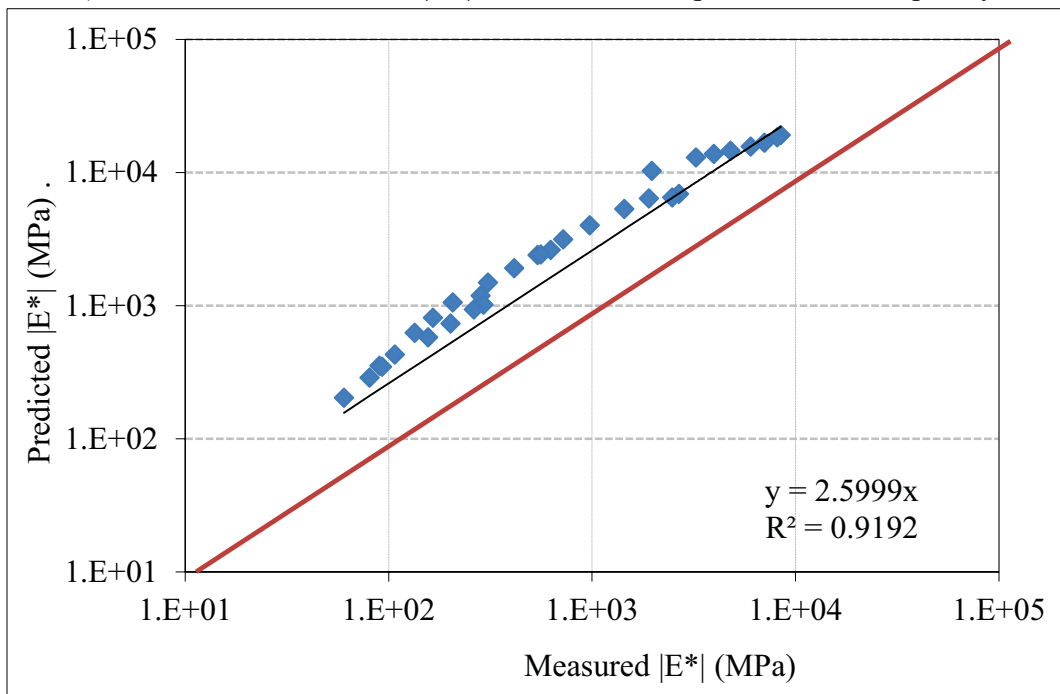
b) Measured |E*| vs. Predicted |E*|

Figure C.13 Summary of Predicted |E*| based on Modified Witczak Model
(Project: Palmer-Wasilla Highway Phase II)
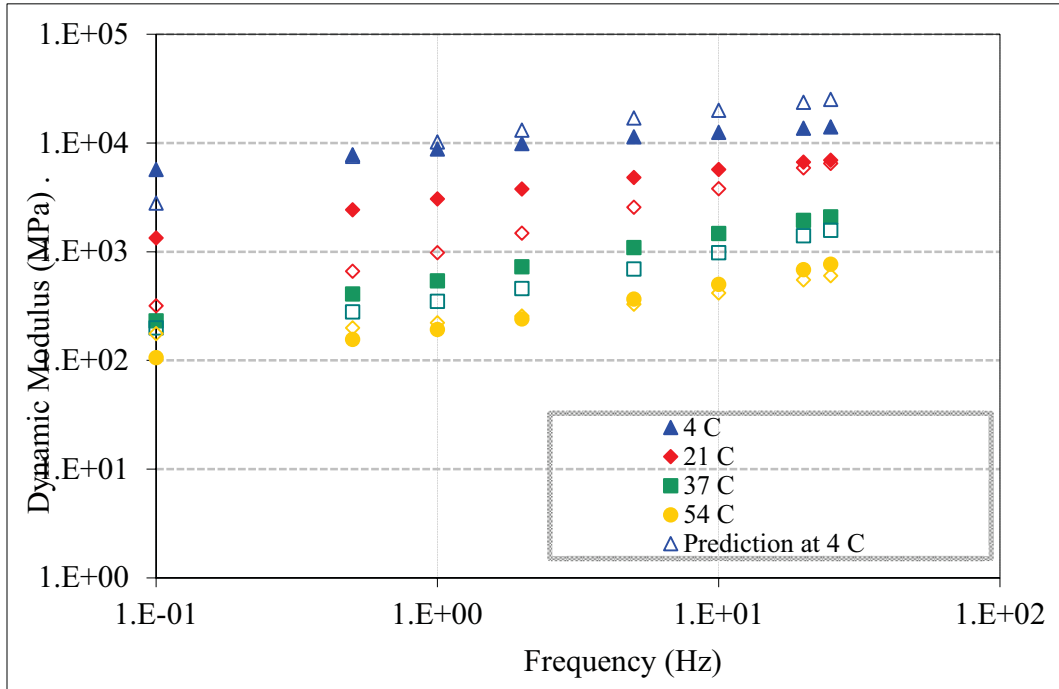
a) Measured and Predicted |E*| at Different Temperature and Frequency
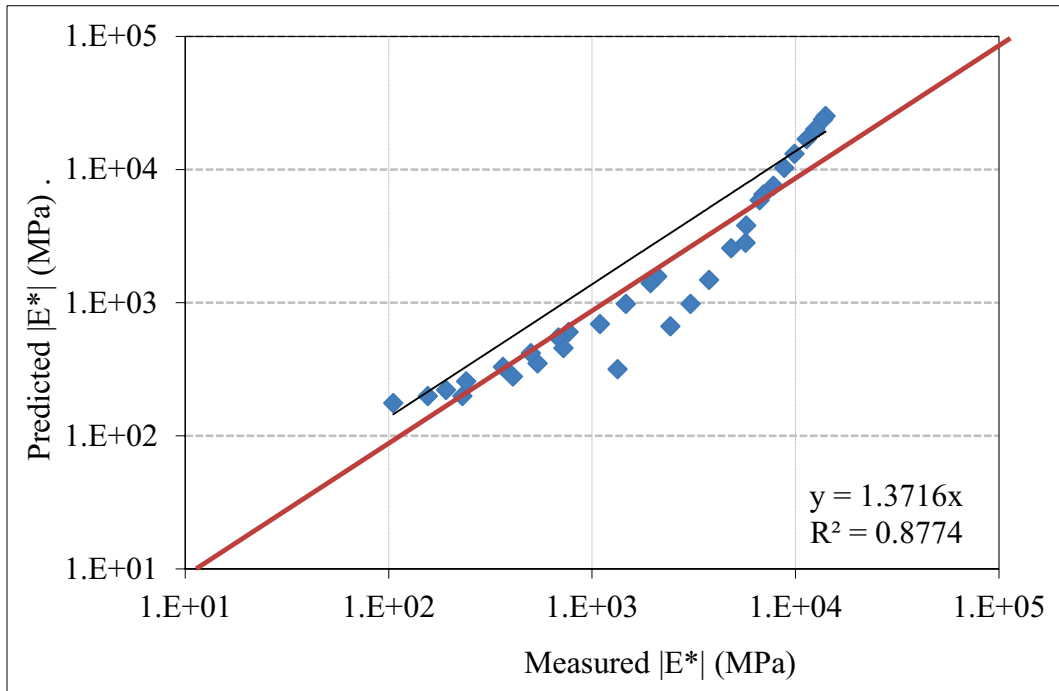
b) Measured |E*| vs. Predicted |E*|

Figure C.14 Summary of Predicted |E*| based on Modified Witczak Model
(Project: Unalakleet Airport Paving)
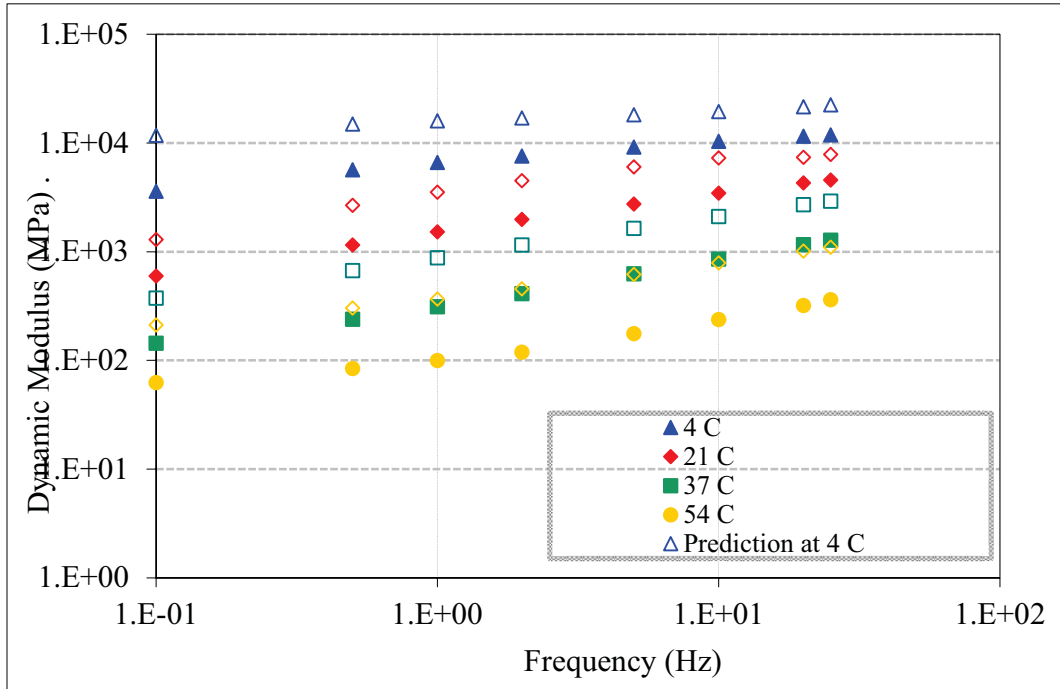
a) Measured and Predicted |E*| at Different Temperature and Frequency
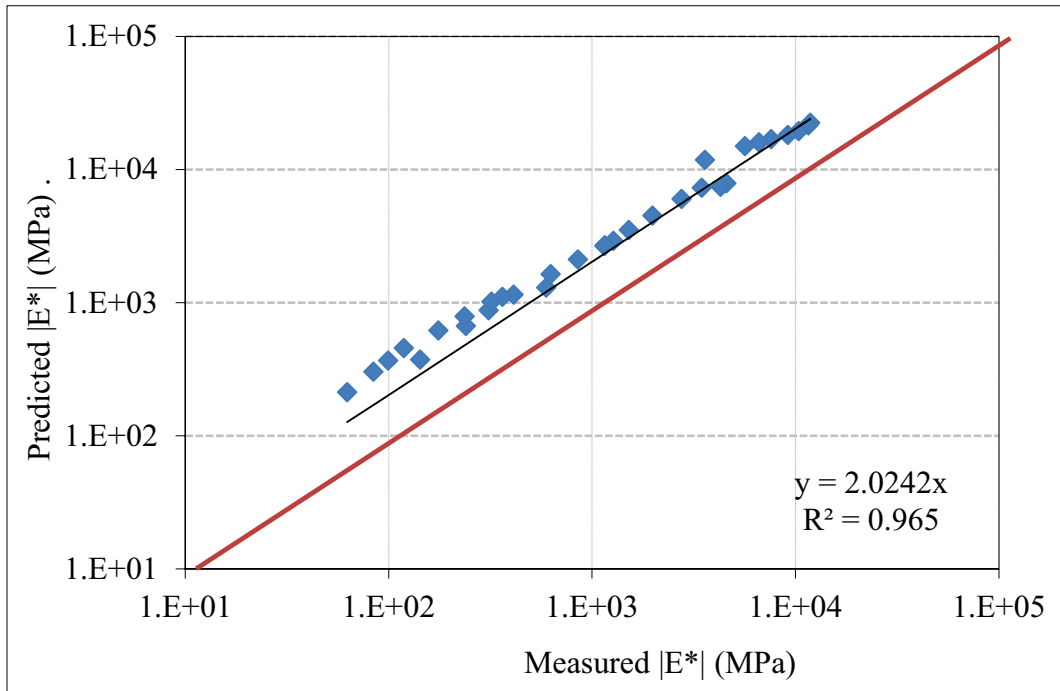
b) Measured |E*| vs. Predicted |E*|

Figure C.15 Summary of Predicted |E*| based on Modified Witczak Model
(Project: Glenn Highway MP 34-42, parks to Palmer Resurf.)

a) Measured and Predicted |E*| at Different Temperature and Frequency

y = 1.3958x
R² = 0.9723
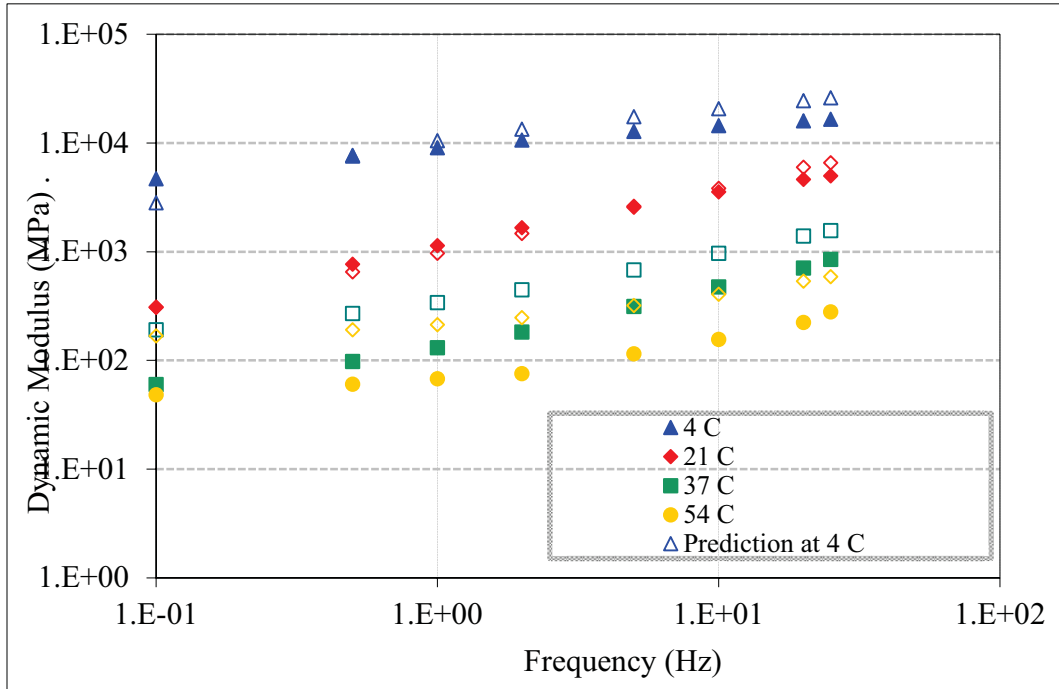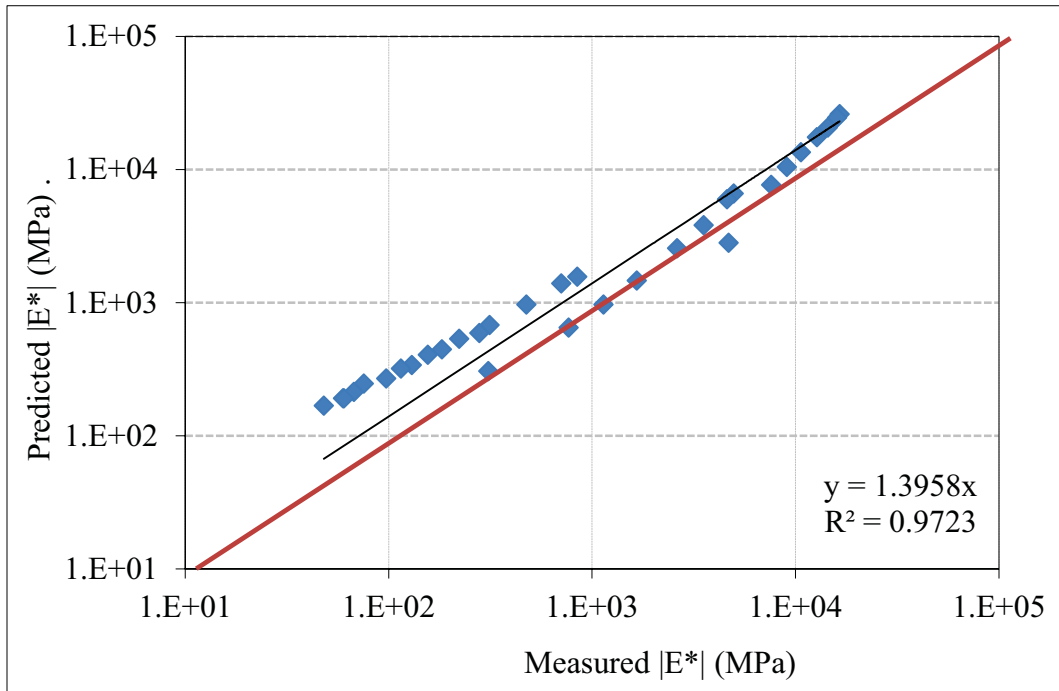
b) Measured |E*| vs. Predicted |E*|

Figure C.16 Summary of Predicted |E*| based on Modified Witczak Model
(Project: Alaska Hwy MP 1267-1314)
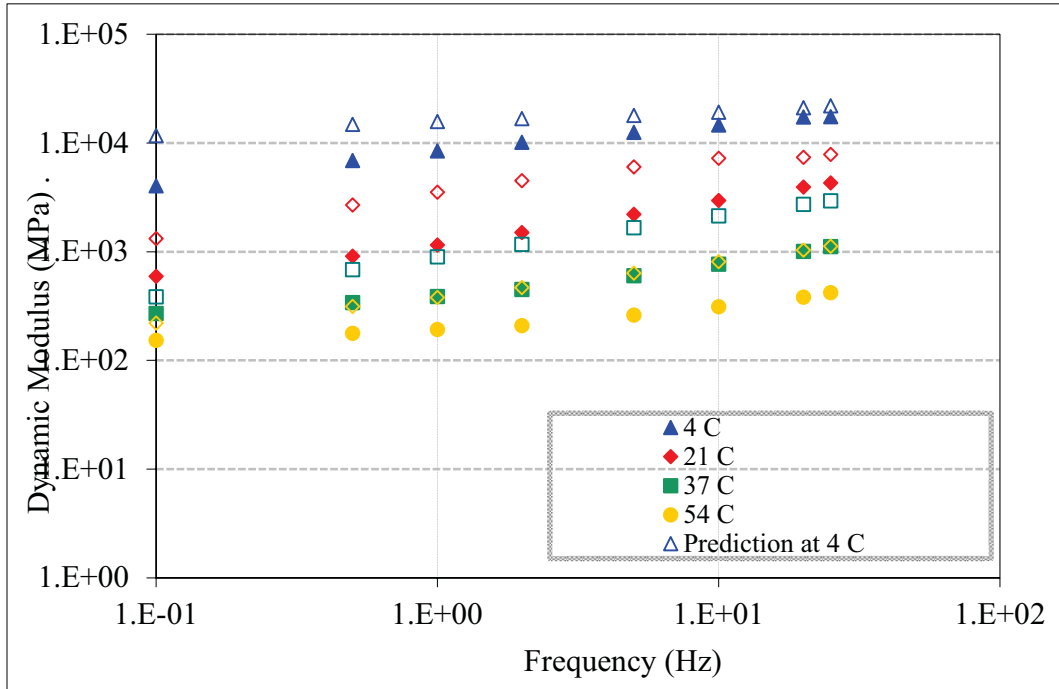
a) Measured and Predicted |E*| at Different Temperature and Frequency
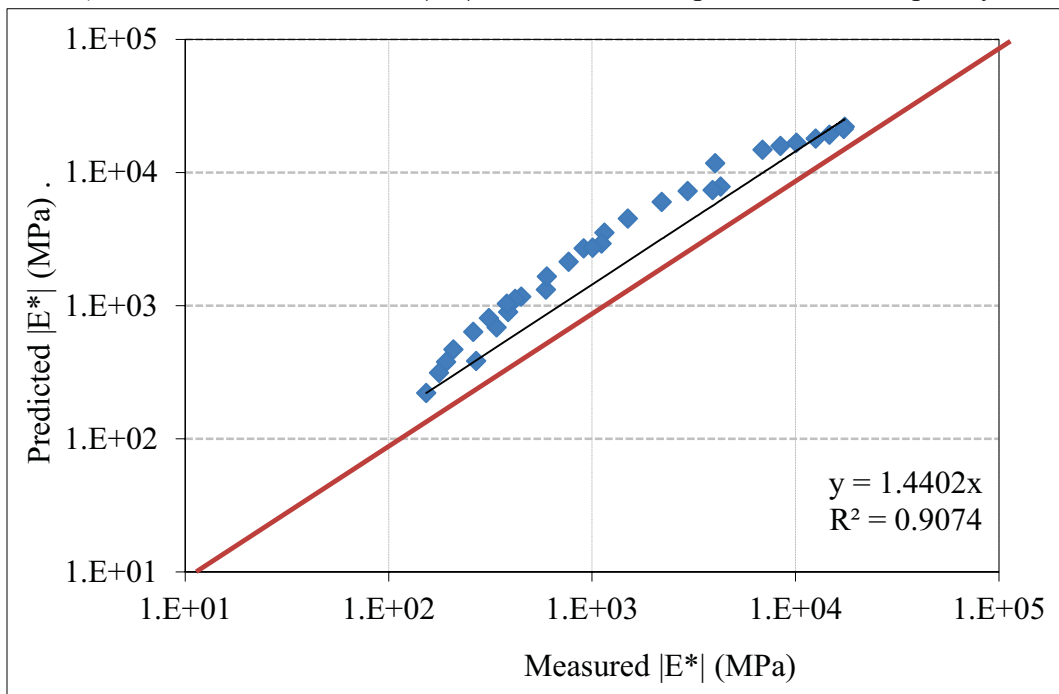
b) Measured |E*| vs. Predicted |E*|

Figure C.17 Summary of Predicted |E*| based on Modified Witczak Model
(Project: AIA runway 7R_25L Rehab.)
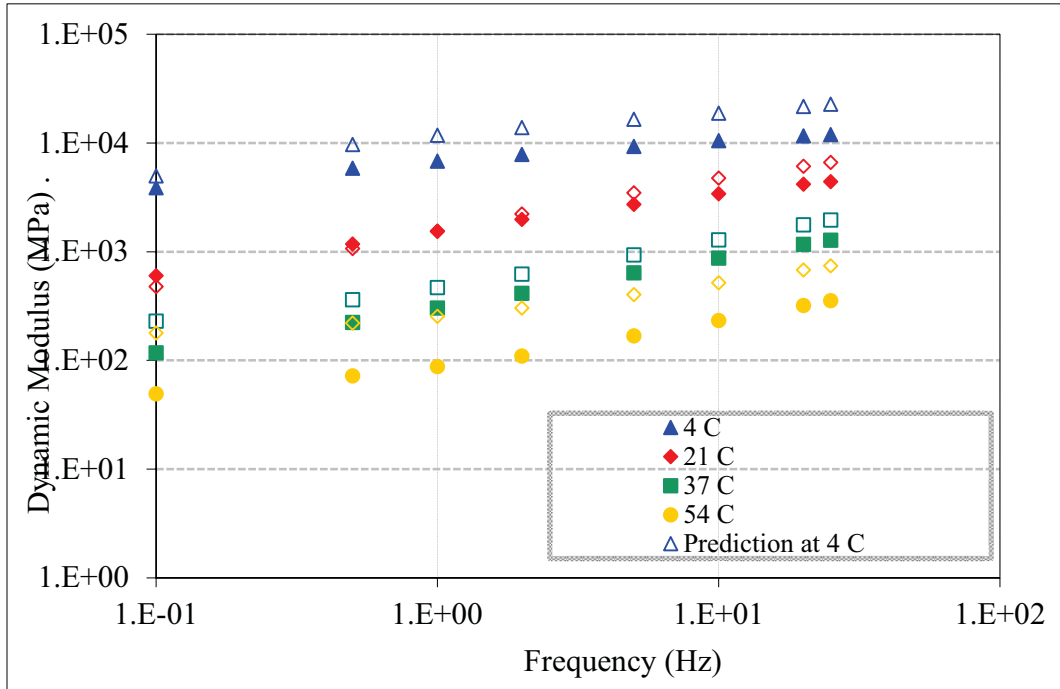
a) Measured and Predicted |E*| at Different Temperature and Frequency
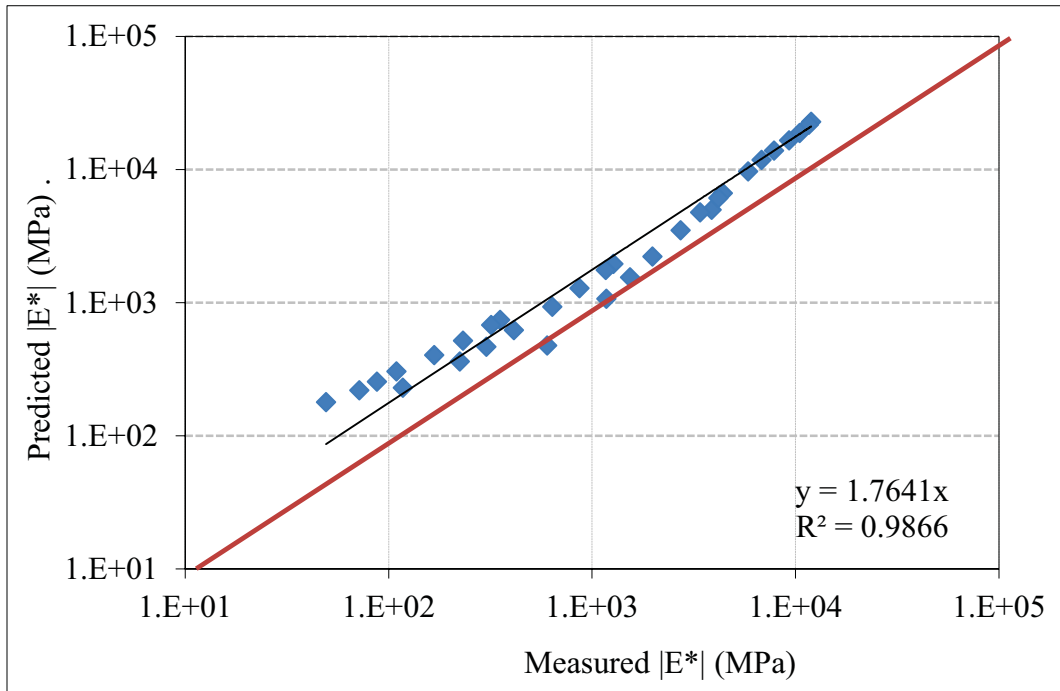
b) Measured |E*| vs. Predicted |E*|

Figure C.18 Summary of Predicted |E*| based on Modified Witczak Model
(Project: Parks Hwy MP 287-305 Rehab.)
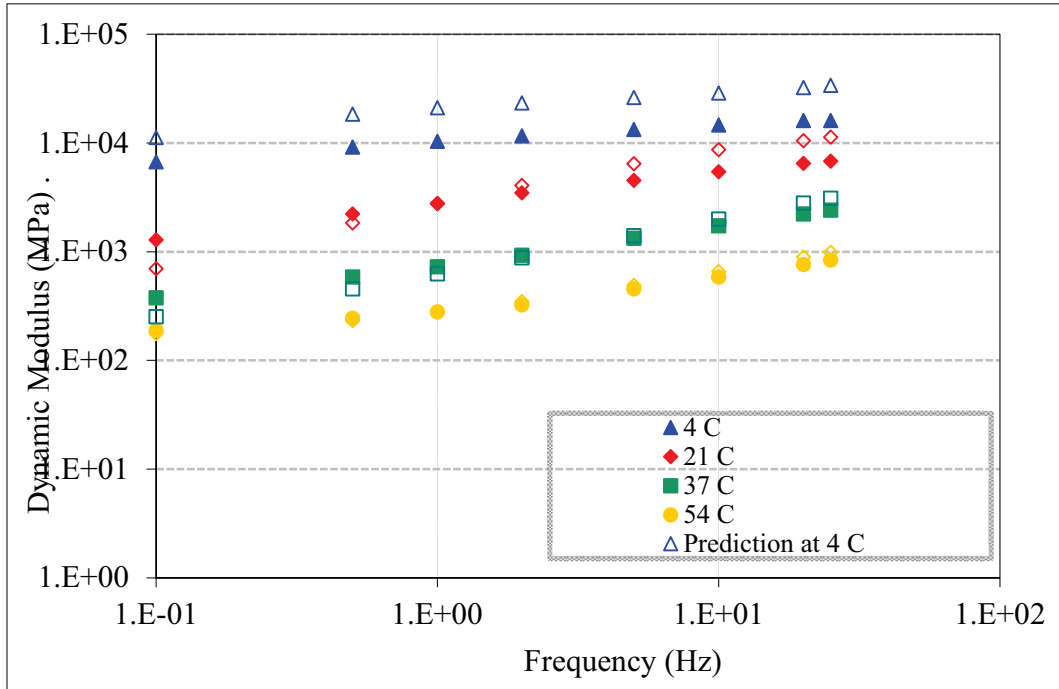
a) Measured and Predicted |E*| at Different Temperature and Frequency
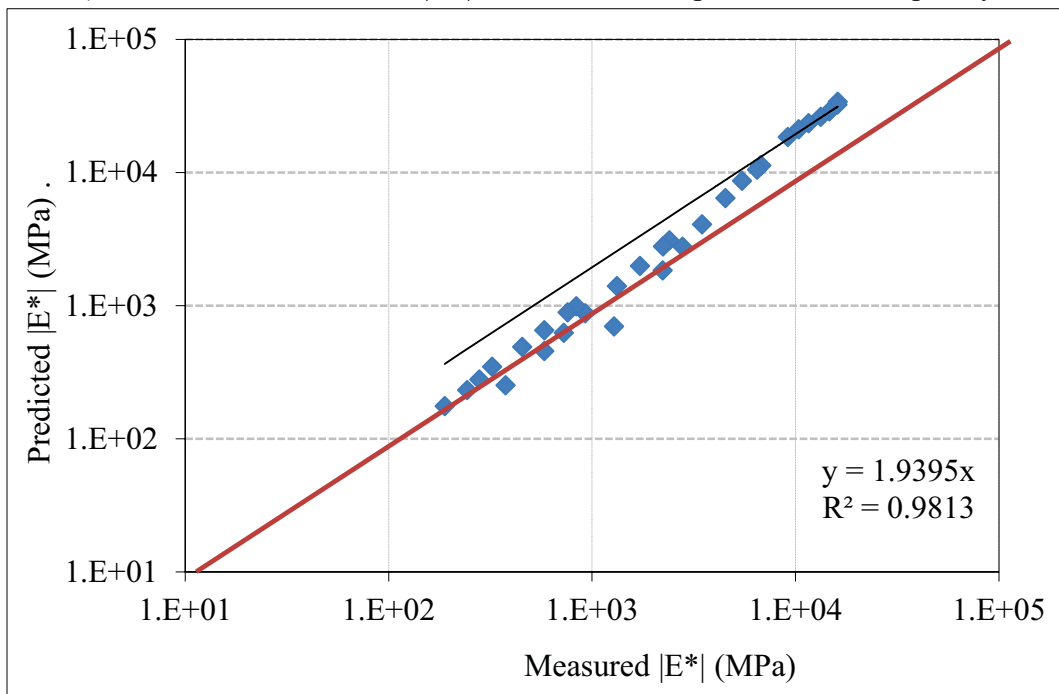
b) Measured |E*| vs. Predicted |E*|

Figure C.19 Summary of Predicted |E*| based on Modified Witczak Model
(Project: PSG Mitkof Highway-Scow Bay to Crystal Lake Hatchery)

APPENDIX D: Predicted |E*| Based on Hirsch Model
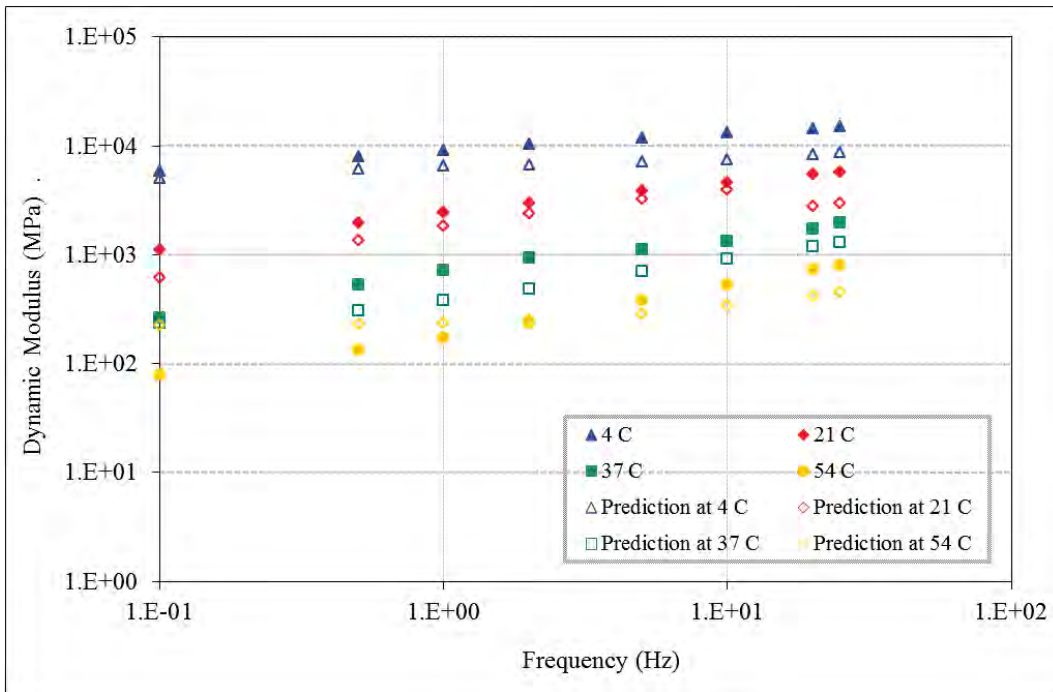
a) Measured and Predicted |E*| at Different Temperature and Frequency
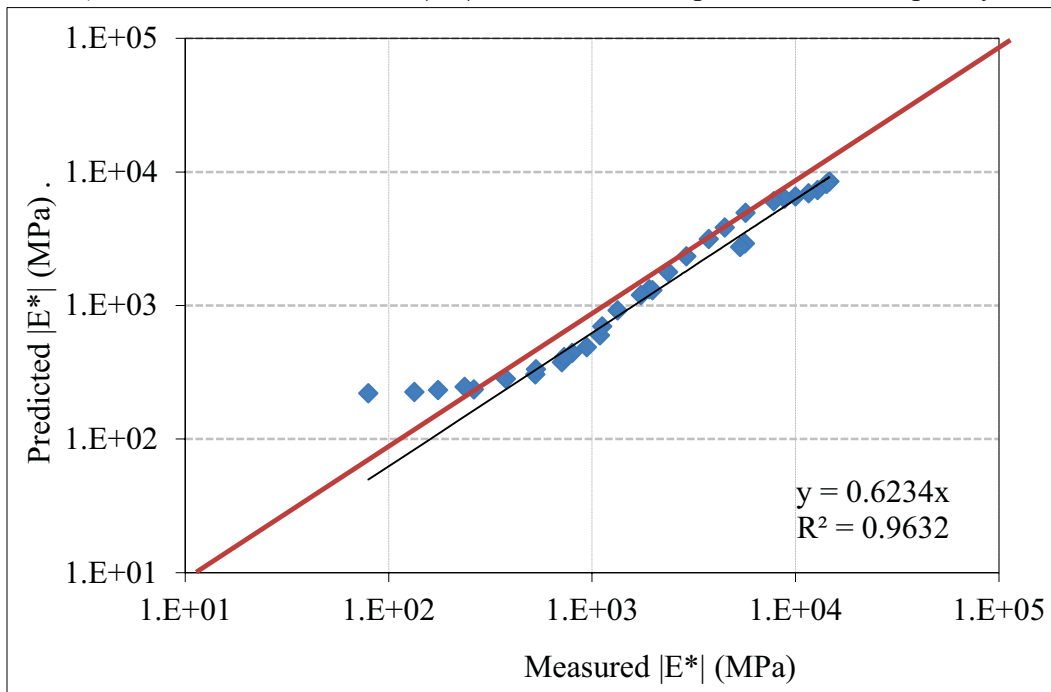
b) Measured |E*| vs. Predicted |E*|

Figure D.1 Summary of Predicted |E*| based on Hirsch Model
(Project: FIA Runway 1L_19R stage 3 (64-34))
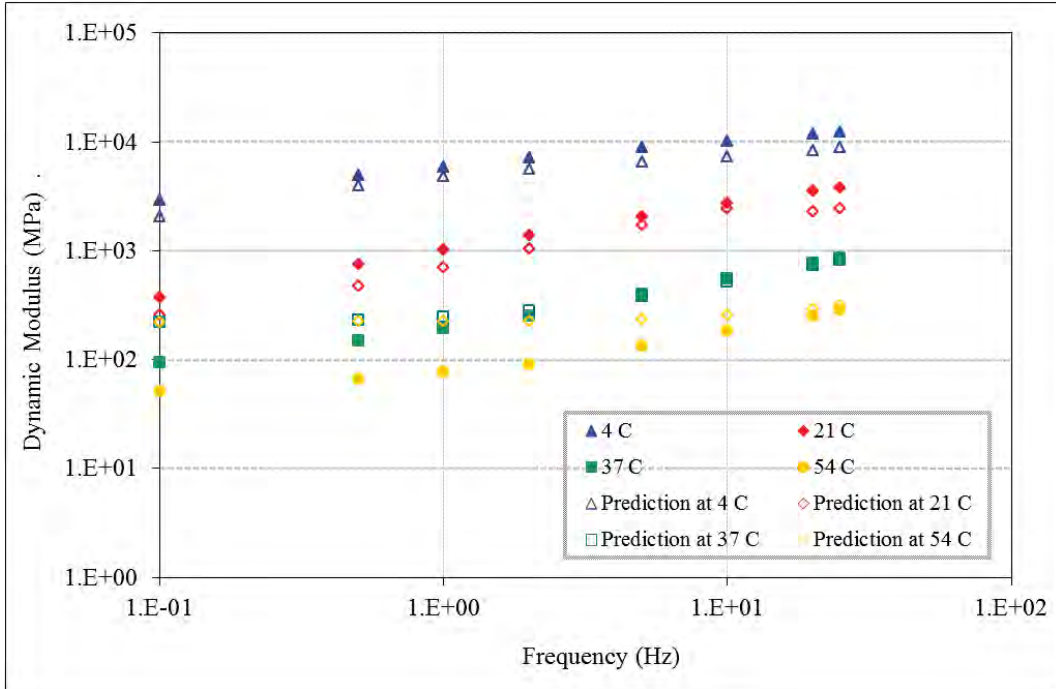
a) Measured and Predicted |E*| at Different Temperature and Frequency
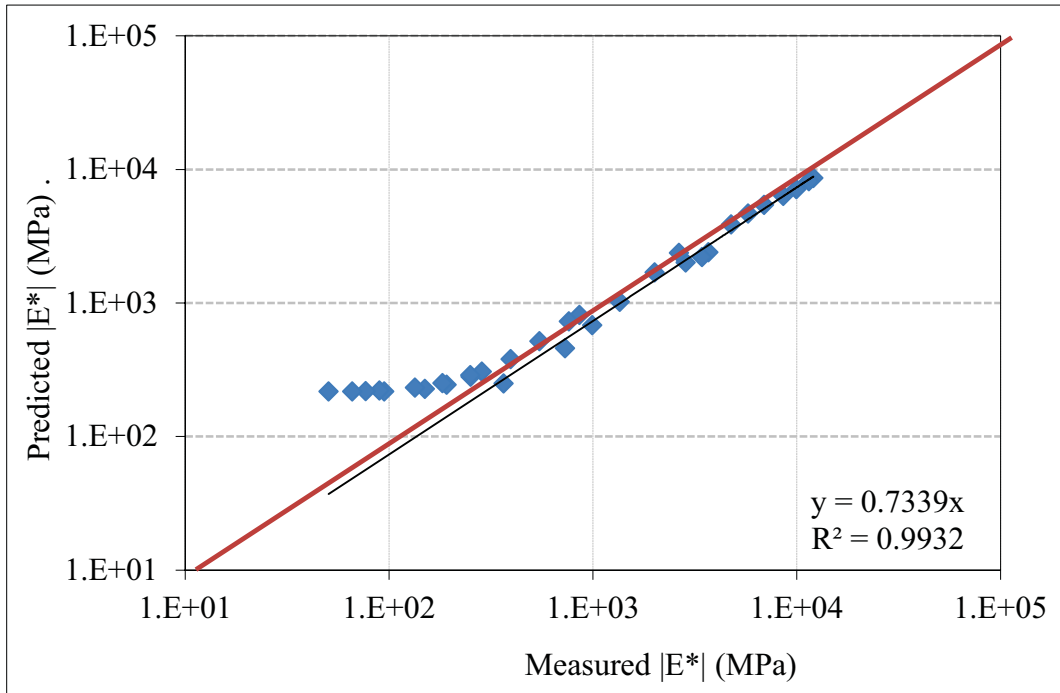
b) Measured |E*| vs. Predicted |E*|

Figure D.2 Summary of Predicted |E*| based on Hirsch Model
(Project: FIA Runway 1L_19R stage 3 (52-34))
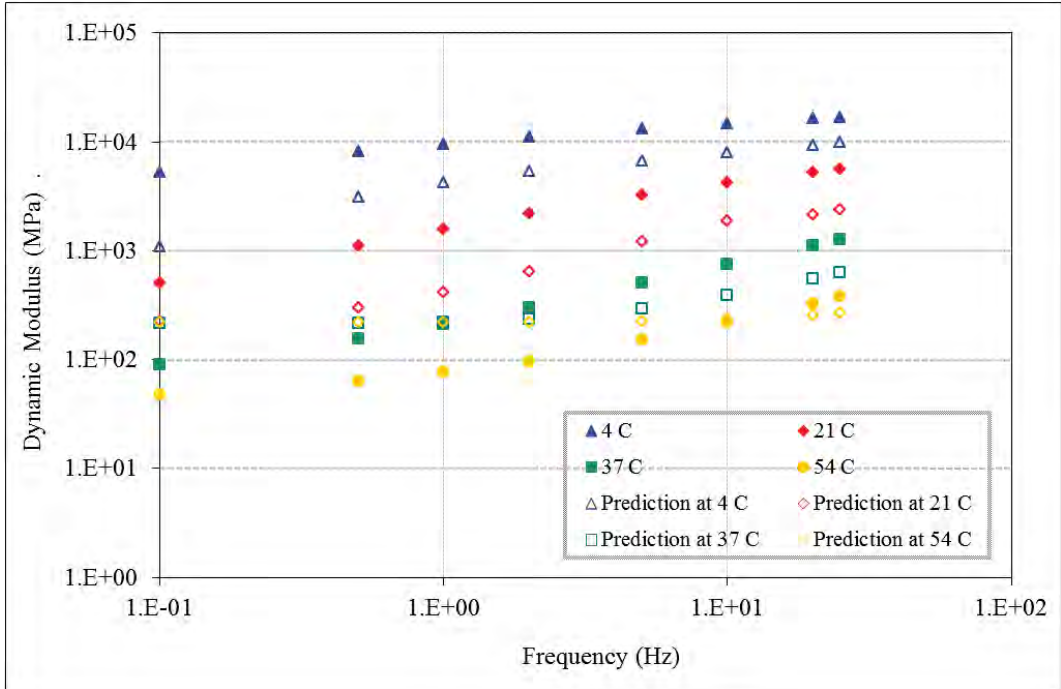
141

a) Measured and Predicted |E*| at Different Temperature and Frequency

$$y = 0.5134x$$
$$R^2 = 0.9685$$
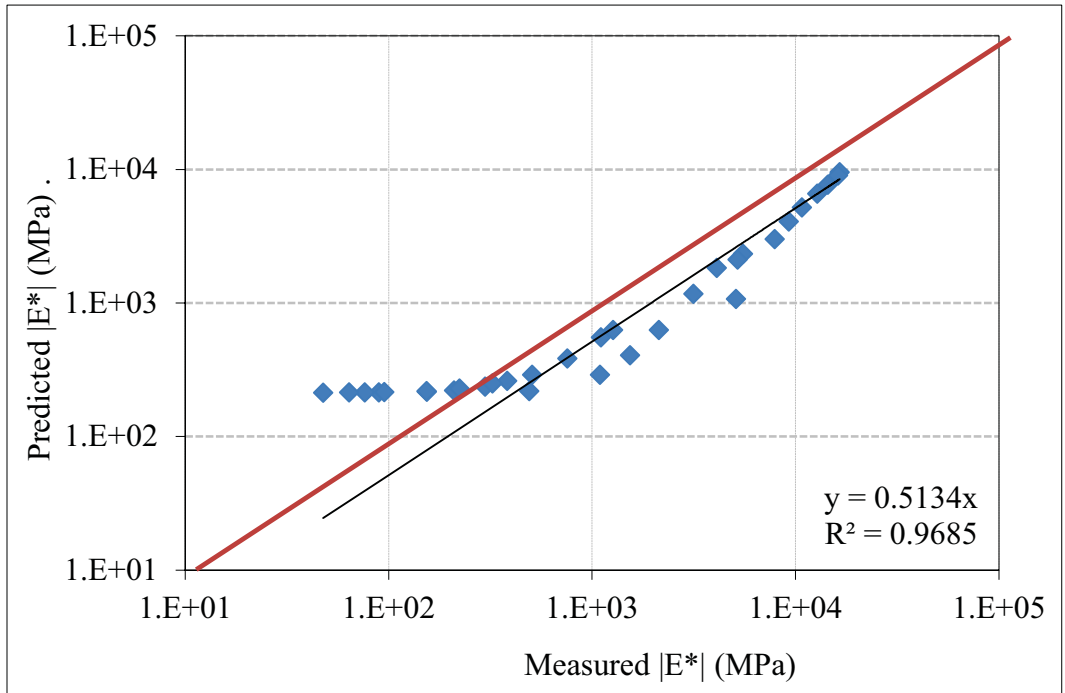
b) Measured |E*| vs. Predicted |E*|

Figure D.3 Summary of Predicted |E*| based on Hirsch Model
(Project: Chena Hot Springs Rd, MD-1)
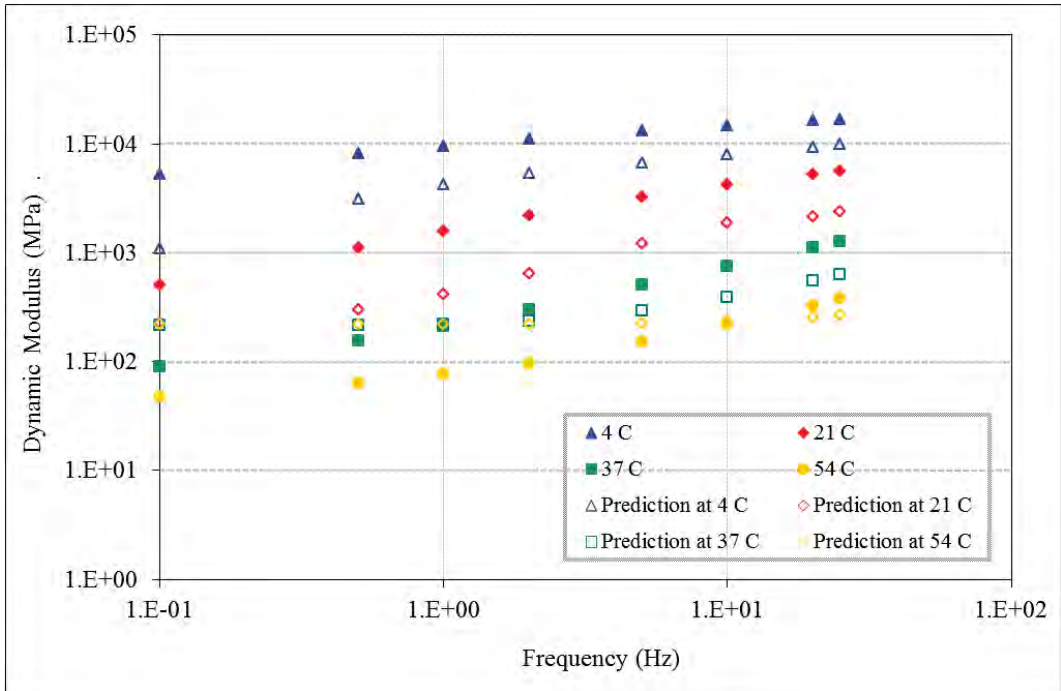
142

a) Measured and Predicted |E*| at Different Temperature and Frequency
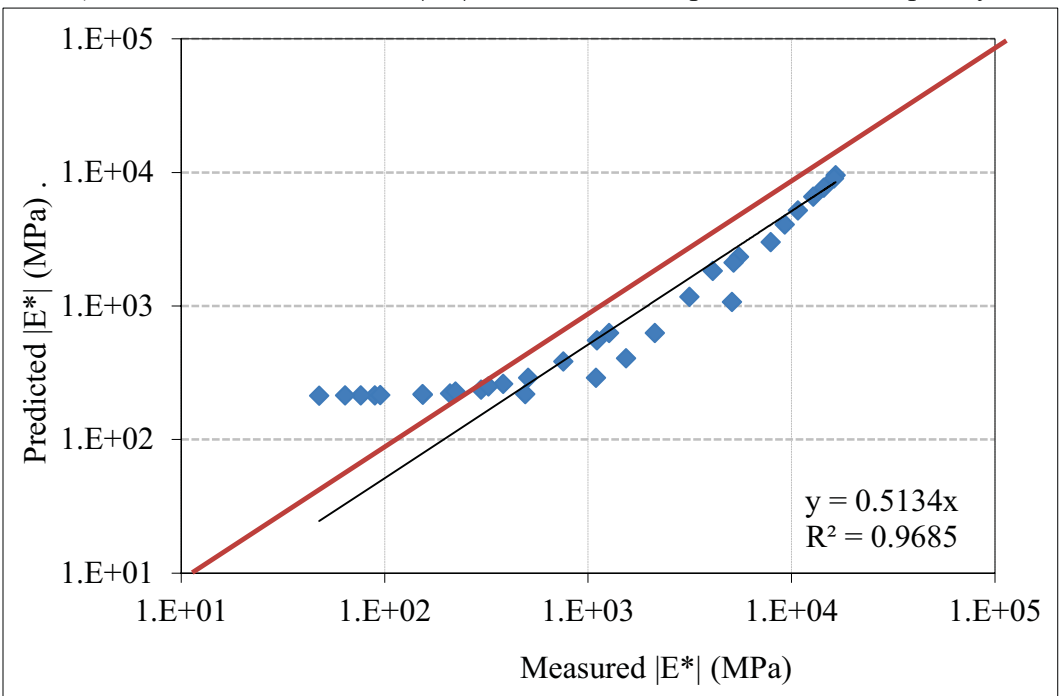
b) Measured |E*| vs. Predicted |E*|

Figure D.4 Summary of Predicted |E*| based on Hirsch Model
(Project: Chena Hot Springs Rd MD-3)
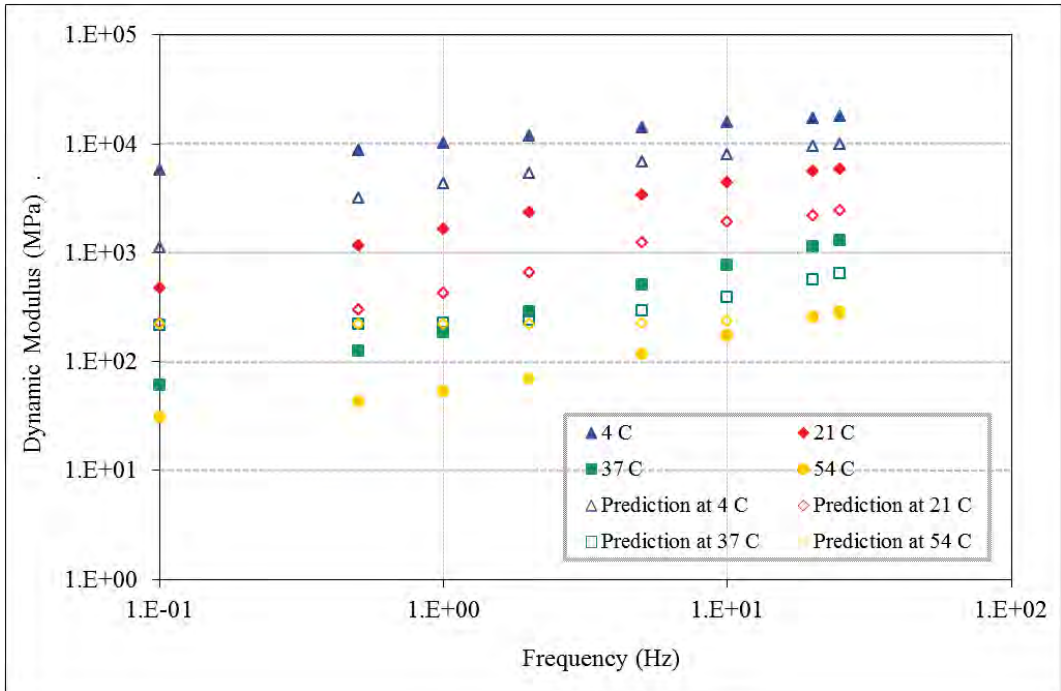
a) Measured and Predicted |E*| at Different Temperature and Frequency

$$y = 0.4934x$$
$$R^2 = 0.9659$$
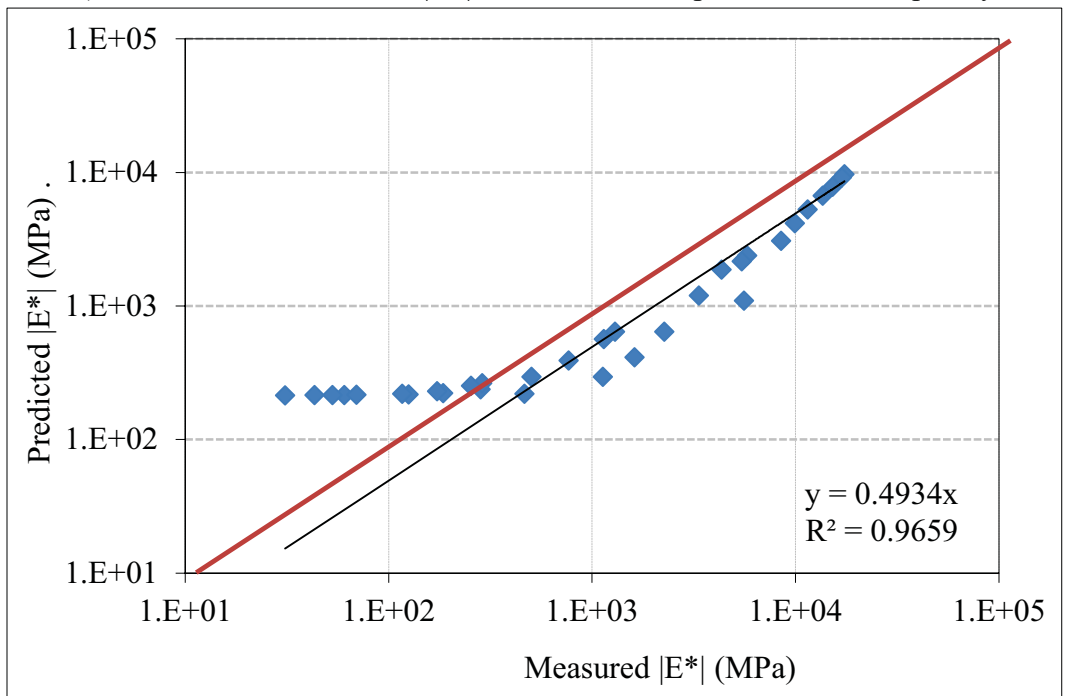
b) Measured |E*| vs. Predicted |E*|

Figure D.5 Summary of Predicted |E*| based on Hirsch Model
(Project: Fairbanks Cowles Street Upgrade)
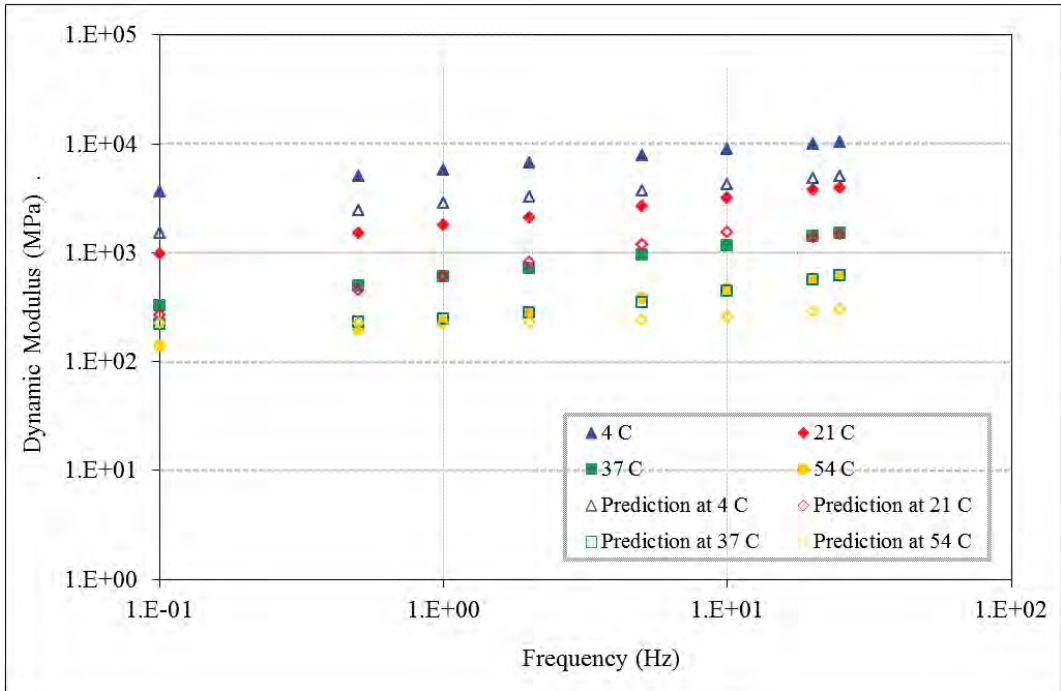
a) Measured and Predicted |E*| at Different Temperature and Frequency
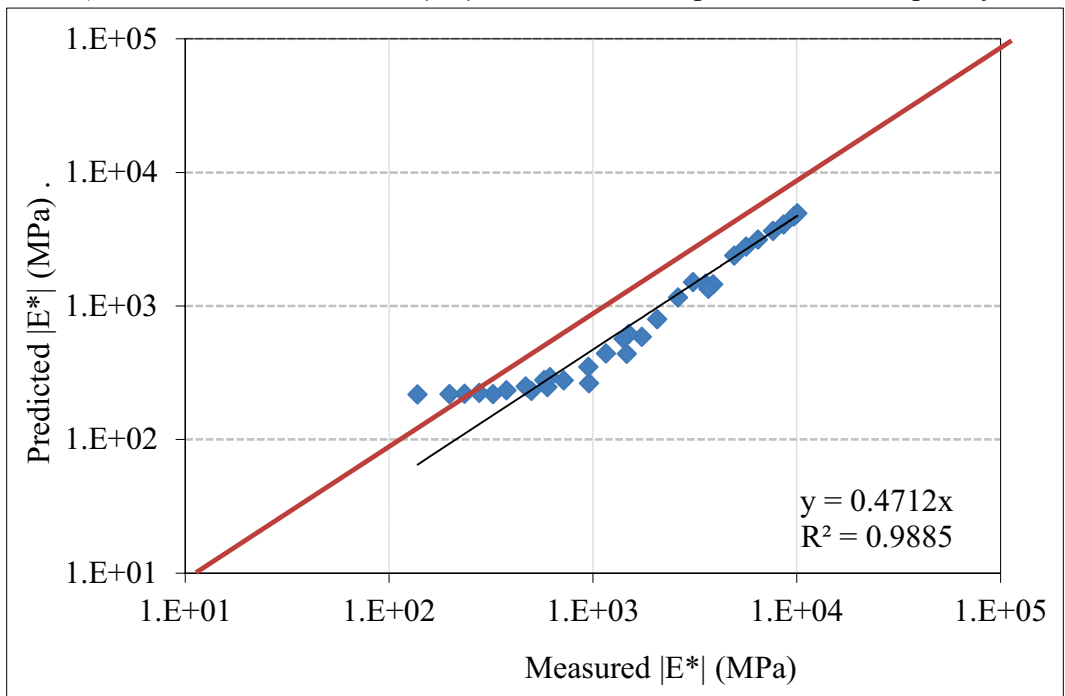
b) Measured |E*| vs. Predicted |E*|

Figure D.6 Summary of Predicted |E*| based on Hirsch Model
(Project: Dalton Hwy. MP 175-197 Rehabilitation)
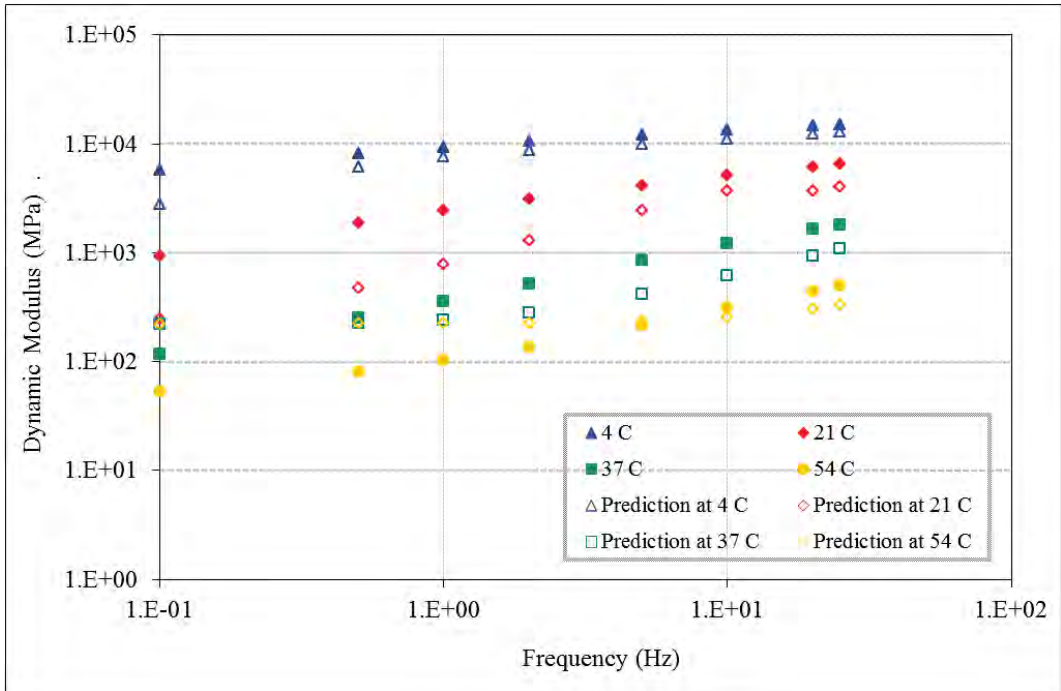
a) Measured and Predicted |E*| at Different Temperature and Frequency
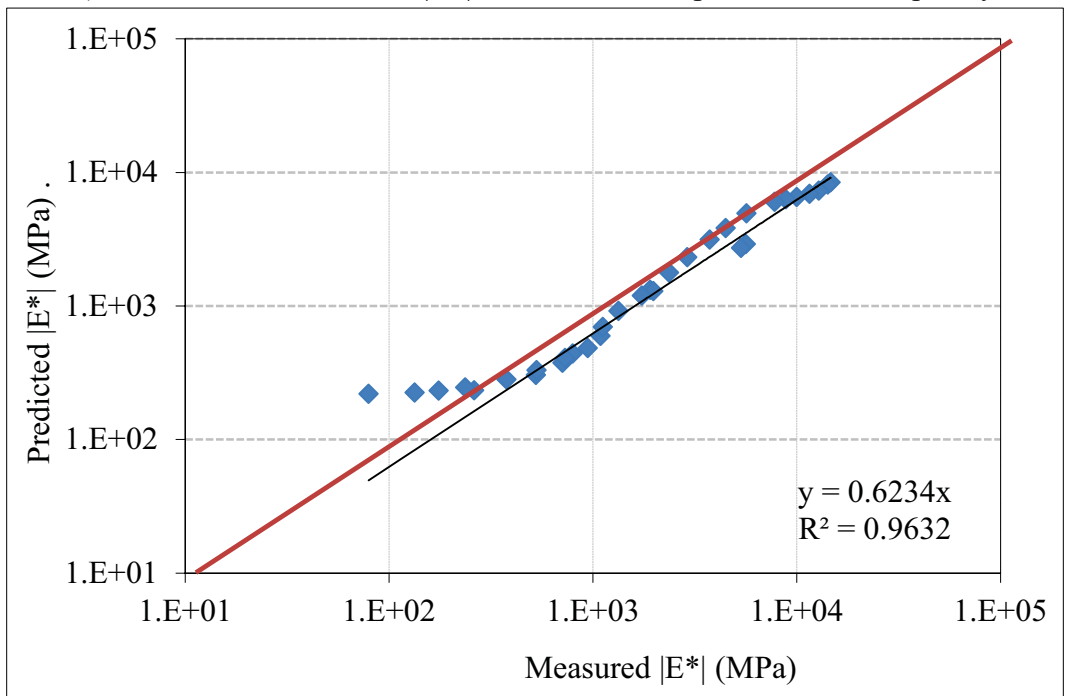
b) Measured |E*| vs. Predicted |E*|

Figure D.7 Summary of Predicted |E*| based on Hirsch Model
(Project: Glen Why MP 92-97 Cascade to Hicks Creek)

146
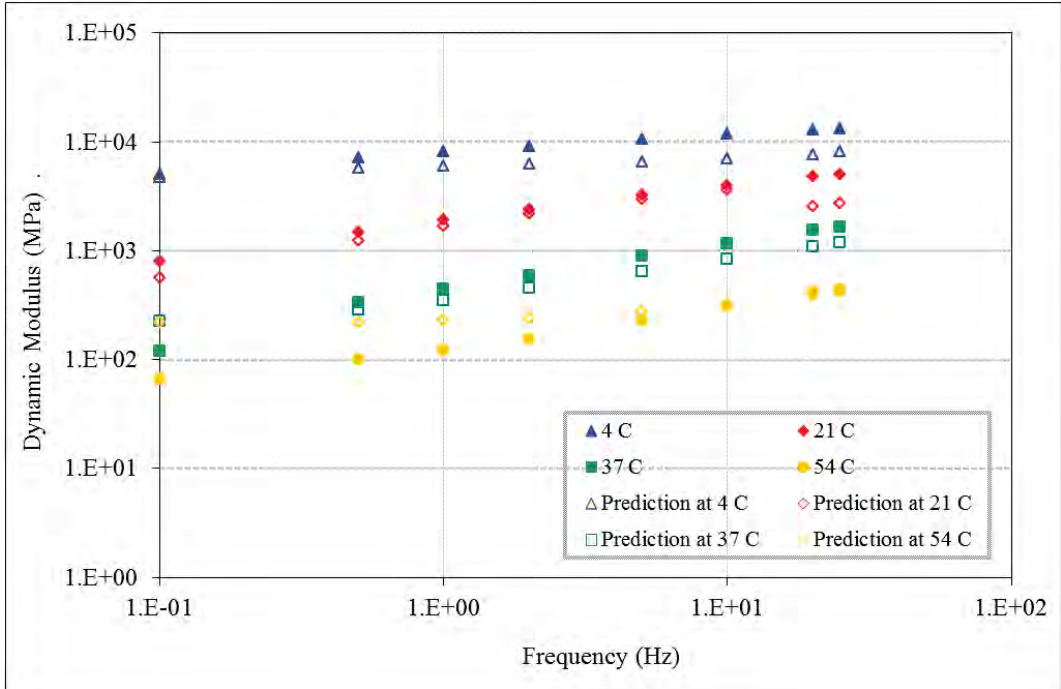
a) Measured and Predicted |E*| at Different Temperature and Frequency
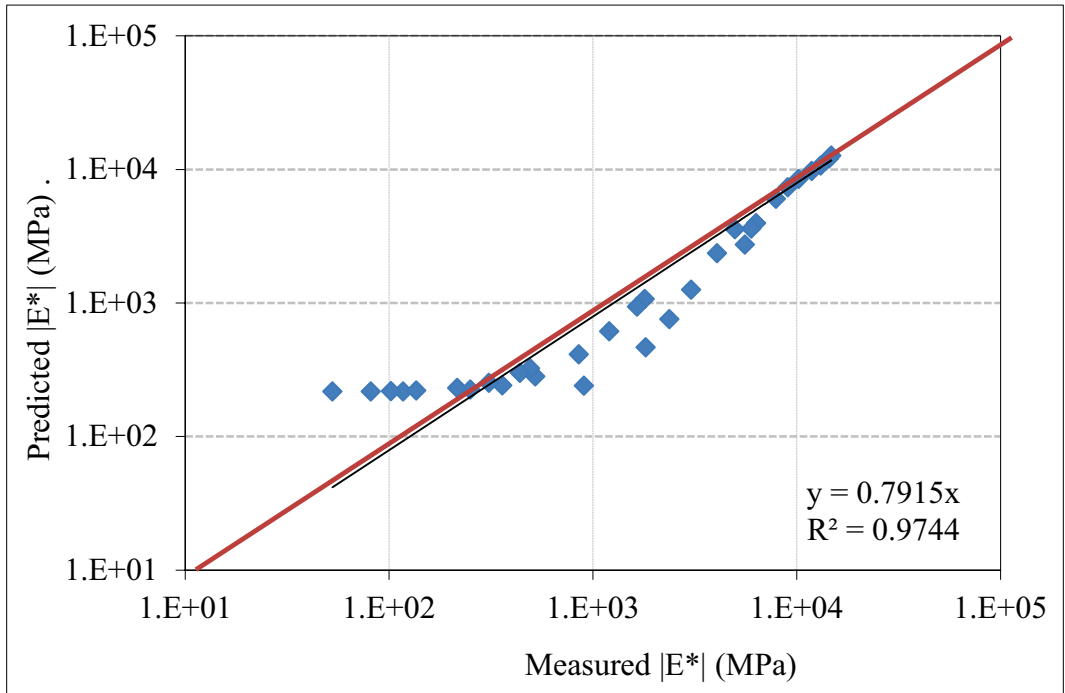
b) Measured |E*| vs. Predicted |E*|

Figure D.8 Summary of Predicted |E*| based on Hirsch Model
(Project: Glenn Highway Gambell to airport MP 0-1.5)

147

a) Measured and Predicted |E*| at Different Temperature and Frequency

$$y = 0.6531x$$
$$R^2 = 0.961$$
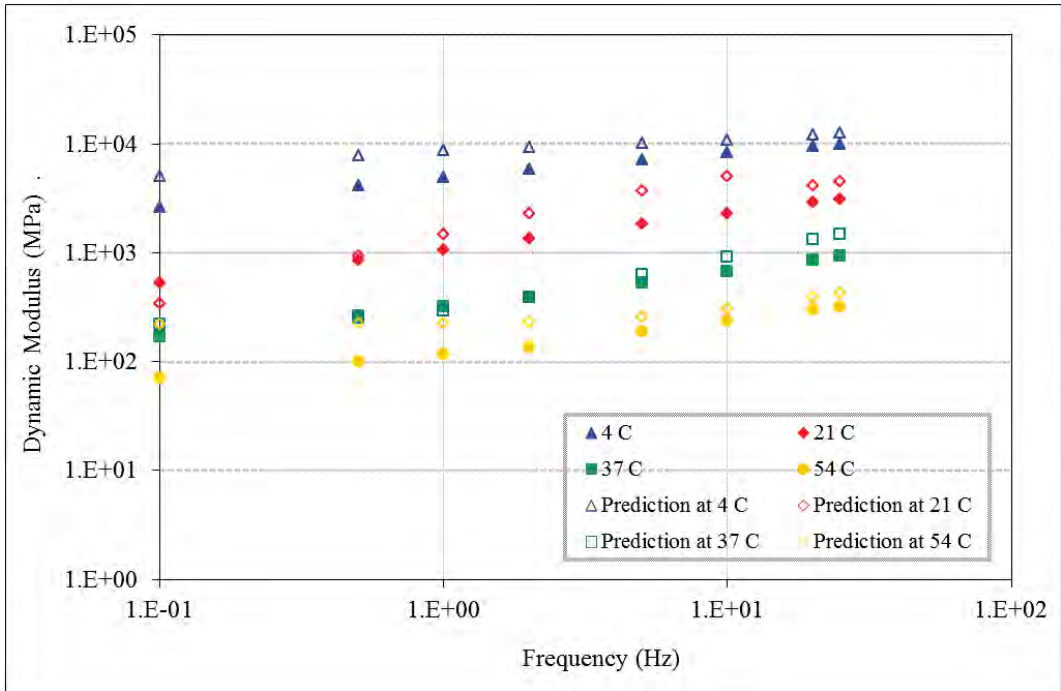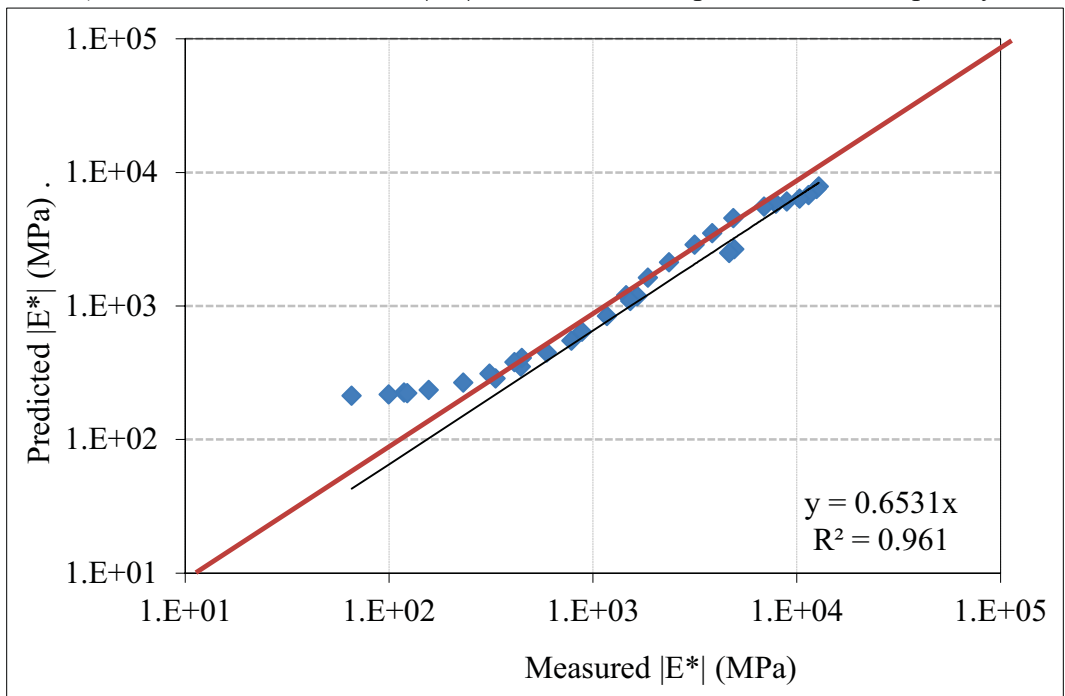
b) Measured |E*| vs. Predicted |E*|

Figure D.9 Summary of Predicted |E*| based on Hirsch Model
(Project HNS Ferry Terminal to Union Street)
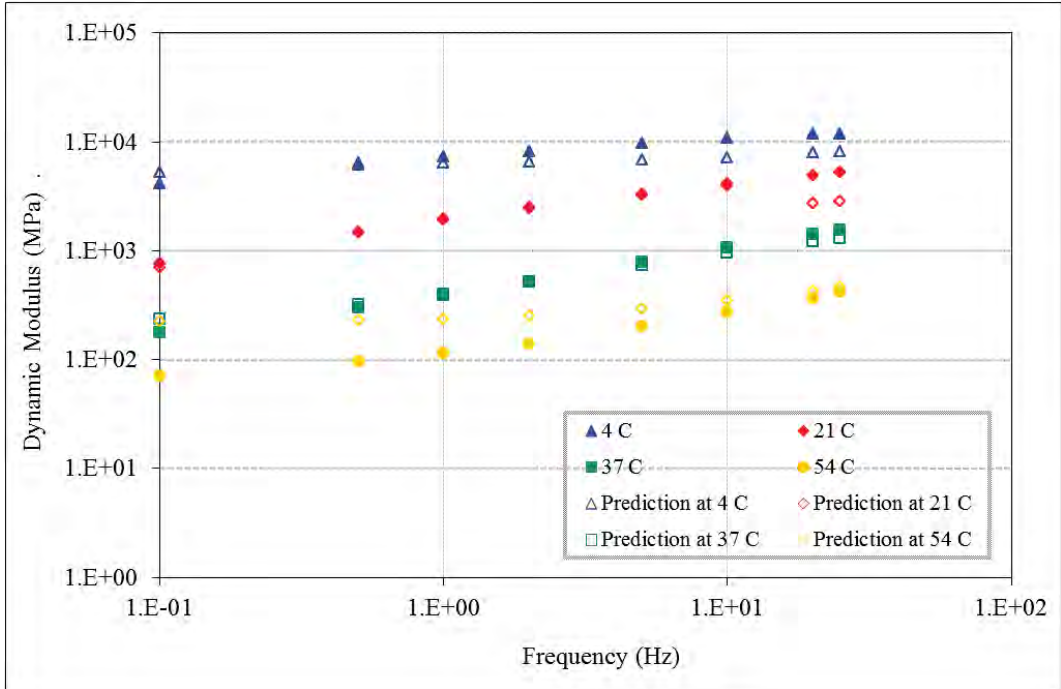
a) Measured and Predicted |E*| at Different Temperature and Frequency

y = 0.7362x
R² = 0.9348
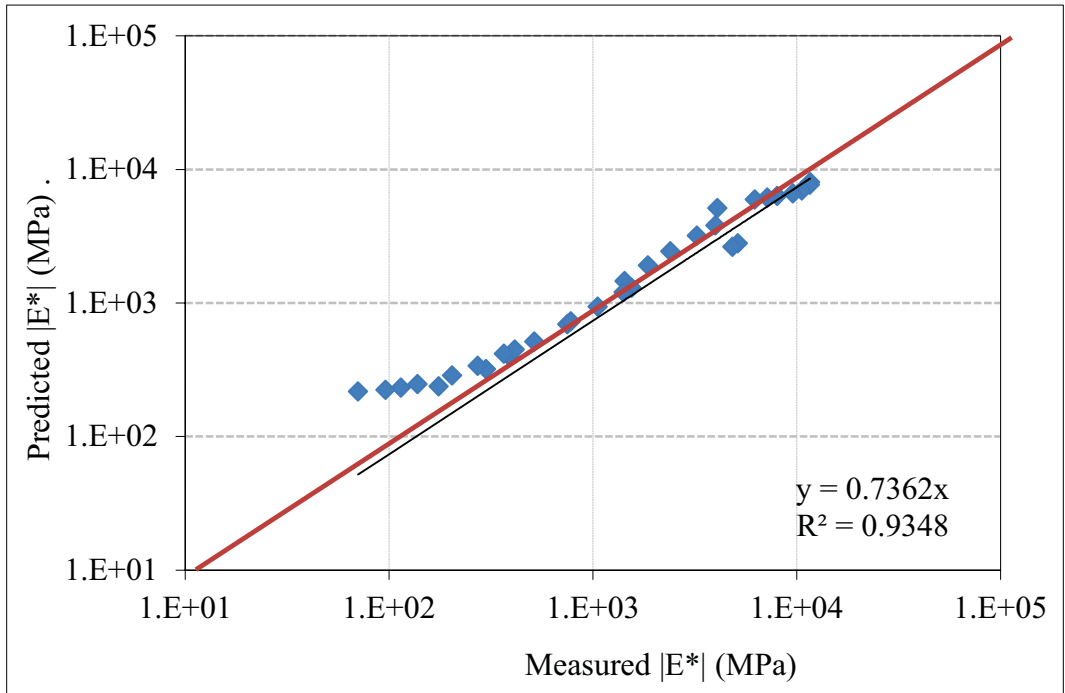
b) Measured |E*| vs. Predicted |E*|

Figure D.10 Summary of Predicted |E*| based on Hirsch Model
(Project: Minnesota Dr Resurfacing: Int'l Airport Rd to 13th)
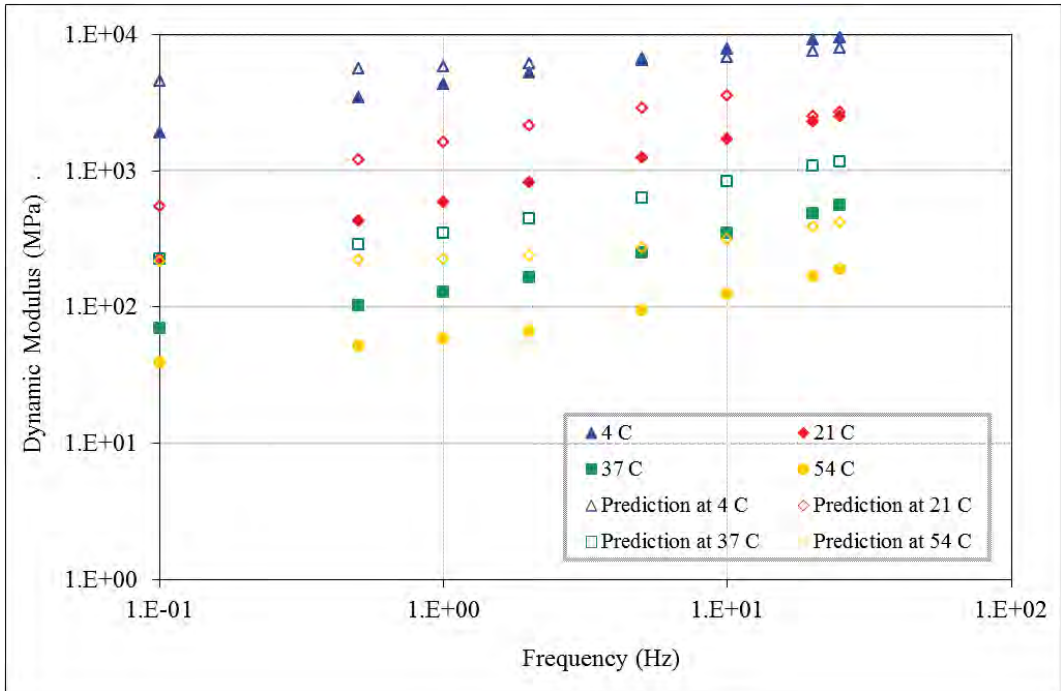
a) Measured and Predicted |E*| at Different Temperature and Frequency
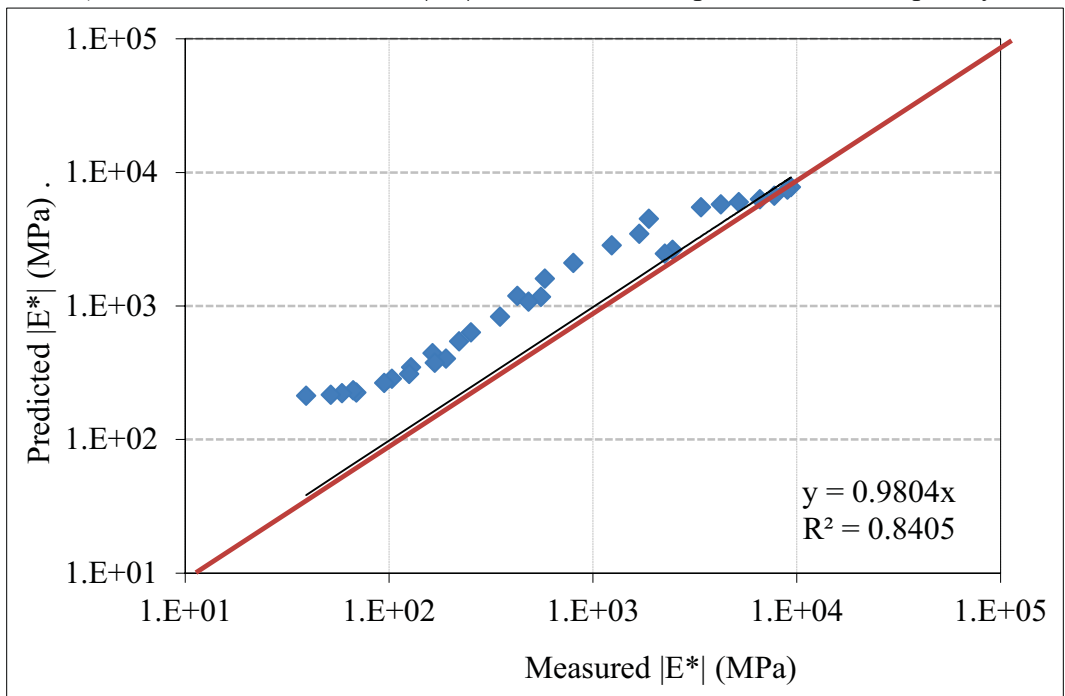
b) Measured |E*| vs. Predicted |E*|

Figure D.11 Summary of Predicted |E*| based on Hirsch Model
(Project: Rich Hwy North Pole Interchange)
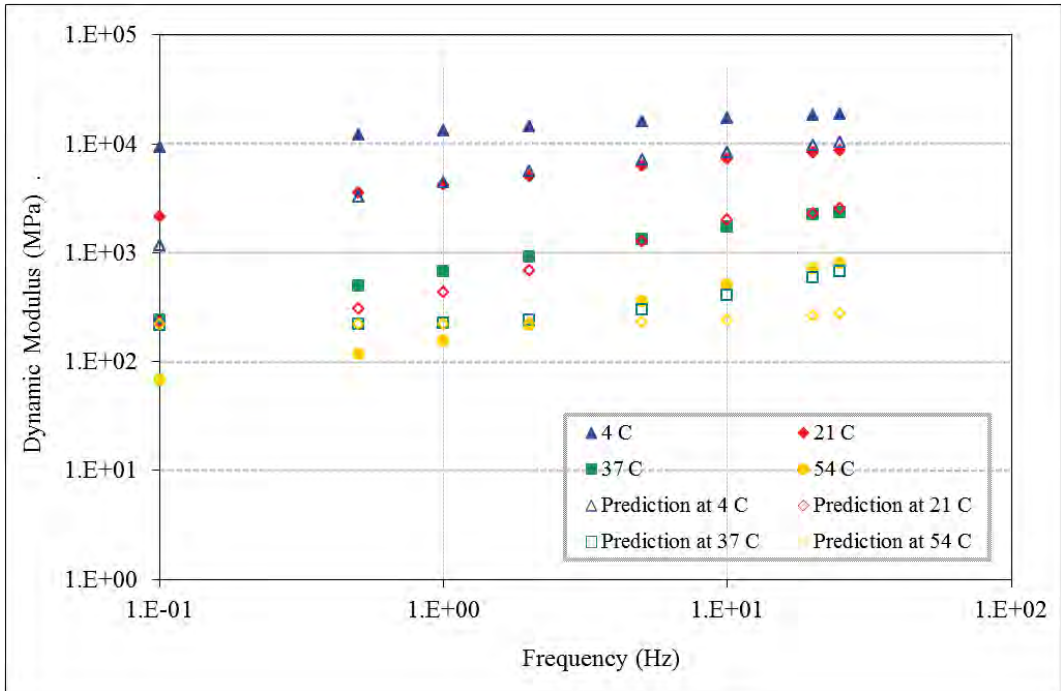
a) Measured and Predicted |E*| at Different Temperature and Frequency
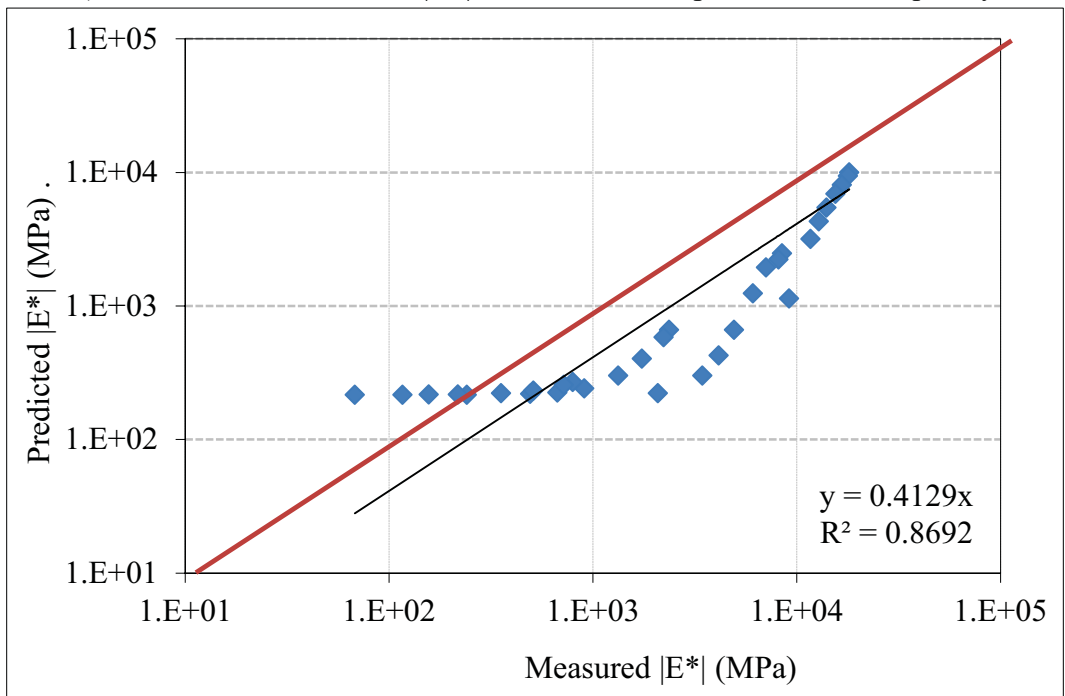
b) Measured |E*| vs. Predicted |E*|

Figure D.12 Summary of Predicted |E*| based on Hirsch Model
(Project: Old Glenn Hwy.: MP 11.5-18)
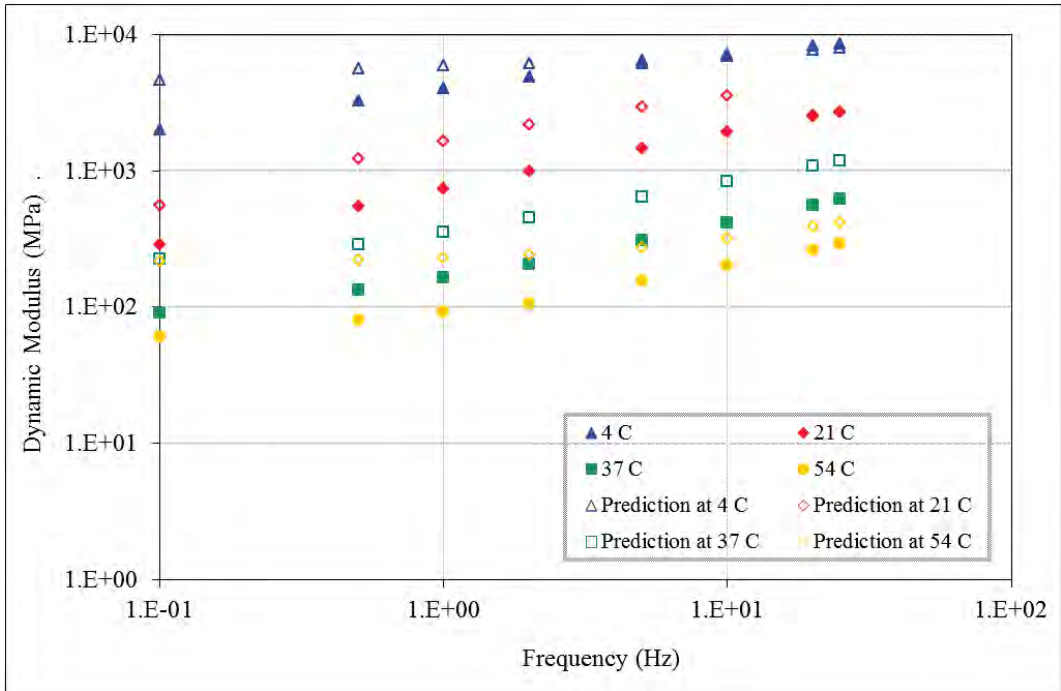
a) Measured and Predicted |E*| at Different Temperature and Frequency

$$y = 1.086x$$
$$R^2 = 0.8766$$
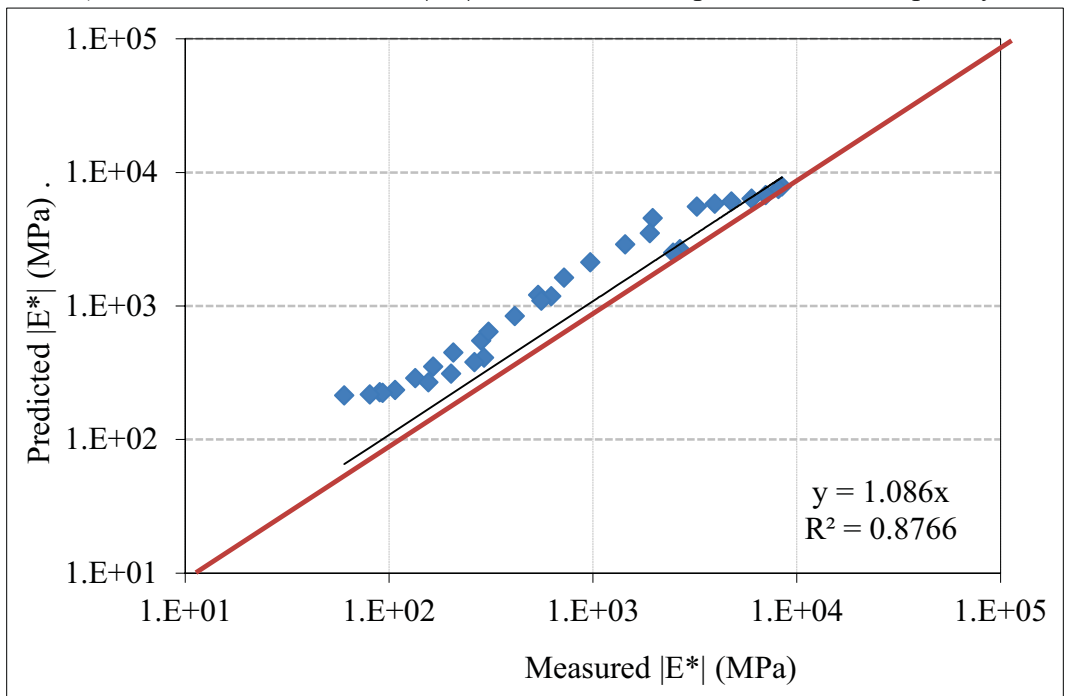
b) Measured |E*| vs. Predicted |E*|

Figure D.13 Summary of Predicted |E*| based on Hirsch Model
(Project: Palmer-Wasilla Highway Phase II)
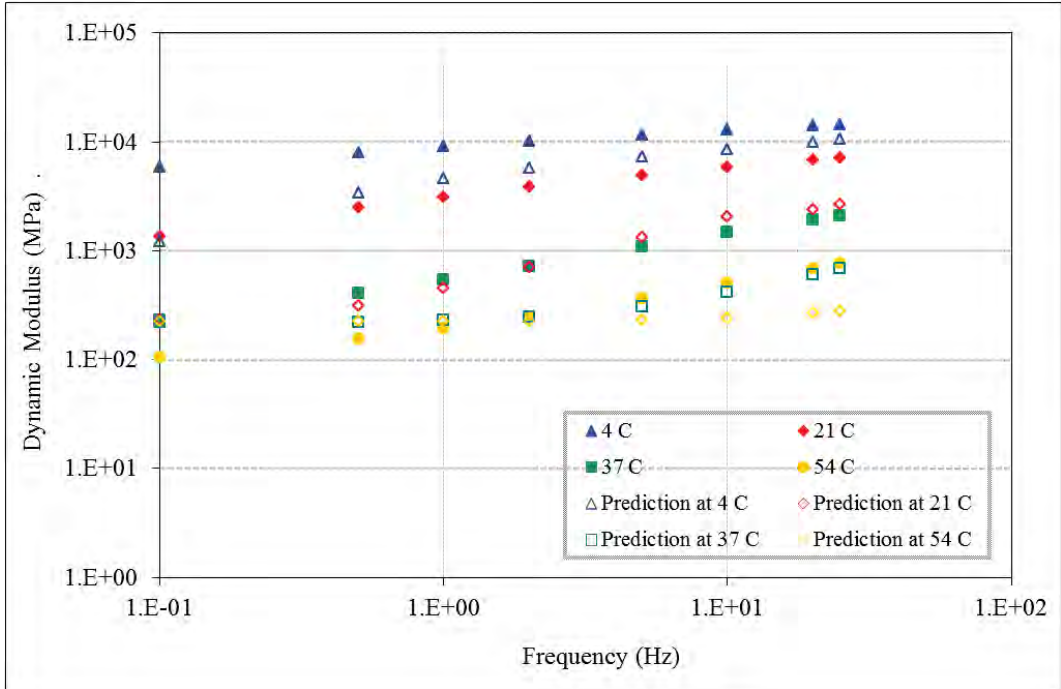
a) Measured and Predicted |E*| at Different Temperature and Frequency

$$y = 0.5762x$$
$$R^2 = 0.8886$$
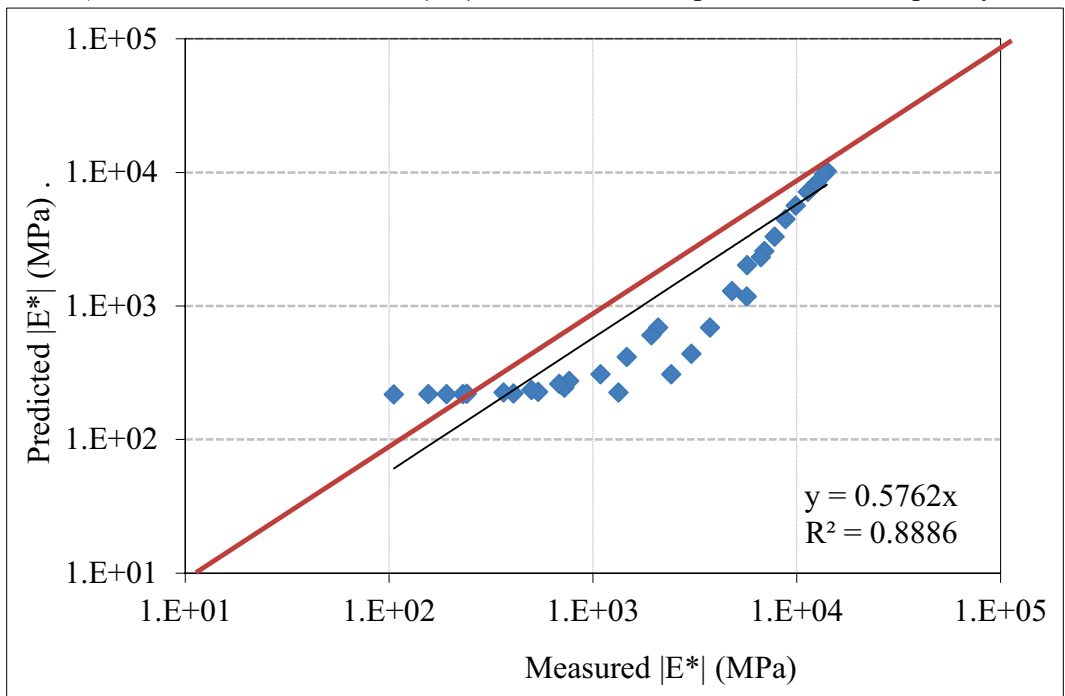
b) Measured |E*| vs. Predicted |E*|

Figure D.14 Summary of Predicted |E*| based on Hirsch Model
(Project: Unalakleet Airport Paving)
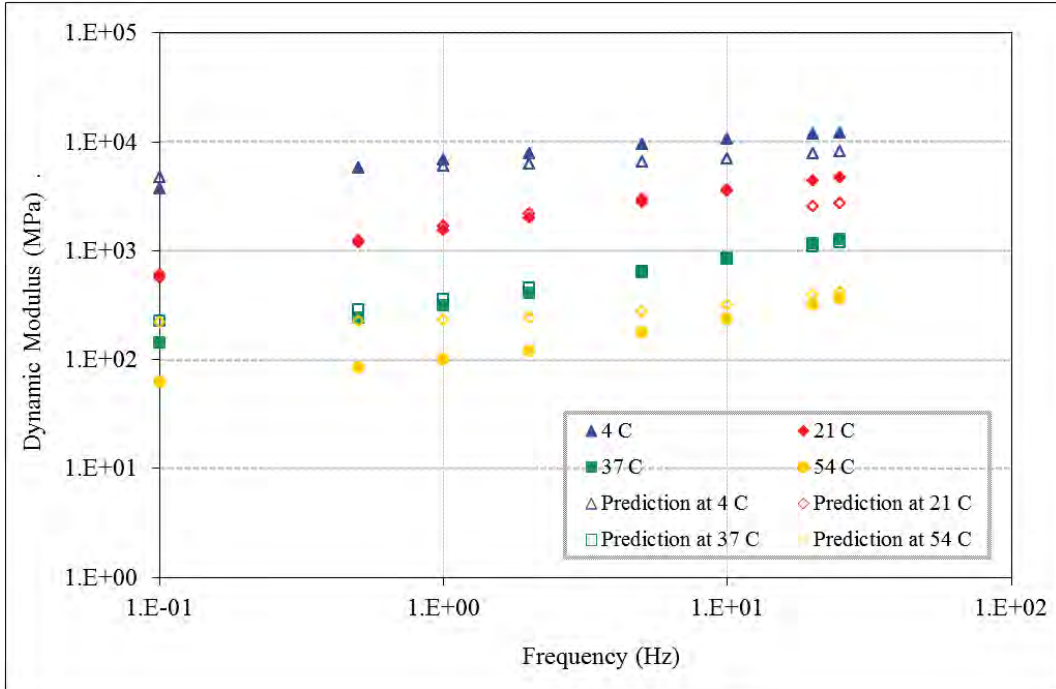
a) Measured and Predicted |E*| at Different Temperature and Frequency

y = 0.7308x
R² = 0.934
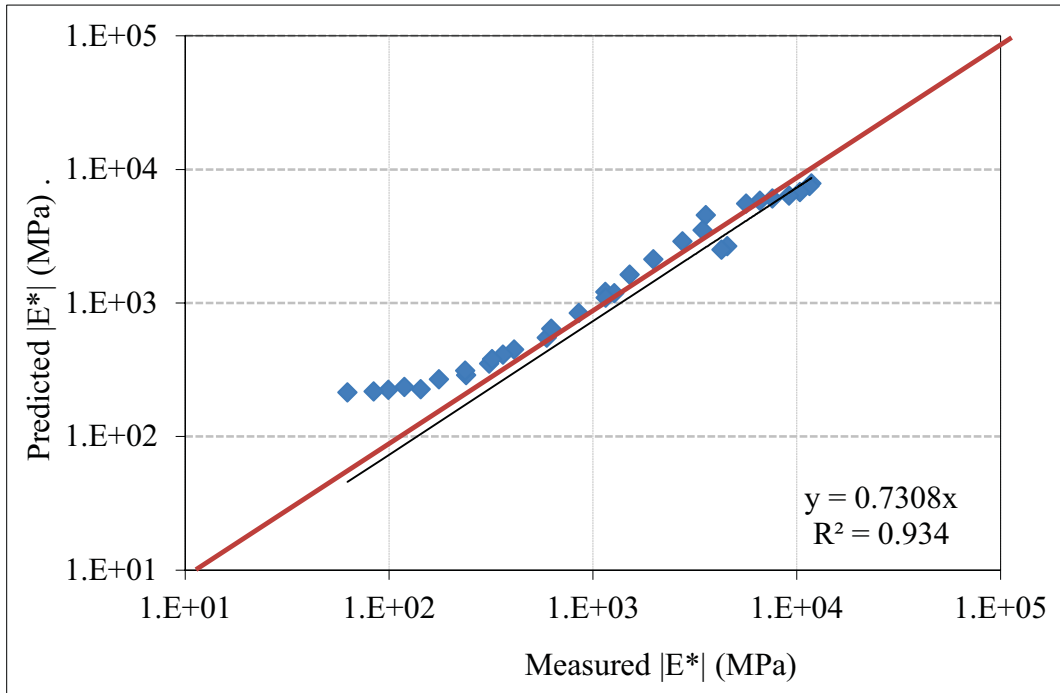
b) Measured |E*| vs. Predicted |E*|

Figure D.15 Summary of Predicted |E*| based on Hirsch Model
(Project: Glenn Highway MP 34-42, parks to Palmer Resurf.)

154
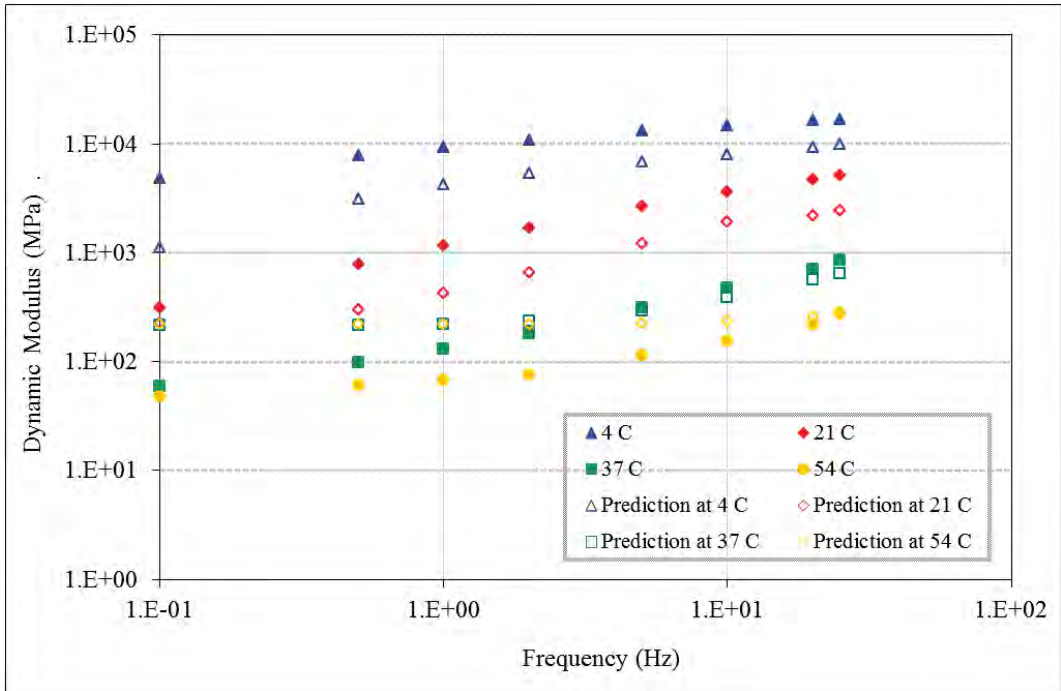
a) Measured and Predicted |E*| at Different Temperature and Frequency
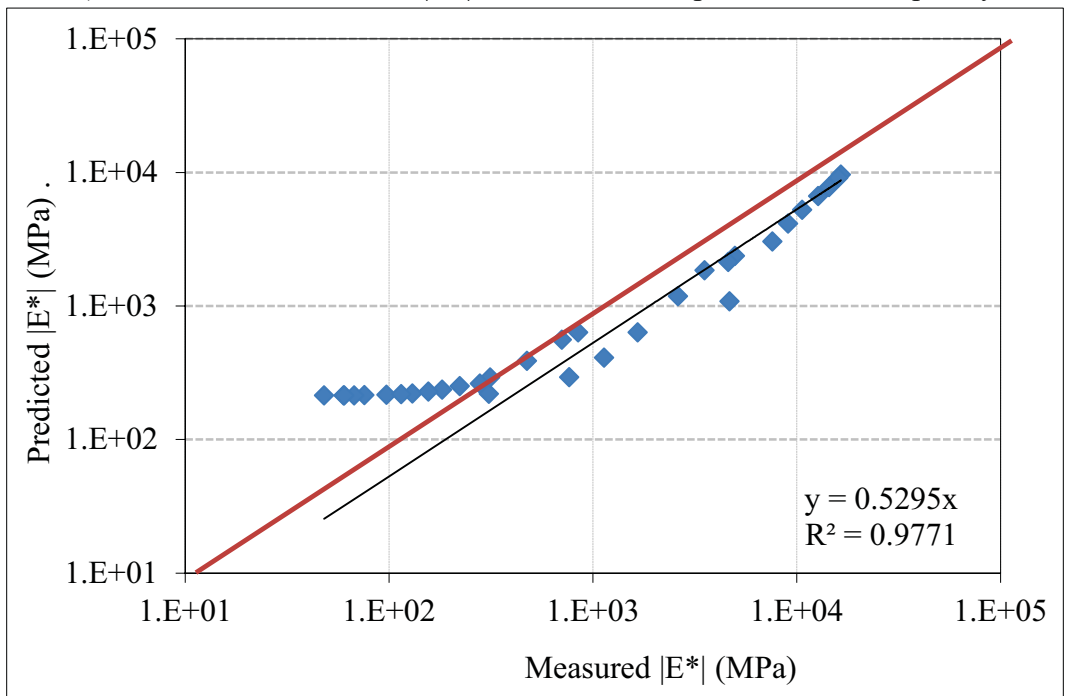
b) Measured |E*| vs. Predicted |E*|

Figure D.16 Summary of Predicted |E*| based on Hirsch Model
(Project: Alaska Hwy MP 1267-1314)
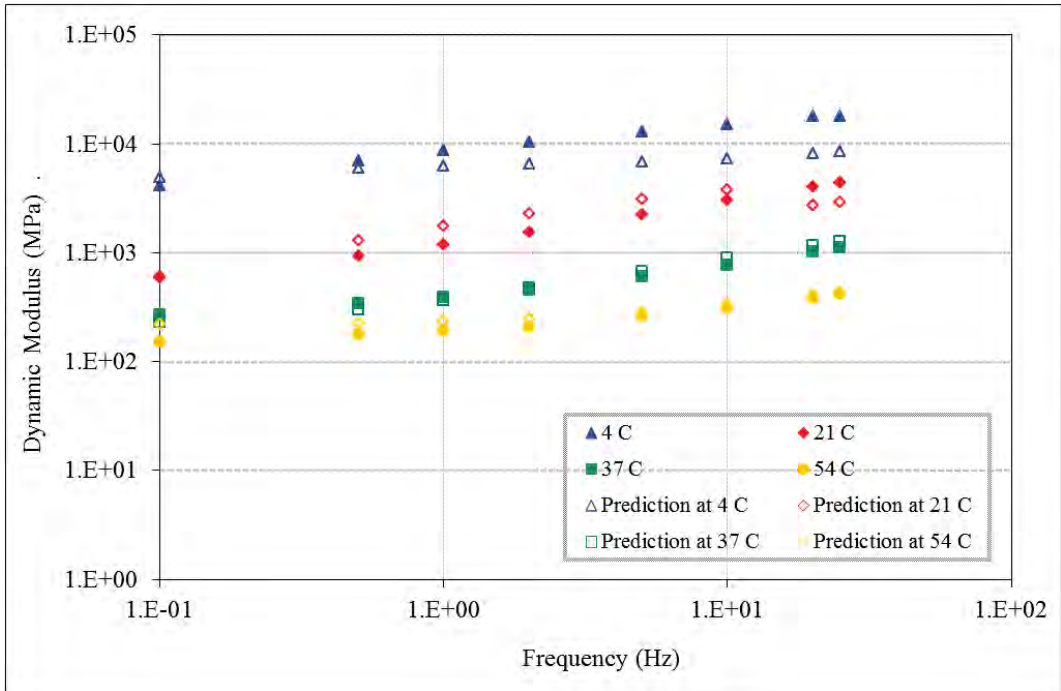
a) Measured and Predicted |E*| at Different Temperature and Frequency

$$y = 0.5477x$$
$$R^2 = 0.8508$$
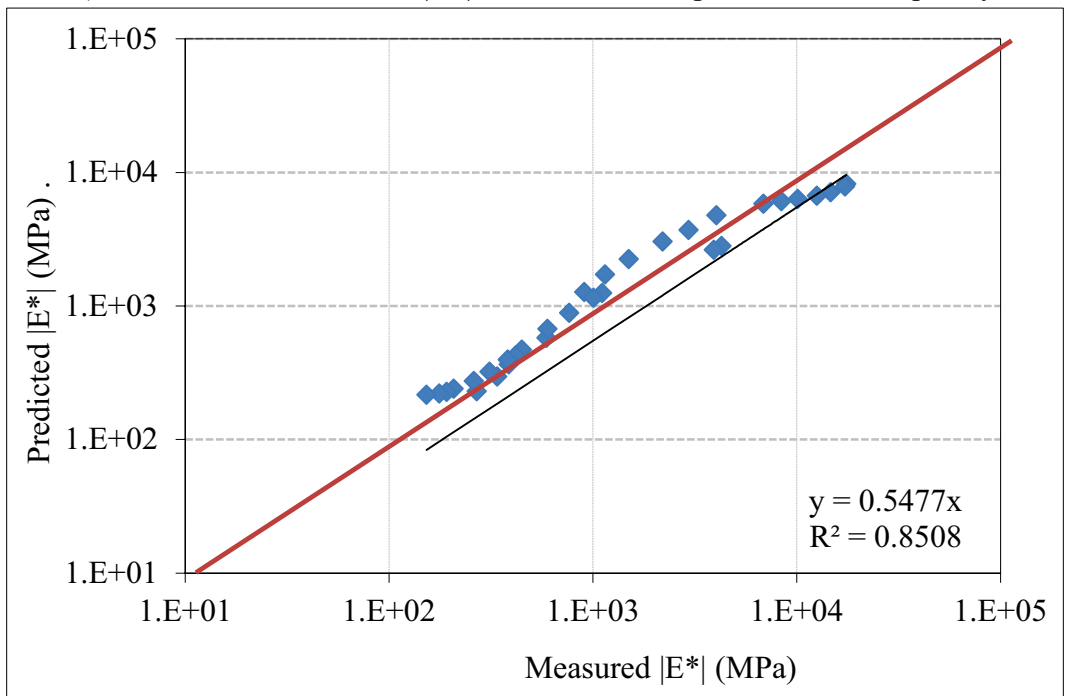
b) Measured |E*| vs. Predicted |E*|

Figure D.17 Summary of Predicted |E*| based on Hirsch Model
(Project: AIA runway 7R_25L Rehab.)
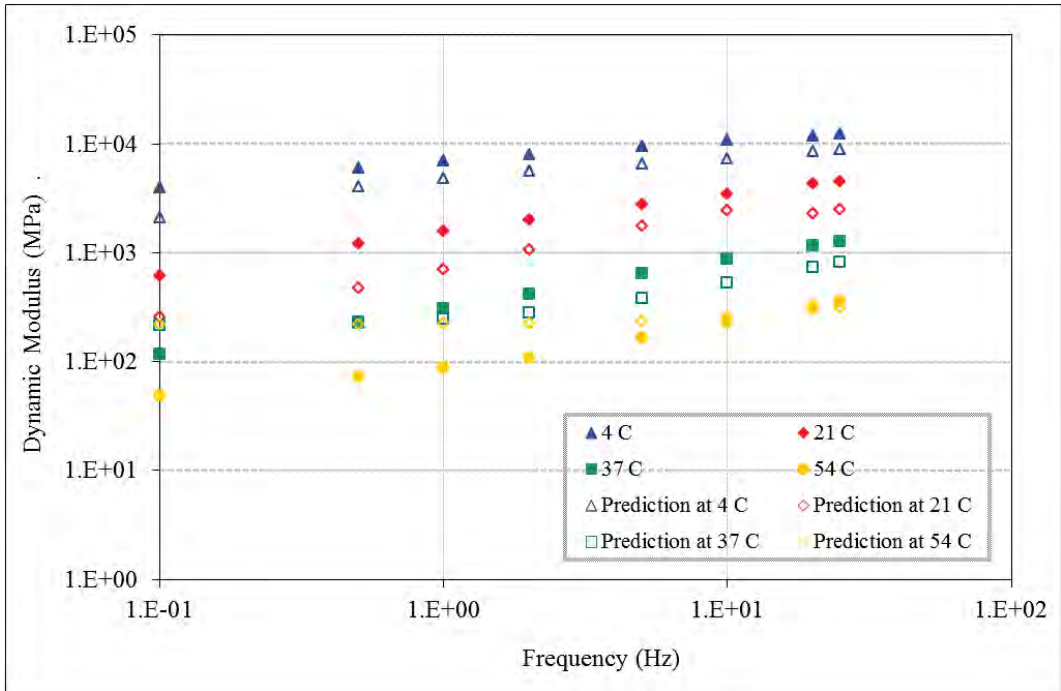
156

a) Measured and Predicted |E*| at Different Temperature and Frequency
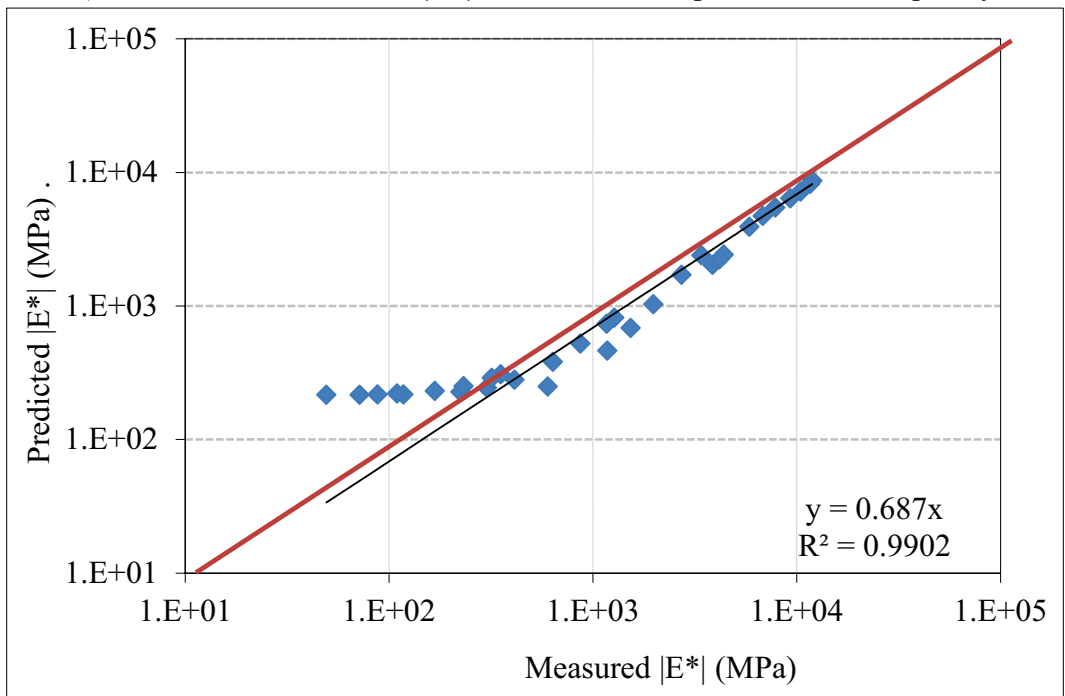
b) Measured |E*| vs. Predicted |E*|

Figure D.18 Summary of Predicted |E*| based on Hirsch Model
(Project: Parks Hwy MP 287-305 Rehab.)
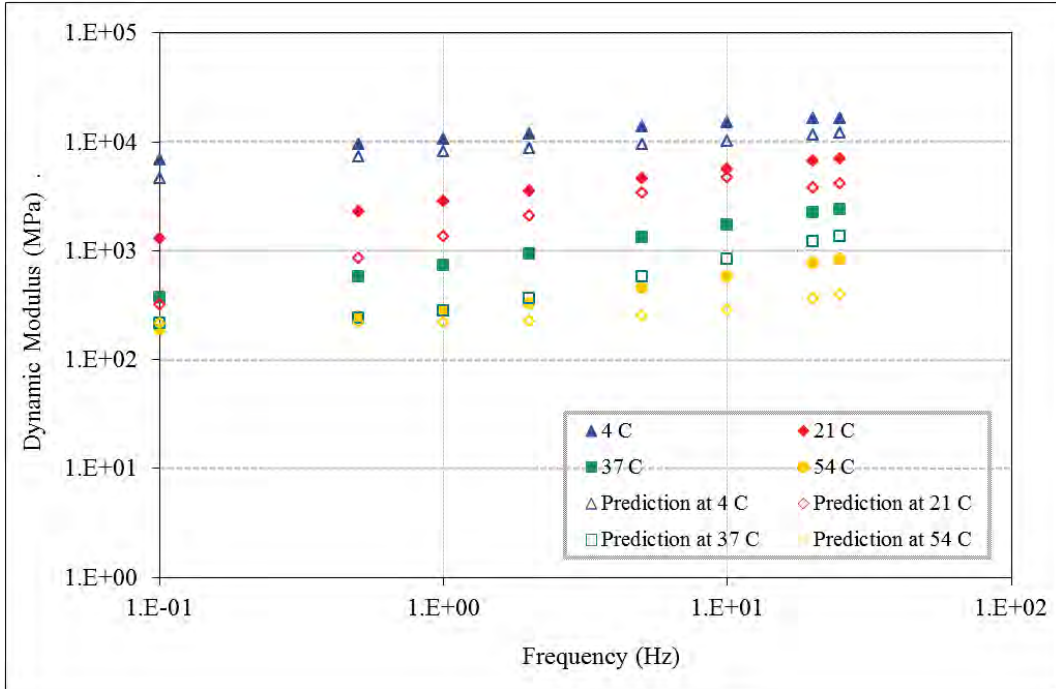
a) Measured and Predicted |E*| at Different Temperature and Frequency
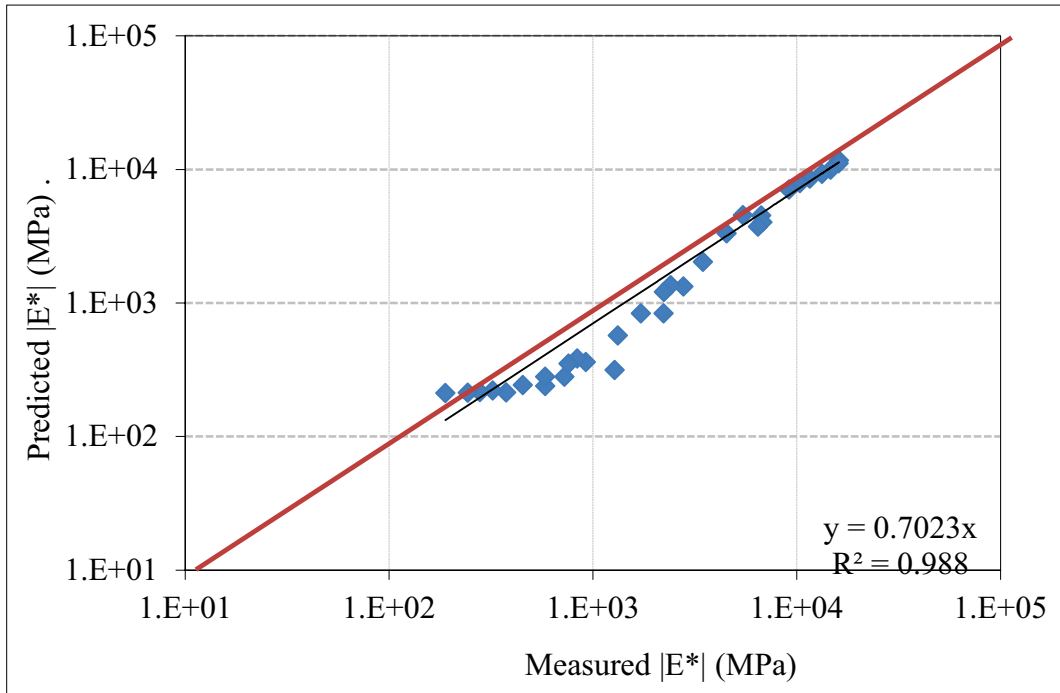
b) Measured |E*| vs. Predicted |E*|

Figure D.19 Summary of Predicted |E*| based on Hirsch Model
(Project: PSG Mitkof Highway-Scow Bay to Crystal Lake Hatchery)
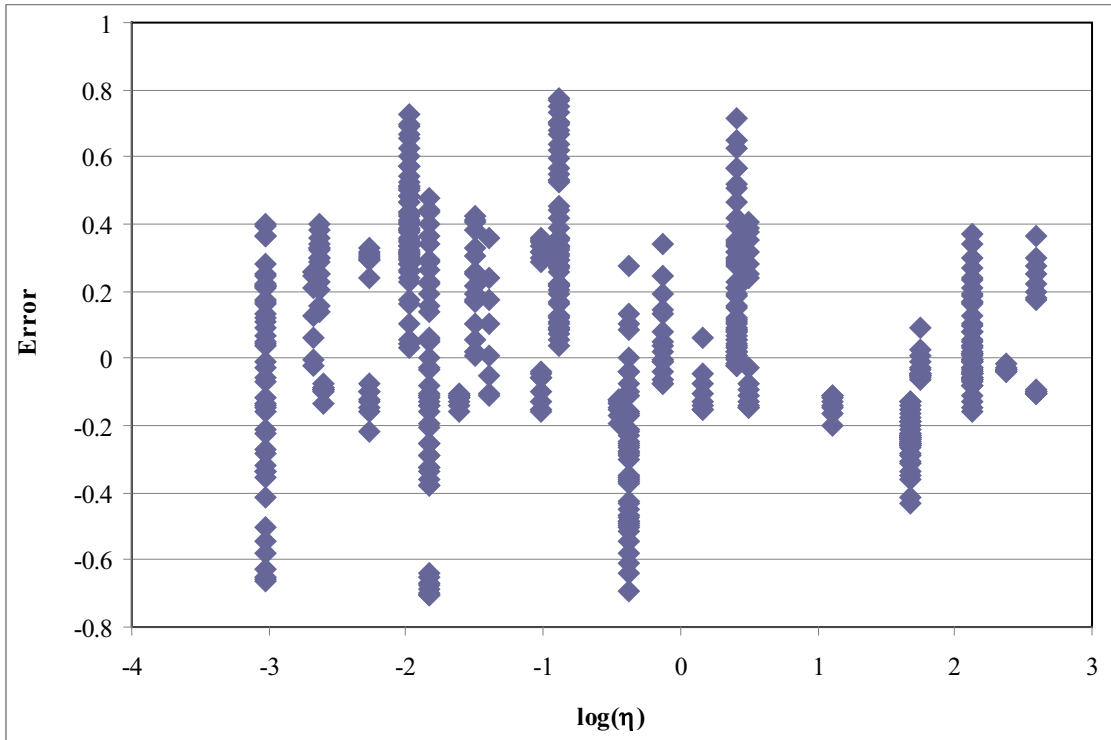
Figure E.1 Error Analyses for Original Witczak Model (η)
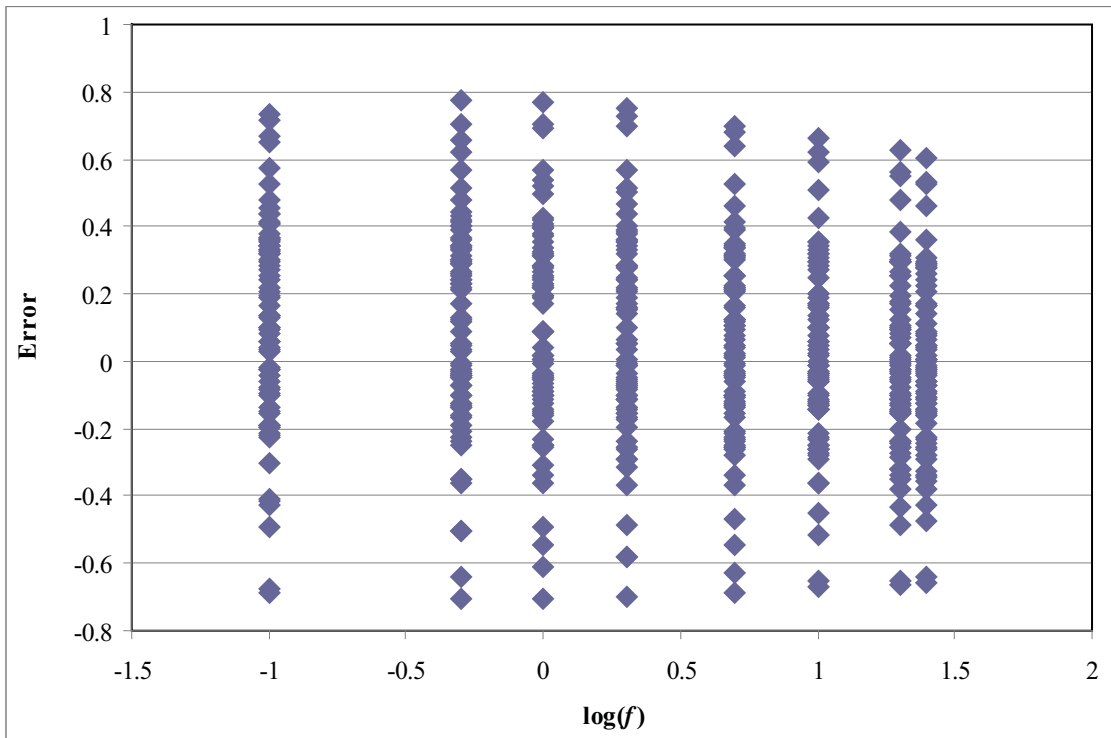
Figure E.2 Error Analyses for Original Witczak Model (*f*)
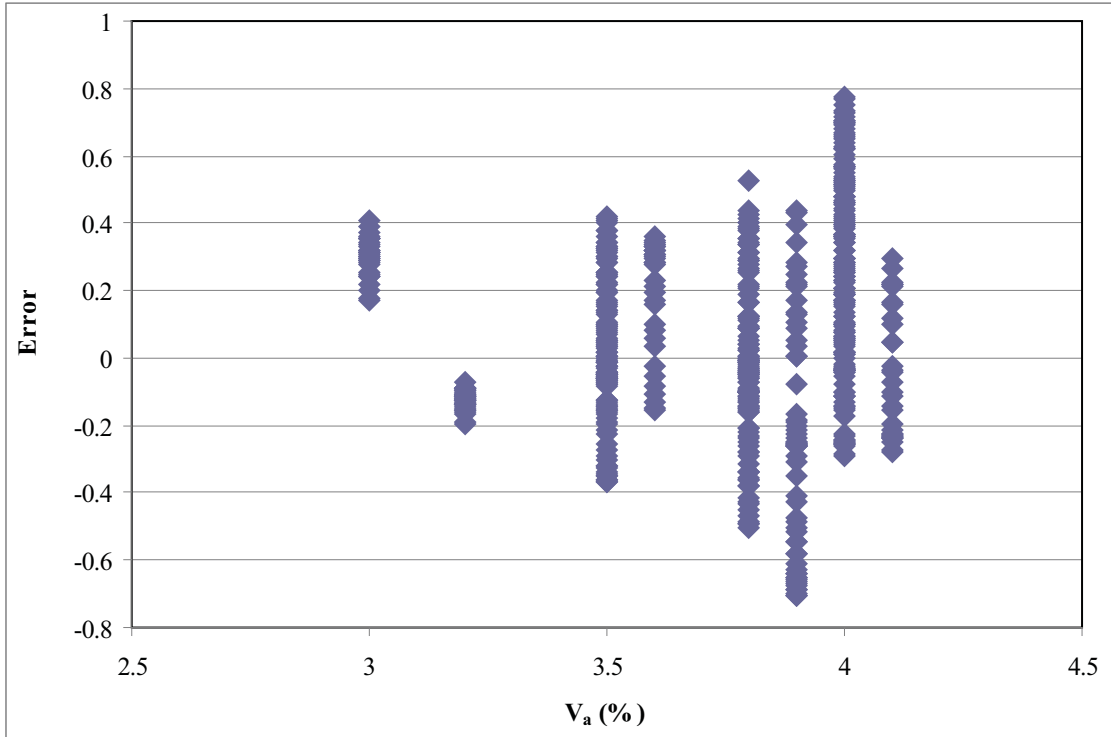
Figure E.3 Error Analyses for Original Witczak Model (Va)
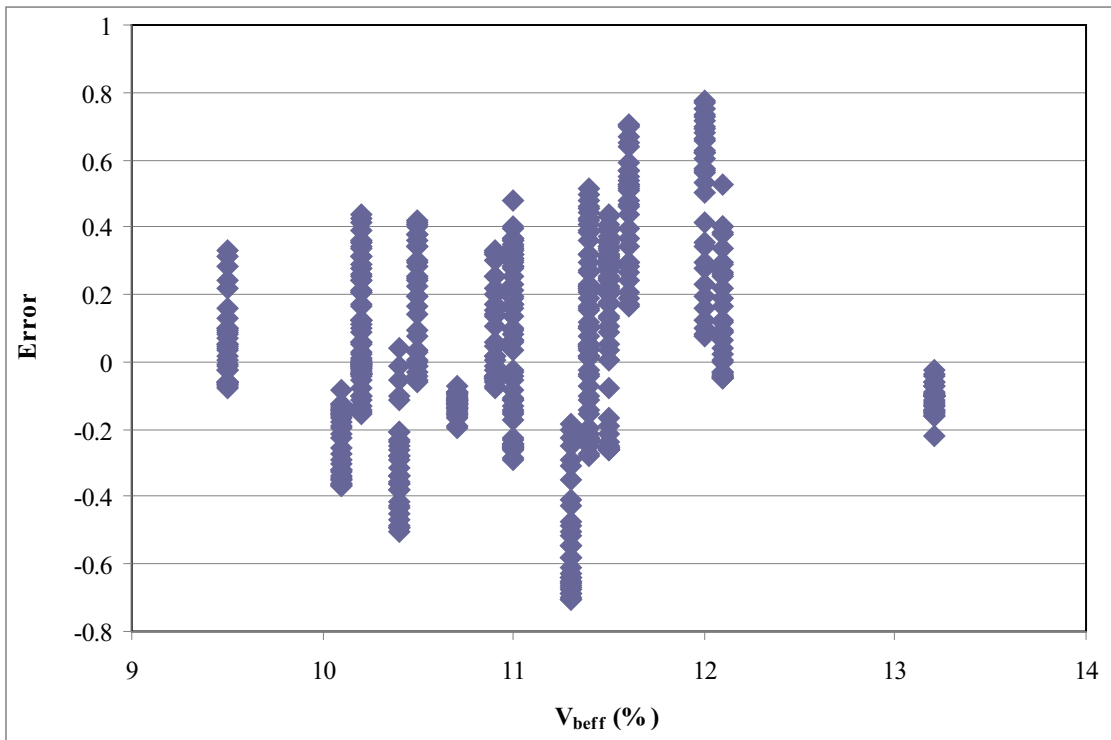
Figure E.4 Error Analyses for Original Witczak Model (V_{beff})

160
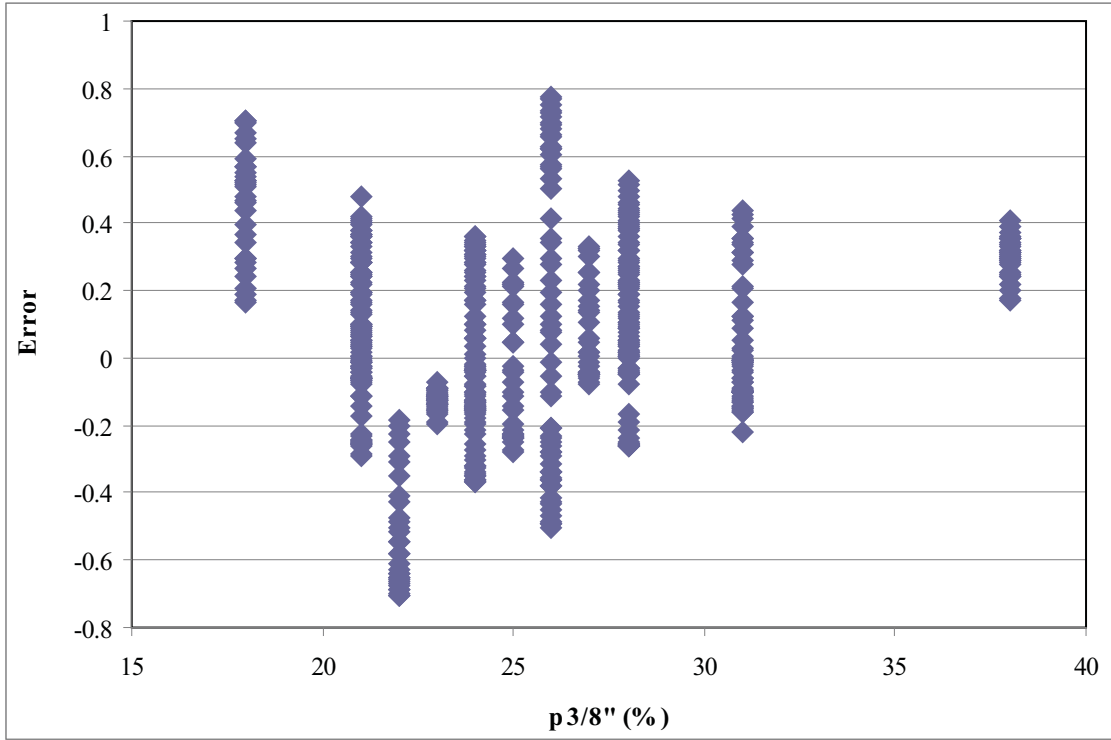
Figure E.5 Error Analyses for Original Witczak Model (p200)
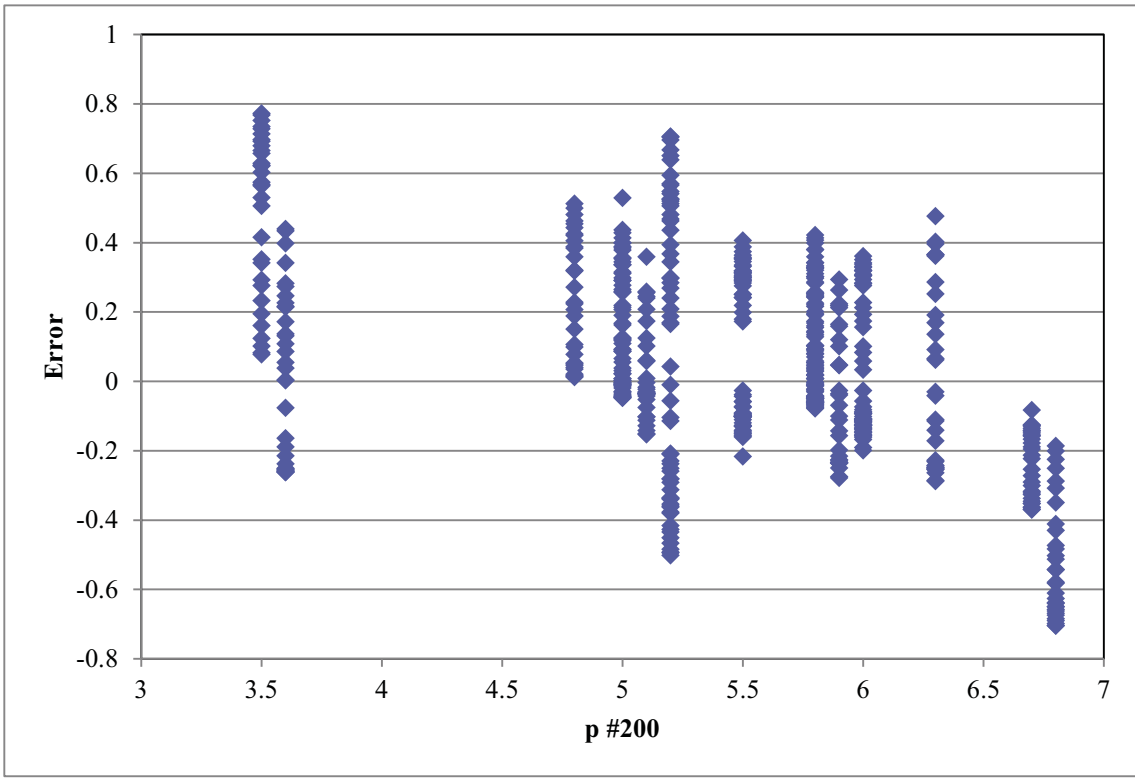
Figure E.6 Error Analyses for Original Witczak Model (p200)

161
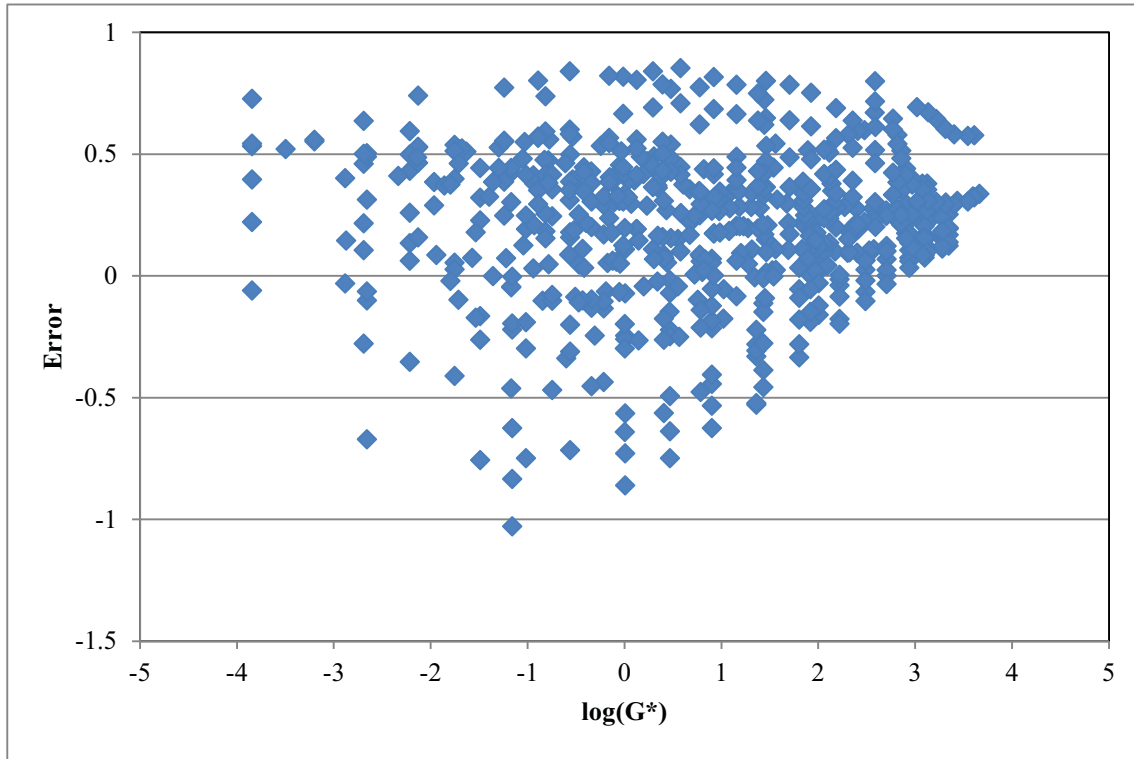
Figure E.7 Error Analysis for Modified Witczak Model (G*)
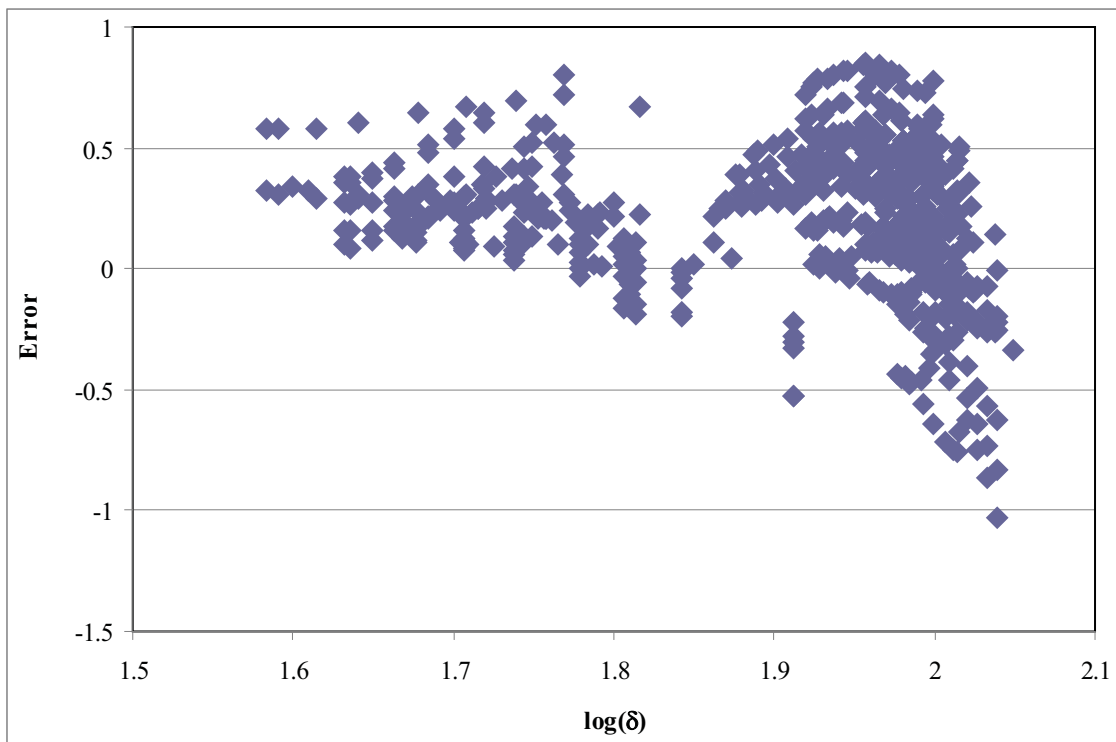
Figure E.8 Error Analysis for Modified Witczak Model (◻)
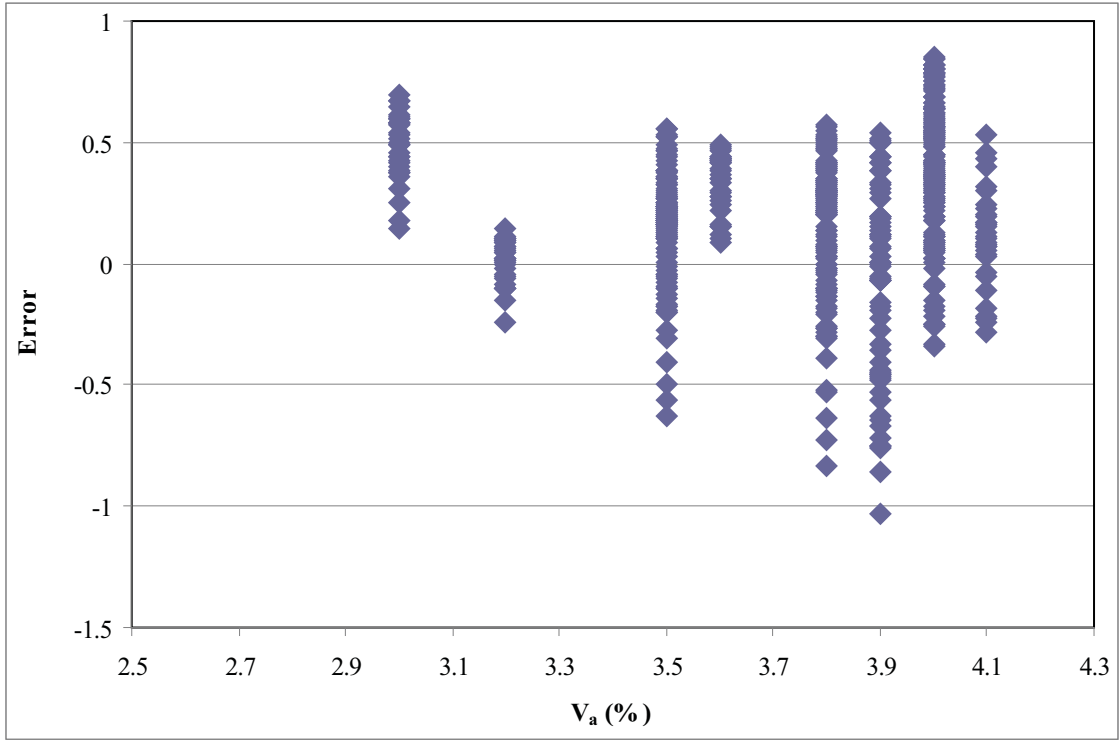
Figure E.9 Error Analysis for Modified Witczak Model (Va)
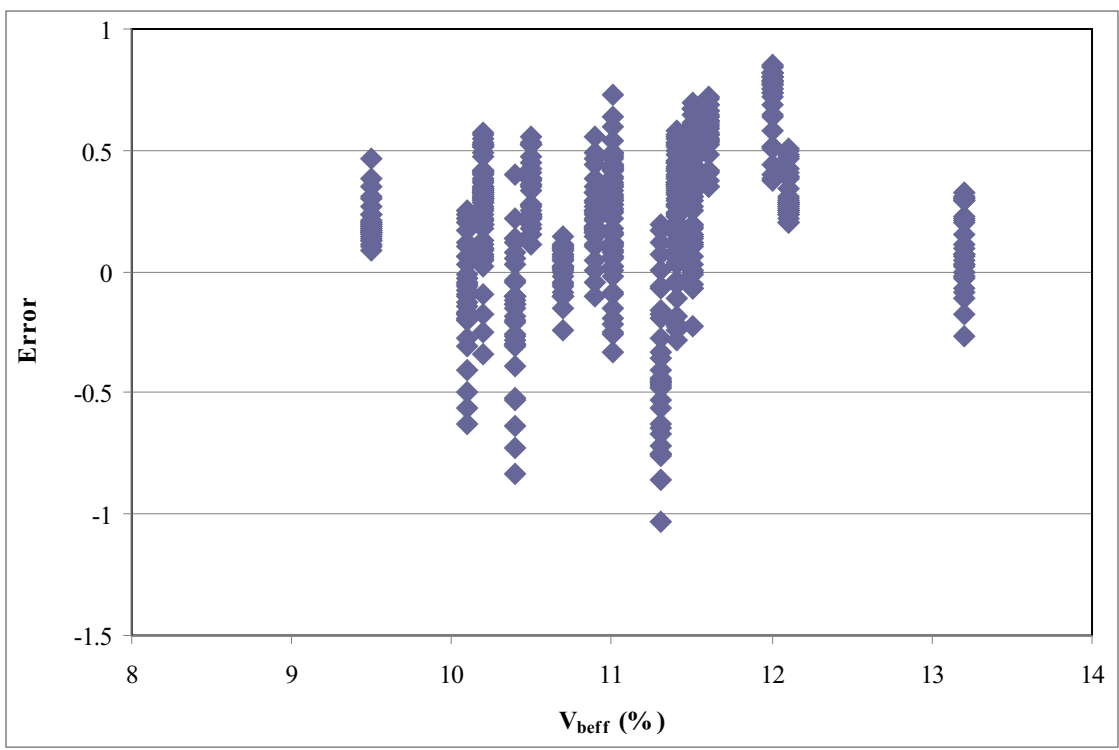
Figure E.10 Error Analysis for Modified Witczak Model (Vbeff)

163
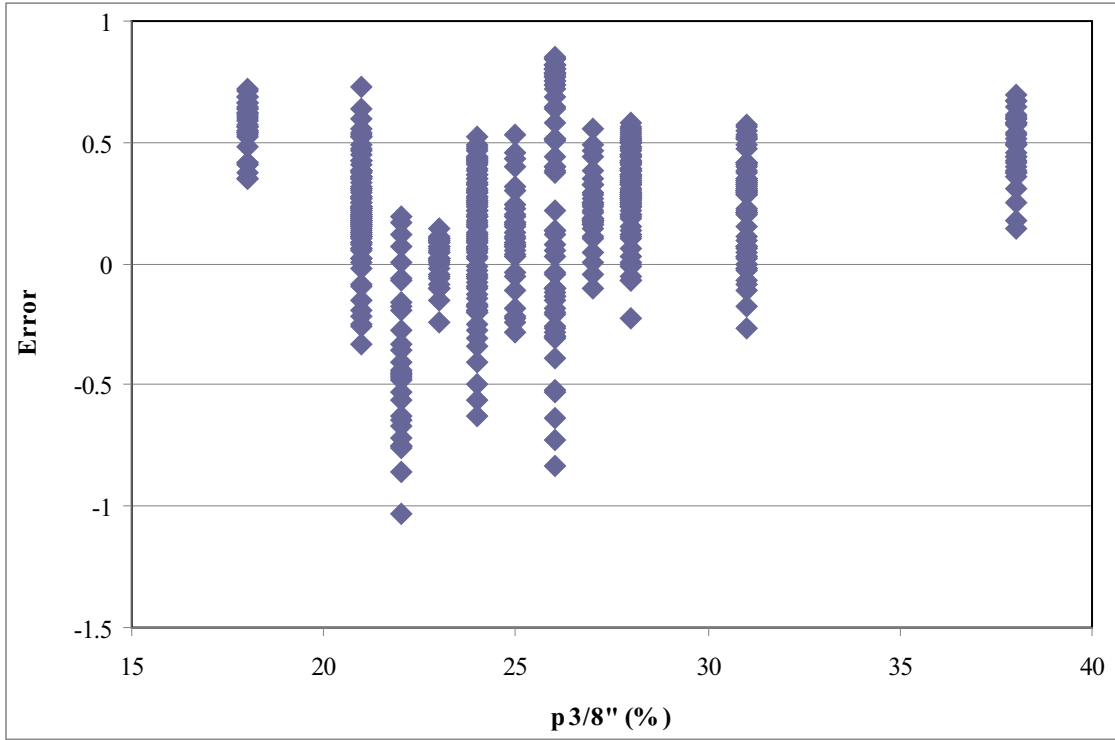
Figure E.11 Error Analysis for Modified Witczak Model (p⅜)
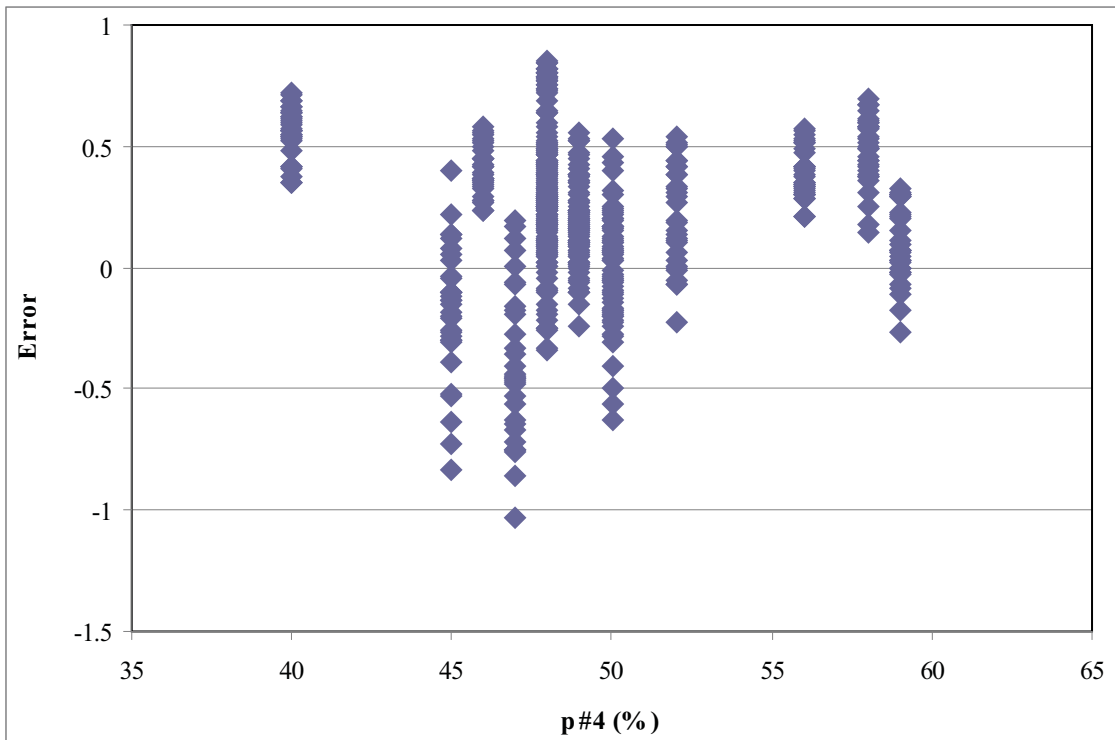
Figure E.12 Error Analysis for Modified Witczak Model (p#4)

164
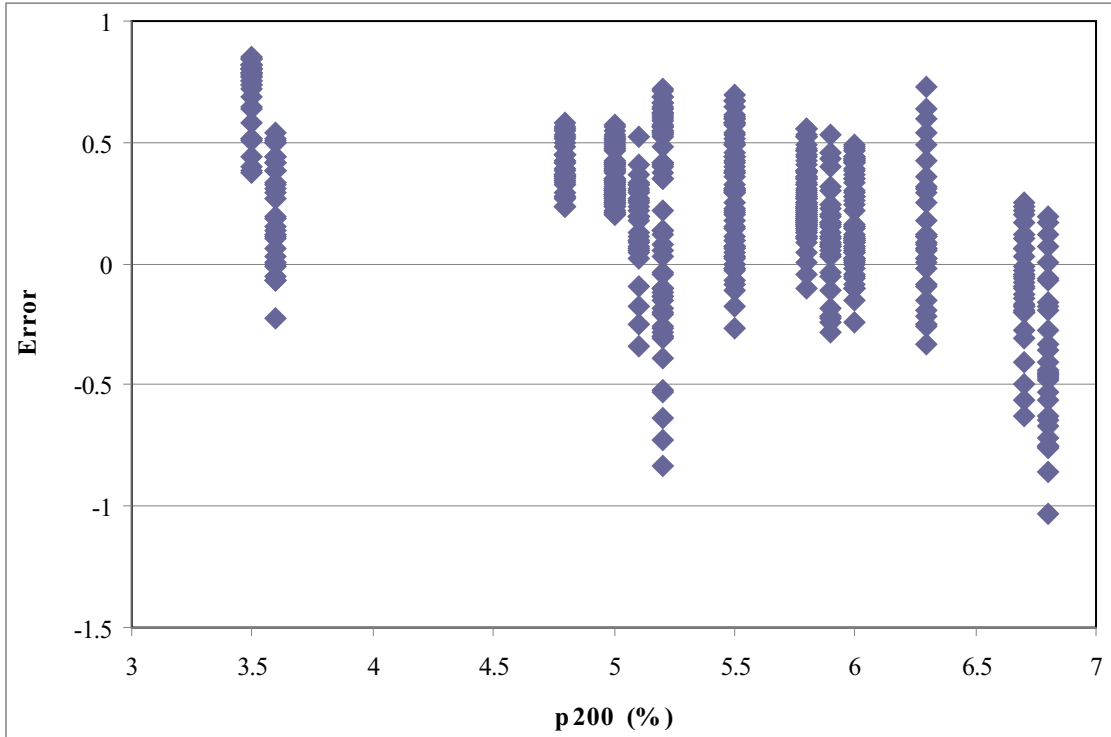
Figure E.13 Error Analysis for Modified Witczak Model (p200)
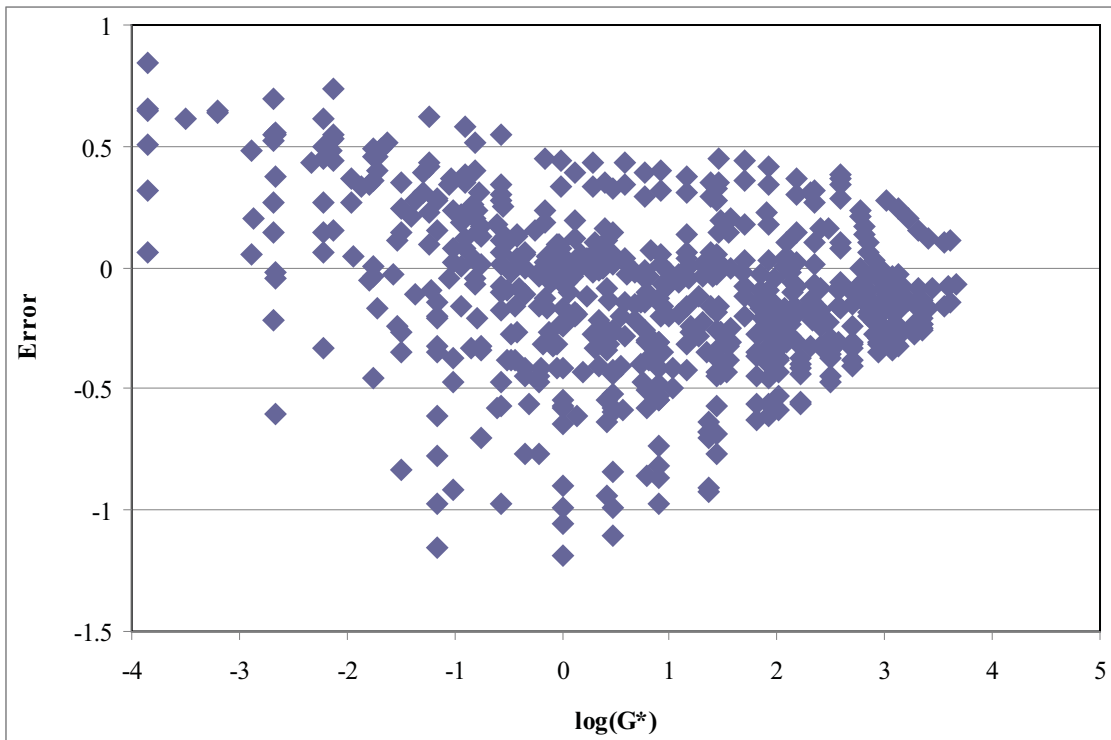
Figure E.14 Error Analysis for Hirsch Model (G*)

165
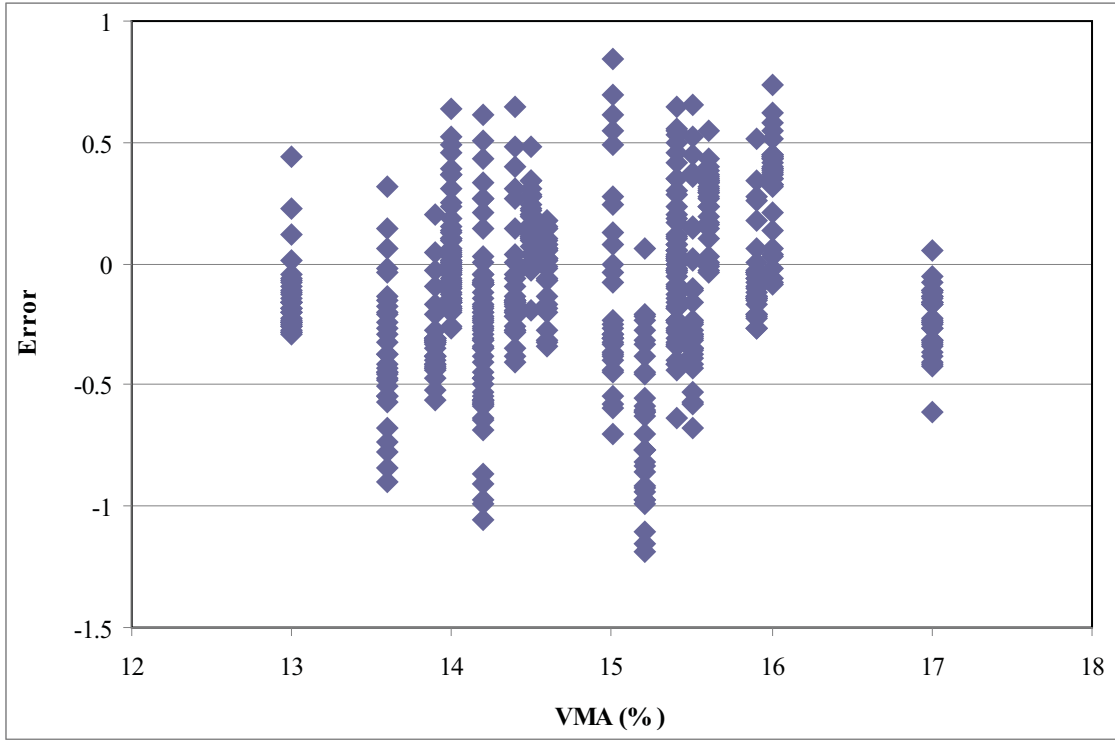
Figure E.15 Error Analysis for Hirsch Model (VMA)
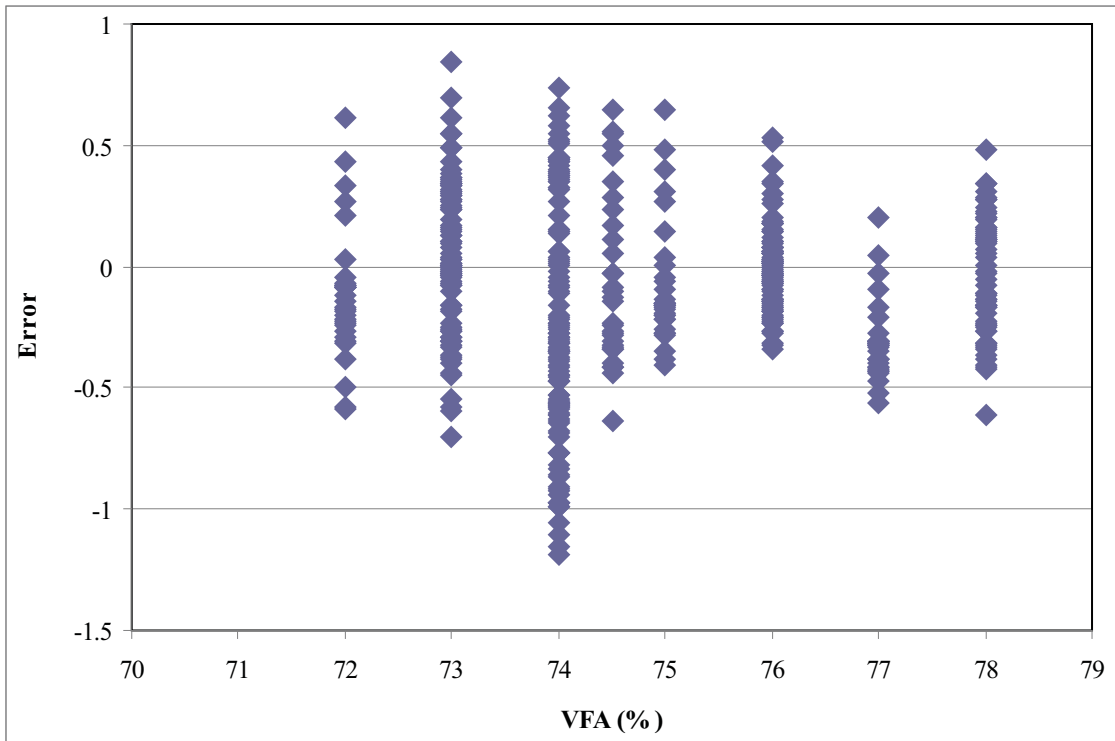
Figure E.16 Error Analysis for Hirsch Model (VFA)